

Copyright  
by  
Michal R. Szymanski  
2011

**The Dissertation Committee for Michal R. Szymanski Certifies that this is the  
approved version of the following dissertation:**

**Helicase-Initiated Assembly of Macromolecular Machines Involved in  
DNA Replication**

**Committee:**

---

Wlodek Bujalowski, PhD, Supervisor

---

Marc C. Morais, PhD, Chair

---

Kay Choi, PhD

---

Roberto Galletto, PhD

---

Andres F. Oberhauser, PhD

---

Dean, Graduate School

**Helicase-Initiated Assembly of Macromolecular Machines Involved in  
DNA Replication**

**by**

**Michal R. Szymanski, B.S.**

**Dissertation**

Presented to the Faculty of the Graduate School of

The University of Texas Medical Branch

in Partial Fulfillment

of the Requirements

for the Degree of

**Doctor of Philosophy**

**The University of Texas Medical Branch**

**August, 2011**

## **Dedication**

With love and gratitude to my parents, Dr. Lidia and Roman Szymanski.

In loving memory of my grandmother, Zofia Szymanska (1921-2008), who raised me  
generating curiosity, passion, and confidence, and showed me that I am able to do  
anything I set my mind to.



## **Acknowledgements**

I would like to express my gratitude to my mentor, “the Boss”, Dr. Wlodek Bujalowski for accepting me to his laboratory, being an exceptional teacher, adviser, and a friend. You noticed my drive and passion for science and believed in me before anybody else did.

Special thanks to Dr. Maria Jezewska who has been of crucial importance through this research project. Most of the hands-on training on experimental techniques described here came from her. You have been a true friend, a source of bottomless support, help, and advice in both scientific and non-scientific problems. Thank you!

Also, I would like to extend my gratitude to Dr. James C. Lee for his countless advice, encouragement, and support.

For continuous guidance in my scientific ventures I want to thank members of my dissertation committee, Dr. Kay Choi, Dr. Roberto Galletto, Dr. Marc Morais, and Dr. Andres Oberhauser.

Thanks to the administrative staff in the laboratory and department. In particular, I would like to express my gratitude to Debora Botting and Rhoda Thompson.

To my family who was always involved during my dissertation, especially to my sister and the best friend Anna, her husband Damian, and my parents Lidia and Roman for their unconditional love, support and patience. I want to thank my grandmother Jozefa Poreba and my aunt and uncle Barbara and Roman Murluk. Through all those years they gave me continuous support, compassion and encouragement.

Deepest thanks to my fiancée, Dr. Alekandra Gmyrek, my inspiration, and a vital driving force during my graduate studies. You have that unrelenting passion, patience, and love to see me through even when I'm grouchy and egocentric.

Thanks to my friends and colleagues Katarzyna Walkiewicz, Kamila Szczesna, Dr. Cecille Bussetta, Dr. Bartosz Szczesny, and Emilio Reyes-Aldrete.

Special thanks to my friends Dr's. Magda and Eric Walkiewicz-Yvon and their kids Sveva and Camil. Your house has always been a true asylum and a perfect escape from Galveston's heat, whether and science wise.

# **Helicase-Initiated Assembly of Macromolecular Machines Involved in DNA Replication**

Publication No. \_\_\_\_\_

Michal R. Szymanski, Ph.D.

The University of Texas Medical Branch, 2011

Supervisor: Wlodek Bujalowski

The research goal of this project is to obtain the first, comprehensive, physical model of the initial phase of the PriA helicase-directed formation of the primosome, a large protein-DNA complex, in *E. coli*, responsible for the restart of the DNA replication after the damage. The primosome, in its final state, comprises of as many as seven different proteins: PriA and DnaB helicases, DnaC, DnaG, DnaT, PriB, and PriC. Multiple and specific protein - protein, and protein - DNA interactions constitute integral part of this large molecular machine and dictate how this molecular motor assembles. However, the mechanistic details on how this intricate complex forms and accomplishes its function are unknown.

In order to be able to put, such a complex molecular machine, together and understand, at the molecular level, its assembly process, discrete protein - protein and protein - DNA interactions of its components must be elucidated. Therefore, to begin with, the examination of the interactions of the PriA helicase, the first player in the

assembly process, with various structures of the DNA, and the effect of the nucleotide cofactors on the interactions was addressed.

The interactions of the PriB protein with PriA-DNA complex are considered to be the next, crucial, step in the assembly process of the primosome. In turn, the interactions of PriB with single stranded and double stranded DNA were examined. Only when such information was available, tertiary complexes could be studied.

Finally, having elucidated the nature of PriA-ssDNA / -dsDNA and PriB-ssDNA / -dsDNA binary complexes, tertiary PriA-PriB-ssDNA, PriA-PriB-dsDNA, PriA-PriB-PAS complexes were examined. Consequently, direct quantitative model of two initial steps in the primosome assembly, involving the PriA and PriB proteins vis-à-vis the minimal primosome assembly site (PAS) of phage phiX174, was proposed.

The studies presented here establish the first quantitative framework to study, at the molecular level, the assembly mechanism of the primosome, a paradigm of a large molecular machine involved in DNA replication. By building on the scaffold established in this research project, subsequent steps in the assembly process will be examined, to grant the first, comprehensive, molecular model of the primosome formation.

## Table of Contents

LIST OF TABLES .....	xviii
LIST OF FIGURES .....	xx
<b>CHAPTER 1: INTRODUCTION</b> .....	1
1.1 GENERAL OVERVIEW.....	1
1.2 DNA REPLICATION.....	2
1.3 DNA DAMAGE AND THE PRIMOSOME .....	3
1.4 RATIONALE FOR THE STUDY .....	4
1.4.1 Central hypothesis and specific aims .....	6
<b>CHAPTER 2: THE <i>ESCHERICHIA COLI</i> PRIA HELICASE SPECIFICALLY RECOGNIZES GAPPED DNA SUBSTRATES</b> .....	10
2.1 ABSTRACT.....	10
2.2 INTRODUCTION .....	11
2.2.1 Replication Restart.....	11
2.2.2 PriA – Dependent Pathway .....	12
2.2.3 Properties of the PriA Helicase.....	14
2.2.4 Rationale for Specific Aim 1 and specific gaps in knowledge .....	16
2.3 MATERIALS AND METHODS.....	17
2.3.1 Buffers and Chemicals.....	17
2.3.2 Water Activity of Buffering Solution .....	18
2.3.3 Nucleotides and Nucleic Acids.....	18
2.3.4 The PriA Protein Purification.....	19
2.3.5 Determination of Extinction Coefficient of PriA.....	19
2.3.6 Fluorescence Measurements .....	21
2.3.7 General Approach to Quantitative Analysis of the Fluorescence Titration Curves of PriA - Gapped DNA Interactions .....	21
2.3.8 Analytical Ultracentrifugation .....	22
2.3.9 Determination of PriA Partial Specific Volume .....	24

2.4 RESULTS .....	24
2.4.1 The PriA Helicase .....	24
2.4.2 Hydrodynamic Properties of PriA .....	24
2.4.3 Binding of the PriA Helicase to the Gapped DNA Substrates.....	28
2.4.4 Maximum Stoichiometry of the PriA Helicase - Gapped DNA Complex. Analytical Sedimentation Equilibrium Studies. ....	30
2.4.5 Statistical Thermodynamic Model of the PriA Helicase Binding to the Gapped DNA Substrates. ....	32
2.4.6 Intrinsic Affinity of the PriA Helicase For the ssDNA Gap as a Function of the Gap Size. ....	34
2.4.7 Interactions of the PriA Helicase With the Gapped DNA Substrates In the Presence of Nucleotide Cofactors. ....	37
2.4.8 Salt Effect on PriA - Gapped DNA Interactions In the Absence of Nucleotide Cofactors.....	42
2.4.9 Salt Effects on PriA - Gapped DNA Interactions With Both Nucleotide-Binding Sites of the Enzyme Saturated With ADP. ....	44
2.5 DISCUSSION .....	47
2.5.1 The Site-Size of the PriA - Gapped DNA Substrate Complexes is Significantly Lower Than the Site-Size of the Enzyme - ssDNA Complex. ....	47
2.5.2 PriA Specifically Recognizes the ssDNA/dsDNA Junction (s) of the Gapped Structures. ....	48
2.5.3 The PriA Helicase Preferentially Recognizes the ssDNA Gap With 5 Nucleotides In the Absence of Nucleotide Cofactors. ....	49
2.5.4 Intrinsic Interactions of the PriA Helicase - ssDNA Gap Indicate Involvement of the ssDNA/dsDNA Junction (s) of the Gapped Structures. The Salt Effect.....	50
2.5.5 The Presence of the Nucleotide in the Strong Nucleotide-Binding Site Eliminates PriA's Size Specific Selectivity for the Gap of 5 Nucleotides.....	52
2.5.6 Saturation of Both Nucleotide-Binging Sites of the PriA Helicase with ADP Restores Enzyme Selectivity for the ssDNA Gap with 5 Nucleotides.....	53
2.5.7 Salt Effect on the Gap Complex Formation when Both Nucleotide- Binding Sites are Saturated with ADP. ....	54
2.5.8 Model of the PriA – Gapped DNA Complex with 5 Nucleotides in the ssDNA Gap.....	55

2.5.9 Functional Implications. ....	57
<b>CHAPTER 3: THE <i>ESCHERICHIA COLI</i> PRIA HELICASE - DOUBLE-STRANDED DNA COMPLEX</b> .....	62
3.1 ABSTRACT.....	62
3.2 INTRODUCTION .....	63
3.3 MATERIALS AND METHODS.....	64
3.3.1 Buffers and Chemicals.....	64
3.3.2 Water Activity of Buffering Solution. ....	65
3.3.3 Nucleotides and Nucleic Acids.....	65
3.3.4 The PriA Protein. ....	66
3.3.5 Fluorescence Measurements. ....	66
3.3.6 Determination of Quantitative Binding Isotherm of the PriA – dsDNA Complexes. ....	67
3.3.7 Analytical Ultracentrifugation Measurements.....	67
3.3.8 Trypsin Digestion Experiments. ....	67
3.3.9 Photo-cross-linking Coupled Trypsin Digestion Experiments. ....	68
3.4 RESULTS .....	69
3.4.1 The Site-Size of the PriA-dsDNA Complex in the Absence of Nucleotide Cofactors.....	69
3.4.2 Analytical Ultracentrifugation Studies. ....	73
3.4.3 Statistical Thermodynamic Model of PriA Binding to the dsDNA.....	75
3.4.4 Binding of PriA to Unmodified dsDNA. Lattice Competition Titration Experiments.....	79
3.4.5 Salt Effect on the PriA – dsDNA 10-mer Complex Formation. ....	82
3.4.6 The Effect of Temperature on the Intrinsic and Cooperative PriA – dsDNA 10-mer Interactions. ....	83
3.4.7 The Effect of Nucleotide Cofactors on the Intrinsic and Cooperative PriA – dsDNA 10-mer Interactions.....	88
3.4.8 Photo – Cross – Linking of the PriA Helicase to ssDNA.....	95
3.5 DISCUSSION.....	98
3.5.1 The Helicase Engages Only the Strong DNA-Binding Subsite in Interactions with the dsDNA.....	98

3.5.2 The Strong DNA – Binding Subsite Is Located on the Helicase Domain of the PriA Helicase. Photo-Cross-Linking Experiments...	100
3.5.3 PriA Preferentially Binds to the dsDNA over the ssDNA.....	100
3.5.4 The PriA Helicase Binds dsDNA with Specific Orientation. ....	101
3.5.5 The Effect of Temperature on the PriA – dsDNA Interactions Indicates Enzyme’s Conformational Flexibility. ....	102
3.5.6 Binding of ADP to the Strong – Nucleotide Binding Site of PriA Increases the Positive Cooperativity of the Enzyme for dsDNA. ....	103
3.5.7 Saturation of Both Nucleotide-Binding Sites with ADP Has a Dramatic Effect on Intrinsic Affinity and Cooperativity of PriA – dsDNA Interactions. ....	103
3.5.8 Only the Intrinsic Affinity, Not the Cooperativity of PriA – dsDNA Interactions is Controlled by ATP $\gamma$ S.....	104
3.5.9 Functional Implications. ....	105

#### **CHAPTER 4: THE *ESCHERICHIA COLI* PRIA HELICASE N-TERMINAL DOMAIN POSES BOTH DNA AND NUCLEOTIDE BINDING SITE.....**

4.1 ABSTRACT.....	110
4.2 INTRODUCTION .....	111
4.3 MATERIALS AND METHODS.....	114
4.3.1 Buffers and Chemicals.....	114
4.3.2 Water Activity of Buffering Solution. ....	115
4.3.3 Nucleotides and Nucleic Acids.....	115
4.3.4 PriA 181aa N-terminal Domain Purification. ....	116
4.3.5 Determination of Extinction Coefficient of PriA 181aa N-terminal Domain. ....	119
4.3.6 Fluorescence Measurements. ....	119
4.3.7 Determination of Quantitative Binding Isotherm of the 181aa N-terminal Domain - DNA Associations or the Nucleotide Binding to the Domain. ....	120
4.3.8 Analytical Ultracentrifugation Measurements.....	121
4.3.9 Determination of Partial Specific Volume of PriA 181aa N-terminal Domain .....	121
4.3.10 Photo-Cross-Linking Experiments.....	121



4.4 RESULTS .....	122
4.4.1 The 181aa N-Terminal Domain of the PriA Helicase. ....	122
4.4.2 The Hydrodynamic properties of the 181aa N-Terminal Domain of PriA Helicase.....	123
4.4.3 Maximum Stoichiometry of the 181aa N-terminal Domain – ssDNA Complexes. ....	125
4.4.4 Number of Nucleotides Directly Engaged in the Interactions with the 181aa N-terminal Domain Dimer. ....	130
4.4.5 Intrinsic Affinities of 181aa N-Terminal Domain – ssDNA Interactions. ....	130
4.4.6 Intrinsic Affinities and Cooperativities of the 181aa N-terminal Domain Binding to the ssDNA Oligomers Which Can Accept Two Dimer Molecules. ....	133
4.4.7 Only One Monomer of the 181aa N-Terminal Domain Dimer Can Effectively Engage in the Interactions with ssDNA. Photo-Cross- Linking Experiments. ....	136
4.4.8 Base Specificity of 181aa N-terminal Domain – ssDNA Interactions. Lattice Competition Titrations Using the MCT. ....	138
4.4.9 Conformational and 3' End Specificity of 181aa N-Terminal Domain – ssDNA Interactions. ....	140
4.4.10 Salt Effect on the 181aa N-Terminal Domain of PriA – ssDNA Interactions. ....	143
4.4.11 The 181aa N-terminal Domain of PriA Helicase Binds Nucleotide Cofactors. ....	143
4.4.12 The Statistical Thermodynamic Model for the Nucleotide Cofactor Binding to the 181N-Terminal Domain Dimer. ....	145
4.4.13 The 181aa N-Terminal Domain – ssDNA Interactions in the Presence of ADP or ATP $\gamma$ S.....	149
4.5 DISCUSSION.....	150
4.5.1 The 181aa N-Terminal Domain Dimer Has Only One Effective ssDNA Binding Site. ....	150
4.5.2 The Small Number of Nucleotides Engaged in Direct Interactions with the ssDNA Indicates That the DNA-Binding Subsites of Intact PriA Helicase are Spatially Separated. ....	152

4.5.3 The Ability of 181aa N-Terminal Domain to Bind to the ssDNA in the Absence of Nucleotide Cofactors Indicates the Presence of Allosteric Domain – Domain Motions in the Intact Enzyme.....	153
4.5.4 The 181aa N-Terminal Domain DNA-Binding Subsite Has Only a Slight Preference for the 3' End of the Nucleic Acid.....	154
4.5.5 The 181aa N-Terminal Domain of PriA Helicase Has a Significant Affinity for dsDNA. ....	155
4.5.6 The DNA-Binding Subsite of the 181aa N-Terminal Domain Lacks Significant Base Specificity in the Interactions with the ssDNA.....	155
4.5.7 The Weak Nucleotide-Binding Site of the Intact PriA Helicase Is Located on the 181aa N-terminal Domain. ....	156
4.5.8 ADP Increases the Intrinsic Affinity of the 181aa N-Terminal Domain - ssDNA Interactions. ....	157
4.5.9 Comparison with Other Works.....	158
4.5.10 Further Functional Implications.....	159

## **CHAPTER 5: INTERACTIONS OF THE *ESCHERICHIA COLI* PRIMOSOMAL PRIB PROTEIN WITH THE DNA.....**

5.1 ABSTRACT.....	163
5.2 INTRODUCTION .....	164
5.3 MATERIALS AND METHODS.....	167
5.3.1 Buffers and Chemicals.....	167
5.3.2 Water Activity of Buffering Solution. ....	168
5.3.3 Nucleic Acids.....	168
5.3.4 The PriB Protein Purification. ....	169
5.3.5 Determination of Extinction Coefficient of the PriB Protein. ....	173
5.3.6 Fluorescence Measurements. ....	173
5.3.7 Determination of Thermodynamically Quantitative Binding Isotherms of the PriB Protein - ssDNA Complexes. ....	174
5.3.8 Analytical Ultracentrifugation Measurements.....	174
5.3.9 Determination of PriB Partial Specific Volume. ....	174
5.3.10 Photo-Cross-Linking Experiments. ....	174
5.4 RESULTS .....	175
5.4.1 The PriB Protein. ....	175
5.4.2 The Hydrodynamic Properties of the PriB Protein. ....	175

5.4.3 The Total Site-Size of the PriB – ssDNA Complex. ....	179
5.4.4 Maximum Stoichiometry of the PriB Dimer – ssDNA Complex Determined by Sedimentation Equilibrium Method. ....	182
5.4.5 Determination of the Site-Size of the PriB Dimer – ssDNA Interactions. ....	186
5.4.6 Intrinsic Affinity of the PriB protein – ssDNA Interactions. ....	186
5.4.7 Intrinsic Affinities and Cooperativities of the PriB protein – ssDNA Interactions. ....	190
5.4.8 The Effect of Salt on the Intrinsic PriB – ssDNA Interactions. ....	193
5.4.9 The Effect of Magnesium on the Intrinsic Interactions of PriB – ssDNA. ....	193
5.4.10 The Effect of Salt on the Intrinsic Affinity and Cooperativity of PriB Dimer – ssDNA Interactions. ....	195
5.4.11 The Effect of Temperature on the Intrinsic PriB – ssDNA Interactions. ....	197
5.4.12 The Base Specificity of PriB – ssDNA Interactions. ....	199
5.4.13 Photo-Cross-Linking of the PriB Dimer To the ssDNA. ....	201
5.5 DISCUSSION .....	203
5.5.1 The Total Site-Size of the PriB Dimer – ssDNA Complex Is $12 \pm 1$ Nucleotides. ....	203
5.5.2 PriB Possesses Only One DNA-Binding Site Located on a Single Monomer of the PriB Dimer .....	204
5.5.3 The PriB Dimer ssDNA-Binding Site Has Functionally Homogenous Structure. ....	205
5.5.4 The PriB Dimer Binds the ssDNA With Significant Positive Cooperativity. ....	206
5.5.5 The Salt Effect on the Intrinsic Affinity of the PriB Dimer –DNA Interactions Indicates Engagement of the Entire Total Binding Site of the Protein .....	207
5.5.6 The PriB Dimer Shows a Very Strong Preference For the Homo- Pyrimidine ssDNA. ....	208
<b>CHAPTER 6: BINDING OF TWO PRIA - PRIB COMPLEXES TO THE PRIMOSOMAL ASSEMBLY SITE INITIATES THE PRIMOSOME FORMATION .....</b>	<b>213</b>
6.1 ABSTRACT.....	213

6.2 INTRODUCTION .....	214
6.3 MATERIALS AND METHODS.....	216
6.3.1 Buffers and Chemicals.....	216
6.3.2 Water Activity of Buffering Solution. ....	216
6.3.3 Nucleotides and Nucleic Acids.....	216
6.3.4 The UV Melting of the PAS Structure.....	218
6.3.5 The PriA and PriB Protein Purification. ....	218
6.3.6 Labeling of the PriA and PriB Protein with Fluorescent Markers.....	218
6.3.7 Fluorescence Measurements. ....	219
6.3.8 Quantitative Determination of Binding Isotherms and Stoichiometries of the PriA - PAS Complexes.....	220
6.3.9 Fluorescence Resonance Energy Transfer (FRET) Measurements. ..	220
6.4 RESULTS .....	222
6.4.1 The Modified PriA and PriB protein. ....	222
6.4.2 The UV Melting of the PAS Substrate. ....	224
6.4.3 Binding of the PriA Helicase to the Fluorescein Labeled PAS Substrate. ....	227
6.4.4 Statistical Thermodynamic Model of the PriA Helicase Binding to the PAS Structure. ....	228
6.4.5 Fluorescence Resonance Energy Transfer (FRET) Results Yield the Location of the Strong PriA Binding Site On the PAS Structure. ...	231
6.4.6 Fluorescent Marker on the PAS Structure Does Not Affect the PriA – 5'-Fl-PAS Interactions. Lattice Competition Titrations.....	233
6.4.7 Binding of the PriA Helicase to PAS in the Presence of ADP and ATP $\gamma$ S. ....	235
6.4.8 The PriA Helicase Interacts with PriB Independent of PAS. ....	238
6.4.9 The PriB Protein Binding to PAS is Negligible.....	240
6.4.10 The Effect of PriB in Solution on the Binding of PriA to PAS. ....	242
6.4.11 The Model of the PriB Effect On the PriA – PAS Interactions. ....	245
6.4.12 The Effect of PriB Protein on the PriA – ssDNA and PriA - dsDNA Interactions. ....	248
6.4.13 The PriA and PriA - PriB – PAS Interactions. The Thermodynamic Cycle.....	251

6.4.14 The Effect of Temperature on the PriA-PAS or PriA-PriB-PAS Complex Formation.....	253
6.4.15 Changes to the PAS Structure Exerted by the PriA and PriA – PriB Binding in the Presence of ATP. FRET Experiments. ....	255
6.5 DISCUSSION.....	259
6.5.1 Binding of Two PriA Molecules to Two Discrete Binding Sites on the PAS Structure Initiates the Primosome Formation. ....	259
6.5.2 The PriB Protein Specifically Binds to the PriA Associated with the Strong Binding Site on the PAS Structure. ....	261
6.5.3 The PriB Protein Induces Conformational Changes in the PriA Protein In the Absence of the DNA Which Specifically Increase the PriA Affinity for the Strong Binding Site On the PAS.....	262
6.5.4 The PriA-PriB Complex Can Recognize the PAS Without Prior Binding of PriA to the DNA.....	263
6.5.5 Only Moderate Conformational Changes in the PAS Structure are Induced by PriA and PriA – PriB Complex in the Presence of ATP.....	264
6.5.6 Further Functional Implications.....	265
<b>CHAPTER 7: CONCLUSIONS AND FUTURE DIRECTIONS .....</b>	<b>269</b>
7.1 CONCLUSIONS.....	269
7.2 FUTURE DIRECTIONS .....	274
APPENDIX .....	277
REFERENCES .....	282
VITA .....	299

## List of Tables

Table 2.1:	Thermodynamic and spectroscopic parameters of the binding of PriA to the gapped DNA substrate containing different numbers of nucleotides in the ssDNA gap, in standard buffer C1005.....	60
Table 2.2:	Thermodynamic and spectroscopic parameters of the binding of the <i>E. coli</i> PriA helicase to the gapped DNA substrate containing 5 nucleotides in the ssDNA gap, in standard buffer C1005, in the presence of different concentrations of ATP $\gamma$ S or ADP .....	61
Table 3.1:	Thermodynamic and spectroscopic parameters of the binding of the <i>E. coli</i> PriA helicase to the double-stranded DNA 10-mer, in buffer C505, and different concentrations of ADP, and ATP $\gamma$ S .....	109
Table 4.1:	Thermodynamic and spectroscopic parameters characterizing the binding of the <i>E. coli</i> PriA helicase 181aa N-terminal domain to etheno-derivatives of ssDNA oligomers in buffer C205 .....	161
Table 4.2:	Macroscopic and intrinsic binding constants, $K_N$ and $K_{in}$ , and the site-size, $n$ , characterizing the binding of the PriA helicase 181aa N-terminal domain to different ssDNA homo-oligomers, dN(pN) <sub>19</sub> , homo-oligomer, dC(pC) <sub>18</sub> pCp, containing phosphate group; at the 3' end, and the dsDNA 10-mer, in buffer C205. The values of the binding constants for the unmodified nucleic acids have been determined using the MCT Method.....	162
Table 5.1:	Thermodynamic and spectroscopic parameters characterizing the binding of the <i>E. coli</i> PriB protein to etheno-derivatives of ssDNA oligomers in buffer C100 .....	211

Table 5.2:	Macroscopic and intrinsic binding constants, $K_{20}$ and $K_{in}$ , and the site-size, $n$ , characterizing the binding of the PriB protein to different ssDNA homo-oligomers, $dN(pN)_{19}$ , in buffer C100. The values of $K_{20}$ for the unmodified 20-mers have been determined using the MCT Method .....	212
Table 6.1:	Fluorescence energy transfer efficiencies, $E_D$ , $E_A$ , $E$ , and the distances, $R$ (Å), between the donor and the acceptor located in the vicinity of the 5' and 3' ends of the PAS substrate (Figure 6.13a), associated with different numbers of the PriA molecules, in the absence and presence of the PriB protein and/or ATP .....	268

## List of Figures

Figure 1.1: Schematic representation of the simplest structure of the primosome formed at the ssDNA of the lagging strand. ....	5
Figure 1.2: After over two decades of research the stoichiometry of the primosome components is still predominantly unknown .....	7
Figure 2.1: Different organisms developed different mechanisms to remove different types of damages encountered by the replication machinery at the replication fork. ....	13
Figure 2.2: PriA is a SF2 superfamily, DEXH-type DNA helicase .....	13
Figure 2.3: Functional organization of the PriA helicase - ssDNA complex. ....	15
Figure 2.4: Gapped DNA substrates used to examine interactions of the PriA helicase with gapped DNAs.....	20
Figure 2.5: 10% SDS polyacrylamide gel of the final step of PriA helicase purification. ....	20
Figure 2.6: PriA in solution sediments as a single homogenous species. ....	25
Figure 2.7: The PriA helicase is a monomer in solution .....	27
Figure 2.8: At saturation, three PriA molecules bind to the examined gapped DNA substrates .....	29
Figure 2.9: Sedimentation equilibrium concentration profile of gapped DNA substrate – PriA Helicase complex. ....	31
Figure 2.10: The dependence of the logarithm of the binding constant $K_G$ and the logarithm of the binding constant $K_{DS}$ .....	36



Figure 2.11: Fluorescence titrations of the gapped DNA substrate with the ssDNA gap of 5 nucleotides, with the PriA helicase in the presence of different nucleotide cofactors .....	38
Figure 2.12: The dependence of the logarithm of the binding constant $K_G$ and the logarithm of the binding constant $K_{DS}$ , in the presence of the nucleotide cofactors .....	40
Figure 2.13: The salt effect on PriA - gapped DNA interactions.....	43
Figure 2.14: Salt effects on PriA - gapped DNA interactions containing $3 \times 10^{-3}$ M ADP.....	45
Figure 2.15: Schematic model of the PriA complex with the gapped DNA substrate. ....	56
Figure 3.1: Two PriA molecules bind to the dsDNA 10-mer at saturation.....	70
Figure 3.2: Three PriA molecules bind to the dsDNA 15-mer at saturation.....	72
Figure 3.3: Typical sedimentation equilibrium concentration profile of the 5'-Fl-dsDNA 10-mer in the presence of PriA helicase.....	74
Figure 3.4: Lattice Competition Titration. ....	81
Figure 3.5: Salt effect on the intrinsic and cooperative PriA – dsDNA 10-mer interactions.....	84
Figure 3.6: Temperature effect on the intrinsic and cooperative PriA – dsDNA 10-mer interactions. ....	87
Figure 3.7: The effect of saturation of the strong nucleotide binding site of PriA with ADP on the intrinsic and cooperative PriA – dsDNA 10-mer interactions.....	90

Figure 3.8: The effect of saturation of both nucleotide binding sites of PriA with ADP on the intrinsic and cooperative PriA – dsDNA 10 – mer interactions.....	92
Figure 3.9: The effect of nucleotides on the intrinsic and cooperative PriA – dsDNA 10-mer interactions. ....	94
Figure 3.10: Trypsin digestion of the PriA helicase.....	96
Figure 3.11: Time dependent trypsin digestion coupled with photo – cross – linking experiments.....	97
Figure 3.12: Schematic, functional models of the PAS-like structure and the ssDNA gap recognition processes by the PriA helicase – nucleotide cofactor complexes.. ....	107
Figure 4.1: Schematic model of the PriA helicase in the complex with the ssDNA and ADP .....	113
Figure 4.2: 15% SDS polyacrylamide gel of the final step of 181aa N-terminal Domain of PriA helicase purification. ....	122
Figure 4.3: 181aa N-terminal domain of PriA in solution sediments as a single homogenous species.....	124
Figure 4.4: Sedimentation equilibrium concentration profile of 181aa N-terminal domain of PriA helicase.....	126
Figure 4.5: Maximum stoichiometry of the 181aa N-terminal domain – ssDNA complexes. ....	128
Figure 4.6: 181aa N-terminal domain – ssDNA interactions. Maximum stoichiometry.....	129

Figure 4.7: The maximum stoichiometry of the 181aa N-terminal domain dimer on the ssDNA oligomer as a function of the length of the oligomer (nucleotides).....	131
Figure 4.8: The dependence of the macroscopic, equilibrium binding constant, $K_N$ , characterizing the binding of the 181aa N-terminal domain dimer to different etheno-derivatives of the ssDNA oligomers, which accept only a single domain dimer, upon the length of the ssDNA oligomer (nucleotides) .....	134
Figure 4.9: Photo-cross-linking of PriA 181aa N-terminal domain to ssDNA 20-mer. ....	139
Figure 4.10: Lattice Competition Titrations. ....	142
Figure 4.11: The salt effect on the 181aa N-terminal domain – ssDNA interactions. ....	144
Figure 4.12: The 181aa N-terminal Domain of the PriA helicase binds nucleotide cofactors. ....	148
Figure 4.13: The 181aa N-Terminal Domain – ssDNA Interactions in the Presence of ADP or ATP $\gamma$ S. ....	151
Figure 5.1: The PriB protein structures .....	166
Figure 5.2: 15% SDS polyacrylamide gel of the final step of the PriB protein purification. ....	176
Figure 5.3: PriB in solution sediments as a single homogenous species.....	177
Figure 5.4: Sedimentation equilibrium concentration profile of PriB.....	178
Figure 5.5: Total site-size of the PriB – ssDNA complex .....	181
Figure 5.6: Interactions of PriB – 35-mer ssDNA.....	183
Figure 5.7: Sedimentation equilibrium studies of PriB – ssDNA complexes. ...	185

Figure 5.8: The site-size of the PriB dimer – ssDNA interactions.....	187
Figure 5.9: The site - size of PriB – ssDNA is $12 \pm 1$ nucleotides.....	189
Figure 5.10: The salt effect on the intrinsic PriB – ssDNA interactions.....	194
Figure 5.11: The salt effect on the intrinsic affinity and cooperativity of PriB – ssDNA interactions. ....	196
Figure 5.12: The temperature effect on the PriB - ssDNA interactions .....	198
Figure 5.13: The base specificity of PriB – ssDNA interactions.. ....	200
Figure 5.14: Photo-cross-linking of PriB to ssDNA. ....	202
Figure 6.1: Modified enzymes were > 99% pure as judged by polyacrylamide electrophoresis with Coomassie Brilliant Blue staining. ....	223
Figure 6.2: The UV melting studies .....	226
Figure 6.3: Two molecules of the PriA helicase bind to the fluorescein labeled PAS substrate. ....	230
Figure 6.4: The location of the strong PriA binding site on the PAS structure.....	232
Figure 6.5: Binding of PriA to unmodified PAS substrate.....	236
Figure 6.6: The PriA helicase interacts with PriB in solution independent of PAS. ....	239
Figure 6.7: The PriB protein binds to PAS structure with low affinity.....	241
Figure 6.8: The presence of PriB in solution has a dramatic effect on the binding of PriA to the PAS structure. ....	244
Figure 6.9: The effect of PriB on PriA - PAS structure interactions. The plausible model. ....	247
Figure 6.10: The PriB protein has virtually no effect on the PriA – ssDNA and dsDNA interactions.....	250

Figure 6.11: Thermodynamic cycles of PriA – PAS, PriA – PAS – PriB, PriA – PriB and PriA – PriB - PAS interactions proposed in the recognition of the strong and weak binding sites on the PAS.....	252
Figure 6.12: Temperature effect on the PriA – PAS and PriA – PriB – PAS interactions.....	254
Figure 6.13: The structural effect of the PriA helicase binding to the PAS. ....	256
Figure 6.14: Pictorial representation of the initial recognition of the PAS by the PriA and PriB proteins in the context of the pre-primosome assembly process, based on the results obtained in this work. ....	266

# CHAPTER 1

## INTRODUCTION

### 1.1 GENERAL OVERVIEW

Binding events are fundamental to the biology of every living organism<sup>1</sup>. From the simple substrate – enzyme and protein – protein interactions to the intricate multiple ligand – enzyme – nucleic acid complexes, binding events control virtually all aspects of life as we know it. A detailed understanding of these complex macromolecular interactions requires understanding of thermodynamics, kinetics and structures of interacting molecules alone and when in the complex<sup>1</sup>. In order to quantify the essential, functionally important forces that stabilize these interactions, thermodynamic tools are used and prove to be extremely powerful, providing the information on macroscopic and intrinsic binding constants, stoichiometries, cooperativities, *i.e.*, the molecular determinants that stabilize examined complexes<sup>1</sup>.

DNA replication, recombination and repair are tightly regulated fundamental processes coordinated by variety of multiple protein complexes including the primosome and the replisome<sup>2-5</sup>. Elucidation of the mechanistic details of the ordered assembly of these essential molecular machines of DNA and RNA metabolism is indispensable for understanding why such processes dysfunction in various diseases such as cancer and human genetic disorders<sup>2-5</sup>. The only efficient way to design competent, rational, therapies for these diseases is to dissect, at the molecular level, elementary protein -

protein and protein – DNA interactions that govern the assembly, and orchestrate faithful transmission of genetic information from one cell generation to the next. In this capacity, helicases, a class of enzymes responsible for virtually all aspects of the DNA and RNA metabolism, are of particular interest<sup>2-5</sup>. It is the helicase activity which transforms the metabolically inactive duplex DNA or RNA into active single stranded form. Numerous human genetic diseases as well as different types of cancer involve defects in proteins that engage in helicase activity<sup>2-5</sup>. However, the mechanistic details on how these fascinating enzymes accomplish their functions are still unknown<sup>2</sup>.

## **1.2 DNA REPLICATION**

DNA replication is a fundamental process in the transmission of the genetic material from one cell generation to the next<sup>2-5</sup>. This process requires the parental duplex DNA to be unwound and form metabolically active single-stranded intermediate<sup>2</sup>. To duplicate their genomes, and separate strands during DNA replication, all cells use a multiprotein apparatus known as the replisome<sup>2-5</sup>. It turns out that the replication machinery is quite conserved among viruses, bacteriophages, prokaryotes, and eukaryotes, and in general, comprises of a helicase to unwind the double stranded DNA, a polymerase(s) to synthesize new strands of DNA, and a clamp loader to organize the complex on the DNA<sup>2-6</sup>.

In the bacterial replication machine, the DnaB protein, the primary replicative helicase, encircles the lagging strand of DNA and uses the energy from ATP hydrolysis to separate the duplex DNA by translocating in 5' to 3' direction within the replication bubble<sup>3-5,7-9</sup>. To prevent formation of unnecessary secondary structures that could obstruct the replication process each individual single strand is then coated with single stranded DNA binding (SSB) proteins<sup>3-5</sup>. DNA Polymerase (Pol) III moves along the

leading arm of the replication fork which is primed only once at the origin of replication, *oriC*, and uses the single stranded DNA as a template to synthesize the daughter strand with high fidelity<sup>3-5</sup>. Heterodimeric  $\beta$  clamp (sliding clamp) tethers Pol III to the DNA thereby confers high processivity of the polymerase and helicase actions<sup>3-6</sup>. Multiprotein clamp loader, in the ATP-dependent fashion, orchestrates  $\beta$  clamp opening and closing around template DNA. It also organizes the replisome by simultaneously binding to Pol II and DnaB<sup>3-6</sup>.

Because of the antiparallel structure of the DNA, on the lagging strand, Pol III translocates in the opposite direction to the progression of the replication fork<sup>3-5</sup>. Here the daughter strand is synthesized in the series of ~1.5 kilobase fragments, the Okazaki pieces<sup>3-5</sup>. This is possible due to the action of the DnaG primase which synthesizes short RNA primers<sup>5,10</sup>. The clamp loader assembles  $\beta$  clamp and Pol III around the RNA primer used by Pol III to jump-start the synthesis of the Okazaki fragment. This creates a DNA loop on the lagging strand<sup>5</sup>. When the synthesis of the daughter strand is completed Pol III discharges the clamp, and the loop collapses<sup>3-5</sup>. In a subsequent step, Pol III binds the new  $\beta$  clamp on the RNA primer upstream and begins synthesis of the next Okazaki fragment<sup>3-5</sup>. When another Okazaki fragment is synthesized, Pol I replaces RNA primers with DNA and a ligase seals the nicks to create a continuous chain of DNA. The process repeats many times until the synthesis is completed<sup>3-5</sup>.

### **1.3 DNA DAMAGE AND THE PRIMOSOME**

Even though Pol III has a very high fidelity, the integrity of the replisome is constantly compromised due to environmental factors and cellular metabolism that induce damages in the genomic DNA and result in the formation of a stalled replication fork<sup>2-5,11-13</sup>. It has been experimentally established that the formation of the stalled



replication fork is an event, which always takes place during replication process, as the lesions on DNA, such as pyrimidine dimers, abasic sites, nicks, or chemical modifications constantly occur<sup>11-13</sup>. When the polymerase encounters DNA damage, the replisome collapses and stalled replication fork is formed<sup>5,11-17</sup>. This situation is detrimental to the cell and without efficient repair mechanism will cause mutations, chromosomal rearrangements, and often cell death<sup>5,11-17,19-21</sup>. In order to prevent the cell death, different organisms employ elaborated pathways to restart DNA replication, independent of *oriC* through the pre-primosome assembly<sup>11-17</sup>. Thus, in *Escherichia coli* cell, six different proteins, DnaB helicase, DnaC, DnaT, PriC, PriB and another helicase, PriA, are engaged in the pre-primosome assembly and function<sup>13-17</sup>. One of the current models suggests that PriA helicase specifically recognizes small ssDNA gap structures and initiates 3' → 5' DNA unwinding, thereby, sets off the assembly process of the pre-primosome<sup>13-17</sup>. Subsequently and sequentially, PriB and DnaT proteins associate with PriA - DNA complex<sup>13-18</sup>. Finally, the DnaB - DnaC complex recognizes the multi-protein scaffold and the ssDNA patch resulting from PriA helicase unwinding and the pre-primosome is formed<sup>13-17</sup>. The transient binding of the primase to the pre-primosome results in a complete primosome (Figure1.1)<sup>13-18</sup>.

#### 1.4 RATIONALE FOR THE STUDY

The physiological description of the pre-primosome and primosome formation, a great scientific achievement in its own merit, leaves as many questions as it answers. The field is left with a number of confusing and contradictory data concerning the initiation, energetics, stability, and the very composition of the pre-primosome, as well as the nature of interactions between different proteins and the DNA (Figure1.2)<sup>5,14,16,18,24-26</sup>. The role of nucleotide cofactors, which dramatically change DnaB, PriA and DnaC behavior has

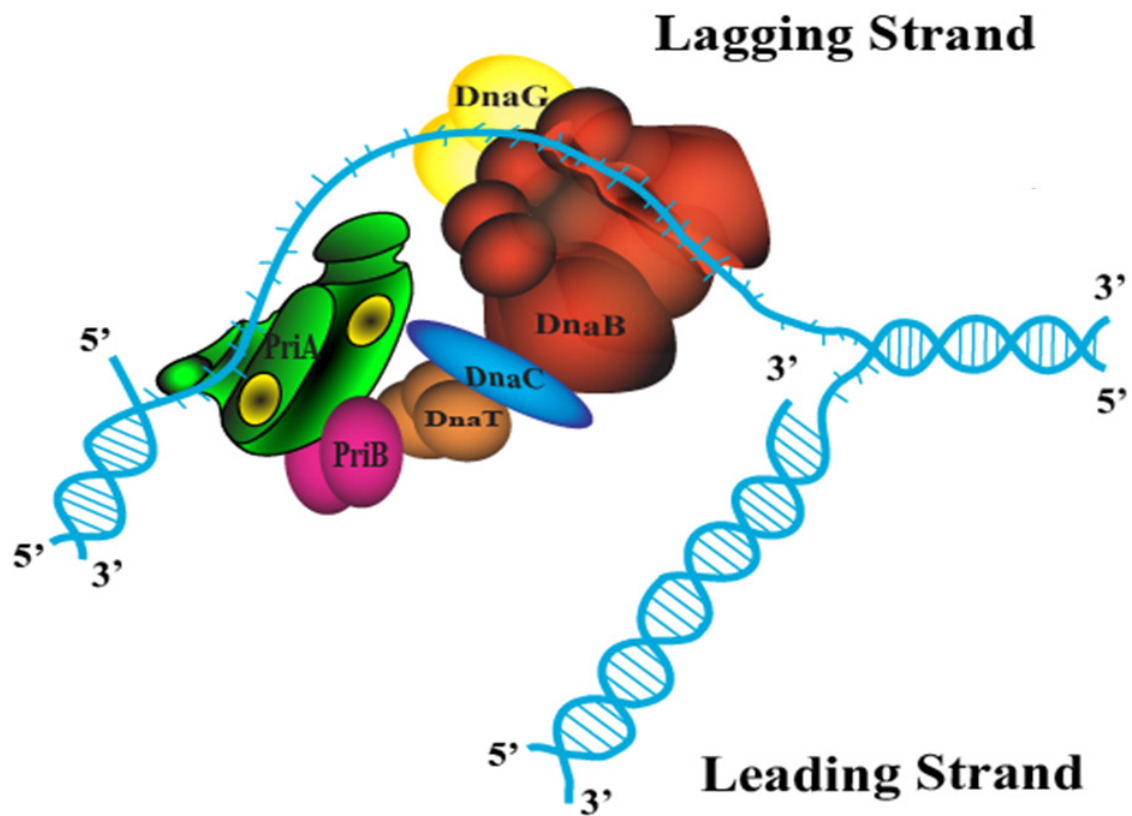


**Figure 1.1** Schematic representation of the simplest structure of the primosome formed at the ssDNA of the lagging strand. Six different *E. Coli* proteins, DnaB helicase, DnaC, DnaG primase, DnaT, PriB and another helicase, PriA, are engaged in the primosome assembly and function.

never been addressed. Direct interactions between PriA and PriB, as well as PriB and DnaT have been indicated, however, due to the semi-quantitative nature of the analyses no mechanistic conclusions could be provided<sup>14,16,18,24-26</sup>. As a consequence, the molecular mechanisms of these specific protein - protein and protein - nucleic acid interactions are largely unknown which obscures elucidation of the biological activities and the rules which govern the assembly process of the primosome, a large molecular machine involved in nucleic acid metabolism.

#### **1.4.1 Central hypothesis and specific aims.**

The research goal of this project is to obtain a physical model of the helicase-directed formation of the pre-primosome and the primosome. Our leading hypothesis is that the PriA helicase specifically recognizes different, yet specific, DNA structures, thereby initiates the assembly process. We postulate that these principal PriA – DNA states of the pre-primosome complex serve as the recognition marks for other proteins involved in the pre-primosome formation. We further postulate that the PriB protein binds to the PriA-DNA and forms a tertiary PriA-PriB-DNA. We hypothesize that interactions within the pre-primosome are controlled by the specific binding of the nucleotide cofactors to the PriA helicase, which allosterically changes the affinities of the enzymes towards DNA, as well as stoichiometries of the helicase – nucleic acid complexes. To test these hypothesis this research project has four major objectives:

**Specific Aim 1: Recognition of the Structures of the Damaged DNA Substrates by the PriA Helicase.** The studies included energetic of the recognition of the gapped ssDNA substrates (**CHAPTER 2**), dsDNA substrates (**CHAPTER 3**), and the allosteric role of ATP and ADP in the recognition process using quantitative fluorescence titration, hydrodynamics, and photo-cross-linking techniques.

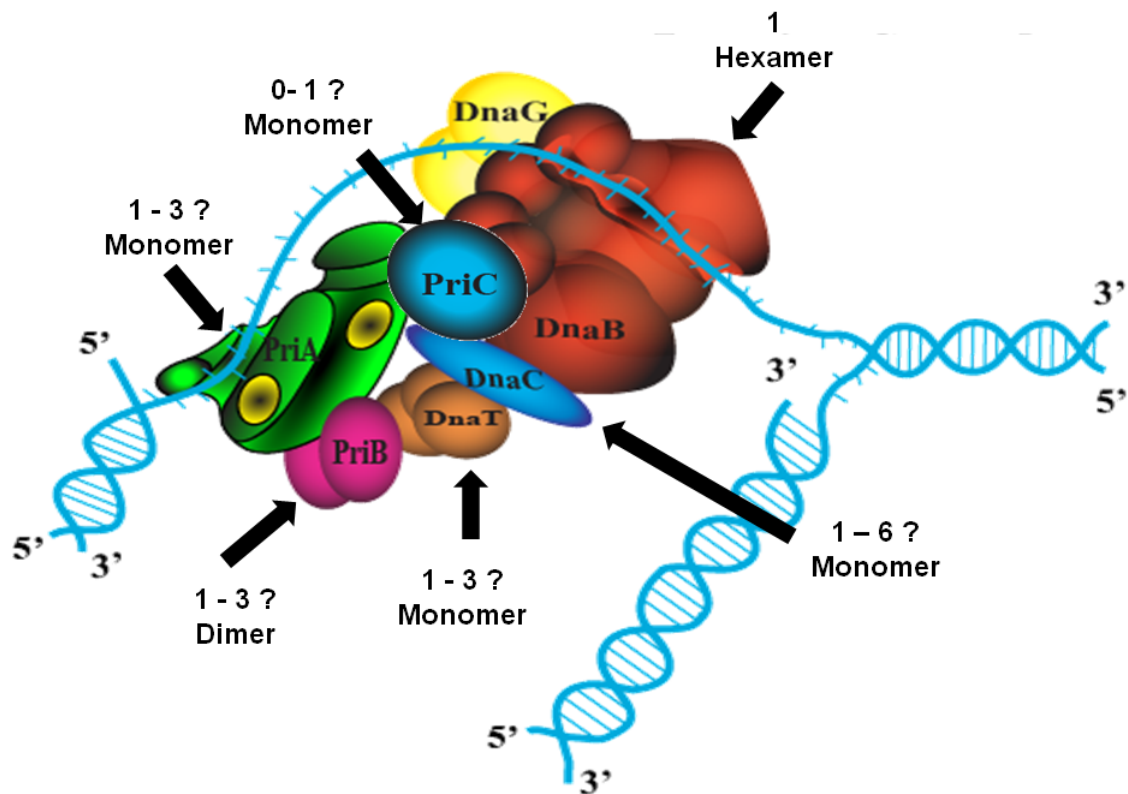


**Figure 1.2** After over two decades of research the stoichiometry of the primosome components is still predominantly unknown. Much less is known about mutual engagement between the proteins, nucleic acid and the role of the nucleotide cofactors in the assembly process.

**Specific Aim 2: The Effect of PriA's N-terminal Domain on the Recognition of the Damaged DNA Structures.** Thermodynamics of the PriA helicase N-terminal domain – ssDNA and dsDNA interactions as well as the allosteric role of ATP and ADP in the recognition process was examined through quantitative fluorescence titration techniques, hydrodynamics, and photo-cross-linking techniques (**CHAPTER 4**).

**Specific Aim 3: Interactions of PriB with the ssDNA and dsDNA.** Energetics of PriB - ssDNA and PriB - dsDNA interactions was examined using quantitative fluorescence titration, analytical ultracentrifugation, and photo-cross-linking techniques (**CHAPTER 5**).

**Specific Aim 4: Initiation of the Primosome Assembly on the Primosome Assembly Site (PAS).** Thermodynamics of the binary PriA-PriB and tertiary PriA-PriB-ssDNA, PriA-PriB-dsDNA, PriA-PriB-PAS complexes was examined. The topology and energetics of formed complexes as well as the allosteric role of ATP and ADP was determined using analytical ultracentrifugation, fluorescence titration, fluorescence resonance energy transfer (FRET), and photo-cross-linking methods (**CHAPTER 6**).

Achieving these research objectives allowed us to formulate the first ever, detailed, molecular model of the initial phase of the pre-primosome assembly, a paradigm molecular machine, directed by the PriA helicase and expose the role of the multiple protein - protein and protein - DNA interactions, as well as the allosteric role of nucleotide cofactors in the assembly process. These studies constitute a fundamental step in elucidation of the entire pre-primosome assembly process in the future.

In conclusion, we will use a comprehensive basic science approach to answer fundamental, biologically meaningful questions. In general, we will argue that in order to fully understand multi-component systems, such as the primosome, which are the building blocks of life; one has to be able to dissect, at the molecular level, multiple

substrates - enzyme interactions which govern these processes. As shown here, wide variety of comprehensive biochemical and biophysical methods provide unique tools to address these essential questions. Only when such fundamental knowledge about the system is available, meaningful and relevant translational approaches could be developed.

## CHAPTER 2

### THE *ESCHERICHIA COLI* PRIA HELICASE SPECIFICALLY RECOGNIZES GAPPED DNA SUBSTRATES<sup>27</sup>

#### 2.1 ABSTRACT

Energetics and specificity of interactions between the *E. coli* PriA helicase and the gapped DNAs have been studied using the quantitative fluorescence titration and analytical ultracentrifugation methods<sup>27</sup>. The PriA – gapped DNA complex has a surprisingly low total site-size corresponding to ~ 7 nucleotides, as compared to the site-size of ~ 20 nucleotides of the enzyme - ssDNA complex<sup>27</sup>. The dramatic difference in stoichiometries indicates that the enzyme predominantly engages the strong DNA-binding subsite in interactions with the gap and assumes a very different orientation in the gap complex, as compared to the complex with the ssDNA<sup>27</sup>. The helicase binds the ssDNA gaps with 4 - 5 nucleotides with the highest affinity, which is ~3 and ~2 orders of magnitude larger than the affinities for the ss and dsDNAs, respectively<sup>27</sup>. In the gap complex, the protein does not engage in cooperative interactions with the enzyme associated with the surrounding dsDNA<sup>27</sup>. Binding of nucleoside tri-phosphate to the strong and weak nucleotide-binding sites of the helicase eliminates the selectivity of the enzyme for the size of the gap, while saturation of both sites with ADP leads to amplified

---

<sup>27</sup>This research was originally published in Journal of Biological Chemistry. Szymanski, M. R., Jezewska, M. J. & Bujalowski, W. (2010). The Escherichia coli PriA helicase specifically recognizes gapped DNA substrates: effect of the two nucleotide-binding sites of the enzyme on the recognition process. *J Biol Chem* 285, 9683-96. © the American Society for Biochemistry and Molecular Biology.

affinity for the ssDNA gap containing 5 nucleotides and engagement of additional protein area in interactions with the nucleic acid<sup>27</sup>.

## **2.2 INTRODUCTION**

Helicases constitute one of the largest classes of enzymes, employed in most of the cellular processes. This fascinating molecular pumps catalyze vectorial unwinding of the duplex DNA to provide an active, single stranded catalytic intermediate required in replication, recombination and repair processes<sup>2,28,29</sup>. These enzymes are motor proteins that couple ATP hydrolysis to unwinding and mechanical translocation along the nucleic acid lattice but also have recently been shown to perform a wide spectrum of functions traditionally not attributed to helicases<sup>2,5,22,23,28-30</sup>. These include remodeling of DNA, RNA, and displacement of proteins and protein complexes from DNA and RNA<sup>28-30</sup>. Since helicases are present in virtually all processes of DNA and RNA metabolism it is not surprising that deficiency in their functions or deregulated expression of these proteins have been connected to various diseases including cancers, developmental defects, and neurodegenerative diseases<sup>19-21,28-31</sup>.

### **2.2.1 Replication Restart.**

The completion of replication which, in *Escherichia coli* takes about 40 min, and 6 – 8 hours in cultured human cells, has to be well coordinated with other cell cycle events and is crucial for stable maintenance of chromosomes<sup>19-21,28-32</sup>. Any malfunction in replication process can lead to a range of disorders; therefore, different organisms developed different mechanisms to restart the replication outside of the origin of replication<sup>19-21,28-32</sup>. This is especially important in bacterial cells where, because of only one origin of replication, the number of replication forks is limited to two per chromosome per generation<sup>19-21,28-33</sup>. Different types of DNA damage like UV radiation,



chemical exposure, formation of abnormal secondary structures, and depletion of nucleotide precursors are only a few common examples that can stall the progression of the replication fork<sup>19-21,28-32</sup>. It is now established that virtually all replication forks formed at *oriC* are derailed at high frequency when encounter DNA damage, collapsing before completing synthesis of the chromosome<sup>33-35</sup>. Different organisms developed different mechanisms to get rid of different damages and different types of damages encountered by the replication fork dictate which restart pathway will be used for the replication fork restoration<sup>34-36</sup>. Even in *E. coli* there are several different repair pathways including: PriA – dependent pathway, PriA – independent and suppressor pathways (Figure 2.1)<sup>32,35,37</sup>.

### **2.2.2 PriA – Dependent Pathway.**

The involvement of the PriA helicase in replication fork restart, and the significance of restart of the replication fork as a housekeeping function were exposed in large part by the phenotypes of null mutations for PriA functions<sup>32,34-36, 38,39</sup>. *priA* null mutants are viable, but grow very poorly<sup>38,39</sup>. These mutants also exhibit activated SOS response which results in filamentous morphology and rich medium sensitivity<sup>38-41</sup>. Another interesting phenotype is that *priA* null cells are highly sensitive to UV radiation and mitomycin C which block ongoing replication<sup>38,42,43</sup>. Further genetic analysis indicated that *priB* or *priC* null cells do not show any defects in growth on their own but *priB* null *priC* null double mutant is very sick<sup>43-46</sup>. In addition, *priB* null, *priC* null or *priA* null, *Rep* null double mutant is lethal<sup>43-46</sup>. These results indicated that the PriA - dependent pathway requires PriB or PriC and while PriA null mutants develop severe growth inhibitory phenotypes, it was suggested that the PriA - dependent pathway is a major replication fork restart pathway<sup>43-46</sup>.

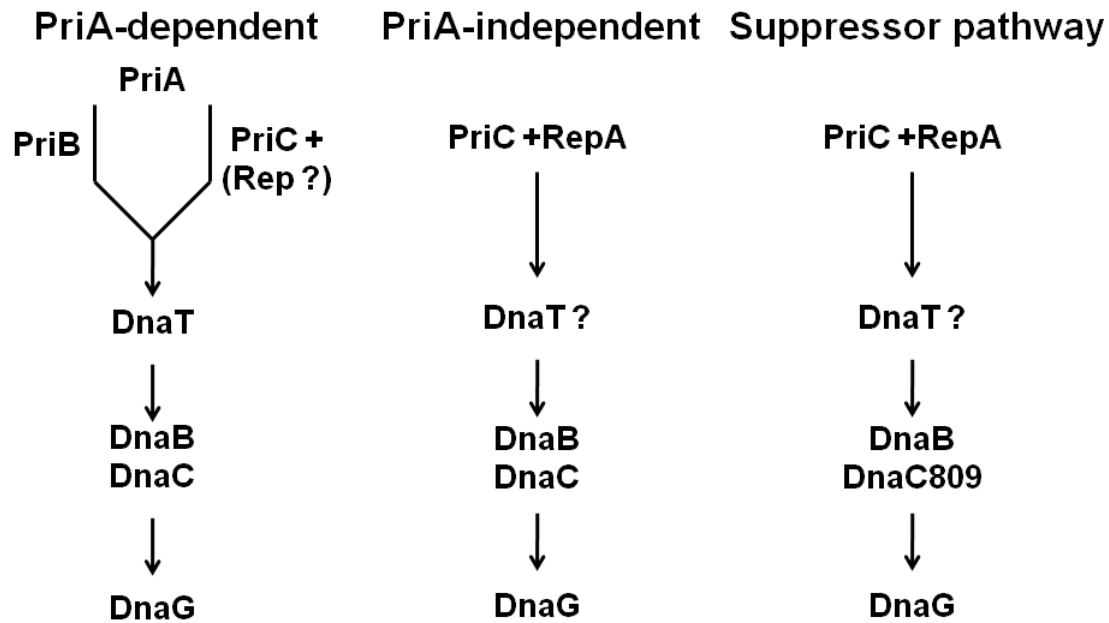


**Figure 2.1** Different organisms developed different mechanisms to remove different types of damages encountered by the replication machinery at the replication fork. In *E. coli* several different repair pathways have been proposed to be of crucial importance. These include PriA – dependent pathway, PriA – independent and suppressor pathways<sup>32,35,37</sup>.

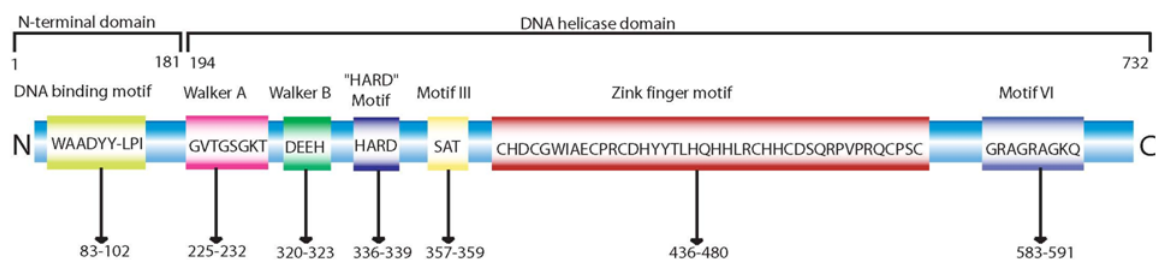


**Figure 2.2** PriA is a SF2 superfamily, DEXH-type DNA helicase. The PriA helicase possesses seven conserved motifs. Presence of these motifs classifies this enzyme as a SF2 superfamily helicase where it defines its own subgroup<sup>32,35,52</sup>.

### 2.2.3 Properties of the PriA Helicase.

The PriA helicase was originally discovered because of its requirement for the synthesis of the complementary strand of bacteriophage phiX174 single-stranded DNA *in vitro*<sup>34-36,47,48</sup>. The gene encoding PriA helicase was cloned and the open reading frame specified a protein of 732 amino acids having a calculated molecular mass of 81.7 kDa<sup>35,49,50</sup>. Ground-breaking sequence analysis by Gorbalenya and co-workers and more up to date comparative structural and functional studies showed that helicases can be classified in several superfamilies (SFs)<sup>51-53</sup>. In this capacity, PriA has the seven amino acid motifs common to most DNA helicases and falls into the SF2 superfamily, where it defines its own subgroup (Figure 2.2)<sup>32,35,52</sup>. PriA is a DEXH-type DNA helicase, exhibits DNA dependent (d)ATP hydrolysis activity, possesses large, unique, zinc-finger motif, and is highly conserved in eubacteria suggesting its important role in bacterial physiology<sup>32,54,55</sup>. Quantitative thermodynamic analyses showed that, in the complex with the ssDNA, the total DNA-binding site of the PriA helicase occludes  $20 \pm 3$  nucleotides of the nucleic acid<sup>27,56-58</sup>. Within the total DNA-binding site, the PriA helicase possesses a strong ssDNA-binding subsite, an area, which has a high ssDNA-affinity and engages in interactions with only  $\sim 5 - 8$  nucleotides of the nucleic acid<sup>27,56-58</sup>. Nevertheless, the intrinsic affinity of the enzyme for the ssDNA is predominantly generated at the strong ssDNA-binding subsite, which is located in the central part of the enzyme molecule, on a structurally separated domain<sup>27,56-58</sup>. The functional organization of the PriA helicase - ssDNA complex is schematically depicted in Figure 2.3a<sup>27,56-58,92</sup>.

Unlike most of the helicases, the PriA protein has a significant affinity for the ssDNA in the absence of the nucleotide cofactors<sup>27,56-58</sup>. It has been shown by the Bujalowski's group that PriA possesses two, strong and weak, nucleotide-binding sites,

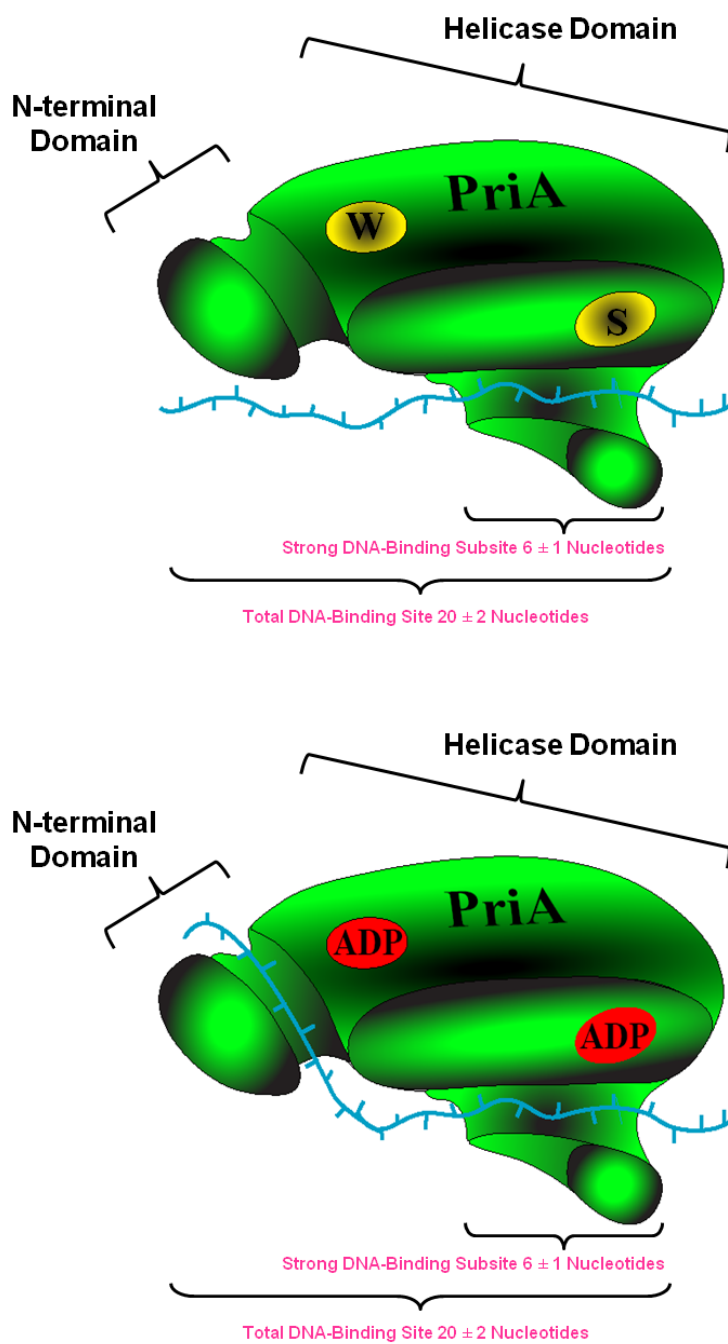


**Figure 2.3 Functional organization of the PriA helicase - ssDNA complex. a.** Total DNA-binding site of the PriA helicase is heterogeneous<sup>56</sup>. **b.** PriA possesses two strong and weak nucleotide-binding sites<sup>61</sup>. Saturation of both nucleotide-binding sites with ADP induces the conformational change and engagement of an additional area of the protein in DNA interactions<sup>27,61</sup>.

which profoundly differ in their affinities for the cofactors and their effects on the intrinsic affinity of the protein for the ssDNA (Figure 2.3a)<sup>27,59-61</sup>. Furthermore, cooperative interactions between the two nucleotide-binding sites indicate intricate communication between the sites<sup>27,59</sup>. Saturation of both nucleotide-binding sites with ADP induces the engagement of an additional area of the protein, possibly the N-terminal domain, in interactions with the ssDNA (Figure 2.3b)<sup>27,61</sup>.

#### **2.2.4 Rationale for Specific Aim 1 and Specific Gaps in Knowledge.**

Activities of the PriA helicase *in vivo* are associated with the ability of the enzyme to interact with both the ss and the dsDNA<sup>12,14,15,27</sup>. This includes the unwinding reaction of the dsDNA, fueled by the hydrolysis of nucleoside triphosphates (NTPs)<sup>14,17,27,57</sup>. During the dsDNA unwinding reaction, the PriA helicase performs a complex free energy transduction process, where the binding and/or hydrolysis of NTPs regulate the enzyme activity, including the affinity toward different conformations of the DNA<sup>14,17,27,57</sup>. Also, the PriA helicase plays a fundamental role in the initiation of recombination and repair processes in the *E. coli* cell, as a major factor that sets off the restart of the stalled replication fork at the damaged DNA sites<sup>11-13,16,27</sup>. In addition, PriA has been indicated to play a fundamental role assembly of the primosome<sup>12,14,15,17,27,34</sup>. Both of these processes, presumably, occur through the recognition of the specific DNA structures, ssDNA gap of the damaged DNA or primosome assembly site, although the nature of this recognition reactions is unknown<sup>11-13,16,27</sup>.

Interactions of the PriA helicase with the ssDNA have been intensively studied but quantitative analyses of the enzyme interactions with the gapped DNA structure has never been addressed<sup>27,56-58,61</sup>. Nothing is known about the stoichiometries, intrinsic energetics, cooperativity, and the role of the nucleotide cofactors in the process of

enzyme binding to the gapped DNA<sup>27</sup>. The role of two nucleotide-binding sites in the recognition process and the effect of structure of the phosphate group of the nucleotides on the ssDNA gap recognition had never been addressed<sup>27,59-61</sup>. In order to understand, at the molecular level, the mechanism of the stalled replication fork restart and the assembly process of the primosome, the information on how PriA interacts with gapped DNA structures is indispensable<sup>14,17,27</sup>. In addition, understanding the role of nucleotide cofactors in these recognition reactions is important for grasping the enzyme mechanisms in both replication and recombination processes<sup>11-13,27</sup>.

In this Chapter, quantitative studies of the ssDNA gap recognition by the PriA helicase and the effect of the nucleotide cofactors on the recognition reaction have been described<sup>27</sup>. The total site-size of the enzyme in the gap complex is ~ 7 nucleotides or base pairs (bps)<sup>27</sup>. This indicates that the PriA helicase, in the complex with the gap, exclusively engages the strong DNA-binding subsite and assumes a different orientation as compared to the complex with the ssDNA<sup>27</sup>. The PriA helicase binds the ssDNA gaps with 4 - 5 nucleotides with the highest affinity without engaging in cooperative interactions with the enzyme molecules associated with the surrounding dsDNA<sup>27</sup>. Binding of ADP to strong and weak nucleotide-binding sites of the enzyme profoundly affects the affinity and stoichiometry of the helicase - gapped DNA complex<sup>27</sup>.

## **2.3 MATERIALS AND METHODS**

### **2.3.1 Buffers and Chemicals**

All solutions used in experiments described in this Chapter were made with distilled and deionized > 18 M $\Omega$  (Milli-Q Plus) water. The standard buffer, C1005, consists of 10 mM sodium cacodylate adjusted to pH 7.0 with HCl at 10°C, 1 mM DTT,

100 mM NaCl, 5 mM MgCl<sub>2</sub>, and 25% glycerol w/v<sup>27</sup>. The standard temperature in all the experiments described herein was 10°C. All experiments described herein were carried out in the standard buffer C1005 unless otherwise specified in the text. All chemicals were reagent grade.

### 2.3.2 Water Activity of Buffering Solution

Water activity “error term” of the standard buffer, C1005, used in this Chapter, had been calculated according to the values in the literature<sup>132,133</sup>. Due to the presence of glycerol and salt in the buffer used here, the water activity “error term” is less than 5%, and is contained within the experimental error in all the experiments presented here<sup>27,132,133</sup>.

### 2.3.3 Nucleotides and Nucleic Acids

ATPγS and ADP were from Sigma (Saint Louis, MI). ATPγS and ADP were of high purity as judged by thin layer chromatography (TLC)<sup>27</sup>. Unmodified nucleic acid oligomers, etheno-derivatives, and fluorescein-labeled ssDNA oligomers were purchased from Midland Certified Reagents (Midland, TX)<sup>27</sup>. All nucleic acids were HPLC purified and at least > 95% pure as judged by electrophoresis on polyacrylamide gel<sup>27</sup>.

To monitor binding, gapped DNA substrates containing etheno-derivative of the adenosine oligomers were used<sup>27</sup>. The concentrations of unlabeled nucleic acids and etheno-derivative of the nucleic acids were determined spectrophotometrically using following the extinction coefficients:  $\epsilon_{257} = 3700 \text{ cm}^{-1}\text{M}^{-1}$  (nucleotide) for  $\epsilon\text{A}$ ,  $\epsilon_{260} = 10000 \text{ cm}^{-1}\text{M}^{-1}$  (nucleotide) for A,  $\epsilon_{260} = 8500 \text{ cm}^{-1}\text{M}^{-1}$  (nucleotide) for G,C and T<sup>27,62</sup>. Gapped substrates were obtained by mixing the labeled ssDNA oligomers of general primary structure, CGCACGTCAG( $\epsilon\text{A}$ )<sub>N</sub>GCAGGCTCGT, with N being a gap size (in red) ranging from 1 to 10 nucleotides, with complementary unmodified oligomers at

given concentrations (Figure 2.4)<sup>27,62</sup>. After mixing, in order to obtain the gap structure, the solution was warmed for 5 minutes at 95°C, and then slowly cooled for a period of ~ 4 - 5 hours to assure appropriate annealing of complementary strands<sup>27,62,63</sup>.

The fluorescein-modified ssDNA oligomer used for sedimentation equilibrium experiments were, 5'-Fl-CGCACGTCAGAAAAAAAAAGCAGGCTCGT, 5'-Fl-CGCACGTCAGAAAAAGCAGGCTCGT, containing fluorescein (Fl) moiety attached to the 5' through phosphoramidate chemistry<sup>27</sup>. The concentrations of the nucleic acids were determined spectrophotometrically using the extinction coefficients:  $\epsilon_{494} = 76000 \text{ cm}^{-1}\text{M}^{-1}$  for fluorescein<sup>27,62,63</sup>. 5'-Fl-labeled gapped substrates were obtained by mixing labeled ssDNA oligomers with complementary unmodified oligomers at appropriate concentration. The mixture was then warmed for 5 minutes at 95°C, and slowly cooled for a period of ~ 4 - 5 hours<sup>27,62,63</sup>.

The integrities of the gapped DNA substrates have been checked by UV melting and analytical ultracentrifugation techniques<sup>27,62,63</sup>. The melting temperature of the examined gapped DNA substrates was ~ 50°C or higher in all studied solution conditions<sup>27,62,63</sup>.

### **2.3.4 The PriA Protein Purification.**

The *E. coli priA* gene was placed in pET30a plasmid (Novagen)<sup>27,56-61,92,99</sup>. The PriA helicase was purified using the protocol previously described by Jezewska *et al.* (Figure 2.5)<sup>56</sup>.

### **2.3.5 Determination of Extinction Coefficient of PriA.**

The concentration of the protein was spectrophotometrically determined, with an extinction coefficient  $\epsilon_{280} = 1.06 \times 10^5 \text{ cm}^{-1}\text{M}^{-1}$  obtained using an approach based on the Edelhoch's method<sup>27,56-61,64,65</sup>.



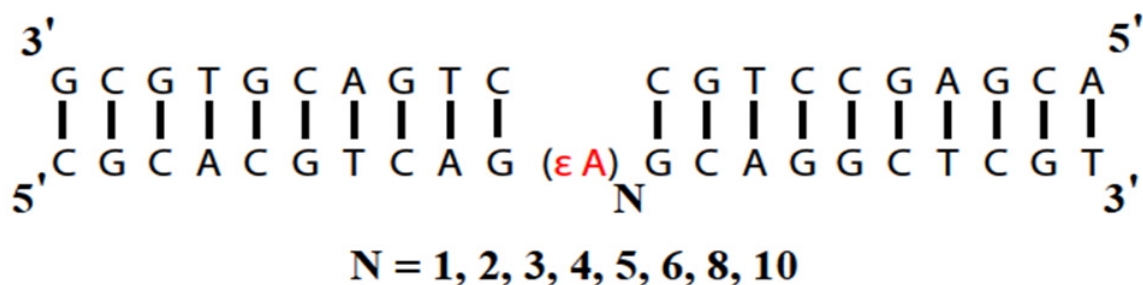


**Figure 2.4 Gapped DNA substrates used to examine interactions of the PriA helicase with gapped DNAs.** The DNA substrates have two dsDNA parts, which are identical in all substrates<sup>27</sup>. The dsDNA parts are separated by the ssDNA of the gap containing 1–10 nucleotides, which are fluorescent, ethenoadenosine residues<sup>27</sup>.

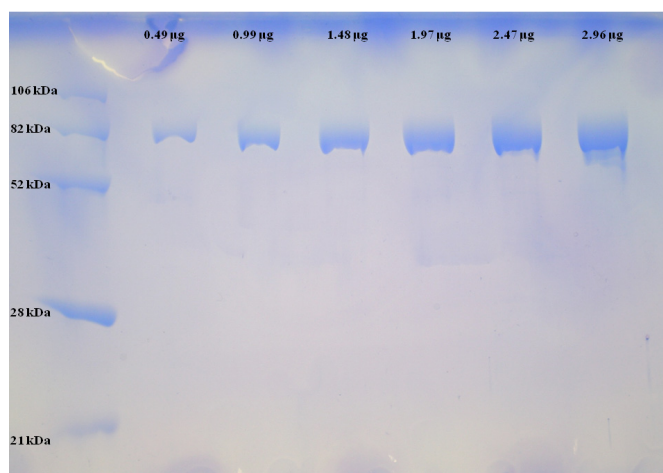


**Figure 2.5 10% SDS polyacrylamide gel of the final step of PriA helicase purification.** Serial dilution clearly shows that employed purification protocol yields ~ 82 kDa PriA protein of high purity<sup>27</sup>.

### 2.3.6 Fluorescence Measurements.

All steady-state fluorescence titrations, described in this Chapter, were performed using the Fluorolog F-11 spectrofluorometer (Jobin Yvon) as previously described<sup>27,56-63</sup>. The temperature of the cuvette holder was regulated by circulating water at  $10.0 \pm 0.1$  °C. The PriA protein binding to the gapped DNA substrates was followed by monitoring the etheno-derivative fluorescence of the nucleic acids ( $\lambda_{\text{ex}} = 325$  nm,  $\lambda_{\text{em}} = 410$  nm)<sup>27</sup>. The relative fluorescence increase,  $\Delta F_{\text{obs}}$ , of the DNA emission upon protein binding is defined as,  $\Delta F_{\text{obs}} = (F_i - F_o)/F_o$ , where  $F_i$  is the fluorescence of the sample at a given titration point “i” and  $F_o$  is the initial fluorescence of the same solution<sup>27,56-63</sup>.

### 2.3.7 General Approach to Quantitative Analysis of the Fluorescence Titration Curves of the PriA – Gapped DNA Interactions.

Binding of the PriA helicase to the gapped DNAs, has been monitored by the fluorescence increase,  $\Delta F_{\text{obs}}$ , of the etheno-derivatives of the nucleic acid<sup>27,56-63</sup>. Quantitative estimates of the total average degree of binding,  $\Sigma\Theta_i$  (average number of bound PriA molecules per gapped DNA) and the free protein concentration,  $P_F$ , independent of any assumption about the relationship between the observed spectroscopic signal,  $\Delta F_{\text{obs}}$ , and  $\Sigma\Theta_i$  was accomplished using an approach previously described<sup>1,7-9,27,56-63</sup>. Briefly, each different possible “i” complex of the PriA protein with the gapped DNA contributes to the experimentally observed relative fluorescence increase,  $\Delta F_{\text{obs}}$ . Thus,  $\Delta F_{\text{obs}}$  is functionally related to  $\Sigma\Theta_i$  by<sup>1,7-9,27,56-63</sup>

$$\Delta F_{\text{obs}} = \Sigma\Theta_i \Delta F_i \quad (2.1)$$

where  $\Delta F_i$  is the maximum relative fluorescence increase of the gapped DNA with the PriA bound in complex "i"<sup>1,7-9,27,56-63</sup>. The same value of  $\Delta F_{obs}$ , obtained at two different total DNA substrate concentrations,  $M_{T1}$  and  $M_{T2}$ , indicates the same physical state of the nucleic acid, *i.e.*, the total average degree of binding,  $\Sigma\Theta_i$ , and the free helicase concentration,  $P_F$ , must be the same<sup>1,7-9,27,56-63</sup>. The values of  $\Sigma\Theta_i$  and  $P_F$  are then related to the known total protein concentrations,  $P_{T1}$  and  $P_{T2}$ , and the known, corresponding total nucleic acid concentrations,  $M_{T1}$  and  $M_{T2}$ , at the same value of  $\Delta F_{obs}$ , by<sup>1,7-9,27,56-63</sup>

$$\Sigma\Theta_i = \frac{(P_{T2} - P_{T1})}{(M_{T2} - M_{T1})} \quad (2.2)$$

and

$$P_F = P_{Tx} - (\Sigma\Theta_i)M_{Tx} \quad (2.3)$$

where  $x = 1$  or  $2$ <sup>1,7-9,27,56-63</sup>. The strategy described above is used in all fluorescence titration experiments described here.

Computer fits were performed using Mathematica (Wolfram, IL) and KaleidaGraph (Synergy Software, PA).

### 2.3.8 Analytical Ultracentrifugation.

Analytical ultracentrifugation experiments were performed with an Optima XL-A analytical ultracentrifuge (Beckman Inc., Palo Alto, CA), equipped with absorbance optics and An60Ti rotor<sup>27</sup>. All experiments described here are at 10°C in the standard buffer C unless otherwise specified in the text (section 2.3.1)<sup>27</sup>.

### a) Sedimentation equilibrium

Sedimentation equilibrium scans were collected using double-sector charcoal-filled 12-mm centerpieces at the absorption band of the PriA protein (280 nm) or fluorescein of the labeled gapped DNA substrate (495 nm)<sup>27</sup>. The sedimentation was considered to be at equilibrium when consecutive scans, separated by time intervals of 8 hrs, were identical<sup>27</sup>. For the n-component system, the total concentration at radial position  $r$ ,  $c_r$ , is defined by<sup>27,66</sup>.

$$c_r = \sum_{i=1}^n c_{bi} \exp \left[ \frac{(1 - \bar{v}_i \rho) \omega^2 M_i (r^2 - r_b^2)}{2RT} \right] + b \quad (2.4)$$

where  $c_{bi}$ ,  $\bar{v}_i$ , and  $M_i$  are the concentration at the bottom of the cell, partial specific volume and molecular weight of "i" component, respectively,  $\rho$  is the density of the solution,  $\omega$  is the angular velocity, and  $b$  is the base-line error term<sup>27,66</sup>. Equilibrium sedimentation profiles were fitted to equation 2.4 with  $M_i$  and  $b$  as fitting parameters<sup>27,66,67</sup>. The speeds of the rotor are indicated in the text<sup>27</sup>.

### b) Sedimentation Velocity

Sedimentation velocity experiments were performed using double-sector charcoal-filled 12-mm centerpieces<sup>66-69,72</sup>. For the PriA protein alone, sedimentation velocity scans were collected at the absorption band of the protein (280 nm)<sup>66-69,72</sup>. The PriA-nucleotide complexes were scanned at 290 nm, where the cofactor absorbance is minimal and the absorbance of the sample is dominated by the signal from the PriA protein<sup>66-69,72</sup>. In addition, in this case the reference cell contains the same concentration of the nucleotide cofactor, allowing to exclusively monitor the absorbance of the protein<sup>72,76</sup>. Time derivative analyses of sedimentation scans were performed with the

software supplied by the manufacturer using averages of 10 - 15 scans for each concentration<sup>66-69,72,76</sup>. In addition, the  $c(s)$  distribution as a function of  $s_{20,w}$  was calculated from the analysis of the velocity profiles using SedFit program<sup>27,68</sup>. The values of the apparent average sedimentation coefficients were corrected to  $s_{20,w}$  for solvent viscosity and temperature to standard conditions<sup>27,66,67,69</sup>. The speeds of the rotor are indicated in the text<sup>27</sup>.

### **2.3.9 Determination of PriA Partial Specific Volume.**

Partial specific volume of the PriA protein ( $v$ ) was calculated from the amino acid composition of the protein according to Lee and Timasheff and was 0.741 mL/g<sup>27,70</sup>.

## **2.4 RESULTS**

### **2.4.1. The PriA Helicase.**

The enzyme was > 99% pure as judged by polyacrylamide electrophoresis with Coomassie Brilliant Blue staining. (Figure 2.5)

### **2.4.2. The Hydrodynamic Properties of PriA.**

The results of thermodynamics and kinetics of PriA – ssDNA and PriA – nucleotide cofactors interactions indicate that the PriA helicase exists in solution as a stable monomer and binds ssDNA and nucleotide cofactors as a monomer<sup>1,27,56-61</sup>. In order to be able to study interactions of PriA helicase with intricate gapped DNA structures, containing both ss and ds DNA parts, oligomeric states and global conformational states of PriA, in different solution conditions, were examined using independent hydrodynamic techniques<sup>27</sup>. The size and the shape of the macromolecule affect its ability to move in the fluid solution and hydrodynamic techniques<sup>66,69,74,75</sup>.

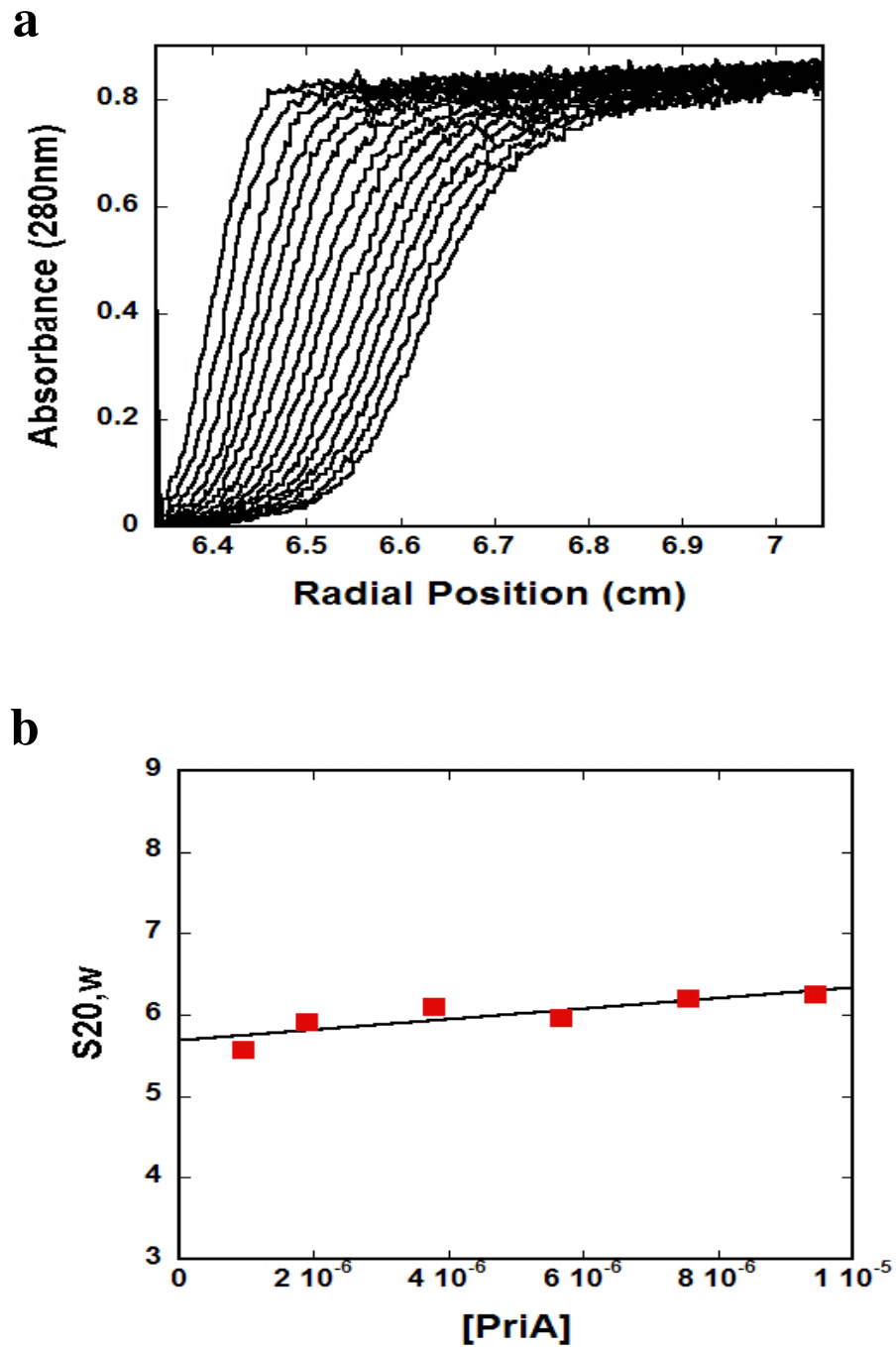


**Figure 2.6** PriA in solution sediments as a single homogenous species. **a.** Typical analytical sedimentation velocity profiles recorded at 280 nm and 60000 rpm for  $[7.55 \times 10^{-5} \text{M}]$  of PriA. **b.** The dependence of the sedimentation coefficient ( $s_{20,w}$ ) upon the PriA concentration.

Sedimentation equilibrium and sedimentation velocity, take advantage of this fact and yield useful information about the molecular weights and shapes of the macromolecule<sup>66,69,72,74,75</sup>.

An example of sedimentation velocity profiles performed at 60000 rpm, monitored at 280 nm, of the PriA protein in the standard buffer C1005 (section 2.3.1) are shown in Figure 2.6a<sup>72</sup>. The concentration of the PriA protein is  $7.55 \times 10^{-5}$  M. Inspection of the profiles clearly shows that there is a single moving boundary<sup>72</sup>. Similar experiments have been performed in the presence of ADP and ATP (data not shown)<sup>72</sup>. The sedimentation coefficient of the PriA protein has been obtained using the time-derivative approach and corrected for solvent viscosity and temperature to standard conditions<sup>27,66,67,69</sup>. The dependence of the sedimentation coefficient ( $s_{20,w}$ ) upon the protein concentration is shown in Figure 2.6b. Within experimental accuracy values of  $s_{20,w}$  are similar and show a little dependence upon in the examined protein concentration range<sup>27,72,76</sup>. The extrapolation of the plots to  $[\text{PriA}] = 0$  provides  $s^{\circ}_{20,w} = 5.58 \pm 0.19$  S in all examined solution conditions (Figure 2.6b)<sup>27,72,76</sup>.

The results of PriA equilibrium analytical ultracentrifugation experiments in the standard buffer C1005 performed at 14000 rpm, monitored at 280 nm (section 2.3.1) are shown in Figure 2.7. The continuous red line is the nonlinear least-squares fit, using the single exponential function defined by equation 2.4 (section 2.3.8). Adding extra exponents does not improve the statistics of the fits (data not shown)<sup>66,67,69</sup>. Similar experiments were performed at different PriA concentrations and different rotor speeds and the results obtained are, within experimental error, identical (data not shown). The fit, in Figure 2.7, provides an excellent description of the experimental curve, indicating the presence of a single species with a molecular mass of  $82000 \pm 8000$  Da. Therefore, the data show that PriA is a monomer in examined solution conditions<sup>27,56</sup>.

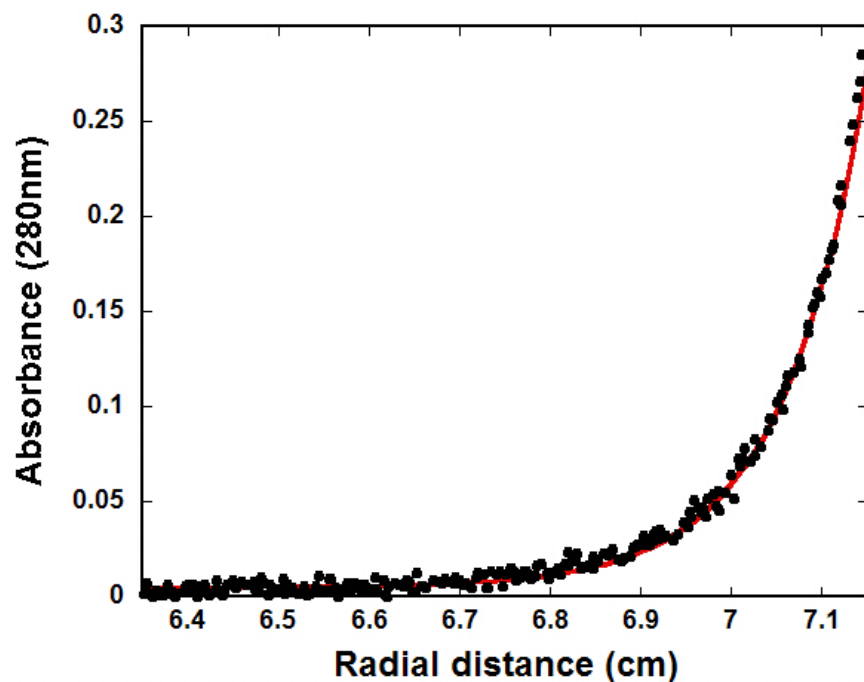


**Figure 2.7 The PriA helicase is a monomer in solution.** Example of sedimentation equilibrium profile recorded at 14000 rpm and monitored at 280 nm. The concentration of PriA was  $9.43 \times 10^{-7}$  M. The solid red line is the nonlinear least-squares fit, using the single exponential function, defined by equation 2.4, with the molecular mass of 80193 Da.



### 2.4.3. Binding of the PriA Helicase to the Gapped DNA Substrates.

The effect of the structure of the DNA substrate on the energetics of the ssDNA gap recognition by the PriA helicase was revealed by examining the interactions of the enzyme with the DNA substrates containing the ssDNA gap substrates depicted in Figure 2.4<sup>27</sup>. All DNA substrates contain two dsDNA parts, each having 10 bps and the primary structure of the dsDNA parts is identical in all gapped DNAs<sup>27</sup>. The dsDNA parts are separated by the ssDNA gap having 1, 2, 3, 4, 5, 6, 8, and 10 nucleotides (Figure 2.4)<sup>27</sup>. Binding of the PriA protein to the fluorescent etheno-derivative of homo-adenosine oligomers is accompanied by the very strong increase of the nucleic acid fluorescence, therefore, the bases in the ssDNA gap are all etheno-adenines ( $\epsilon$ A), which provide the fluorescence signal to monitor the binding process<sup>27,56-61</sup>.

Fluorescence titrations of the gapped DNA substrate, having the ssDNA gap of 4 nucleotides with the PriA helicase at three different nucleic acid concentrations, in the standard buffer C1005 are shown in Figure 2.8a<sup>27</sup>. The shift of the titration curve at higher nucleic acid concentrations results from the fact, that more protein is required to induce the same fluorescence change of the DNA<sup>1,7-9,27,56-63</sup>. To quantitatively obtain the total average degree of binding,  $\Sigma\Theta_i$ , independent of any assumption about the relationship between the observed signal and the degree of binding, the titration curves in Figure 2.8a have been analyzed, using the approach described in section 2.3.6 and 2.3.7 in this Chapter<sup>1,7-9,27,56-63</sup>. Figure 2.8b shows the dependence of the observed relative fluorescence increase as a function of  $\Sigma\Theta_i$ <sup>27</sup>. The plot is nonlinear indicating the presence of at least two binding phases<sup>1,7-9,27,56-63</sup>. Separation of the titration curves allowed determining  $\Sigma\Theta_i$  up to  $\sim 2.6$ . In the high affinity phase, the total average degree of binding reaches the value of  $1 \pm 0.2$  corresponding to binding of a single molecule of the PriA

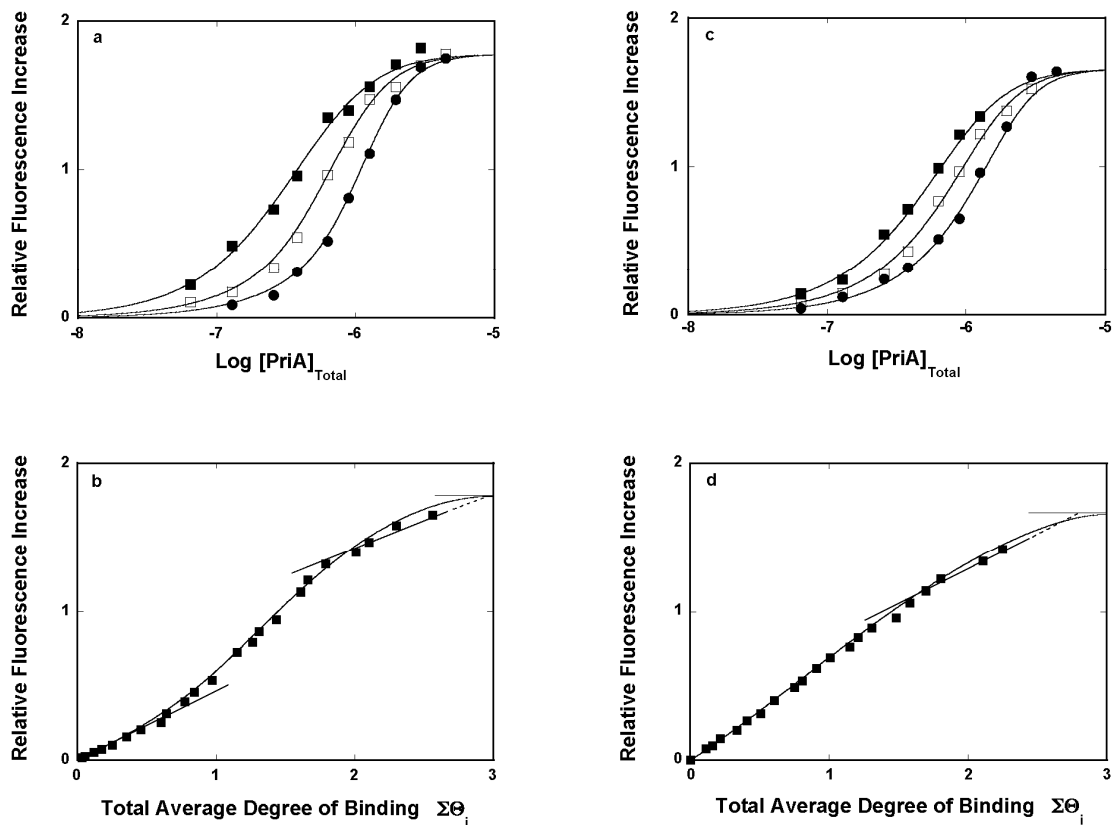


**Figure 2.8** At saturation, three PriA molecules bind to the examined gapped DNA substrates. **a.** Fluorescence titrations of the gapped DNA substrate with the ssDNA gap having 4 nucleotides at three different concentrations of the nucleic acid:  $1 \times 10^{-7}$  M (■),  $3 \times 10^{-7}$  M (□), and  $6 \times 10^{-7}$  M (●)<sup>27</sup>. **b.** The dependence of the relative fluorescence increase,  $\Delta F$ , upon the degree of binding,  $\Sigma\Theta_i$ , of the PriA DNA complex<sup>27</sup>. **c.** Fluorescence titrations of the gapped DNA substrate with 10 nucleotides in the ssDNA gap with the PriA helicase at three different concentrations of the nucleic acid:  $1 \times 10^{-7}$  M (■),  $3 \times 10^{-7}$  M (□), and  $6 \times 10^{-7}$  M (●)<sup>27</sup>. **d.** The dependence of the relative fluorescence increase,  $\Delta F$ , upon the degree of binding,  $\Sigma\Theta_i$ , of the PriA DNA complex<sup>27</sup>. The solid straight line is the limiting slope of the low affinity binding phase. The dashed line is an extrapolation of the total average degree of binding to the maximum value of the observed fluorescence increase<sup>27</sup>.

helicase<sup>27</sup>. Extrapolation of the low affinity phase to the maximum fluorescence increase,  $\Delta F_{\max} = 1.8 \pm 0.1$ , provides  $\Sigma\Theta_i = 3.0 \pm 0.2$ , therefore, at saturation, three PriA molecules bind to the examined gapped DNA substrate<sup>27</sup>.

No change in the maximum stoichiometry of the PriA - gapped DNA substrate was observed for the nucleic acid containing ssDNA gap with 10 nucleotides<sup>27</sup>. Fluorescence titrations of the gapped DNA with the ssDNA of 10 nucleotides with the PriA protein at three different nucleic acid concentrations are shown in Figure 2.8c<sup>27</sup>. Separation of the titration curves allows determining the total average degree of binding,  $\Sigma\Theta_i$ , up to  $\sim 2.3$ <sup>27</sup>. The plot of the dependence of the relative fluorescence increase of the nucleic acid as a function of  $\Sigma\Theta_i$  is also nonlinear indicating the presence of at least two binding phases (Figure 2.8d)<sup>27</sup>. Extrapolation of the weak affinity phase to the maximum fluorescence increase  $\Delta F_{\max} = 1.7 \pm 0.1$  provides  $\Sigma\Theta_i = 2.8 \pm 0.2$  and, surprisingly, the gapped DNA substrate with the ssDNA gap of 10 nucleotides can also accommodate three PriA molecules<sup>27</sup>.

#### **2.4.4 Maximum Stoichiometry of the PriA Helicase - Gapped DNA Complex.**

##### **Analytical Sedimentation Equilibrium Studies.**

Unexpectedly large number of the PriA molecules binding to the gapped DNA substrates has been further addressed using the independent sedimentation equilibrium technique<sup>27,67,76-80</sup>. In these studies we utilize the gapped DNA substrate, which contains fluorescein at its 5' end<sup>27</sup>. The structure of the substrate is analogous to the DNA substrate used in the binding experiments (section 2.2.3)<sup>27</sup>. In this approach, the sedimentation equilibrium profile of the nucleic acid can be exclusively monitored at the fluorescein absorption band, without any interference of the protein absorbance<sup>27,76-81</sup>.

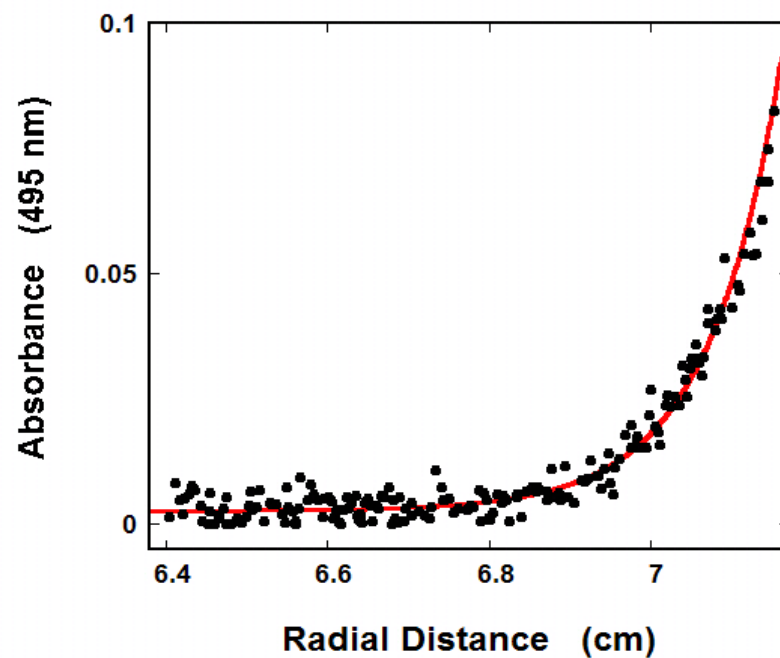


**Figure 2.9 Sedimentation equilibrium concentration profile of gapped DNA substrate – PriA Helicase complex.** 5'-Fl-Gapped DNA substrate containing 5 nucleotides in the ssDNA gap, in the presence of the PriA helicase recorded at 495 nm and at 8000 rpm<sup>27</sup>. Concentrations of the nucleic acid and the protein are  $1 \times 10^{-6}$  M and  $2 \times 10^{-5}$  M, respectively<sup>27</sup>. The *red line* is the nonlinear least squares fit to single exponential function, with a single species having a molecular mass of  $242 \pm 15$  kDa<sup>27</sup>.

In addition, the experiments have been performed at the large excess of the PriA protein to assure complete saturation of the nucleic acid over the entire equilibrium profile<sup>27,76-81</sup>. Because the molecular weight of the gapped DNA substrate with 5 nucleotides and 10 nucleotides in the ssDNA gap is  $\sim 15$  kDa, the formation of the complex between the gapped DNA substrate and the PriA protein ( $\sim 82$  kDa) will result in a large increase of the apparent molecular weight of the nucleic acid<sup>27,76-81</sup>.

Sedimentation equilibrium profiles of the gapped DNA substrates in the presence of the PriA protein and recorded at the fluorescein absorption band (495 nm) in the standard buffer C1005 are shown in Figure 2.9<sup>27</sup>. The concentrations of the protein and nucleic acid are  $2.0 \times 10^{-5}$  M and  $1.0 \times 10^{-6}$  M, respectively<sup>27</sup>. The solid line is the nonlinear least squares fits, using the single exponential function defined eq. 2.4 (section 2.3.8)<sup>27</sup>. Adding additional exponents does not improve the statistics of the fits (data not shown) which provide excellent description of the experimental curves indicating the presence of a single species with the molecular weight of  $242 \pm 15$  kDa, for the gapped DNA substrates with 5 nucleotides. In case of the gapped substrate with 10 nucleotides in the ssDNA gap, the molecular weight of the complex was determined to be  $255 \pm 15$  kDa (data not shown)<sup>27</sup>. As a result, the equilibrium sedimentation data confirm that three PriA molecules associate with selected gapped DNA substrate, which is in excellent agreement with the fluorescence titration results (section 2.4.3)<sup>27</sup>.

#### **2.4.5 Statistical Thermodynamic Model of the PriA Helicase Binding to the Gapped DNA Substrates.**

Selected gapped DNA substrates comprise of three structural regions, which may serve as specific binding sites, the ssDNA gap with the ssDNA/dsDNA junctions, and two dsDNA parts on both sides of the gap Figure 2.4<sup>27</sup>. Since a single PriA molecule

binds to the gapped structure in high-affinity phase, it must correspond to the formation of a complex with the ssDNA gap<sup>1,27,67,82</sup>. The low affinity phase must then correspond to the association of the remaining two PriA molecules with two dsDNA parts of the substrate<sup>1,27,67,82</sup>. The simplest model of the association of the PriA helicase with the gapped DNA can be described as ligand binding to two different classes of binding sites<sup>27</sup>. One class containing a single binding site and the other one containing two equivalent binding sites including potential cooperative interactions between the protein associated with the ssDNA gap and the enzyme molecules bound to the dsDNA parts<sup>1,27,67,82</sup>. The partition function,  $Z_G$ , of the system is then defined as,

$$Z_G = 1 + (K_G + 2K_{DS})P_F + (2\sigma K_G K_{DS})P_F^2 + K_G K_{DS} \sigma P_F^3 \quad (2.5)$$

where  $K_G$  and  $K_{DS}$  are the equilibrium binding constants describing the association with the ssDNA gap and the dsDNA parts of the DNA substrate, respectively, and  $\sigma$  is the cooperativity parameter<sup>1,27,67,82</sup>. The total average degree of binding,  $\Sigma\Theta_i$ , is then

$$\Sigma\Theta_i = \frac{(K_G + 2K_{DS})P_F + 2(2\sigma K_G K_{DS})P_F^2 + 3K_G K_{DS} \sigma P_F^3}{Z_G} \quad (2.6)$$

The observed relative fluorescence increase,  $\Delta F_{obs}$ , is described by

$$\Delta F_{obs} = \frac{\Delta F_1 (K_G + 2K_{DS})P_F + \Delta F_2 (2\sigma K_G K_{DS})P_F^2 + \Delta F_3 K_G K_{DS} \sigma P_F^3}{Z_G} \quad (2.7)$$

A formidable number of independent parameters, in equations 2.5 – 2.7, namely,  $K_G$ ,  $K_{DS}$ ,  $\sigma$ ,  $\Delta F_1$ ,  $\Delta F_2$ , and  $\Delta F_3$ , in equations 2.5 – 2.7; precludes their accurate determination

in a single, fitting procedure<sup>1,27,67,82</sup>. In order to extract the information on some of those parameters the following strategy was applied<sup>1,27,67,82</sup>. The value of  $\Delta F_G$  is the slope,  $\Delta F_G = \partial \Delta F / \partial (\Sigma \Theta_i)$ , of the initial part of the plots in Figures 2.8b and 2.8d which provide  $\Delta F_G = 0.46 \pm 0.05$  and  $\Delta F_G = 0.62 \pm 0.05$ , for the gapped DNA substrate with 4 and 10 nucleotides in the gap, respectively<sup>1,27,67,82</sup>. The value of  $\Delta F_3$  is known from the titration curves, (Figure 2.8a and Figure 2.8c), which provide  $\Delta F_3 = 1.8 \pm 0.1$  and  $\Delta F_3 = 1.7 \pm 0.1$  for the corresponding gapped DNA substrates<sup>1,27,67,82</sup>. Knowing  $\Delta F_1$ , the value of  $K_G$  can be estimated from the analysis of the dependence of  $\Sigma \Theta_i$ , as a function of the protein concentration which provides  $K_G = (4 \pm 1) \times 10^7 \text{ M}^{-1}$  and  $K_G = (2.5 \pm 0.6) \times 10^6 \text{ M}^{-1}$  for the considered gapped DNA substrates<sup>1,27,67,82</sup>. As a result, there are three outstanding parameters that have to be determined,  $K_{DS}$ ,  $\sigma$ , and  $\Delta F_2$ <sup>1,27,67,82</sup>. The solid lines in Figure 2.8a and Figure 2.8c are nonlinear least squares fits of the experimental titration curves using equations 2.5 – 2.7, and provide an excellent description of the experimental titration curves with  $K_{DS} = (1.6 \pm 0.4) \times 10^6 \text{ M}^{-1}$ ,  $\sigma = 1 \pm 0.3$ ,  $\Delta F_2 = 1.8 \pm 0.1$ , and  $K_{DS} = (1.7 \pm 0.4) \times 10^6 \text{ M}^{-1}$ ,  $\sigma = 1 \pm 0.3$ , and  $\Delta F_2 = 1.7 \pm 0.1$ , for the gapped substrates with 4 and 10 nucleotides in the gap, respectively<sup>1,27,67,82</sup>.

#### **2.4.6 Intrinsic Affinity of the PriA Helicase For the ssDNA Gap as a Function of the Gap Size.**

Analogous thermodynamic analyses have been performed for the entire series of the gapped DNA substrates differing in the size of the ssDNA gap respectively<sup>1,27,67,82</sup>. The obtained binding and spectroscopic parameters are included in Table 2.1<sup>27</sup>. All examined gapped DNA substrates bind three PriA molecules, including the DNA substrate with a single nucleotide in the gap<sup>27</sup>. Formation of the gap complex induces only a moderate change of the etheno-adenosines in the gap but binding of the next

enzyme molecule to the dsDNA part of the substrates induces the major fluorescence increase of the nucleic acids, indicating significant rearrangement of the structure of the complex affecting the ssDNA gap<sup>27</sup>. Nonetheless, the values of  $\sigma \approx 1$ , is independent of the size of the ssDNA gap, indicating the absence of cooperative interactions between the PriA molecule bound in the gap complex and the enzyme molecules associated with the dsDNA part of the gapped DNA substrates<sup>27</sup>. Association of the third PriA molecule does not cause any change of the nucleic acid fluorescence resulting in  $\Delta F_2 = \Delta F_3$  and indicates that the structure of the substrate is unaffected, as compared to the complex with the two PriA molecules bound (Table 2.1)<sup>27</sup>.

The dependence of the logarithm of the binding constant,  $K_G$ , describing the formation of the gap complex as well as the binding constant,  $K_{DS}$ , characterizing the association of the enzyme to the dsDNA parts of the gapped DNA substrates, upon the length of the ssDNA gap is shown in Figure 2.10<sup>27</sup>. For the gapped DNA substrate with 1 nucleotide in the ssDNA gap, the value of  $K_G$  is practically the same as the value of  $K_{DS}$ , which characterizes the binding of the enzyme to the dsDNA of the gapped DNA substrates<sup>27</sup>. The value of  $K_G$  steadily and strongly increases with the size of the gap up to 5 nucleotides, where it is  $\sim 2$  orders of magnitude higher than  $K_{DS}$ <sup>27</sup>. Thus, in the absence of the nucleotide cofactors the PriA helicase specifically recognizes the ssDNA gaps of 4 - 5 nucleotides<sup>27</sup>. With the size of the gap 6 nucleotides,  $K_G$  sharply decreases and for the gap with 10 nucleotides reaches the value similar to the value of the  $K_{DS}$  (Figure 2.10)<sup>27</sup>. Surprisingly, the values of  $K_{DS}$  are not affected by the size of the ssDNA gap and are, within the experimental accuracy, the same for all examined gapped DNA substrates<sup>27</sup>.



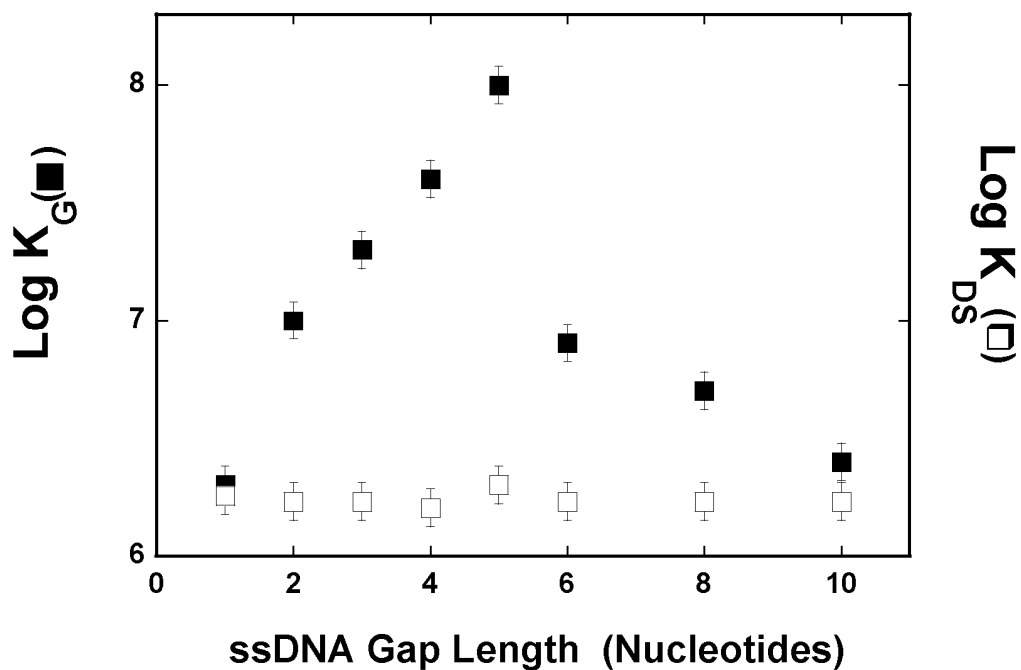


**Figure 2.10** The dependence of the logarithm of the binding constant  $K_G$  (■) and the logarithm of the binding constant  $K_{DS}$  (□), characterizing the PriA-gapped DNA complex and the association of the PriA helicase with the dsDNA of the gapped DNA substrates, respectively, upon the length of the ssDNA gap<sup>27</sup>.

#### **2.4.7 Interactions of the PriA Helicase With the Gapped DNA Substrates In the Presence of Nucleotide Cofactors.**

The PriA helicase possesses two, strong and weak nucleotide-binding sites, which dramatically affect the enzyme interactions with the ssDNA (Figure 2.3, section 2.2.3)<sup>27,59-61</sup>. In the next set of experiments, we address the effect of ADP and ATP nonhydrolyzable analog, ATP $\gamma$ S, on the recognition of the ssDNA gap substrates by the PriA helicase<sup>27</sup>. Fluorescence titrations of the gapped DNA substrate with the ssDNA gap of 5 nucleotides, with the PriA helicase at two different nucleic acid concentrations, in the standard buffer C1005, containing  $1 \times 10^{-5}$  M ADP, are shown in Figure 2.11a<sup>27</sup>. At this concentration of ADP, only the strong nucleotide-binding site of the enzyme saturated with the cofactor<sup>27,59-61</sup>. The quantitative analysis of the titration curves has been performed as described above, in the section 2.4.5, for the studies in the absence of the cofactors and show that, again, even in the presence of ADP, three PriA molecules associate with the gapped DNA<sup>27</sup>. The solid lines in Figures 2.11a are nonlinear least squares fits of the experimental titration curves using equations 2.5 – 2.7. It is evident that the presence ADP in the strong nucleotide-binding site does not affect the maximum stoichiometry of the complex and has little effect on the relative fluorescence increases with  $\Delta F_1 \approx 0.33$  and  $\Delta F_2 = \Delta F_3 \approx 1.67$ , indicating that the structure of the gap complex is similar to the structure of the corresponding complex formed in the absence of the cofactor (Figure 2.11a and Table 2.1)<sup>27</sup>. Interestingly, the values of both  $K_G \approx 2 \times 10^7 \text{ M}^{-1}$  and  $K_{DS} \approx 4.8 \times 10^5 \text{ M}^{-1}$  are diminished by a factor of  $\sim 5$ , as compared to the affinities observed in the absence of the cofactor<sup>27</sup>. Nevertheless, ADP does not affect the cooperativity of the PriA helicase binding to the gapped DNA, which remains the same as in the absence of nucleotide cofactors<sup>27</sup>.

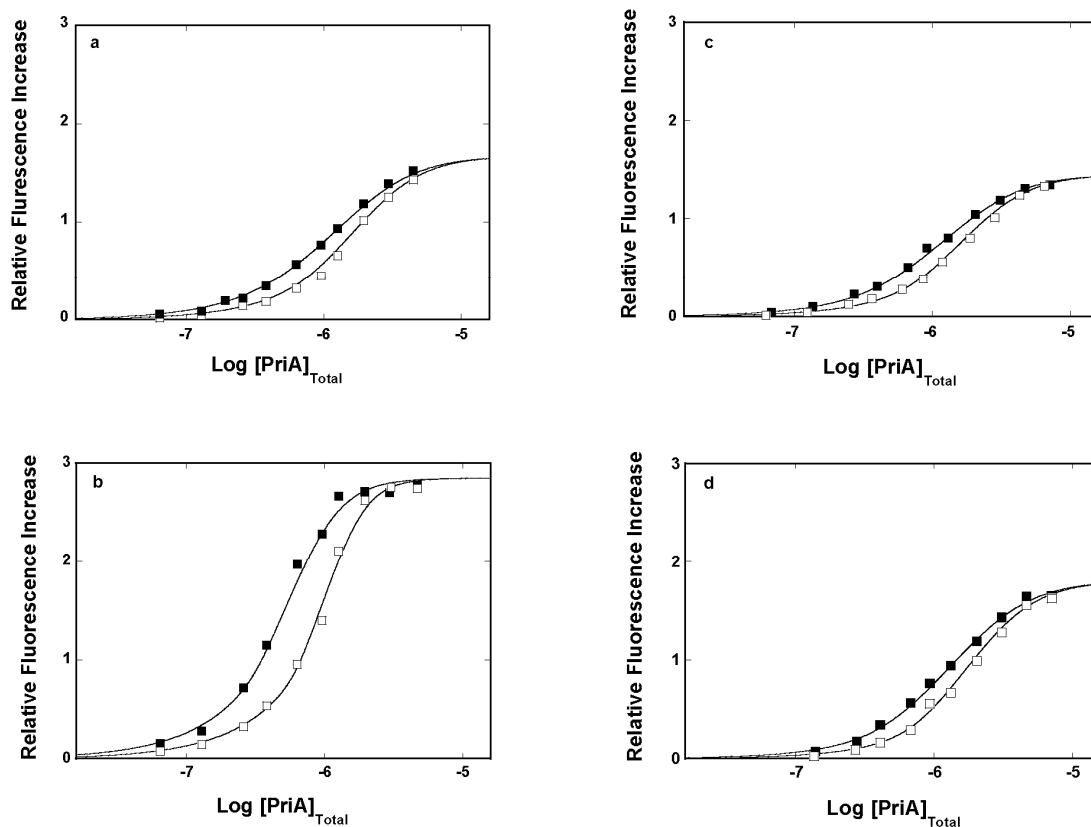


**Figure 2.11** Fluorescence titrations of the gapped DNA substrate with the ssDNA gap of 5 nucleotides, with the PriA helicase in the presence of different nucleotide cofactors. **a.** Containing  $1 \times 10^{-5}$  M ADP, at two different concentrations of the nucleic acid:  $1 \times 10^{-7}$  M (■) and  $3 \times 10^{-7}$  M (□). **b.** Containing  $3 \times 10^{-3}$  M ADP, at two different concentrations of the nucleic acid:  $1 \times 10^{-7}$  M (■) and  $3 \times 10^{-7}$  M (□). **c.** Containing  $1 \times 10^{-5}$  M ATP $\gamma$ S, at two different concentrations of the nucleic acid:  $1 \times 10^{-7}$  M (■) and  $3 \times 10^{-7}$  M (□). **d.** Containing  $3 \times 10^{-3}$  M ATP $\gamma$ S, at two different concentrations of the nucleic acid:  $1 \times 10^{-7}$  M (■) and  $3 \times 10^{-7}$  M (□). The solid lines in all panels are nonlinear least squares fits of the fluorescence titration curves according to the three-site binding model described in section 2.4.5<sup>27</sup>.

When both nucleotide-binding sites are saturated with the cofactor, in the presence of high ADP concentration, PriA recognizes the same gapped DNA substrate in a very different way<sup>27,59-61</sup>. Fluorescence titrations of the gapped DNA substrate, which has the ssDNA gap of 5 nucleotides, with the PriA helicase at two different nucleic acid concentrations, in the standard buffer C1005, containing  $3 \times 10^{-3}$  M ADP, are shown in Figure 2.11b<sup>27</sup>. The presence of ADP in both nucleotide-binding sites dramatically affects the enzyme interactions with the gapped DNA, however, the maximum stoichiometry is not changed and three PriA molecules associate with the gapped DNA<sup>27</sup>. The solid lines in Figure 2.11b are nonlinear least squares fits of the experimental titration curves using equations 2.5 – 2.7. The presence ADP in both nucleotide-binding sites is strongly manifested in the change in the relative fluorescence increase with  $\Delta F_1 \approx 0.8$  and  $\Delta F_2 = \Delta F_3 \approx 2.85$ , indicating a significant change in the structure of the complex as compared to the structure of the complex formed in the absence of the cofactor, or the in the presence of the low ADP concentrations (Figure 2.11a, Figure 2.11b, and Table 2.1).<sup>27</sup>. Moreover, the value of  $K_G$  is strongly increased to  $\sim 5 \times 10^8 \text{ M}^{-1}$  with  $K_{DS} \approx 2.5 \times 10^6 \text{ M}^{-1}$  and  $\sigma \approx 1$  is the same, as observed in the absence of the cofactor<sup>27</sup>.

Fluorescence titrations of the gapped DNA substrate, containing 5 nucleotides in the ssDNA gap, with the PriA helicase in the standard buffer C1005, with  $1 \times 10^{-4}$  M and  $3 \times 10^{-3}$  M ATP $\gamma$ S, are shown in Figure 2.11c and Figure 2.11d<sup>27</sup>. There is a dramatic difference between the situations when the nucleotide-binding sites of the PriA helicase are engaged in interactions with ADP as compared to ATP $\gamma$ S<sup>27</sup>. Both low and the high ATP $\gamma$ S concentrations induce virtually the same relative increases of the nucleic acid fluorescence accompanying the formation of the gap complex<sup>27</sup>. The values of  $\Delta F_1$  are very similar to the fluorescence changes accompanying the enzyme binding in the absence of cofactor, or in the presence of the low ADP concentration (Figure 2.11a)<sup>27</sup>.

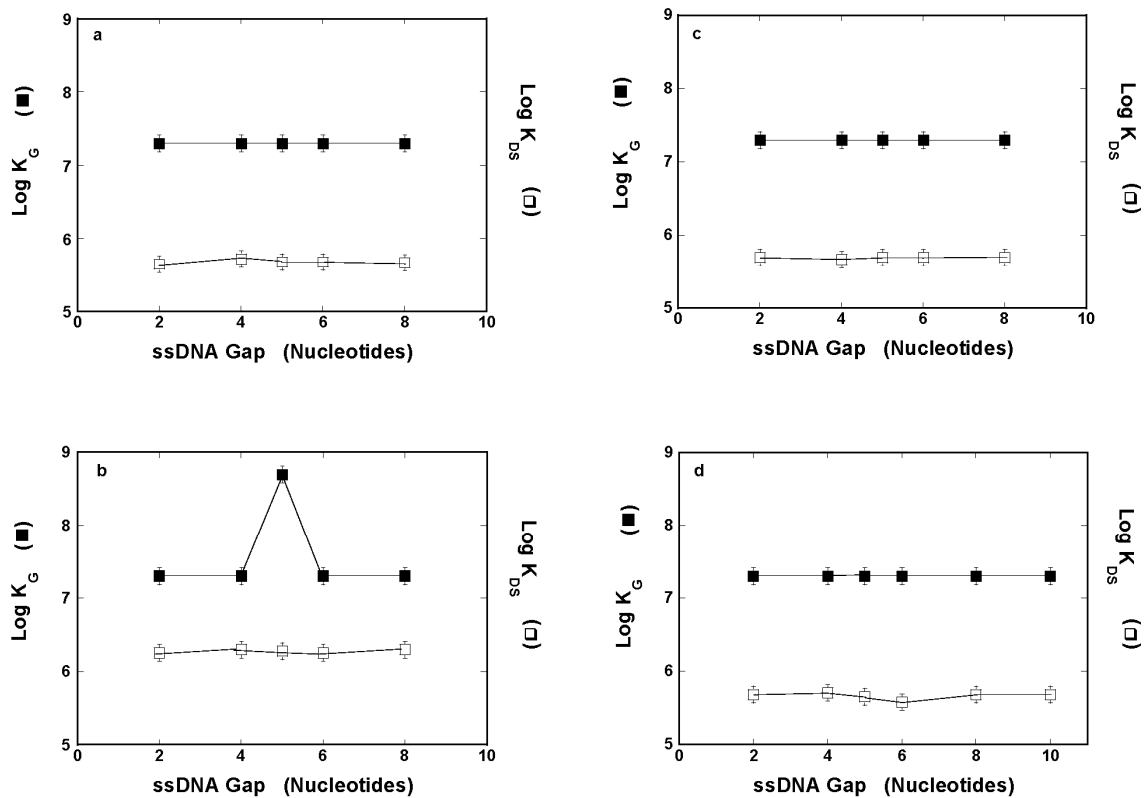


**Figure 2.12** The dependence of the logarithm of the binding constant  $K_G$  (■) and the logarithm of the binding constant  $K_{DS}$  (□), characterizing the gap complex and the association with the dsDNA, respectively, upon the length of the ssDNA gap in buffer C1005 containing: **a.** Containing  $1 \times 10^{-5}$  M ADP. **b.** Containing  $3 \times 10^{-3}$  M ADP. **c.** Containing  $1 \times 10^{-4}$  M  $\text{ATP}\gamma\text{S}$ . **d.** Containing  $3 \times 10^{-3}$  M  $\text{ATP}\gamma\text{S}$ . The solid lines in all panels connect the data points and do not have a theoretical basis<sup>27</sup>.

Saturation of both nucleotide-binding sites with ATP $\gamma$ S decreases the binding constant,  $K_G$ , by a factor of  $\sim 5$  to  $\sim 2 \times 10^7 \text{ M}^{-1}$ , and  $K_{DS}$  by a factor of  $\sim 4$  to  $\sim 5 \times 10^5 \text{ M}^{-1}$ . Thus, in the presence ATP $\gamma$ S, at the concentration saturating both nucleotide-binding sites, the PriA helicase has the lowest affinity in the gap complex and for the dsDNA parts of the nucleic acid of all examined states of the enzyme with or without the cofactors<sup>27</sup>. Again, as observed for the ADP, ATP $\gamma$ S does not affect the cooperativity of the binding process<sup>27</sup>.

Analogous studies of the PriA helicase association with the gapped DNA substrates in the presence of ADP and ATP $\gamma$ S have been performed for the DNA substrates of different size of the ssDNA gaps (data not shown)<sup>27</sup>. The dependence of the logarithm of  $K_G$  and  $K_{DS}$  upon the length of the ssDNA gap in the presence of  $1 \times 10^{-5} \text{ M}$  ADP is shown in Figure 2.12a<sup>27</sup>. In this case, when ADP saturates only the strong nucleotide-binding site of the PriA helicase, the enzyme binds with a significant affinity to the gap over the dsDNA, although the affinity is independent of the length of the ssDNA gap<sup>27</sup>. The dependence of the logarithm of  $K_G$  and  $K_{DS}$  upon the length of the ssDNA gap in the presence of the high ADP concentration ( $3 \times 10^{-3} \text{ M}$ ) is shown in Figure 2.12b<sup>27</sup>. In this state, where two nucleotide-binding sites are saturated with ADP, the enzyme shows significant preference for the ssDNA gap with 5 nucleotides in the gap over the gaps with different number of the nucleotides<sup>27</sup>.

Corresponding dependences of the logarithm of  $K_G$  and  $K_{DS}$  upon the length of the ssDNA gap in the presence of the low ( $1 \times 10^{-4} \text{ M}$ ) and high ( $3 \times 10^{-3} \text{ M}$ ) ATP $\gamma$ S concentrations are shown in Figure 2.12c and Figure 2.12d, respectively<sup>27</sup>. Unlike the effect exerted by ADP in the strong or weak nucleotide-binding site, saturation of exclusively the strong or both nucleotide-binding sites with ATP $\gamma$ S does not distinguish any particular gapped DNA substrate<sup>27</sup>. In these two cases, all gap complexes are

characterized by  $K_G \approx 2 \times 10^7 \text{ M}^{-1}$ <sup>27</sup>. Yet, the enzyme binds with the preferential affinity to the ssDNA gaps, as compared to the dsDNA, independently of the length of the ssDNA gap and the affinity difference is amplified by the lower dsDNA affinity of the helicase in the presence of the ATP analog<sup>27</sup>.

#### **2.4.8 Salt Effect on PriA - Gapped DNA Interactions In the Absence of Nucleotide Cofactors.**

To gain further insight into how the PriA helicase recognizes the gapped DNA substrates, the salt effect on the enzyme binding to the gapped DNA containing the ssDNA gap with 5 nucleotides was examined<sup>27</sup>. Fluorescence titrations of the gapped DNA substrate with the PriA protein in the standard buffer C1005, containing different concentrations of NaCl are shown in Figure 2.13a<sup>27</sup>. As the concentrations of NaCl increases the titration curves shift toward higher total protein concentrations, a representative of a decrease in macroscopic affinity of the helicase - gapped DNA complex<sup>27</sup>. Correspondingly, maximum relative fluorescence change that goes along with the binding process decreases indicating the change in the structure of the complex<sup>27</sup>. The quantitative analysis of the titration curves have been performed as described above in section 2.4.5 and 2.4.7. The solid lines in Figure 2.13a are nonlinear least squares fits of the experimental titration curves using equations 2.5 – 2.7<sup>27</sup>. The dependence of the logarithm of the binding constants,  $K_G$  and  $K_{DS}$  upon the logarithm of [NaCl] (log-log plot) is shown in Figure 2.13b<sup>27,83,84</sup>. The plots are clearly linear in examined salt concentration ranges, however, there is a major differences between the values of their slopes, with  $\partial \log K_G / \partial \log [\text{NaCl}] = -6.1 \pm 0.7$ , and  $\partial \log K_{DS} / \partial \log [\text{NaCl}] = -3.8 \pm 0.5$ <sup>27,83,84</sup>. These numbers indicate that the formation of the gap complex is accompanied by the net release of ~6 ions, while the binding of the dsDNA is accompanied by the net

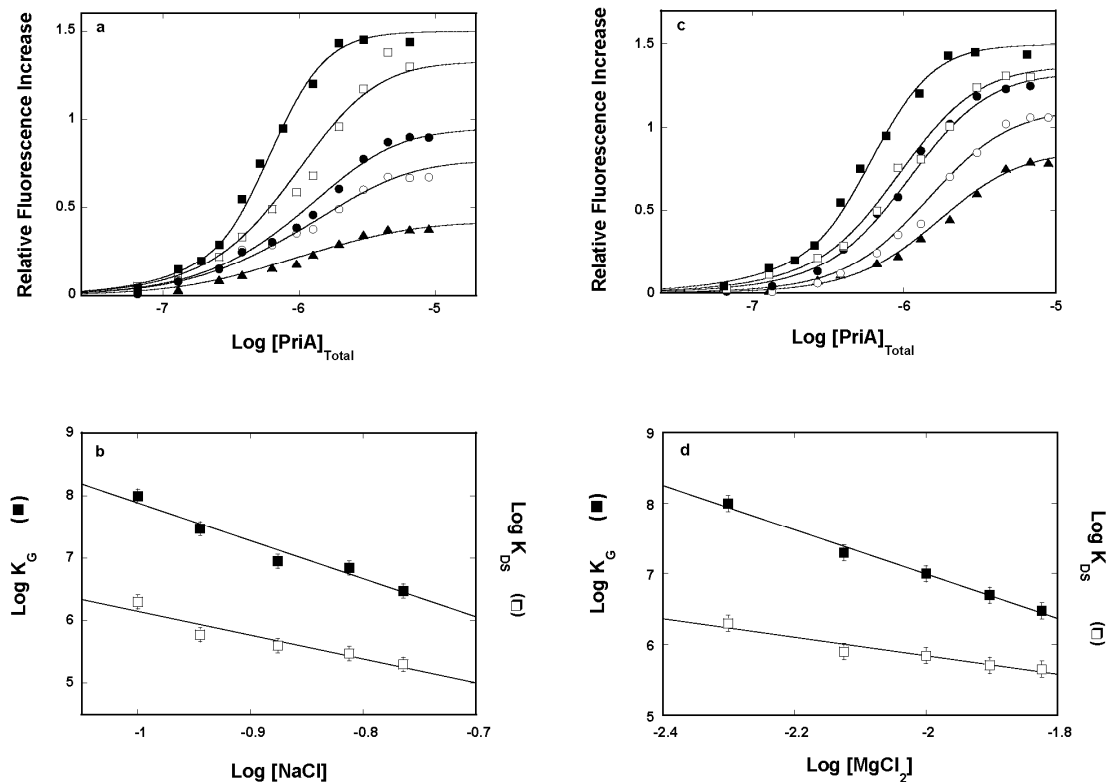


**Figure 2.13 The salt effect on PriA - gapped DNA interactions.** **a.** Fluorescence titrations of the gapped DNA substrate [ $3 \times 10^{-7}$  M] with the ssDNA gap having 5 nucleotides with PriA containing different NaCl concentrations: 100 mM (■), 113.5 mM (□), 130 mM (●), 154 mM (○), and 172 mM (▲)<sup>27</sup>. The solid lines are nonlinear least squares fits of the titration curves, using the three-site binding model, with  $\sigma = 1$ ,  $\Delta F_1$ ,  $\Delta F_{\max}$ ,  $K_G$ , and  $K_{DS}$  of 0.3, 1.5,  $1 \times 10^8$  M<sup>-1</sup>, and  $2 \times 10^6$  M<sup>-1</sup> (■); 0.3, 1.33,  $3 \times 10^7$  M<sup>-1</sup>, and  $6 \times 10^5$  M<sup>-1</sup> (□); 0.29, 0.95,  $9 \times 10^6$  M<sup>-1</sup>, and  $4 \times 10^5$  M<sup>-1</sup> (●); 0.29, 0.77,  $7 \times 10^6$  M<sup>-1</sup>, and  $3 \times 10^5$  M<sup>-1</sup> (○); and 0.26, 0.42,  $3 \times 10^6$  M<sup>-1</sup>, and  $2 \times 10^5$  M<sup>-1</sup> (▲). **b.** The dependence of the logarithm of  $K_G$  (■) and  $K_{DS}$  (□) upon the logarithm of [NaCl]<sup>27</sup>. The solid lines are linear least squares fits, which provide the slope  $\delta \log K_G / \delta \log [\text{NaCl}] = -6.1 \pm 0.7$  and  $\delta \log K_{DS} / \delta \log [\text{NaCl}] = -3.8 \pm 0.5$ , respectively<sup>27</sup>. **c.** Fluorescence titrations of the same gapped DNA substrate with PriA at different MgCl<sub>2</sub> concentrations: 5 mM (■), 7.5 mM (□), 10 mM (●), 12.5 mM (○), and 15 mM (▲)<sup>27</sup>. Binding parameters are as follows:  $\sigma = 1$ ,  $\Delta F_1$ ,  $\Delta F_{\max}$ ,  $K_G$ , and  $K_{DS}$  of 0.3, 1.5,  $1 \times 10^8$  M<sup>-1</sup>, and  $2 \times 10^6$  M<sup>-1</sup> (■); 0.23, 1.37,  $2 \times 10^7$  M<sup>-1</sup>, and  $8 \times 10^5$  M<sup>-1</sup> (□); 0.18, 1.33,  $1 \times 10^7$  M<sup>-1</sup>, and  $7 \times 10^5$  M<sup>-1</sup> (●); 0.1, 1.11,  $6 \times 10^6$  M<sup>-1</sup>, and  $5.1 \times 10^5$  M<sup>-1</sup> (○); and 0.07, 0.86,  $3 \times 10^6$  M<sup>-1</sup>, and  $4.5 \times 10^5$  M<sup>-1</sup> (▲). **d.** The dependence of the logarithm of  $K_G$  (■) and  $K_{DS}$  (□) upon the logarithm of [MgCl<sub>2</sub>]<sup>27</sup>. The solid lines are linear least squares fits, which provide the slope  $\delta \log K_G / \delta \log [\text{MgCl}_2] = -3.1 \pm 0.7$  and  $\delta \log K_{DS} / \delta \log [\text{MgCl}_2] = -1.3 \pm 0.5$ , respectively<sup>27</sup>.



release of only  $\sim 4$  ions<sup>27,83,84</sup>.

Fluorescence titrations of the same gapped DNA substrate with the PriA helicase in the standard buffer C1005, containing different  $\text{MgCl}_2$  concentrations, are shown in Figure 2.13c. As in the case of  $\text{NaCl}$ , increasing concentrations of  $\text{MgCl}_2$  strongly decreases the macroscopic affinity of the enzyme for the gapped DNA substrate and the observed relative fluorescence changes accompanying the formation of the complex<sup>27</sup>. The solid lines in Figures 2.13c are nonlinear least squares fits of the experimental titration curves using equations 2.5 – 2.7 described in section 2.4.5<sup>27</sup>. The dependence of the logarithm of the binding constants,  $K_G$  and  $K_{DS}$  upon the logarithm of  $[\text{MgCl}_2]$  is shown in Figure 2.13d<sup>27,83,84</sup>. Similar to the effect of  $\text{NaCl}$ , there is a significant difference between the values of the slope of the plots, with  $\partial \log K_G / \partial \log [\text{MgCl}_2] = -3.1 \pm 0.5$  and  $\partial \log K_{DS} / \partial \log [\text{MgCl}_2] = -1.3 \pm 0.3$ , respectively<sup>27,83,84</sup>. Notice, that the values of the slopes are approximately half of the values of the slopes determined for  $\text{NaCl}$  Figure 2.13d<sup>27</sup>. This large discrepancy in the thermodynamic response of  $K_G$  and  $K_{DS}$  to the changes in  $\text{NaCl}$  or  $\text{MgCl}_2$  concentrations clearly shows that the helicase forms a very different complex with the ssDNA gap, as compared to the complex formed with the dsDNA<sup>27,83,84</sup>. In any case, increasing  $\text{NaCl}$  or  $\text{MgCl}_2$  concentrations does not affect the cooperativity of the PriA association with the gapped DNA as evident by the constant value of  $\sigma \approx 1$ <sup>27</sup>.

#### **2.4.9 Salt Effects on PriA - Gapped DNA Interactions With Both Nucleotide-Binding Sites of the Enzyme Saturated With ADP.**

Fluorescence titrations of the gapped DNA substrate with 5 nucleotides in the ssDNA gap and the PriA helicase in the standard buffer C1005, containing  $3 \times 10^{-3}$  M ADP at different  $\text{NaCl}$  concentrations, are shown in Figure 2.14a<sup>27</sup>. The macroscopic

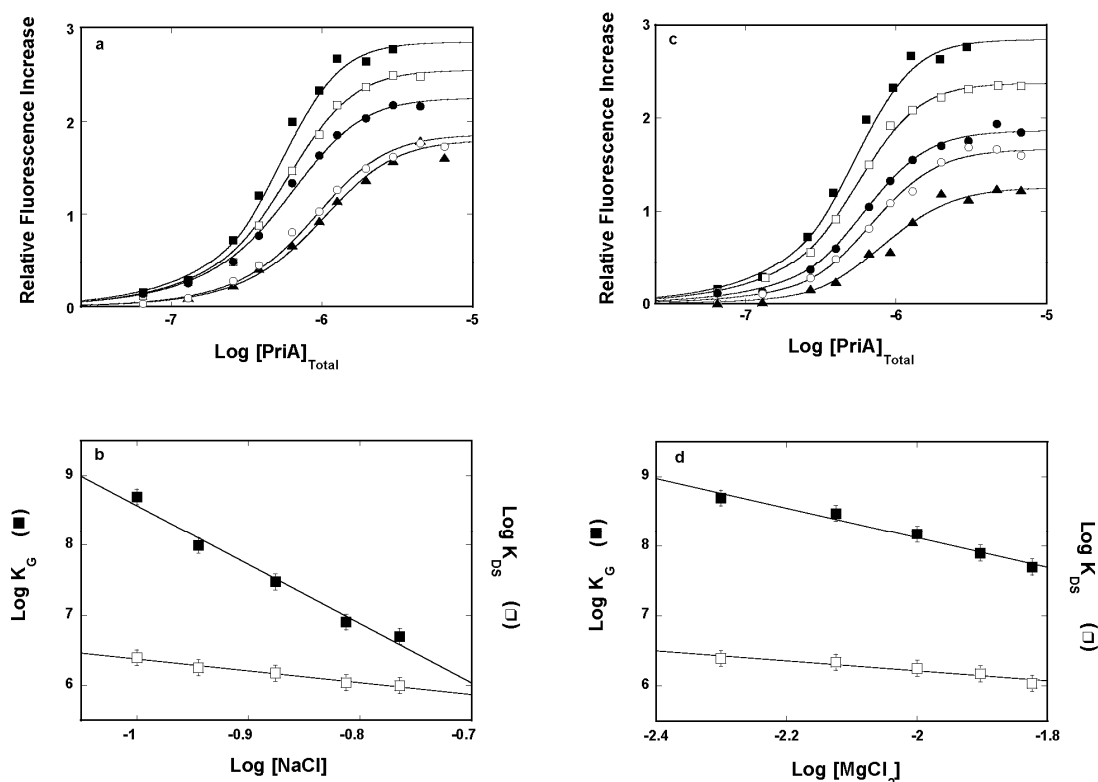


**Figure 2.14 Salt effects on PriA - gapped DNA interactions containing  $3 \times 10^{-3}$  M ADP.** **a.** Fluorescence titrations of the gapped DNA substrate [ $3 \times 10^{-7}$  M] with the ssDNA gap having 5 nucleotides with the PriA helicase, containing  $3 \times 10^{-3}$  M ADP at different [NaCl]: 100 mM (■), 113.5 mM (□), 130 mM (●), 154 mM (○), and 172 mM (▲)<sup>27</sup>. The solid lines are nonlinear least squares fits of the titration curves, using the three-site binding model with  $\sigma = 1$ ,  $\Delta F_1$ ,  $\Delta F_{\max}$ ,  $K_G$ , and  $K_{DS}$ : 0.8, 2.85,  $5 \times 10^8$  M<sup>-1</sup>, and  $2.5 \times 10^6$  M<sup>-1</sup> (■); 0.7, 2.55,  $1 \times 10^8$  M<sup>-1</sup>, and  $1.8 \times 10^6$  M<sup>-1</sup> (□); 0.7, 2.25,  $3 \times 10^7$  M<sup>-1</sup>, and  $1.5 \times 10^6$  M<sup>-1</sup> (●); 0.3, 1.86,  $8 \times 10^6$  M<sup>-1</sup>, and  $1.1 \times 10^6$  M<sup>-1</sup> (○); and 0.3, 1.8,  $5 \times 10^6$  M<sup>-1</sup>, and  $1 \times 10^6$  M<sup>-1</sup> (▲)<sup>27</sup>. **b.** The dependence of the logarithm of  $K_G$  (■) and  $K_{DS}$  (□) upon the logarithm of [NaCl]<sup>27</sup>. The solid lines are linear least squares fits, with the slope  $\delta \log K_G / \delta \log [\text{NaCl}] = -8.5 \pm 1.0$  and  $\delta \log K_{DS} / \delta \log [\text{NaCl}] = -1.8 \pm 0.4$ , respectively<sup>27</sup>. **c.** Fluorescence titrations of the same gapped DNA substrate with the PriA helicase containing  $3 \times 10^{-3}$  M ADP and at different [MgCl<sub>2</sub>]: 5 mM (■), 7.5 mM (□), 10 mM (●), 12.5 mM (○), and 15 mM (▲). Binding parameters are as follows with  $\sigma = 1$ ,  $\Delta F_1$ ,  $\Delta F_{\max}$ ,  $K_G$ , and  $K_{DS}$  of 0.8, 2.85,  $5 \times 10^8$  M<sup>-1</sup>, and  $2.5 \times 10^6$  M<sup>-1</sup> (■); 0.65, 2.38,  $3 \times 10^8$  M<sup>-1</sup>, and  $2.2 \times 10^6$  M<sup>-1</sup> (□); 0.4, 1.87,  $1.5 \times 10^8$  M<sup>-1</sup>, and  $1.8 \times 10^6$  M<sup>-1</sup> (●); 0.25, 1.67,  $8 \times 10^7$  M<sup>-1</sup>, and  $1.5 \times 10^6$  M<sup>-1</sup> (○); and 0.1, 1.26,  $5 \times 10^7$  M<sup>-1</sup>, and  $1.1 \times 10^6$  M<sup>-1</sup> (▲)<sup>27</sup>. **d.** The dependence of the logarithm of  $K_G$  (■) and  $K_{DS}$  (□) upon the logarithm of [MgCl<sub>2</sub>]. The solid lines are linear least squares fits with the slope  $\delta \log K_G / \delta \log [\text{MgCl}_2] = -2.1 \pm 0.5$  and  $\delta \log K_{DS} / \delta \log [\text{MgCl}_2] = -0.7 \pm 0.2$ , respectively<sup>27</sup>.

affinity of the helicase - gapped DNA complex and the maximum relative fluorescence change, accompanying the binding process, decrease with the increase of NaCl concentration, same as it was observed in the absence of the cofactor<sup>27</sup>. However, the relative fluorescence change is much higher as compared to the case in the absence of ADP (Figure 2.13a)<sup>27</sup>. The solid lines in Figures 2.14a are nonlinear least squares fits to the experimental titration curves using equations 2.5 – 2.7 (section 2.4.5)<sup>27</sup>. The dependence of the logarithm of the binding constants,  $K_G$  and  $K_{DS}$  upon the logarithm of NaCl concentration is shown in Figure 2.14b<sup>27,83,84</sup>. The slopes are:  $\partial \log K_G / \partial \log [\text{NaCl}] = -8.5 \pm 1$  and  $\partial \log K_{DS} / \partial \log [\text{NaCl}] = -1.8 \pm 0.4$ , respectively, therefore, the net number of ions released in the formation of the gap complex is increased to  $\sim 8 - 9$ , while the net number of ions released decreases to  $\sim 2$  for the enzyme binding to the dsDNA, as compared to the complex formation in the absence of the cofactor (section 2.4.8)<sup>27,83,84</sup>. As a result, PriA with both nucleotide-binding sites saturated with ADP, bound to the gapped DNA structure, shows dramatically different thermodynamic response to the changes of salt concentration in solution as compared to the response of the system in the absence of the cofactor (Figure 2.13, section 2.4.8)<sup>27,83,84</sup>.

Fluorescence titrations of the corresponding gapped DNA substrate with the PriA helicase in the standard buffer C1005 containing  $3 \times 10^{-3}$  M ADP and different  $\text{MgCl}_2$  concentrations, are shown in Figure 2.14c, and the dependences of the logarithm of the binding constants,  $K_G$  and  $K_{DS}$  upon the logarithm of  $[\text{MgCl}_2]$  (log-log plots) are shown in Figure 2.14d<sup>27</sup>. The values of the slopes for the gap complex and the binding to the dsDNA in the presence of high ADP concentrations are  $\partial \log K_G / \partial \log [\text{MgCl}_2] = -2.1 \pm 0.5$  and  $\partial \log K_{DS} / \partial \log [\text{NaCl}] = -0.7 \pm 0.2$ <sup>27,83,84</sup>. Notice, the net number of ions released in the association with the dsDNA, is approximately half of the corresponding value

determined for NaCl<sup>27</sup>. On the other hand, the number ions released in the formation of the gap complex, ~2, is significantly lower than half of ~8 - 9 ions released in response to the increased NaCl concentration<sup>27,83,84</sup>.

## **2.5 DISCUSSION**

### **2.5.1 The Site-Size of the PriA - Gapped DNA Substrate Complexes is Significantly Lower Than the Site-Size of the Enzyme - ssDNA Complex.**

A site-size of the protein - nucleic acid complex is a model-independent parameter and defines the total number of nucleotides occluded by the bound protein<sup>1,7-9,27,56-58,62,81,85-89,84</sup>. Recall, that the PriA helicase occludes ~ 20 nucleotides when in the complex with the ssDNA (Figure 2.3)<sup>27,56-58</sup>. Therefore, the large number of PriA molecules associating with the examined gapped DNA structures, described above, is rather startling<sup>27</sup>. Three PriA molecules are bound to all gapped DNA structures with the ssDNA gap ranging from 1 to 10 nucleotides (Figure 2.4 and Table 2.1)<sup>27</sup>. The shortest and the longest gapped DNA substrates are 21- and 30-mer in length, therefore, the average site-size of the PriA helicase in the gap complex must correspond to ~7 - 10 nucleotides<sup>27</sup>. Consequently, the site-size of PriA - dsDNA must be much shorter than ~ 20 nucleotides, observed for the PriA helicase - ssDNA interactions, and fluctuating around 7 - 10 bps<sup>27,56-58</sup>.

There are two, rather obvious but important aspects of these results<sup>27</sup>. First, to achieve such a small site-size, PriA in a complex with the gap structures must be bound in a different orientation than in the complex with the ssDNA<sup>27</sup>. This different orientation is indicated by different responses to the changes salt concentration in solution and very different relative fluorescence changes accompanying the formation of the gap complex as compared to the binding of PriA to the ssDNA (section 2.5.4)<sup>27,56-58</sup>. In the same way,

different responses to the changes salt concentration in solution and very different relative fluorescence changes accompanying the formation of the complex with ds parts of the gapped DNA structures indicate that orientation of the helicase in the gap complex is different from the orientation in the complex with the dsDNA(section 2.5.4)<sup>27,56-58</sup>. Second, as mentioned above, small maximum stoichiometry of PriA-gapped DNA complex, can only be understood in the context of the heterogeneous structure of the total DNA-binding site of the PriA helicase, previously demonstrated by the Bujalowski's lab<sup>27,56-58</sup>. Within the total DNA-binding site, PriA contains the strong DNA-binding subsite that, in the complex with the ssDNA, occludes ~ 5-8 nucleotides (Figure 2.3)<sup>27,56-58</sup>. The minimum sites-size of ~ 7 nucleotides of the gap complex described herein indicates that the helicase engages its strong DNA-binding binding site and binds the gapped substrates in the specific orientation<sup>27</sup>. The same should be true for the dsDNA (see Chapter 3)<sup>27</sup>.

### **2.5.2 PriA Specifically Recognizes the ssDNA/dsDNA Junction (s) of the Gapped Structures.**

The value of the binding constant,  $K_G$ , characterizing the PriA helicase affinity for the ssDNA gap with 5 nucleotides in the gap is  $\sim 1 \times 10^{-8} \text{ M}^{-1}$  and is  $\sim 3$  and orders of magnitude higher than the enzyme's affinity for the ssDNA ( $\sim 8 \times 10^{-4} \text{ M}^{-1}$ ) in the same solution conditions<sup>27,56-58</sup>. In the case of dsDNA parts of the gapped DNA structures, the PriA helicase affinity is  $\sim 2 \times 10^{-6} \text{ M}^{-1}$ , which is  $\sim 2$  orders of magnitude higher than the enzymes affinity for the ssDNA, in the same solution conditions (Figure 2.10 and Table 2.1)<sup>27,56-58</sup>. In addition, gapped substrates with 3, 4, and 6 nucleotides in the gap have affinities  $\sim 2$  orders of magnitude higher than the corresponding affinity of the ssDNA(Figure 2.10 and Table 2.1)<sup>27,56-58</sup>. It is evident that the intrinsic affinity of enzyme

for the ssDNA in the gap does not play a significant role in the ssDNA gap recognition<sup>27</sup>. In addition, formation of the gap complex goes along with moderate changes of the etheno-adenosine fluorescence increase ranging from 0.3 to 0.8 (Table 2.1), whereas direct binding of PriA to the corresponding etheno-derivatives of the ssDNA adenosine homo-polymers induces much larger relative fluorescence increase of  $\sim 2.5 - 2.9$ <sup>27,56-58</sup>.

The fluorescence of  $\epsilon A$  is not very sensitive to the polarity of the environment and compared to the free  $\epsilon AMP$ , the emission of etheno-oligomers is quenched 8-10 fold, primarily, by the dynamic process of an intramolecular collision<sup>27,90,91</sup>. To wit, the fluorescence increase is caused by the conformational change of the nucleic acid and reflects the increased separation and restricted mobility of the nucleic acid bases<sup>27,81,90,91</sup>. It is evident that the formation of the PriA - gap complexes goes along with very modest values of the relative fluorescence increase, as a result the enzyme does not affect the structure of the ssDNA in the gap to the same extent as in the complex with the ssDNA alone, *i.e.*, the interactions with the ssDNA are much less direct in the gap complex<sup>27,90,91</sup>. These results strongly indicate that, in the complex with the gapped DNA structures, PriA predominantly engages the ssDNA/dsDNA junction rather than the ssDNA of the gap<sup>27</sup>. Should the ssDNA play a dominant role in the recognition of the gapped DNA structure, the gaps with 8 and 10 nucleotides would have the highest affinities of the gap complex and the highest relative fluorescence changes accompanying the formation of the complex, but this is not experimentally observed<sup>27</sup>.

### **2.5.3 The PriA Helicase Preferentially Recognizes the ssDNA Gap With 5 Nucleotides In the Absence of Nucleotide Cofactors.**

In the absence of nucleotide cofactors, the binding constant,  $K_G$ , progressively and strongly increases, from a gap containing 1 to the gap containing 5 nucleotides where

it is  $\sim 2$  orders of magnitude higher than the value of  $K_G$  describing interactions of PriA with gap of 1 (Figure 2.10 and Table 2.1)<sup>27,56-58</sup>. However, this dramatic increase of the affinity is not accompanied by increase of the fluorescence of the etheno-adenosines in the gap, comparable to the fluorescence increase observed in the complex with the ssDNA (section 2.5.1 and 2.5.2), indicating a little change of the structure of the ssDNA of the gap, *i.e.*, weak engagement of the enzyme in interactions with the ssDNA of the gap (section 2.5.1 and 2.5.2 and Table 2.1)<sup>27,56-58</sup>. It stands to reason that PriA recognizes the spatial separation between two ss/dsDNA junctions of the gap, the size of the gap, with the ssDNA/dsDNA junctions being the “attachment points” of the enzyme (section 2.5.2)<sup>27,56-58</sup>. Interestingly, the sharp decrease of the value of  $K_G$  for the gapped DNA starting with 6 nucleotides in the ssDNA gap supports this conclusion<sup>27</sup>. It is likely that this behavior results from the fact that, in longer gaps, PriA loses one of the attachment points, which goes beyond the optimal size of the gap that can be accommodated by the strong DNA-binding subsite of the protein<sup>27,56-58</sup>. These results corroborate well with an idea that PriA binds gapped substrates with specific orientation and that there is a strict geometrical requirement for the optimal recognition of the size of the gap<sup>27</sup>.

#### **2.5.4 Intrinsic Interactions of the PriA Helicase - ssDNA Gap Indicate Involvement of the ssDNA/dsDNA Junction (s) of the Gapped Structures. The Salt Effect.**

The difference between the salt effect on the PriA - ssDNA interactions and in the PriA helicase - gap complex, with the ssDNA gap of 5 nucleotides, is staggering<sup>27,56-58</sup>. While the slope of the log-log plot is  $\partial \log K_G / \partial \log [\text{NaCl}] = -6.1 \pm 0.7$ , the analogous slope, obtained in the same solution conditions, for the PriA - ssDNA 10-mer, which only engages the strong DNA-binding subsite of the helicase, is  $\partial \log K_{10} / \partial \log [\text{NaCl}] = -2.5 \pm$

0.4<sup>27,57</sup>. Clearly, the net number of ions released,  $\sim 6$ , in the formation of the gap complex is larger than the number of the nucleotides in the ssDNA gap. Additionally, since in the interactions with the gapped DNA substrates the enzyme does not engage the ssDNA of the gap to the same extent as in the direct binding to the ss nucleic acid, the number of ions released from the ssDNA of the gaps should be much smaller than observed for the ssDNA binding but this is not experimentally observed<sup>27,57</sup>. These data provide strong evidence that both ssDNA/dsDNA junctions of the gap are involved in interactions with the strong-DNA binding site of the helicase<sup>27</sup>. The slope of the log-log plot obtained in the presence of different concentrations of  $\text{MgCl}_2$ , is  $\partial \log K_G / \partial \log [\text{MgCl}_2] = -3.1 \pm 0.5$ , and is approximately half of what is observed for the effect of NaCl (Figure 2.13b and Figure 2.13d), strongly suggesting that magnesium and sodium cations compete for the same ionic interactions in the complex and the interactions are predominantly electrostatic in nature<sup>27,83,84</sup>.

In the case of the PriA helicase – ssDNA interactions, the increase of the salt concentration in solution strongly increases the positive cooperative interactions, which at high concentrations of NaCl becomes an important part of the free energy of binding<sup>27,57</sup>. No cooperative interactions between PriA molecules bound in the gap complex were detected and the increase in NaCl or  $\text{MgCl}_2$  concentration in solution does not change  $\sigma$ , which within experimental error is 1 in all experiments described in this Chapter<sup>27</sup>. The lack of any effect in the salt concentration changes on the cooperative interactions reinforces the conclusion that the enzyme is bound in very different and specific orientation in the gap complex than in the complex with the ssDNA<sup>27,57</sup>. This different orientation eliminates favorable interacting contacts between bound protein molecules, which are stabilized by the ion binding to the PriA protein<sup>27</sup>. In contrast,  $\partial \log K_{DS} / \partial \log [\text{NaCl}] = -3.8 \pm 0.5$ , and  $\partial \log K_{DS} / \partial \log [\text{MgCl}_2] = -1.3 \pm 0.3$ , are comparable



to the values of the corresponding slopes,  $\sim -3$  and  $\sim -1.7$ , respectively, determined for the direct interactions of the strong DNA-binding site of PriA with the ssDNA. This similar thermodynamic response of two systems to the salt concentration changes in solution suggests similar involvement of the nucleic acid in interactions with the PriA protein<sup>27,57,83,84</sup>.

#### **2.5.5 The Presence of the Nucleotide in the Strong Nucleotide-Binding Site Eliminates PriA's Size Specific Selectivity for the Gap of 5 Nucleotides.**

When the nucleotide cofactor is exclusively bound to the strong-nucleotide-binding site of the PriA helicase there is no significant effect on the enzyme interactions with the ssDNA<sup>27,57,59-61</sup>. Similarly, in the case of the gap complex, low ADP or ATP $\gamma$ S concentrations only slightly affect  $\Delta F_1$ ,  $\Delta F_2$ , and  $\Delta F_3$ , as compared to the same parameters determined in absence of the cofactors, indicating similar structures of the formed complexes (Table 2.1 and Table 2.2)<sup>27</sup>. Notice, in the presence of the low nucleotide concentrations, the values of  $K_G$  for the gaps with 4 and 5 nucleotides are significantly diminished, as compared to the corresponding affinities observed in the absence of cofactor<sup>27</sup>. Hence, PriA no longer specifically recognizes ssDNA gaps of 4 to 5 nucleotides<sup>27</sup>. Interestingly, the values of  $K_G$  are increased for the remaining examined gapped DNAs, as compared to the corresponding affinities observed in the absence of cofactor (Figure 2.12a and Figure 2.12c)<sup>27</sup>. The value of  $K_{DS}$  is also diminished for all examined gapped substrates, as compared to the values observed in the absence of cofactor<sup>27</sup>. Because the efficiency of the gap recognition should be measured with respect to the surrounding dsDNA, the PriA enzyme with the strong nucleotide-binding site saturated with ADP or ATP analog, preserves and even augments its recognition efficiency for some gaps<sup>27</sup>. Nevertheless, all examined gapped DNA substrates are now

characterized by the same  $K_G$  (Figure 2.12a and Figure 2.12c)<sup>27</sup>. In other words, as mentioned above, the preference of the enzyme for the gap with 4 - 5 nucleotides, seen in the state without nucleotide cofactors, is lost and the helicase binds equally well to the ssDNA gaps of different sizes (Figure 2.10, Figure 2.12a, and Figure 2.12c)<sup>27</sup>.

#### **2.5.6 Saturation of Both Nucleotide-Binding Sites of the PriA Helicase with ADP Restores Enzyme Selectivity for the ssDNA Gap with 5 Nucleotides.**

The effect of the saturation of the both nucleotide-binding sites with ATP nonhydrolyzable analog, ATP $\gamma$ S, is the same as observed for the nucleotide binding to the strong-nucleotide binding site (Figure 2.11c, Figure 2.11d, Figure 2.12c, and Figure 2.12d)<sup>27</sup>. The preference of the enzyme for the gap with 4 - 5 nucleotides, seen in the state without nucleotide cofactors, is lost and the helicase binds equally well to the ssDNA gaps of different sizes (Figure 2.12d)<sup>27</sup>. Different behavior is observed when both the strong and the weak nucleotide-binding sites are saturated with ADP (Figure 2.11b and Figure 2.12b)<sup>27</sup>. At high concentration of ADP, the relative fluorescence changes,  $\Delta F_1$ ,  $\Delta F_2$ , and  $\Delta F_3$ , are considerably increased, especially for the ssDNA gap with 5 nucleotides, demonstrating more extensive engagement of the ssDNA of the gap in interactions with the enzyme<sup>27,56-60</sup>. In that state, the PriA helicase binds preferentially to the ssDNA gap with 5 nucleotides, as the value of  $K_G$  is increased by a factor of  $\sim 5$ <sup>27</sup>. In addition, the affinity is, within the experimental error, the same for all other gaps (Figure 2.12b)<sup>27</sup>. Interestingly, the value of  $K_{DS}$  remains the same as determined in the absence of any cofactor, and as a result, the enzyme has a preference for the gap with 5 nucleotides over the ssDNA gaps with different numbers of nucleotides than 5, and over the dsDNA (Figure 2.12)<sup>27</sup>.

### 2.5.7 Salt Effect on the Gap Complex Formation when Both Nucleotide-Binding Sites are Saturated with ADP.

When both nucleotide-binding sites of PriA are saturated with ADP, the slope of the log-log plot is  $\partial \log K_G / \partial \log [\text{NaCl}] = - 8.5 \pm 1$  (Figure 2.14a, Figure 2.14b, and Table 2.2)<sup>27</sup>. Thus, the net number of ions released,  $\sim 8 - 9$  a significantly larger than  $\sim 6$  ions determined for the complex in the absence of the nucleotide cofactors and approximately two times larger than the number of the nucleotides in the ssDNA gap of the examined gapped DNA substrate (Figure 2.13a, Figure 2.13b, and Table 2.2)<sup>27,57,83,84</sup>. In spite of the fact that the value of  $\Delta F_1$  is increased, it is still significantly lower than  $\Delta F_{\text{max}}$  observed in the direct binding to the ssDNA, indicating less pronounced contact with the ssDNA in the gap<sup>27,56-59</sup>. Although additional ion release from the ssDNA gap cannot be excluded, such a large increase in the net number of ions released upon gap complex formation indicates that the enzyme engages additional area in interactions with the nucleic acid and additional fragment of the DNA outside the gap complex, presumably through the opening of the DNA-binding area at the N-terminus of the protein<sup>27,56-59</sup>. Notice, the slope of the log-log plot obtained in the presence of different  $\text{MgCl}_2$  concentrations  $\partial \log K_G / \partial \log [\text{MgCl}_2] = - 2.1 \pm 0.5$ , is significantly lower than expected, if magnesium cations simply replace sodium ions in the ion exchange (Figure 2.14d and Table 2.2)<sup>27,83,84</sup>. The diminished slope of  $\partial \log K_G / \partial \log [\text{MgCl}_2]$  strongly suggests that a specific uptake of magnesium cations by the enzyme, associated with the presence nucleotide cofactor, compensates the observed net number of ion released<sup>27,83,84</sup>. The same uptake of magnesium cations should also diminish the slope of the  $\partial \log K_{\text{DS}} / \partial \log [\text{MgCl}_2]$ , which is also experimentally observed<sup>27</sup>. The value of  $\partial \log K_{\text{DS}} / \partial \log [\text{MgCl}_2] = - 1.3 \pm 0.3$ , observed in the absence of the nucleotide cofactor, is reduced to  $\partial \log K_{\text{DS}} / \partial \log [\text{MgCl}_2] =$

-  $0.7 \pm 0.2$ , for the enzyme with both nucleotide-binding site saturated with ADP (Figure 2.13, Figure 2.14, and Table 2.2)<sup>27,83,84</sup>.

#### **2.5.8 Model of the PriA – Gapped DNA Complex with 5 Nucleotides in the ssDNA Gap.**

Based on the results described in this Chapter, the pictorial model of the PriA - gapped DNA substrate complex, containing 5 nucleotides in the ssDNA gap, in the absence of the nucleotide cofactors, is shown in Figure 2.15a<sup>27</sup>. The PriA helicase binds gapped DNA substrates using its strong DNA-binding subsite located on the protruding domain in a specific orientation, which allows for the enzyme unwinding of the dsDNA in 3' -> 5' direction<sup>27,56-59</sup>. Predominantly the ssDNA/dsDNA junctions are engaged in interactions with the helicase when in the complex<sup>27</sup>. Together these interactions match the geometry and structural flexibility of the strong DNA-binding subsite and lead to the amplified affinity for the gapped DNA substrate and different thermodynamic response to the changes of the salt concentrations in solution<sup>27</sup>. Another schematic model of the PriA complex with the gapped DNA substrate, containing the ssDNA gap with 5 nucleotides in the presence of high ADP concentration, which saturates both nucleotide-binding sites of PriA, is shown in Figure 2.15b<sup>27</sup>. Again, the enzyme predominantly engages the ssDNA/dsDNA junctions in interactions with the gapped DNA substrate, however, saturation of both nucleotide-binding sites with ADP induces conformational transition of the enzyme and opens additional interacting area, possibly, on the N-terminus domain, which engages additional fragment of the gapped DNA substrate, analogously to the complexes with the ssDNA<sup>27,56-59</sup>. As a result, the PriA helicase completely saturated with ADP has increased affinity for the gap DNA substrate with 5 nucleotides and the complex manifests a different thermodynamic response to the changes of the salt

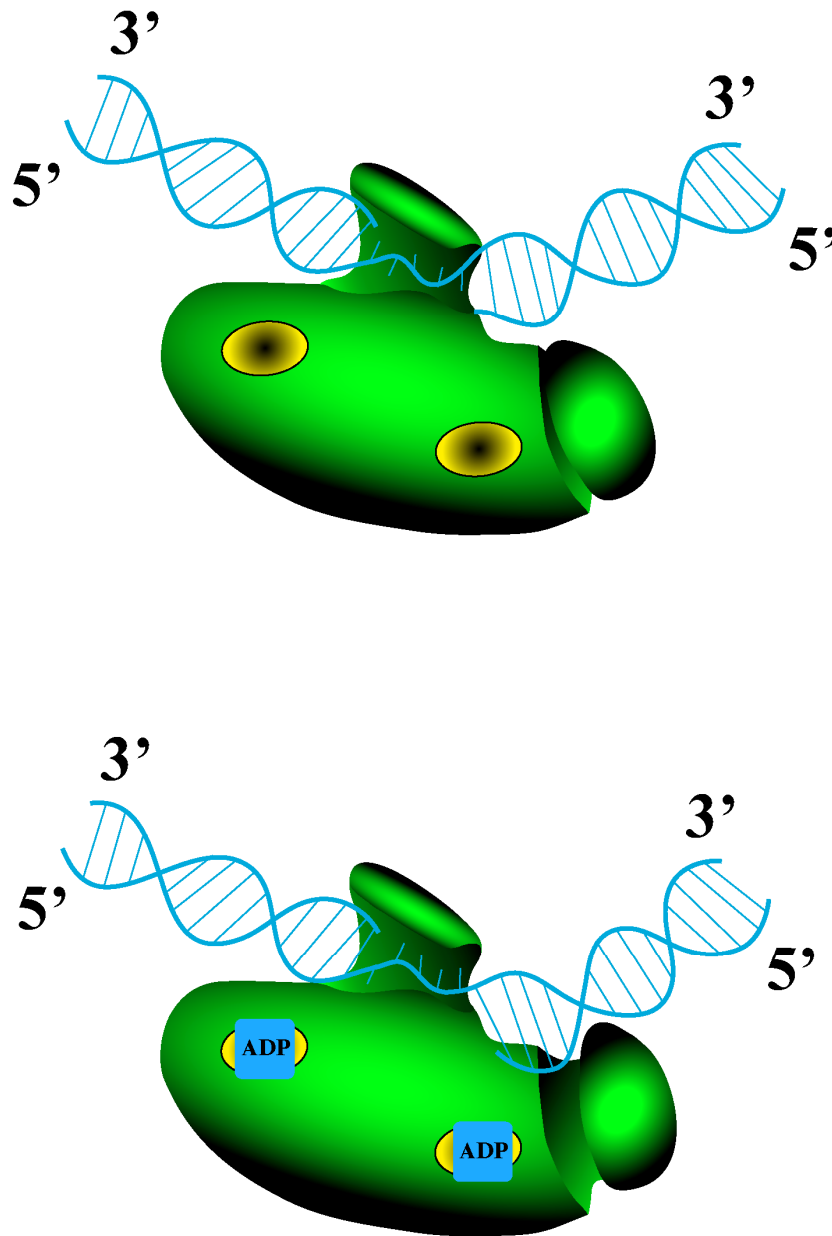


**Figure 2.15 Schematic model of the PriA complex with the gapped DNA substrate.**  
**a.** In the absence of the nucleotide cofactors the enzyme binds the gapped DNA substrate using its strong DNA-binding subsite engaging the ssDNA/dsDNA junctions<sup>27</sup>. **b.** Saturation of both nucleotide-binding sites with ADP induces conformational transition of the enzyme and opens additional interacting area which engages further fragment of the gapped DNA substrate<sup>27</sup>.

concentration in solution, as compared to the gap complex formed in the absence of ADP<sup>27</sup>.

### **2.5.9 Functional Implications.**

Biochemical studies indicated that in order to initiate the assembly of the primosome, the PriA helicase requires a small ssDNA gap of ~ 5 nucleotides<sup>14,17,27</sup>. About the same time, thermodynamic studies indicated that the total site-size of the PriA - ssDNA is ~ 20 nucleotides, which is much too large for the observed gap recognition process<sup>27,56-60</sup>. Nonetheless, these studies, as well as the findings described herein, provide the first indication on how PriA could adjust to different sizes of the ssDNA and recognizes gapped DNA substrates<sup>27,56-60</sup>. Studies in this work show that the recognition of the short ssDNA gap is accomplished by PriA binding in a specific orientation, which allows the enzyme to engage only the strong DNA-binding subsite in the gap complex<sup>27</sup>. The selectivity for the ssDNA gap with 5 nucleotides is the consequence of matching the site-size of the strong DNA-binding subsite of the helicase to the size of the gapped DNA substrate<sup>27</sup>. Yet, the enzyme can recognize even shorter ssDNA gaps than 5 nucleotides, although with lower efficiency<sup>27</sup>. The lack of cooperative interactions between multiple PriA molecules bound in the gap complex and the enzyme molecules associated with the surrounding dsDNA strongly suggests that a single PriA molecule participates in the recognition of the ssDNA gap at the stalled replication fork<sup>27</sup>. On the other hand, for the gaps with 8 or 10 nucleotides in length, the PriA helicase has significantly lower, if any, gap-recognition capabilities<sup>27</sup>. It is likely that for these longer gaps a different pathway of the restart of the replication fork is activated<sup>27</sup>. In fact, it has been indicated that for the large ssDNA gaps, the PriC - Rep (PriA-independent) and not PriA - PriB (PriA-dependent) pathway may be operational (Figure 2.1, section 2.2.1 and 2.2.2)<sup>11-14,27,35,43,45</sup>.

Out of five different states of the enzyme with respect to the engagement of its two nucleotide-binding sites in interactions with the cofactor, examined in this work, only two states, without nucleotide cofactors and with two nucleotide-binding sites saturated with ADP show dramatic preference for the ssDNA gap with 5 nucleotides<sup>27</sup>. Yet, there is a significant difference between these two states<sup>27</sup>. In the absence of the cofactors, the enzyme predominantly recognizes the size of the ssDNA gap, without extensively engaging the ssDNA of the gap or any additional fragments of the nucleic acid<sup>27</sup>. On the other hand, in the state with both nucleotide-binding sites saturated with ADP, the enzyme engages both the ssDNA/dsDNA junctions and an additional fragment of the surrounding DNA<sup>27</sup>. Recognition of the size of the gap seems to be a more efficient in finding the short ssDNA gap than a process which involves conformational rearrangements and engagement of an additional fragment of the nucleic acid<sup>27</sup>. Thus, it is probable that the state of the enzyme without bound nucleotide cofactors is the state which is used in the recognition of the ssDNA gap<sup>27</sup>.

The states of the enzyme with bound nucleotide cofactors, to one or both nucleotide-binding sites, could be employed in the post-recognition stage<sup>27</sup>. Therefore, binding of the nucleotide cofactors to both nucleotide-binding sites would regulate the PriA affinity for the gap, in the state when the enzyme is already bound to the gapped DNA substrate<sup>27</sup>. Notice, saturation of the strong nucleotide-binding site with ADP or ATP eliminates the enzyme preference for the gap of 4 - 5 nucleotides<sup>27</sup>. Recall, the ssDNA affinity does not play a role in the gap recognition, thus, the saturation of the strong nucleotide-binding site seems to increase the affinity of the enzyme for the ssDNA/dsDNA junction<sup>27</sup>. Because the strong site is the major ATPase site of the PriA helicase, in this state, the enzyme, placed at the ssDNA/dsDNA junction, is ready to perform the dsDNA unwinding reaction in the post recognition stages<sup>27</sup>. Similar role can

be executed by the state where both nucleotide-binding sites are saturated with ATP<sup>27</sup>. The state with both nucleotide-binding sites saturated with ADP stabilizes the gap complex and allows the enzyme to engage additional binding area in interactions with the nucleic acid<sup>27</sup>. This activity would be necessary to achieve the recognition of the fork not just the ssDNA gap<sup>27</sup>. Exchange for ATP in both sites would diminish the stability of the gap complex, as the recognition is already achieved<sup>27</sup>. This would allow the enzyme to bind to the ssDNA/dsDNA junction in the 3' -> 5' direction and initiate the unwinding reaction in the presence of ATP in preparing for the entry of the DnaB - DnaC complex into the primosome<sup>11-14,27,35,43,45</sup>.



**Table 2.1.** Thermodynamic and spectroscopic parameters of the binding of the *E. coli* PriA helicase to the gapped DNA substrate containing different numbers of nucleotides in the ssDNA gap, in standard buffer C1005\*.

ssDNA Gap	1	2	3	4	5	6	8	10
Stoichiometry	3	3	3	3	3	3	3	3
$K_G$	$(2.0 \pm 0.4) \times 10^6$	$(1.0 \pm 0.2) \times 10^7$	$(2.0 \pm 0.4) \times 10^7$	$(4.0 \pm 1.0) \times 10^7$	$(1.0 \pm 0.2) \times 10^8$	$(8.0 \pm 2.0) \times 10^8$	$(5.0 \pm 1.3) \times 10^6$	$(2.5 \pm 0.6) \times 10^6$
$K_{DS}$	$(1.8 \pm 0.5) \times 10^6$	$(1.7 \pm 0.5) \times 10^6$	$(1.7 \pm 0.5) \times 10^6$	$(1.6 \pm 0.4) \times 10^6$	$(2.0 \pm 0.5) \times 10^6$	$(1.7 \pm 0.4) \times 10^6$	$(1.7 \pm 0.4) \times 10^6$	$(1.7 \pm 0.4) \times 10^6$
$\sigma$	$1 \pm 0.3$	$1 \pm 0.3$	$1 \pm 0.3$	$1 \pm 0.3$	$1 \pm 0.3$	$1 \pm 0.3$	$1 \pm 0.3$	$1 \pm 0.3$
$\Delta F_1$	$0.80 \pm 0.05$	$0.73 \pm 0.05$	$0.45 \pm 0.05$	$0.46 \pm 0.05$	$0.31 \pm 0.05$	$0.35 \pm 0.05$	$0.33 \pm 0.05$	$0.62 \pm 0.05$
$\Delta F_2 = \Delta F_3$	$3.0 \pm 0.1$	$3.1 \pm 0.1$	$1.7 \pm 0.1$	$1.8 \pm 0.1$	$1.5 \pm 0.1$	$1.8 \pm 0.1$	$1.7 \pm 0.1$	$1.7 \pm 0.1$

\*The errors are standard deviations determined using 3 - 4 independent titration experiments.

Table 2.2. Thermodynamic and spectroscopic parameters of the binding of the *E. coli* PriA helicase to the gapped DNA substrate containing 5 nucleotides in the ssDNA gap, in standard buffer C1005, in the presence of different concentrations of ATP $\gamma$ S or ADP\*.

Conditions	Stoichiometry	$K_c(M^{-1})$	$K_{DS}(M^{-1})$	$\sigma$	$\Delta F_1$	$\Delta F_2 = \Delta F_3$	$dLog K_c /$	$dLog K_{DS} /$	$dLog K_c /$	$dLog [MgCl_2]$	$dLog [MgCl_2]$
5 mM MgCl <sub>2</sub>	3	(1.0 $\pm$ 0.2) $\times 10^8$	(2.0 $\pm$ 0.6) $\times 10^6$	1 $\pm$ 0.3	0.31 $\pm$ 0.05	1.5 $\pm$ 0.1	-6.1 $\pm$ 0.7	-3.8 $\pm$ 0.5	-3.1 $\pm$ 0.5	-	-1.3 $\pm$ 0.3
1 $\times 10^{-5}$ M ADP	3	(2.0 $\pm$ 0.6) $\times 10^7$	(4.8 $\pm$ 1.6) $\times 10^5$	1 $\pm$ 0.3	0.33 $\pm$ 0.05	1.67 $\pm$ 0.12	-	-	-	-	-
3 $\times 10^{-3}$ M ADP	3	(5.0 $\pm$ 1.6) $\times 10^8$	(2.5 $\pm$ 0.6) $\times 10^6$	1 $\pm$ 0.3	0.80 $\pm$ 0.05	2.85 $\pm$ 0.15	-8.5 $\pm$ 1	-1.8 $\pm$ 0.4	-2.1 $\pm$ 0.5	-	-0.7 $\pm$ 0.2
1 $\times 10^{-4}$ M ATP $\gamma$ S	3	(2.0 $\pm$ 0.6) $\times 10^7$	(5.0 $\pm$ 1.6) $\times 10^5$	1 $\pm$ 0.3	0.25 $\pm$ 0.05	1.45 $\pm$ 0.11	-	-	-	-	-
3 $\times 10^{-3}$ M ATP $\gamma$ S	3	(2.0 $\pm$ 0.6) $\times 10^7$	(4.5 $\pm$ 1.5) $\times 10^5$	1 $\pm$ 0.3	0.22 $\pm$ 0.05	1.8 $\pm$ 0.1	-	-	-	-	-

\*The errors are standard deviations determined using 3 - 4 independent titration experiments.

## CHAPTER 3

### THE *ESCHERICHIA COLI* PRIA HELICASE - DOUBLE-STRANDED DNA COMPLEX<sup>92</sup>

#### 3.1 ABSTRACT

The *E. coli* PriA helicase complex with the double-stranded DNA, the location of the strong DNA-binding subsite, and the effect of the nucleotide cofactors, bound to the strong and weak nucleotide-binding site of the enzyme on affinity of the enzyme for dsDNA, have been examined using the fluorescence titration, analytical ultracentrifugation, and photo-cross-linking techniques<sup>92</sup>. The total site-size of the PriA - dsDNA complex is dramatically lower than the site-size of the enzyme - ssDNA complex, and is only  $5 \pm 1$  bps<sup>92</sup>. PriA binds to dsDNA using its strong ssDNA-binding subsite but in an orientation very different from the complex with the ssDNA<sup>92</sup>. The strong DNA-binding subsite of the enzyme is located on the helicase domain of the PriA protein<sup>92</sup>. Surprisingly, intrinsic affinity for the dsDNA is considerably higher than the ssDNA affinity and the binding process is accompanied by a significant positive cooperativity<sup>92</sup>. Binding of nucleotide cofactors to the strong and weak nucleotide-binding sites of the helicase profoundly affects the intrinsic affinity and the cooperativity, without affecting the stoichiometry<sup>92</sup>. Binding of ATP analog to either site diminishes the intrinsic affinity but preserves the cooperativity<sup>92</sup>. Binding of ADP to the strong site leads to a dramatic increase of the cooperativity and barely affects the affinity, while saturation

---

<sup>92</sup> This research was originally published in Journal of Molecular Biology. Szymanski, M. R., Jezewska, M. J. & Bujalowski, W. (2010). The *Escherichia coli* PriA helicase-double-stranded DNA complex: location of the strong DNA-binding subsite on the helicase domain of the protein and the affinity control by the two nucleotide-binding sites of the enzyme. *J Mol Biol* 402, 344-62. Reproduced with permission.

of both sites with ADP strongly increases the affinity and eliminates the cooperativity<sup>92</sup>. As a result, the coordinated action of both nucleotide-binding sites on the PriA - dsDNA interactions depends on the structure of the phosphate group<sup>92</sup>. The results presented here are significant for the enzyme activities in recognizing primosome assembly site or the ssDNA gaps<sup>92</sup>.

### 3.2 INTRODUCTION

As it was shown in Chapter 1 and Chapter 2, the PriA helicase is a key enzyme in *E. coli* DNA replication and is involved in other major processes of the DNA metabolism, including recombination, and repair<sup>1,5,11-18,27,32-36,92</sup>. The enzyme plays a paramount role in the ordered assembly of the primosome, a large molecular machine engaged in DNA priming<sup>5,11-17,27,92</sup>. In this capacity, PriA has also been proposed as the major factor that initiates the restart of the stalled replication fork by recognizing specific DNA structure at the damaged DNA sites<sup>5,11-17,27,92</sup>.

The interactions of PriA with the ssDNA have been intensively studied and are described in the introduction to Chapter 2 (section 2.2.3)<sup>27</sup>. In addition, it was quantitatively revealed by Szymanski *et al.* that the PriA helicase can specifically recognize and bind to the small single stranded gaps in the DNA (Chapter 2)<sup>27</sup>. Interestingly, the results presented in Chapter 2 demonstrated that more than one PriA molecule was bound to the gapped DNA substrate, indicating that the site-size of the PriA – dsDNA complex is significantly lower, as compared to the site-size of the complex with the ssDNA<sup>27,92</sup>. Moreover, the binding process was affected by the presence of nucleotide cofactors<sup>27,92</sup>. This was a very interesting finding, as it is not generally expected that the helicase would bind to the dsDNA. The complexity of the gapped DNA structures, used in that studies, precluded quantitative characterization of

the enzyme - dsDNA association beyond macroscopic affinities<sup>27,92</sup>. Therefore, Chapter 3 is a logical continuation of Chapter 2 where the recognition of the damaged DNA structures by the PriA helicase was examined (section 1.4.1 and section 2.2.4)<sup>27</sup>.

Interactions of the PriA helicase with the dsDNA have never been suggested, nor quantitatively examined<sup>92</sup>. In fact, very little is known about the quantitative energetics and dynamics of interactions of other well-studied helicases with the dsDNA<sup>27,92</sup>. The interactions with the dsDNA are particularly important in the case of the PriA protein, where in the processes of the primosome formation and stalled replication fork restart, the enzyme encounters mostly dsDNA<sup>2,5,11,14,27,92</sup>. Therefore, direct quantitative examination of PriA - dsDNA interactions and the effect of the nucleotide cofactors on these interactions are of fundamental importance for understanding the recognition process of the stalled replication fork substrates by the PriA helicase<sup>27,92</sup>. In addition, elucidation of the mechanism of PriA - dsDNA interactions will add to our understanding of the intricate process of primosome assembly, and, in general, the mechanism of the helicase action in DNA metabolism<sup>27,92</sup>. Thus, in Chapter 3, direct quantitative studies of the PriA - dsDNA interactions and the effect of the nucleotide cofactors on these interactions have been described<sup>92</sup>.

### **3.3 MATERIALS AND METHODS**

#### **3.3.1 Buffers and Chemicals.**

All solutions used in experiments described in this Chapter were made with distilled and deionized >18 M $\Omega$  (Milli-Q Plus) water<sup>92</sup>. The standard buffer was buffer C505 with 10 mM sodium cacodylate adjusted to pH 7.0 with HCl at 10°C, 1 mM DTT, 50 mM NaCl, 5 mM MgCl<sub>2</sub>, and 25% glycerol w/v<sup>92</sup>. The standard temperature in all the experiments described herein was 10°C. All experiments were carried out in the standard

buffer C505 unless otherwise specified in the text. Trypsin, and trypsin inhibitor were from Sigma (Saint Louis, MI). All chemicals were reagent grade.

### **3.3.2 Water Activity of Buffering Solution.**

Water activity “error term” of the standard buffer C505, used throughout this Chapter, had been calculated according to the values described in the literature<sup>132,133</sup>. Due to the presence of the glycerol and salt, the water activity “error term” is less than 5%, and is contained within the experimental error of all the experiments presented here<sup>27,132,133</sup>.

### **3.3.3 Nucleotides and Nucleic Acids.**

ATP $\gamma$ S and ADP were from Sigma (Saint Louis, MI). ATP $\gamma$ S and ADP were of high purity as judged by thin layer chromatography (TLC). Unmodified nucleic acid oligomers, etheno-derivatives, and fluorescein-labeled ssDNA oligomers and were purchased from Midland Certified Reagents (Midland, TX)<sup>92</sup>. All nucleic acids were HPLC purified and at least >95% pure as judged by electrophoresis on polyacrylamide gel.

To monitor binding, dsDNA substrates were build from modified ssDNA oligomers containing a fluorescent label, fluorescein (Fl), attached to the 5' end of the DNA through phosphoramidate chemistry mixed with unmodified oligomers<sup>92</sup>. The sequences of the labeled oligomers were: Fl-CTGACGTGCG, Fl-CTGACGTGCGGATGC, and Fl-CTGACGTGCGGATGCGGACG for 10-, 15-, and 20-mer respectively<sup>92</sup>. The concentrations of the nucleic acids were determined spectrophotometrically using the extinction coefficients:  $\epsilon_{260} = 10000 \text{ cm}^{-1}\text{M}^{-1}$  (nucleotide) for A,  $\epsilon_{260} = 8500 \text{ cm}^{-1}\text{M}^{-1}$  (nucleotide) for G,C and T<sup>27,62</sup>. The degree of labeling of fluorescent labeled nucleic acid was determined spectrophotometrically using

the extinction coefficients  $\epsilon_{494} = 76000 \text{ cm}^{-1}\text{M}^{-1}$  for fluorescein<sup>27,62,63</sup>. 5'-FI-labeled dsDNA substrates were obtained by mixing labeled ssDNA oligomers with complementary unmodified oligomers at appropriate concentration<sup>92</sup>. The mixture was then warmed for 5 minutes at 95°C, and slowly cooled for a period of ~ 4 - 5 hours<sup>27,62,63,92</sup>. The etheno derivative of the ssDNA 18-mer, dεA(pεA)<sub>17</sub>, used for competition studies, was obtained by modification with chloroacetaldehyde<sup>90-92</sup>. The concentration of etheno-derivative of the nucleic acids was determined spectrophotometrically using following the extinction coefficients:  $\epsilon_{257} = 3700 \text{ cm}^{-1}\text{M}^{-1}$  (nucleotide) for εA<sup>56,57,81,87,90-92</sup>.

The integrities of the dsDNA substrates have been checked by UV melting and analytical ultracentrifugation techniques<sup>27,62,63,92</sup>. The melting temperature of the examined dsDNA substrates was ~54°C or higher in the studied solution conditions<sup>27,62,63,92</sup>.

### 3.3.4 The PriA Protein.

The *E. coli* PriA protein has been purified using the protocol previously described by Jezewska *et al.* (section 2.3.4 and 2.4.1)<sup>27,56,57,92</sup>.

### 3.3.5 Fluorescence Measurements.

All steady-state fluorescence titrations, described in this Chapter, were performed using the Fluorolog F-11 spectrofluorometer (Jobin Yvon) as previously described<sup>27,56-63,92</sup>. The temperature of the cuvette holder was regulated by circulating water at  $10.0 \pm 0.1$  °C. The PriA protein binding to the dsDNA substrates was followed by monitoring the emission of the fluorescein-labeled nucleic acid ( $\lambda_{\text{ex}} = 485 \text{ nm}$ ,  $\lambda_{\text{em}} = 520 \text{ nm}$ ) or, in the case competition studies, etheno-derivative fluorescence of the nucleic acids ( $\lambda_{\text{ex}} =$

325 nm,  $\lambda_{em} = 410$  nm)<sup>27,81,92</sup>. The relative fluorescence increase,  $\Delta F_{obs}$ , of the DNA emission upon protein binding is defined as,  $\Delta F_{obs} = (F_i - F_o)/F_o$ , where  $F_i$  is the fluorescence of the sample at a given titration point “i” and  $F_o$  is the initial fluorescence of the same solution<sup>27,56-63,81,92</sup>.

### **3.3.6 Determination of Quantitative Binding Isotherm of the PriA – dsDNA Complexes.**

In this Chapter, we followed the binding of the PriA helicase to the DNA oligomers by monitoring the fluorescence increase,  $\Delta F$ , of the Fl-labeled DNA or etheno-derivative of the nucleic acid<sup>92</sup>. To obtain quantitative estimates of the total average degree of binding,  $\Sigma\Theta_i$  (average number of bound PriA molecules per DNA oligomer) and the free protein concentration,  $P_F$ , independent of any assumption about the relationship between the observed spectroscopic signal and  $\Sigma\Theta_i$ , we applied an approach previously described in section 2.3.7<sup>1,56,57,82,87,92</sup>. Computer fits were performed using Mathematica (Wolfram, IL) and KaleidaGraph (Synergy Software, PA)<sup>92</sup>.

### **3.3.7 Analytical Ultracentrifugation Measurements.**

All analytical ultracentrifugation experiments were performed with an Optima XL-A analytical ultracentrifuge (Beckman Inc., Palo Alto, CA), as we previously described in section 2.3.8<sup>27,66-69,72,76,82,92</sup>.

### **3.3.8 Trypsin Digestion Experiments.**

Trypsin stock solution in the concentration of 0.2 mg/ml, PriA stock solution in the concentration of 0.74 mg/ml, and trypsin inhibitor stock solution in the concentration of 10 mg/ml were all prepared on ice in the standard buffer C505<sup>92</sup>. The PriA protein was mixed with trypsin on ice at the 37 : 1 PriA to trypsin molar ratio<sup>92</sup>. The reaction was



allowed to proceed and aliquots of 10  $\mu$ L were taken at given time points<sup>92</sup>. The digestion reaction was stopped by adding 2  $\mu$ L of trypsin inhibitor and SDS loading buffer<sup>92</sup>. The reaction mixture was then immersed in  $\sim 95$  °C water bath for 4 minutes, allowed to cool down, centrifuged and loaded onto 10% SDS polyacrylamide gel<sup>92</sup>. The sample was run at constant voltage and the gel was stained with Coomassie Brilliant Blue<sup>92</sup>. Several different PriA protein - trypsin molar ratios were examined to obtain the optimal time dependence of the digestion reaction<sup>92</sup>.

### **3.3.9 Photo-cross-linking Coupled Trypsin Digestion Experiments.**

Time-dependent digestion of the PriA helicase - ssDNA complex with trypsin has been performed in the standard buffer C505<sup>92</sup>. The ssDNA oligomer, dT(pT)<sub>19</sub> has been labeled at the 5' end with [<sup>32</sup>P], using polynucleotide kinase<sup>40,92,93</sup>. The concentrations of PriA and nucleic acid are chosen to ensure saturation of the binding process<sup>92</sup>. The complex was mixed with the protease at the 37 : 1 PriA - trypsin molar ratio. Several different PriA protein - trypsin molar ratios were examined to obtain the optimal time dependence of the digestion reaction<sup>92</sup>. The samples (total volume 40  $\mu$ L) were placed on Parafilm, at  $\sim 10$ °C, and irradiated for 20 minutes, at a distance of 11 cm, using a mineral lamp (model UVG-11) with a maximum output of 254 nm<sup>92</sup>. The reaction was stopped by adding trypsin inhibitor, subsequently, adding SDS loading buffer, and immersing the sample in  $\sim 95$ °C water bath for 4 minutes<sup>92</sup>. The samples collected at different time intervals of the protease reaction were loaded on 10% SDS polyacrylamide gel and electrophoresis was performed at a constant voltage<sup>92</sup>. The gels were stained with Coomassie Brilliant Blue and scanned, using the phosphorimager SI (Molecular Dynamics, PA)<sup>92</sup>. The controls were performed to determine the optimal time for photo-

cross-linking and to avoid possible degradation of the protein by prolonged exposure to the UV light<sup>92</sup>.

### 3.4 RESULTS

#### 3.4.1 The Site-Size of the PriA-dsDNA Complex in the Absence of Nucleotide Cofactors.

Alike the interactions of the PriA helicase with the ssDNA, association of the enzyme with the dsDNA is not accompanied by sufficient changes of the protein tryptophan fluorescence suitable to examine the binding process<sup>27,56-58,92</sup>. However, the association of the PriA helicase with dsDNA oligomers, labeled at the 5' of one of the ssDNA strands with fluorescein, is accompanied by a significant increase of the nucleic acid fluorescence, allowing us to perform high-resolution studies of the enzyme - dsDNA complex formation<sup>27,56-58,92</sup>. Selected dsDNA oligomers contain a random sequence of bases with 70% G-C base pairs content<sup>92</sup>. The length of the oligomers are 10, 15, and 20 base pairs, similar to the site-size of the strong DNA-binding subsite (~ 5 - 7 nucleotides) and the total (~ 20 nucleotides) DNA-binding site of the PriA helicase - ssDNA complex (Figure 2.3)<sup>27,56-58,92</sup>.

Fluorescence titrations of the 5'-Fl-dsDNA 10-mer with the PriA helicase at two different nucleic acid concentrations, in buffer C505 are shown in Figure 3.1a<sup>92</sup>. The maximum observed relative fluorescence increase,  $\Delta F_{\max}$ , is ~ 0.4. Titration curves, such as in Figure 3.1a, have been analyzed by using the quantitative approach outlined in sections 2.3.7 and section 3.3.5<sup>1,56,57,82,87,92</sup>. The dependence of the observed relative fluorescence increase,  $\Delta F$ , as a function of the total average degree of binding,  $\Sigma \Theta_i$ , of the PriA protein on the dsDNA 10-mer is shown in Figure 3.1b<sup>92</sup>. The plot is clearly

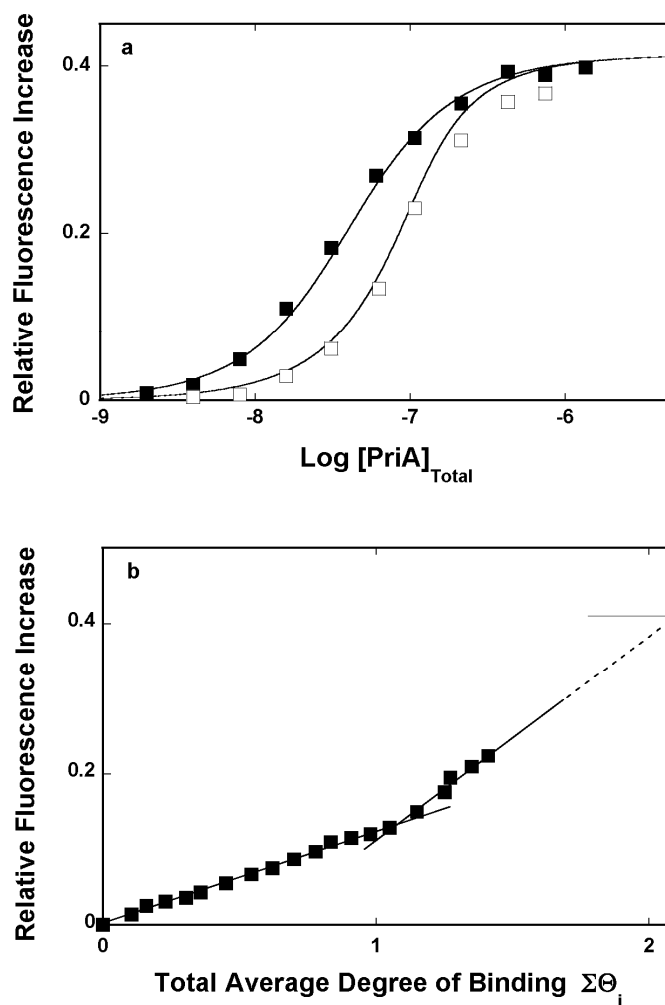


**Figure 3.1 Two PriA molecules bind to the dsDNA 10-mer at saturation. a.** Fluorescence titrations of the 5'-Fl-dsDNA 10-mer with the PriA protein at two different nucleic acid concentrations:  $1 \times 10^{-8}$  M (■),  $5 \times 10^{-8}$  M (□) (oligomer)<sup>92</sup>. The continuous lines are nonlinear least-squares fits of the titration curves, using the statistical thermodynamic model described by equations 3.1 – 3.3<sup>92</sup>. **b.** Dependence of the relative fluorescence increase of the dsDNA 10-mer,  $\Delta F$ , upon the total average degree of binding,  $\Sigma\Theta_i$  (■)<sup>92</sup>. The continuous lines indicate the limiting slopes of the plot at the low and high enzyme concentration range, respectively, and have no theoretical basis<sup>92</sup>. The broken line is the extrapolation of  $\Delta F$  to the maximum value of  $\Delta F_{\max}$ <sup>92</sup>.

nonlinear indicating the presence of two binding phases with a modest increase of  $\Delta F$  to  $\sim 0.12$  describing the binding of the first PriA molecule to the oligomer<sup>92</sup>. Subsequently, the values of  $\Delta F$  significantly increase in the second binding phase and extrapolation of the second phase to the maximum value of the fluorescence increase,  $\Delta F_{\text{max}} = 0.41 \pm 0.03$ , gives the maximum value of  $\Sigma\Theta_i = 2.1 \pm 0.2$ <sup>92</sup>. Thus, at saturation, two PriA molecules bind to the dsDNA 10-mer<sup>92</sup>.

Fluorescence titrations of the 5'-FI-dsDNA 15-mer with the PriA helicase, at two different nucleic acid concentrations, are more complex and are shown in Figure 3.2a<sup>92</sup>. The titration curves clearly show at least two binding phases, however, in this case, the binding phases differ in the induced changes in the nucleic acid fluorescence<sup>92</sup>. In the high-affinity phase, PriA binding induces an increase of the DNA oligomer fluorescence, while in the low-affinity phase the fluorescence quenching process is observed<sup>92</sup>. Figure 3.2b shows the dependence of the observed relative fluorescence increase,  $\Delta F$ , as a function of  $\Sigma\Theta_i$  of the PriA helicase on the 15-mer<sup>92</sup>. The selected DNA concentrations provide separation of titration curves up to  $\Delta F \sim 0.25$ <sup>92</sup>. The total average degree of binding up to  $\Sigma\Theta_i \sim 1.6$ , indicating that two PriA molecules bind the dsDNA 15-mer in the high-affinity phase (Figure 3.2b)<sup>92</sup>. However, the binding process continues into the low affinity phase (Figure 3.2a), indicating that additional PriA molecule(s) associate with the nucleic acid<sup>92</sup>. In addition, fluorescence titrations of the 5'-FI-dsDNA 20-mer with PriA helices show similar behavior as the 5'-FI-dsDNA 15-mer dsDNA substrate. However, in the case of 20-mer dsDNA, binding of four PriA molecules is observed (data not shown)<sup>92</sup>.

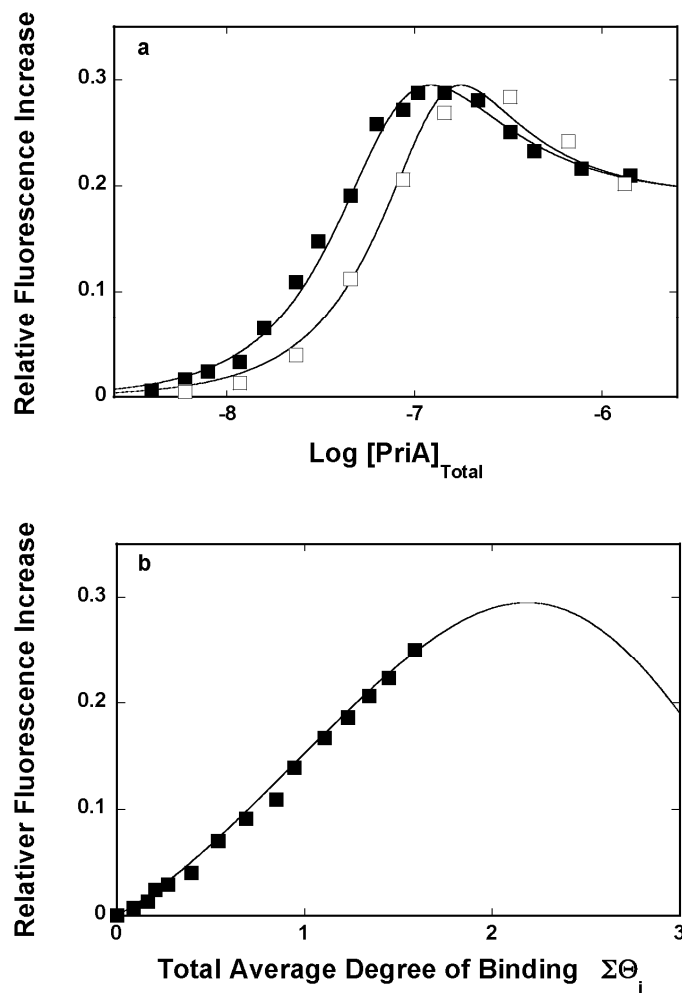


**Figure 3.2 Three PriA molecules bind to the dsDNA 15-mer at saturation. a.** Fluorescence titrations of the 5'-Fl-dsDNA 15-mer with the PriA protein at two different nucleic acid concentrations:  $1 \times 10^{-8}$  M (■),  $5 \times 10^{-8}$  M (□) (oligomer)<sup>92</sup>. The continuous lines are nonlinear least-squares fits of the titration curves, using the statistical thermodynamic model described by equations 3.4 – 3.7<sup>92</sup>. **b.** Dependence of the relative fluorescence increase of the dsDNA 10-mer,  $\Delta F$ , upon the total average degree of binding,  $\Sigma\Theta_i$  (■)<sup>92</sup>. The continuous line indicates is a simulation of the relative fluorescence increase as a function of the total average degree of binding with  $K_{15} = 1 \times 10^7 \text{ M}^{-1}$  and  $\omega = 8$ <sup>92</sup>.

### 3.4.2 Analytical Ultracentrifugation Studies.

The maximum stoichiometry of the PriA - dsDNA complex, has been addressed using independent sedimentation equilibrium method<sup>27,81,92</sup>. The experiments were facilitated by the fact that the nucleic acid concentration, at the absorption band of fluorescein (495 nm), can be exclusively monitored in the presence of the high enzyme concentration without any interference from the protein absorbance<sup>27,81,92</sup>. Characteristic sedimentation equilibrium concentration profile of the dsDNA 10-mer, labeled at the 5' end with fluorescein is shown in Figure 3.3 (section 3.3.3 and section 3.3.7)<sup>92</sup>. The enzyme is in a large molar excess over the nucleic acid, assuring complete saturation of the DNA across whole sedimentation equilibrium profile<sup>92</sup>. The solid line is a nonlinear least-square fit to a single exponential function in equation 2.4 (section 2.3.8)<sup>27,92</sup>. Including additional exponential terms does not cause significant improvement of the statistics of the fit (data not shown)<sup>27,81,92</sup>. The analysis of the concentration profiles provides a molecular weight of  $156000 \pm 15000$ <sup>92</sup>. Since the molecular weights of the PriA helicase and the nucleic acid oligomer are  $\sim 82000$  and  $\sim 6300$ , respectively, the obtained data show that, at saturation, the PriA protein forms a 2:1 complex with the dsDNA 10-mer (section 2.3.8 and section 2.4.2)<sup>27,81,92</sup>. Analogous experiments with the 5'-Fl-dsDNA 15-mer provided the molecular weight of the complex,  $\sim 250000$ , indicating the presence of three enzyme molecules in the complex (data not shown)<sup>92</sup>.

There are two important facets of the thermodynamic and sedimentation equilibrium data presented above<sup>92</sup>. First, at saturation, two and three PriA molecules bind to the dsDNA 10- and 15-mer, demonstrating that the enzyme forms a single type of complex with the dsDNA and entail only 5 base pairs to engage the nucleic acid<sup>92</sup>. In other words, the site-size of the PriA - dsDNA complex is  $n = 5 \pm 1$  base pairs<sup>92</sup>. This

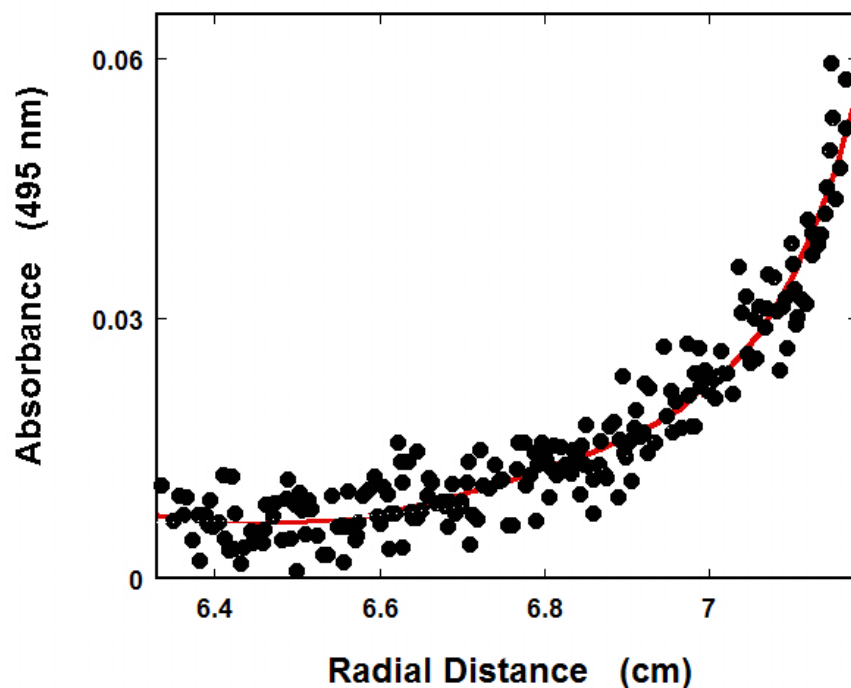


**Figure 3.3** Typical sedimentation equilibrium concentration profile of the 5'-Fl-dsDNA 10-mer in the presence of PriA helicase. The concentration of the nucleic acid and the helicase are  $2.6 \times 10^{-7}$  M and  $8 \times 10^{-6}$  M, respectively<sup>92</sup>. The profile has been recorded at 8000 rpm and monitored at 495 nm<sup>92</sup>. The continuous line is the nonlinear least-squares fit to single exponential function (equation 2.4) with a single species having a molecular weight of  $156,000 \pm 15,000$ <sup>92</sup>.

behavior is dramatically different from PriA binding to the ssDNA where the site-size of the complex is  $\sim 20$  nucleotides<sup>56-58</sup>. In addition, these results corroborate well with our data on PriA-gapped DNA interactions, where we postulated that the PriA helicase can bind to the dsDNA parts of the gaped DNA structures with a site-size much smaller than that predicted for the ssDNA interactions (Chapter 2)<sup>27,92</sup>. Second, the maximum total degree of binding of the PriA protein on the dsDNA 10-mer is not affected by a  $\sim 10$ -fold increase of the oligomer concentration (data not show)<sup>92</sup>. The independence of the enzyme - dsDNA stoichiometry upon the short oligomer concentrations provides a solid thermodynamic proof that only a single DNA-binding subsite of the protein engages in interactions with the nucleic acid<sup>1,27,56-58,92</sup>. The  $\sim 10$ -fold increase of the 10-mer concentration would easily detect a weak interactions with another DNA-binding site on the PriA helicase, characterized by the intrinsic binding constant lower by at least  $\sim 1 - 2$  orders of magnitude than the observed affinity<sup>1,27,92</sup>. This kind of behavior would be evident by a change in the stoichiometry of the complex, however, this is not experimentally observed<sup>1,27,92</sup>. In conclusion, the results strongly indicate that the PriA protein binds the dsDNA by using its strong DNA-binding subsite<sup>27,56-58,92</sup>.

### 3.4.3 Statistical Thermodynamic Model of PriA Binding to the dsDNA.

The simplest statistical thermodynamic model that describes the binding of two PriA molecules to the dsDNA 10-mer is defined by the partition function,  $Z_{10}$ , as<sup>1,27,56-58,81,84,92</sup>

$$Z_{10} = 1 + (N - n + 1)K_{10}[P_F] + \omega (K_{10}[P_F])^2 \quad (3.1)$$



where  $N$  is the total number of base pairs in the oligomer ( $N = 10$ ),  $n$  is the site-size of the PriA- dsDNA complex ( $n = 5$ ), and  $\omega$  is the parameter characterizing the cooperative interactions between the bound protein molecules<sup>1,27,56-58,81,84,92</sup>. The total average degree of binding,  $\Sigma\Theta_i$ , is expressed by simple statistical thermodynamic formula,  $\partial\ln Z_{10}/\partial\ln[P_F]$ , as

$$\Sigma\Theta_i = \frac{[(N-n+1)K_{10}P_F + 2\omega(K_{10}P_F)^2]}{Z_{10}} \quad (3.2)$$

Therefore, the experimental relative fluorescence increase,  $\Delta F$ , of the dsDNA 10-mer is

$$\Delta F = \Delta F_1 \left[ \frac{(N-n+1)K_{10}P_F}{Z_{10}} \right] + \Delta F_{\max} \left[ \frac{\omega(K_{10}P_F)^2}{Z_{10}} \right] \quad (3.3)$$

where  $\Delta F_1$  is the relative molar fluorescence increase associated with binding of the first PriA molecule to the dsDNA 10-mer, and  $\Delta F_{\max}$  is the relative fluorescence increase accompanying binding of two PriA molecules to the dsDNA substrate<sup>1,27,81,84,92</sup>.

Because of the nonlinear dependence of the observed signal as a function of the total average degree of binding, quantitative analysis of PriA binding to the dsDNA 10-mer, requires both the fluorescence titration curve (Figure 3.1a) and the dependence of the observed  $\Delta F$  as a function of  $\Sigma\Theta_i$  (Figure 3.1b)<sup>1,27,81,84,87,92,94,95</sup>. The value of  $\Delta F_1$  can be determined from the initial part of the plot in Figure 3.1b, as,  $\Delta F_1 = \partial\Delta F/\partial\Sigma\Theta_i$ , which provides  $\Delta F_1 = 0.12 \pm 0.03$ <sup>92</sup>. The value of  $\Delta F_{\max}$  can be estimated from the plateau of the titration curves at high enzyme concentrations, which provides  $\Delta F_{\max} = 0.41 \pm 0.03$ <sup>92</sup>. Having that information, there are only two remaining parameters that must be

determined,  $K_{10}$  and  $\omega$ <sup>1,92,94,95</sup>. The solid lines in Figure 3.1a are the nonlinear least squares fits of the experimental titration curves to equations 3.1 – 3.3, with  $K_{10}$  and  $\omega$  as the fitting parameters<sup>92</sup>. As seen in the Figure 3.1a, the model provides an excellent description of the binding process<sup>1,92</sup>. The values of the binding and spectroscopic parameters are included in Table 3.1<sup>92</sup>. The intrinsic binding constant,  $K_{10} \sim 1.6 \times 10^7 \text{ M}^{-1}$ , is significantly larger than the analogous parameter, previously obtained for the ssDNAs in similar solution conditions<sup>27,56-59,92</sup>. Surprisingly, the value of  $\omega \approx 10$  indicates that, unlike the binding to the ssDNA, where  $\omega \approx 1 - 2$ , interactions of the PriA protein with the dsDNA are characterized by significant positive cooperativity<sup>27,56-59,92</sup>.

Because three PriA molecules associate with dsDNA 15-mer estimation of the binding parameters is much more intricate<sup>92</sup>. The binding system can be directly treated by the exact combinatorial theory for large ligand binding to a finite linear, homogeneous lattice<sup>1,84,92</sup>. The partition function,  $Z_{15}$ , is defined as

$$Z_{15} = \sum_{k=0}^g \sum_{j=0}^{k-1} P_N(k, j) (K_{15} P_F)^k \omega^j \quad (3.4)$$

where  $g$  is the maximum number of ligand molecules which may bind to the finite nucleic acid lattice (for the nucleic acid lattice  $N$  residues long,  $g = N/n$ ),  $K_{15}$  is the intrinsic binding constant,  $\omega$  is the cooperative interaction parameter,  $k$  is the number of ligand molecules bound, and  $j$  is the number of cooperative contacts between the  $k$  bound ligand molecules in a particular configuration on the lattice<sup>1,84,92</sup>. The combinatorial factor  $P_N(k, j)$  is the number of distinct ways that  $k$  ligands bind to a lattice with  $j$  cooperative contacts and is defined by<sup>92</sup>

$$P_N(k,j) = \frac{[(N - nk + 1)!(k - 1)!]}{[(N - nk + j + 1)!(k - j)!(k - j - 1)!]} \quad (3.5)$$

The total average degree of binding,  $\Sigma\Theta_i$ , is then<sup>92</sup>

$$\Sigma\Theta_i = \frac{\sum_{k=1}^g \sum_{j=0}^{k-1} k P_N(k,j) (K_{15} P_F)^k \omega^j}{\sum_{k=0}^g \sum_{j=0}^{k-1} P_N(k,j) (K_{15} P_F)^k \omega^j} \quad (3.6)$$

The value of the relative fluorescence increase,  $\Delta F$ , at any titration point, is defined as<sup>92</sup>

$$\Delta F = \Delta F_1 \left[ \frac{(N - n + 1) K_{15} P_F}{Z_{15}} \right] + \Delta F_2 \left[ \frac{\sum_{j=0}^{k-1} P_N(k,j) (K_{15} P_F)^k \omega^j}{Z_{15}} \right] + \Delta F_3 \left[ \frac{(K_{15} P_F)^3 \omega^2}{Z_{15}} \right] \quad (3.7)$$

where  $\Delta F_1$ ,  $\Delta F_2$ , and  $\Delta F_3$  are the relative molar fluorescence increases accompanying the binding of one, two, and three PriA molecules to the 15-mer<sup>92</sup>. Notice, the value of  $\Delta F_1$  can be determined from the initial part of the plot in Figure 3.2b, as,  $\Delta F_1 = \partial\Delta F / \partial\Sigma\Theta_i$ , which provides  $\Delta F_1 = 0.09 \pm 0.03$ <sup>92</sup>. The value of  $\Delta F_3 = 0.19 \pm 0.03$  can also be estimated from the plots in Figure 3.2a, therefore, there are three independent parameters,  $\Delta F_2$ ,  $K_{15}$ , and  $\omega$ , which must be determined<sup>92</sup>. The solid lines in Figure 3.2a are nonlinear least squares fits of the titration curves using equations 3.4 – 3.7<sup>92</sup>.

The value of intrinsic binding constant,  $K_{15} = (1 \pm 0.4) \times 10^7 \text{ M}^{-1}$  and the cooperativity parameter  $\omega = 8 \pm 4$  are, within experimental error, the same as determined

for the 10-mer<sup>56-59,92</sup>. Such a similarity in intrinsic affinities and cooperativity values eliminates possible end effect in studied interactions<sup>1,56-59,92</sup>. Similar to the 10-mer, the largest increase of the nucleic acid fluorescence occurs for the complex with two PriA molecules, with  $\Delta F_2 = 0.43 \pm 0.04$ , however, the value of  $\Delta F_3 \approx 0.19$ , characterizing the complex with three PriA molecules, indicates that association of the third enzyme molecule induces a quenching of the nucleic acid fluorescence (Figures 3.2a)<sup>92</sup>.

#### **3.4.4 Binding of PriA to Unmodified dsDNA. Lattice Competition Titration Experiments.**

In order to make sure that the presence of the fluorescent marker has no effect on the binding process, quantitative analysis of the PriA helicase binding to unmodified dsDNA 10-mer has been performed using the Macromolecular Competition Titration method (MCT)<sup>1,81,87,92,95</sup>. In these studies, we use, as a reference fluorescent nucleic acid, the etheno derivative of the ssDNA 18-mer, dεA(pεA)<sub>17</sub>, whose interactions with the PriA helicase has been extensively studied by the Bujalowski's group<sup>1,56-61,92</sup>. It was established that a single PriA molecule binds ssDNA 18-mer and the association process is accompanied by a large fluorescence increase originating from the oligomer<sup>1,56-61,92</sup>. Recall, that for the fluorescein labeled dsDNA 10-mer, the partition function,  $Z_{10}$ , is described by equation 3.1 (section 3.4.3). The partition function for the reference ssDNA 18-mer is:

$$Z_{18} = 1 + K_R P_F \quad (3.8)$$

where  $K_R$  is the macroscopic binding constant of the PriA helicase to the 18-mer<sup>92</sup>. The concentration of PriA, bound to the reference and unmodified nucleic acid,  $P_b$ , at total concentrations  $M_{TR}$  and  $M_{TS}$ , respectively, is then:

$$P_b = (\Sigma\Theta_i)_R M_{TR} + (\Sigma\Theta_i)_S M_{TS} \quad (3.9)$$

and

$$P_b = \left[ \frac{K_R P_F}{Z_{18}} \right] M_{TR} + \left[ \frac{(N-n+1) K_{10S} P_F + 2 \omega_S (K_{10S} P_F)^2}{Z_{10}} \right] M_{TS} \quad (3.10)$$

where  $(\Sigma\Theta_i)_R$  and  $(\Sigma\Theta_i)_S$  are the total average degree of binding of the protein on the reference 18-mer and unmodified dsDNA 10-mer, respectively<sup>92</sup>.  $K_{10S}$ , and  $\omega_S$  are intrinsic binding constant and the cooperativity parameter for the unmodified dsDNA 10-mer<sup>92</sup>. The observed relative fluorescence increase of the reference nucleic acid,  $\Delta F$ , is then

$$\Delta F = \Delta F_{\max} \left[ \frac{K_R P_F}{1 + K_R P_F} \right] \quad (3.11)$$

where

$$P_F = P_T - P_b \quad (3.12)$$

and  $P_T$  is the total concentration of the PriA helicase<sup>92</sup>. Both, binding constant of PriA for the ssDNA 18-mer,  $K_R = (1.6 \pm 0.3) \times 10^6 M^{-1}$ , and, maximum relative fluorescence

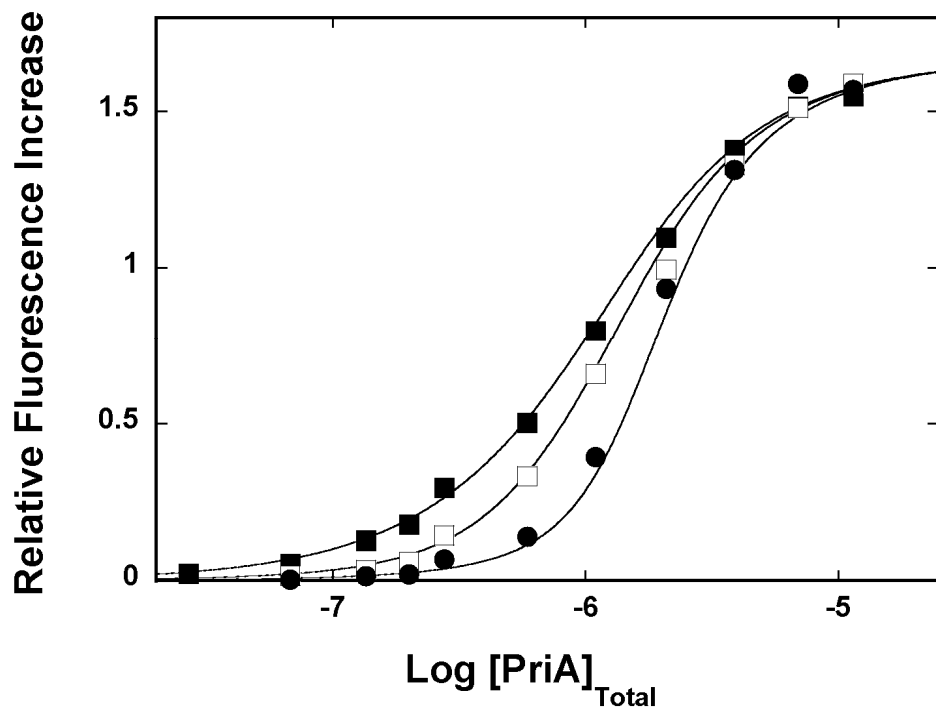


**Figure 3.4 Lattice Competition Titration.** Fluorescence titrations of the fluorescent reference ssDNA 18-mer, dεA(pεA)<sub>17</sub> [ $1 \times 10^{-6}$  M] with the PriA protein in the absence (■) and presence of two different concentrations of the unmodified dsDNA 10-mer:  $1.5 \times 10^{-7}$  M (□) and  $5 \times 10^{-7}$  M (●)<sup>92</sup>. The continuous lines are nonlinear least-squares fits of the titration curves using equations 3.8 – 3.11 (section 3.4.4) with the binding constant for dεA(pεA)<sub>17</sub>,  $K_{18}=1.6 \times 10^6 \text{ M}^{-1}$  and  $\Delta F_{\text{max}} = 1.67$ , and the intrinsic binding constant,  $K_{10S} = 8 \times 10^6 \text{ M}^{-1}$  and  $\omega_S = 6$ , for the unmodified dsDNA 10-mer<sup>92</sup>.

increase associated with this process,  $\Delta F_{\max} = 1.7 \pm 0.05$ , have been determined in independent fluorescence titrations in the absence of the unmodified oligomer<sup>1,56-61,92</sup>.

Fluorescence titrations of dεA(pεA)<sub>17</sub>, with the PriA helicase, in the absence and presence of two different concentrations of the unmodified dsDNA 10-mer, are shown in Figure 3.4<sup>92</sup>. A significant shift of the binding isotherm, in the presence of unmodified dsDNA 10-mer, indicates efficient competition with dεA(pεA)<sub>17</sub> for the PriA helicase<sup>1,81,87,92,95</sup>. The solid lines in Figure 3.4 are nonlinear least squares fits of the experimental titrations with  $K_{10S}$  and  $\omega_S$  as independent fitting parameters, using equations 3.8 – 3.12<sup>92</sup>. The binding constant is  $K_{10S} = (8 \pm 1.5) \times 10^6 \text{ M}^{-1}$  and the cooperativity parameter,  $\omega_S = 6 \pm 2$ <sup>92</sup>. It is clear that binding of the enzyme to unmodified dsDNAs is characterized by parameters very similar to the parameters describing the enzyme binding to the fluorescein-labeled 10-mer ( $K_{10} = (1.6 \pm 0.6) \times 10^7 \text{ M}^{-1}$  and  $\omega_S = 10 \pm 3$ )<sup>92</sup>. In other words, the presence of the fluorescein marker has a very little effect on the enzyme interactions with dsDNA and can be proficiently used to monitor the binding process<sup>92</sup>. Notice, the strong competition of the dsDNA with the ssDNA oligomer clearly shows that both nucleic acids bind to the same DNA-binding site of the enzyme<sup>92</sup>.

#### **3.4.5 Salt Effect on the PriA – dsDNA 10-mer Complex Formation.**

To better understand the nature of PriA – dsDNA interactions the salt effect on the association process was examined<sup>92</sup>. Fluorescence titrations of the 5'-Fl-dsDNA 10-mer with the PriA helicase, in buffer C505, containing different NaCl concentrations, are shown in Figure 3.5a<sup>92</sup>. Increasing salt concentration significantly decreases the affinity of the enzyme for the DNA<sup>92</sup>. The solid lines in Figure 3.5a are nonlinear least squares fits of the experimental titration curves to equations 3.1 – 3.3 (section 3.4.3)<sup>92</sup>. The

dependence of the logarithm of the intrinsic binding constant,  $K_{10}$ , and cooperativity parameter,  $\omega$ , upon the logarithm of the NaCl concentration (log-log plots), are shown in Figure 3.5b and Figure 3.5c, respectively<sup>1,27,81,83,84,92</sup>. The plots are linear, within experimental accuracy, giving the slopes  $\partial \log K_{10} / \partial \log [\text{NaCl}] = - 3.1 \pm 0.5$  and  $\partial \log \omega / \partial \log [\text{NaCl}] = - 1 \pm 0.3$ , respectively<sup>92</sup>. Hence, the net release of  $\sim 3$  and  $\sim 1$  ions accompanies the intrinsic and cooperative interactions<sup>1,27,81,83,84,92</sup>. The salt effect on the intrinsic affinity observed here is very similar to analogous salt effect on the enzyme complex with the ssDNA<sup>56-58,92</sup>. Contrary to the complex with the ssDNA, where cooperativity increases with the increase of NaCl concentration, the cooperativity of PriA binding to the dsDNA decreases with the increase of NaCl concentration<sup>56-58,92</sup>.

#### **3.4.6 The Effect of Temperature on the Intrinsic and Cooperative PriA – dsDNA 10-mer Interactions.**

Further, the nature of the intrinsic and cooperative interactions in the PriA - dsDNA complex were studied by examining the temperature effect on the enzyme binding to the dsDNA 10-mer<sup>27,81,92</sup>. Fluorescence titrations representing 5'-Fl-dsDNA 10-mer interaction with the PriA helicase, performed at different temperatures, are shown in Figure 3.6a<sup>92</sup>. The behavior of the system is very complex and in the range from 5°C to 10°C, the values of  $\Delta F_{\text{max}}$  slightly increase with the increase in temperature<sup>92</sup>. As the temperature increases from 10°C to 20°C, the relative fluorescence increase, decreases<sup>92</sup>. It should be mentioned that in examined temperature range (from 5°C to 20°C), the dsDNA fully preserves its duplex structure (section 3.3.3)<sup>92</sup>. Thus, the data representing temperature effect on the PriA – dsDNA interactions provide a strong indication that the structure of the PriA enzyme undergoes significant changes as the temperature of the sample increases<sup>92</sup>. The solid lines in Figure 3.6a are nonlinear least squares fits of the



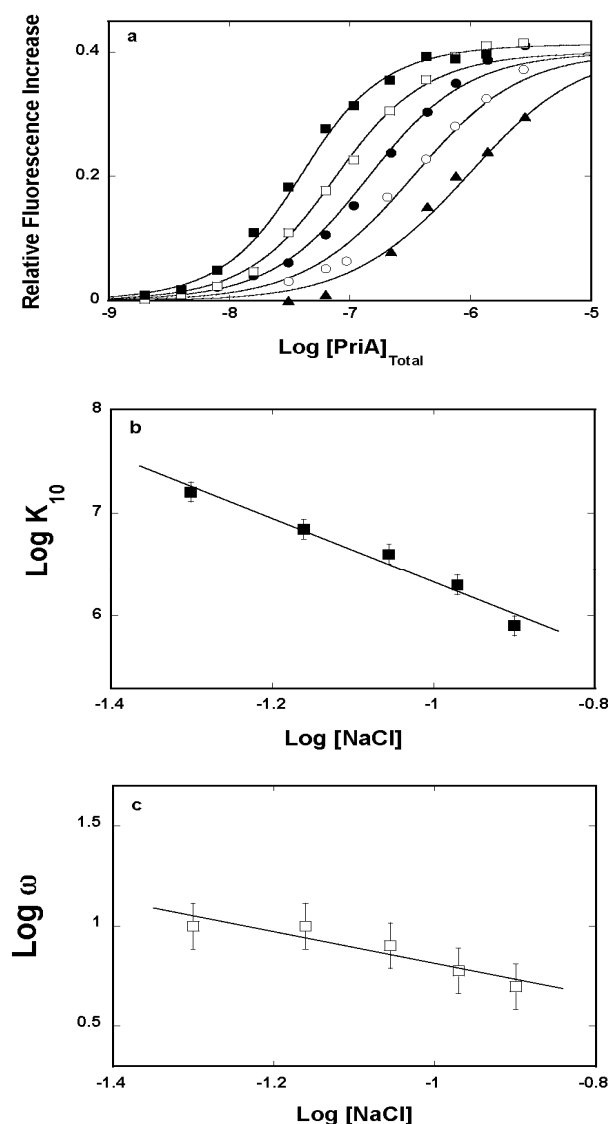


**Figure 3.5 Salt effect on the intrinsic and cooperative PriA – dsDNA 10-mer interactions.** **a.** Fluorescence titrations of the 5'-Fl-dsDNA 10-mer with the PriA protein at different NaCl concentrations: 50 mM (■), 69 mM (□), 88 mM (●), 107 mM (○), 126 mM (▲)<sup>92</sup>. The continuous lines are nonlinear least-squares fits of the titration curves to the model described by equations 3.1 – 3.3 with  $\Delta F_1 = 0.124$  and  $\Delta F_{\max} = 0.4$ , and  $K_{10}$  and  $\omega$  as follows:  $1.6 \times 10^7 \text{ M}^{-1}$  and 10 (■),  $7.0 \times 10^6 \text{ M}^{-1}$  and 10 (□),  $4.0 \times 10^6 \text{ M}^{-1}$  and 8 (●),  $2.0 \times 10^6 \text{ M}^{-1}$  and 6 (○),  $8.0 \times 10^5 \text{ M}^{-1}$  and 5 (▲)<sup>92</sup>. **b.** The dependence of the logarithm of the intrinsic binding constant,  $K_{10}$ , upon the logarithm of NaCl concentration. The continuous line is a linear least squares fit, which provides the slope  $\partial \log K_{10} / \partial \log [\text{NaCl}] = -3.1 \pm 0.6$ <sup>92</sup>. **c.** The dependence of the logarithm of the cooperativity parameter,  $\omega$ , upon the logarithm of NaCl concentration<sup>92</sup>. The continuous line is a linear least-squares fit, which provides the slope  $\partial \log \omega / \partial \log [\text{NaCl}] = -1 \pm 0.3$ <sup>92</sup>.

experimental titration curves using equations. 3.1 – 3.3 (section 3.4.3)<sup>92</sup>.

Figure 3.6b shows the dependence of the natural logarithm of the intrinsic binding constant,  $K_{10}$ , upon the reciprocal of temperature (Kelvin) (van't Hoff plot)<sup>92,95</sup>. Even though the error in determining  $K_{10}$  is large, the plot is, without a doubt, nonlinear<sup>92,95</sup>. The value of  $K_{10}$  decreases as the temperature decreases and arrives at a minimum around  $\sim 10$  °C, from where it starts to increase as the temperature continues to drop<sup>92</sup>. As a result, the observed nonlinear van't Hoff plot in Figure 3.6b indicates that there are two temperature-dependent binding processes in the enzyme association with dsDNA 10-mer<sup>66,92,95</sup>.

The simplest thermodynamic model, which could explain the experimentally determined nonlinear behavior of the van't Hoff plot in Figure 3.6b, includes a transition of the PriA helicase between two conformations and the binding of the dsDNA 10-mer to each conformation with different intrinsic affinities, described as



where  $P_L$  is the conformation of the PriA in the low temperature range,  $P_H$  is the corresponding conformation of the enzyme in the high temperature range<sup>66,92,95</sup>.  $C_{11}$ ,  $C_{12}$ ,  $C_{21}$ , and  $C_{22}$  are complexes of the helicase with the 10-mer, containing one or two enzyme molecules, with the low-temperature and high-temperature conformation of the helicase, respectively<sup>66,92,95</sup>.  $K_C$ , is the equilibrium constant characterizing the transition,

$P_L < - > P_H$ , while the binding of the enzyme in the  $P_L$  and  $P_H$  conformation is described by the intrinsic binding constants,  $K_{10L}$  and  $K_{10H}$ , respectively. The overall intrinsic binding constant,  $K_{ov}$ , is then defined by<sup>92,95</sup>

$$K_{ov} = \frac{K_{10L} + K_{10H}K_C}{1 + K_C} \quad (3.16)$$

The temperature dependence of the equilibrium constants present in equation 3.16 are described by

$$K_{10L} = K_{10L}(T_R) \exp \left[ -\frac{\Delta H_{10L}}{R} \left( \frac{1}{T} - \frac{1}{T_R} \right) \right] \quad (3.17)$$

$$K_{10H} = K_{10H}(T_R) \exp \left[ -\frac{\Delta H_{10H}}{R} \left( \frac{1}{T} - \frac{1}{T_R} \right) \right] \quad (3.18)$$

$$K_C = K_C(T_R) \exp \left[ -\frac{\Delta H_C}{R} \left( \frac{1}{T} - \frac{1}{T_R} \right) \right] \quad (3.19)$$

$K_{10L}(T_R)$  and  $K_{10H}(T_R)$ , are the intrinsic binding constants of the helicase in the  $P_L$  and  $P_H$  conformations at a reference temperature,  $T_R$ <sup>92</sup>.  $K_C(T_R)$  is the equilibrium constant describing the enzyme conformational transition at  $T_R$ <sup>92</sup>.  $\Delta H_{10L}$  and  $\Delta H_{10H}$  are the enthalpy changes characterizing the enzyme binding in the  $P_L$  and  $P_H$  conformation, respectively<sup>92</sup>.  $\Delta H_C$  is the enthalpy change representing the transition,  $P_L < - > P_H$ <sup>92</sup>. The reference temperature,  $T_R$ , is 10°C, for the low and 20°C for the high temperature conformation, respectively<sup>92</sup>. The reference temperature for the  $P_L < - > P_H$  transition is taken at 10°C<sup>92</sup>. The values of  $K_{10L}(T_R)$  and  $K_{10H}(T_R)$  are experimentally available, however, other

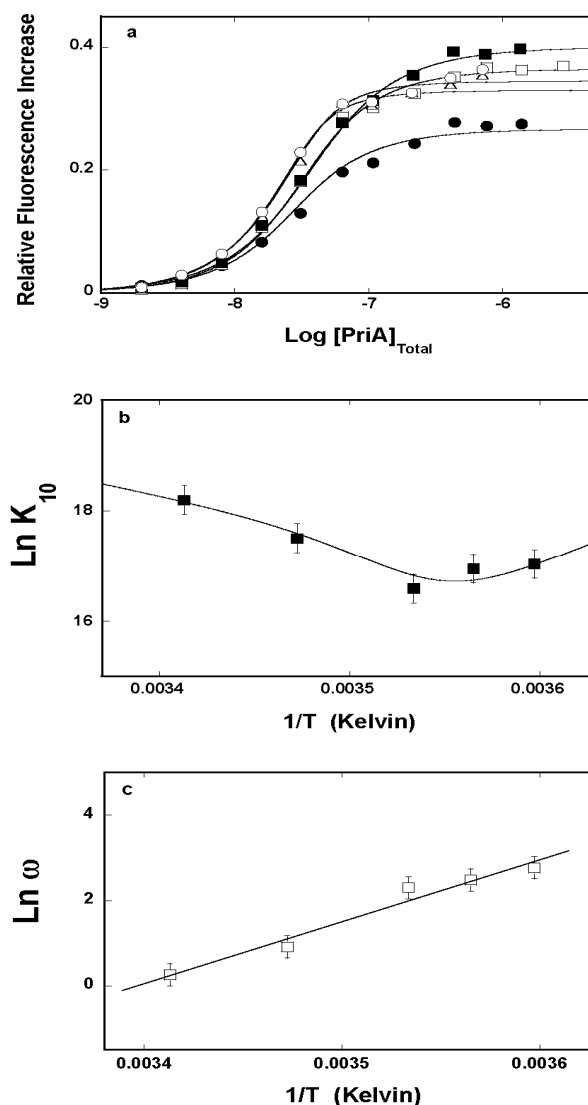


**Figure 3.6 Temperature effect on the intrinsic and cooperative PriA – dsDNA 10-mer interactions.** **a.** Fluorescence titrations of the 5'-Fl-dsDNA 10-mer [ $1.5 \times 10^{-8}$  M] with the PriA protein at different temperatures (°C): 5 ( $\Delta$ ), 7.5 ( $\circ$ ), 10 ( $\blacksquare$ ), 15 ( $\square$ ), and 20 ( $\bullet$ ). The continuous lines are nonlinear least-squares fits of the titration curves, using the model described by equations 3.1 – 3.3<sup>92</sup>. **b.** The dependence of the natural logarithm of the intrinsic binding constant,  $K_{10}$ , upon the reciprocal of the temperature (van't Hoff plot)<sup>92</sup>. The continuous line is the nonlinear least squares fit of the experimental plot to the model of binding of two PriA molecules in two different conformations, defined by equations 3.16 – 3.19<sup>92</sup>. **c.** The dependence of the natural logarithm of the cooperativity parameter,  $\omega$ , upon the reciprocal of temperature<sup>92</sup>. The continuous line is a linear least-squares fit, which provides the slope  $\Delta H_{\omega} = -28.9$  kcal/mol<sup>92</sup>.

parameters, in equations 3.16 – 3.19, must be estimated from the plot in Figure 3.6b<sup>92</sup>. The slopes in the low and high temperature range supply the estimates of enthalpy changes characterizing the enzyme binding in the P<sub>L</sub> and P<sub>H</sub> conformation,  $\Delta H_{10L} = 14 \pm 6$  kcal/mol and  $\Delta H_{10H} = -27 \pm 11$  kcal/mol<sup>92</sup>. As a consequence, there are only two unknown parameters,  $K_C(T_R)$  and  $\Delta H_C$ <sup>92</sup>. The solid line in Figure 3.6b is the nonlinear least squares fit of the plot to equations 3.16 – 3.19 providing  $K_C(10^\circ\text{C}) = 0.1 \pm 0.05$  and  $\Delta H_C = 60 \pm 30$  kcal/mol<sup>92</sup>. Even though there is a considerable error in these parameters, the value of  $\Delta H_C$  suggests that the PriA protein endures a significant structural transition, characterized by a large positive enthalpy change<sup>92</sup>. The value of  $K_C(10^\circ\text{C})$  indicates that below  $\sim 10^\circ\text{C}$ , the PriA helicase exists in the P<sub>L</sub> state<sup>92</sup>. On the other hand, introducing the value of  $\Delta H_C$  into equation 3.19, gives the value of  $K_C \approx 4$  already at  $20^\circ\text{C}$ , indicating that the enzyme is in the P<sub>H</sub> state in the high temperature range<sup>92</sup>.

The dependence of the natural logarithm of the cooperativity parameter,  $\omega$ , upon the reciprocal of temperature, in Figure 3.6c, looks dramatically different from the intrinsic affinity plot (Figure 3.6b)<sup>92</sup>. Within experimental accuracy, the plot is linear, and the values of  $\omega$  decrease as the temperature increases<sup>92</sup>. The slope of the plot provides  $\Delta H_\omega = -29 \pm 10$  kcal/mole<sup>92</sup>. The cooperative interactions strongly decrease with temperature; furthermore, the value of  $\Delta H_\omega$  indicates that at temperature higher than  $20^\circ\text{C}$ , the enzyme binding to the dsDNA is characterized by negative cooperativity<sup>92</sup>.

#### **3.4.7 The Effect of Nucleotide Cofactors on the Intrinsic and Cooperative PriA – dsDNA 10-mer Interactions.**

As indicated above, the PriA helicase possesses two strong and weak nucleotide-binding sites, which dramatically affect the enzyme interactions with the ssDNA, particularly in the presence of ADP (Figure 2.3)<sup>27,59-61,92</sup>. Therefore, in the next set of

experiments, we examined the effect of ADP and the ATP nonhydrolyzable analog, ATP $\gamma$ S, on the PriA – dsDNA interactions<sup>92</sup>. Fluorescence titrations of the 5'-FI-dsDNA 10-mer with the PriA helicase at two different nucleic acid concentrations, in buffer C505, containing  $1 \times 10^{-5}$  M ADP, are shown in Figure 3.7a<sup>92</sup>. Only the strong nucleotide-binding site of the PriA helicase is saturated with the cofactor at this ADP concentration<sup>27,59-61,92</sup>. The maximum relative fluorescence increase,  $\Delta F_{\max}$ , obtained in this experiment is  $\sim 0.3$ , which is lower than  $\sim 0.4$  found in the absence of nucleotide cofactors (Figure 3.1 and Table 3.1)<sup>92</sup>. The dependence of the relative fluorescence increase,  $\Delta F$ , as a function of the total average degree of binding,  $\Sigma\Theta_i$ , of the PriA protein on the 5'-FI-dsDNA 10-mer is shown in Figure 3.7b<sup>92</sup>. Within experimental accuracy, the plot is linear, a behavior which is also different from the one observed in the absence of the cofactors (Figure 3.1b)<sup>92</sup>. The value of  $\Sigma\Theta_i$ , could be determined up to  $\sim 1.2$ , and extrapolation of the plot to the maximum value of the relative fluorescence increase,  $\Delta F_{\max} = 0.29 \pm 0.03$ , gives the maximum value of  $\Sigma\Theta_i = 2.2 \pm 0.2$ <sup>92</sup>. Thus, at saturation, two PriA molecules, with the strong nucleotide-binding site associated with ADP, bind to the 10-mer<sup>92</sup>. The spectroscopic titration curves in Figure 3.7a have been analyzed using the binding model described above (section 3.4.3)<sup>92</sup>. The solid lines in Figure 3.7a are the nonlinear least squares fits of the titration curves to equations 3.1 – 3.3 with  $K_{10}$  and  $\omega$  as fitting parameters (section 3.4.2 and Table 3.1)<sup>92</sup>. Exclusive saturation of the strong nucleotide-binding site with ADP has a very modest effect on the value of the intrinsic binding constant,  $K_{10}$ , which is diminished only by a factor of  $\sim 2$ <sup>92</sup>. Notice, the dramatic effect observed in the case of the cooperativity parameter, which increases by a factor of  $\sim 5$  (Table 3.1)<sup>92</sup>. These results, as well as different values of  $\Delta F_1$  and  $\Delta F_{\max}$ , point toward the fact that the orientation of the enzyme on the dsDNA is affected by the bound cofactor<sup>92</sup>.

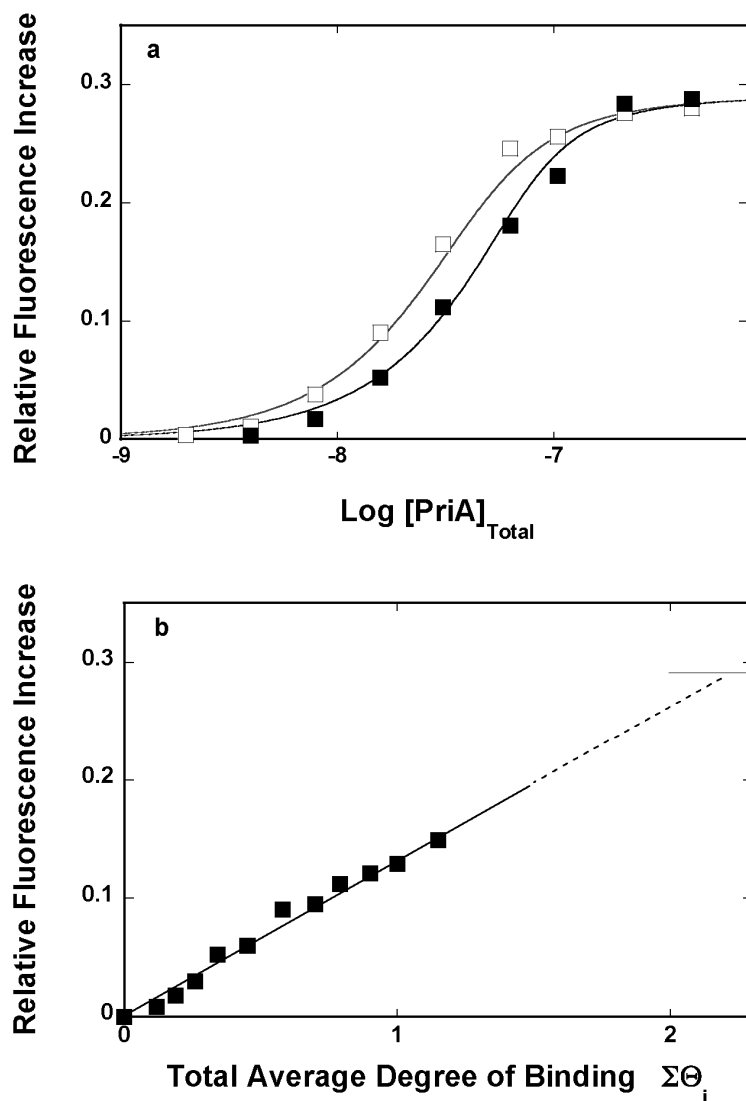


**Figure 3.7** The effect of saturation of the strong nucleotide binding site of PriA with ADP on the intrinsic and cooperative PriA – dsDNA 10-mer interactions. **a.** Fluorescence titrations of the 5'-Fl-dsDNA 10-mer with the PriA helicase in the presence of  $1 \times 10^{-5}$  M ADP, at two different nucleic acid concentrations:  $1 \times 10^{-8}$  M (□) and  $2.5 \times 10^{-8}$  M (■) (oligomer). The continuous lines are nonlinear least-squares fits of the titration curves, using the statistical thermodynamic model described by equations 3.1 – 3.3. **b.** Dependence of the relative fluorescence increase of the dsDNA 10-mer,  $\Delta F$ , upon the total average degree of binding of PriA helicase on the nucleic acid (■). The continuous line follows the experimental points and has no theoretical basis. The broken line is the extrapolation of  $\Delta F$  to  $\Delta F_{\max} = 0.29$ <sup>92</sup>.

Radically different behavior is observed when both nucleotide-binding sites of the PriA helicase are saturated with ADP<sup>92</sup>. Fluorescence titrations of the 5'-Fl-dsDNA 10-mer with the PriA helicase at two different nucleic acid concentrations, in buffer C505, containing  $3 \times 10^{-3}$  M ADP, are shown in Figure 3.8a<sup>92</sup>. At this ADP concentration, both the strong and the weak nucleotide-binding sites are saturated with the nucleotide<sup>27,59-61,92</sup>. The maximum relative fluorescence increase,  $\Delta F_{\max}$ , is  $\sim 0.9$ , which is significantly higher than  $\sim 0.4$  and  $\sim 0.3$  obtained in the absence, or with only the strong nucleotide-binding site saturated with ADP (Table 3.1)<sup>92</sup>. The dependence of the relative fluorescence increase,  $\Delta F$ , as a function of the total average degree of binding,  $\Sigma\Theta_i$ , of the PriA protein on the 5'-Fl-dsDNA 10-mer is shown in Figure 3.8b<sup>92</sup>. Again, the plot is nonlinear, as observed in the absence of the nucleotide cofactors, indicating the presence of two binding phases (Figure 3.1b)<sup>92</sup>. The value of  $\Sigma\Theta_i$ , was determined up to  $\sim 1.6$  with binding of the first PriA molecule characterized by  $\Delta F_1$  of  $0.21 \pm 0.03$ <sup>92</sup>. In the second binding phase,  $\Delta F$  strongly increases and extrapolation of the plot to  $\Delta F_{\max} = 0.93 \pm 0.03$ , gives the maximum value of  $\Sigma\Theta_i = 2.0 \pm 0.2$ <sup>92</sup>. Hence, saturation of both nucleotide-binding sites with ADP does not affect the stoichiometry of the PriA - dsDNA complex<sup>27,59-61,92</sup>. Analysis of the titration curves in Figure 3.8a has been performed as described above for the analogous studies in the absence of the cofactors (section 3.4.2)<sup>92</sup>.  $\Delta F_1$  and  $\Delta F_{\max}$  are both known and the solid lines in Figure 3.8a are the nonlinear least squares fits of the experimental titration curves to equations 3.1 – 3.3, with  $K_{10}$  and  $\omega$  as the fitting parameters (Table 3.1)<sup>92</sup>. It looks like the saturation of both the strong and the weak nucleotide-binding site with ADP dramatically increases the intrinsic binding constant,  $K_{10}$ , from  $\sim 1.6 \times 10^7 \text{ M}^{-1}$  to  $\sim 1.3 \times 10^8 \text{ M}^{-1}$  (Table 3.1)<sup>92</sup>. Interestingly, when corrected for the difference in salt concentrations, the affinity for dsDNA is  $\sim 2$  and  $\sim 1$  orders higher than the intrinsic affinities obtained for homo-purine and homo-pyrimidine



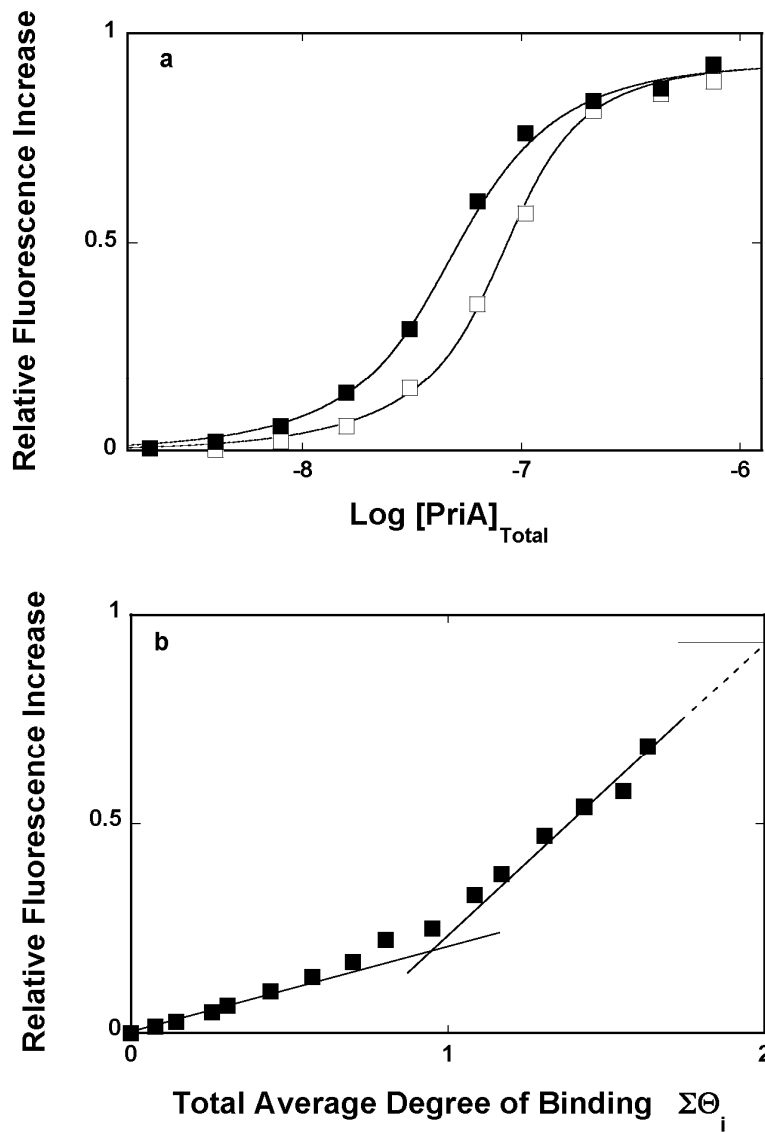


**Figure 3.8 The effect of saturation of both nucleotide binding sites of PriA with ADP on the intrinsic and cooperative PriA – dsDNA 10 – mer interactions. a.** Fluorescence titrations of the 5'-Fl-dsDNA 10-mer with the PriA helicase in the presence of  $3 \times 10^{-5}$  M ADP, at two different nucleic acid concentrations:  $1 \times 10^{-8}$  M (■) and  $2.5 \times 10^{-8}$  M (□) (oligomer)<sup>92</sup>. The continuous lines are nonlinear least-squares fits of the titration curves, using the statistical thermodynamic model described by equations 3.1 – 3.3<sup>92</sup>. **b.** Dependence of the relative fluorescence increase of the dsDNA 10-mer,  $\Delta F$ , upon the total average degree of binding of PriA helicase on the nucleic acid (■)<sup>92</sup>. The continuous line follows the experimental points and has no theoretical basis. The broken line is the extrapolation of  $\Delta F$  to  $\Delta F_{\max}=0.93$ <sup>92</sup>.

ssDNA, respectively<sup>1,27,56-59,92</sup>. On the other hand, the cooperativity parameter,  $\omega \sim 2$  is strongly diminished by a factor of  $\sim 23$  as compared to  $\omega \sim 45$ , in the situation when only the strong nucleotide-binding site is engaged in interactions with ADP<sup>92</sup>. In addition, the values of the spectroscopic parameters  $\Delta F_1$  and  $\Delta F_{\max}$  are significantly higher than the values of the same parameters obtained in the absence of the nucleotide cofactors, or at the low ADP concentration, which is a good indication that the orientation of the enzyme on the dsDNA is affected when both nucleotide sites are saturated with ADP<sup>27,92</sup>.

At the same time, different behavior is observed when the nucleotide-binding sites of PriA are engaged in interactions with ATP $\gamma$ S<sup>92</sup>. The use of this nonhydrolyzable analog of ATP is dictated by the fact that the PriA helicase does not hydrolyze it on the time scale of the binding experiments, both in the absence or the presence of the dsDNA<sup>27,56-61,92</sup>. Fluorescence titrations of the 5'-Fl-dsDNA 10-mer with the PriA helicase in buffer C505, containing  $1 \times 10^{-4}$  M and  $3 \times 10^{-3}$  M ATP $\gamma$ S, are shown in Figure 3.9<sup>92</sup>. For comparison, titrations of the 5'-Fl-dsDNA 10-mer, at the same nucleic acid concentration, in the presence of low and high concentrations of ADP are included in Figure 3.9 as well<sup>92</sup>. Analysis of the titration curves in the presence of ATP $\gamma$ S has been performed as described above, using equations 3.1 – 3.3 (Table 3.1)<sup>92</sup>. The difference between the effects of the saturation of the two nucleotide-binding sites with the nucleoside di-phosphate or nucleoside tri-phosphate is stunning<sup>92</sup>. Both the low and high ATP $\gamma$ S concentrations stimulate, within experimental accuracy, the same maximum relative increases of the nucleic acid fluorescence with,  $\Delta F_1$ , virtually the same and similar to the emission changes accompanying the enzyme binding in the absence of any cofactor, or in the presence of low ADP concentration (Table 3.1)<sup>92</sup>. Exclusive saturation of the strong nucleotide-binding site with ATP $\gamma$ S lowers the intrinsic binding constant,

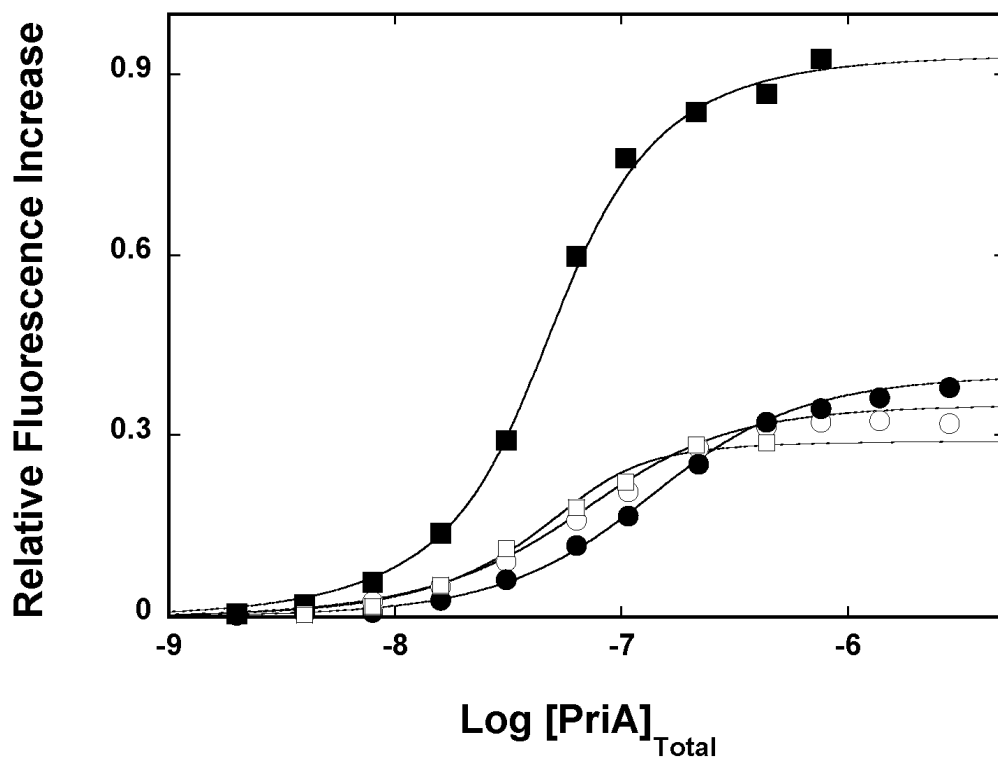


**Figure 3.9 The effect of nucleotides on the intrinsic and cooperative PriA – dsDNA 10-mer interactions.** Fluorescence titrations of the 5'-Fl-dsDNA 10-mer [ $2.5 \times 10^{-8}$  M (oligomer)] with the PriA helicase in the presence of  $1 \times 10^{-5}$  M (○) ATPγS,  $3 \times 10^{-5}$  M (●) ATPγS,  $1 \times 10^{-5}$  M (□) and  $3 \times 10^{-5}$  M (■) ADP. The continuous lines are nonlinear least-squares fits of the titration curves, using the statistical thermodynamic model described by equations 3.1 – 3.3 <sup>92</sup>.

$K_{10}$ , by a factor of  $\sim 2.5$ , while saturation of both nucleotide-binding sites lowers the intrinsic affinity by a factor  $\sim 5$  (Table 3.1)<sup>92</sup>. Therefore, in the presence ATP $\gamma$ S, the enzyme has the lowest intrinsic affinity of all examined enzyme states with or without the cofactors<sup>92</sup>. Interestingly, ATP $\gamma$ S does not affect the cooperativity of PriA binding to dsDNA, which, in this case, remains the same or slightly higher than in the absence of nucleotide cofactors (Table 3.1)<sup>92</sup>.

#### **3.4.9 Photo – Cross – Linking of the PriA Helicase to ssDNA.**

The involvement of PriA domains in the interactions with the ss and the dsDNA has been addressed using the UV irradiation<sup>40,81,92,93</sup>. UV irradiation produces covalent linkage between nucleic acid bases and amino acid residues, resulting in a "zero-length" cross-linking with minimal perturbation to the protein - nucleic acid complex<sup>40,81,92,93</sup>. Among the nucleic acid bases, thymine is by far the most reactive in the photo-cross-linking reactions, therefore, parallel to the thermodynamic studies, we performed photo-cross-linking experiments of the PriA protein complex with the radioactive [<sup>32</sup>P]-dT<sub>20</sub> (section 3.3.8)<sup>40,81,92,93</sup>. Recall, in the absence of cofactors, only a single PriA molecule, using its strong DNA-binding subsite, associates with the ssDNA 20-mer<sup>27,56-58,92</sup>. As shown by the Lattice Competition Titration in section 3.4.4 both the ssDNA and the dsDNA compete for the same binding site, that is, the dsDNA also binds to the strong DNA-binding subsite<sup>92</sup>. Since the X-ray structure of the PriA helicase is unknown, the location of strong DNA-binding subsite within the domain structure of the enzyme is unknown<sup>92</sup>. [<sup>32</sup>P]-dT<sub>20</sub>, photo-cross-links with the PriA protein more efficiently than the dsDNA, therefore, it was used in this experiment<sup>92</sup>.

The following strategy was applied to address the domain-location of the strong DNA-binding subsite of the PriA enzyme<sup>92</sup>. Trypsin digestion of the PriA protein, in the

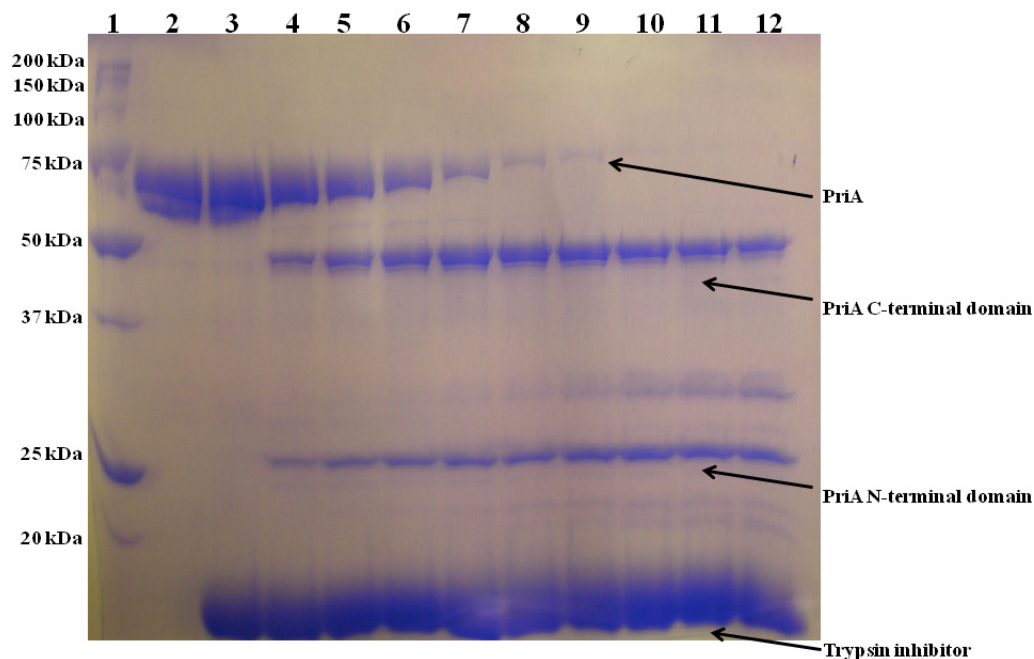


**Figure 3.10 Trypsin digestion of the PriA helicase.** 10% SDS polyacrylamide gel of the PriA protein subjected to the time-dependent trypsin digestion and stained with Coomassie Brilliant Blue<sup>92</sup>. Lanes in the gel are as follows: 1, molecular markers, 2, PriA, 3, PriA and trypsin inhibitor, 4 - 12 time-dependant trypsin digestion reaction. Lane 4, 1 min; lane 5, 3 min; lane 6, 5 min; lane 7, 10 min; lane 8, 20 min; lane 9, 30 min; lane 10, 45 min; lane 11, 60 min; lane 12, 90 min<sup>92</sup>.

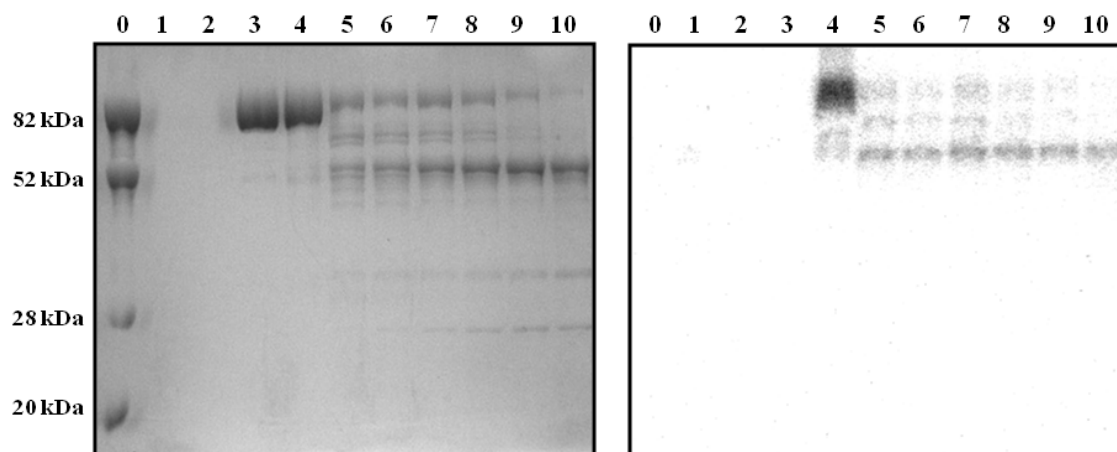


**Figure 3.11 Time dependent trypsin digestion coupled with photo – cross – linking experiments. a.** 10% SDS polyacrylamide gel of the PriA protein – [<sup>32</sup>P]-dT<sub>20</sub> complex subjected to the time-dependent trypsin digestion and stained with Coomassie Brilliant Blue<sup>92</sup>. The lannes in the gel are as follows: 0, contains the molecular markers; 1, contains 5'-[<sup>32</sup>P]-dT<sub>20</sub> alone without irradiation; 2, contains 5'-[<sup>32</sup>P]-dT<sub>20</sub> alone after irradiation; 3, contains the PriA protein-[<sup>32</sup>P]-dT<sub>20</sub> complex in the absence of the protease prior to irradiation; 4, contains the PriA protein-[<sup>32</sup>P]-dT<sub>20</sub> complex, in the absence of the protease after irradiation; 5 to 10 contain the PriA protein-[<sup>32</sup>P]-dT<sub>20</sub> complex in the presence of the constant trypsin concentration, collected at different time intervals of the digestion reaction<sup>92</sup>. Lane 5, 1 min; lane 6, 3 min; lane 7, 5 min; lane 8, 10 min; lane 9, 20 min; lane 10, 30 min. **b.** Autoradiogram of the same 10% SDS polyacrylamide gel of the PriA protein – [32P]-dT<sub>20</sub> complex, as shown in panel **a.**<sup>92</sup>.

presence and absence of the ssDNA (dT<sub>20</sub>), yields the large fragment of the protein (helicase domain of ~ 500 amino acids), and two smaller fragments, one of which was shown to correspond to ~ 210 amino acids of the N-terminal domain. The identity of the protein fragments were confirmed by mass spectrometry (Figure 3.10, section 3.3.8)<sup>92,97,98</sup>. The digestion experiments have been performed using the UV photo-cross-linked PriA - [<sup>32</sup>P]-dT<sub>20</sub> complex, at PriA concentration, which completely saturates the nucleic acid<sup>27,56-61,92</sup>. Figure 3.11a illustrates SDS-PAGE, stained with Coomassie Brilliant Blue, of UV irradiated PriA protein - [<sup>32</sup>P]-dT<sub>20</sub> sample, in the presence of trypsin, as a function of time<sup>92</sup>. The full length PriA protein band at ~ 82,000 diminishes with time as the band corresponding to the helicase domain (~ 53,000) and two fragments corresponding to the N-terminal domain (~ 26,000 and ~ 35,000) appear<sup>92</sup>. Figure 3.11b shows the autoradiogram of the same gel<sup>92</sup>. Two dominant radioactive bands appear on the gel, at the molecular weight of ~ 85,000, and ~ 55,000, corresponding to the PriA protein and the helicase domain complex with [<sup>32</sup>P]-dT<sub>20</sub><sup>92</sup>. The nucleic acid only slightly affects PriA's gel mobility in the cross-linked PriA protein - and helicase domain - DNA complex<sup>92</sup>. It is evident that the strong DNA-binding subsite, which is able to engage both the ss and the dsDNA, is located on the large helicase domain of the PriA protein<sup>92</sup>. This is in excellent agreement with the proposed location of the strong DNA-binding subsite, based on quantitative thermodynamic and kinetic studies<sup>27,56-61,92</sup>.

### **3.5 DISCUSSION**

#### **3.5.1 The Helicase Engages Only the Strong DNA-Binding Subsite in Interactions with the dsDNA.**

The strong DNA-binding subsite of the PriA helicase occludes only 5 - 7 nucleotides, at the same time, the orientation of PriA molecule bound to the ssDNA is

such that the enzyme always occludes  $\sim 20$  nucleotides. (Figure 2.3)<sup>27,56-61,92</sup>. Interestingly, the total site-size of the PriA - dsDNA complex determined in this work, is  $n = 5 \pm 1$  bps, and is dramatically lower than the total site-size of the PriA - ssDNA complex<sup>27,56-61,92</sup>. There are two significant aspect of this finding. First and foremost, the site-size of the complex is, within experimental accuracy, identical to the site-size of the strong DNA-binding subsite, pointing toward the fact that the helicase exclusively engages the strong DNA-binding subsite in interactions with the dsDNA<sup>27,56-61,92</sup>. It is also evident in the competition experiments where the PriA helicase efficiently commpeets for the dsDNA<sup>27,56-61,92</sup>. Second, in order to achieve such a small total site-size, PriA must assume different orientation in the complex with dsDNA, as compared to the complex with the ssDNA<sup>27,92</sup>. As shown in Chapter 2, in studies of PriA – gapped DNA interactions, the average site-size of the PriA helicase in the gapped DNA complex and PriA – dsDNA complex, must correspond to  $\sim 7 - 10$  nucleotides/bps<sup>27,92</sup>. The total site-size of the PriA - dsDNA complex directly examined here ( $n = 5 \pm 1$  bps) may seem smaller from the observed binding to the gapped DNA<sup>27,92</sup>. The difference results from the fact that the PriA molecule bound to the ssDNA of the gapped DNA structure also engages parts of the dsDNA adjacent to both sides of the ssDNA gap<sup>92</sup>. As a result, only a single PriA molecule is able to bind to each of the duplex DNA parts of the gapped DNA (Figure 2.15)<sup>27,92</sup>.

Notice the nonlinear dependence of  $\Delta F$  as a function of  $\Sigma \Theta_i$  in the Figure 3.1b<sup>92</sup>. This behavior can be easily understood in the context of the statistical thermodynamic model, which provides an excellent description of the binding process (section 3.4.3)<sup>92</sup>. The first bound enzyme molecule experiences multiple potential binding sites and, on average, is at some distance from the fluorescence marker located at the 5' end of the DNA<sup>92</sup>. Because of the fact that the strong DNA-binding subsite is engaged in the



interactions with the dsDNA, the second PriA molecule binds in a closer distance from the marker, inducing a further change of its emission intensity<sup>92</sup>.

### **3.5.2 The Strong DNA – Binding Subsite Is Located on the Helicase Domain of the PriA Helicase. Photo-Cross-Linking Experiments.**

Earlier thermodynamic analysis hinted that the strong DNA-binding subsite is centrally located within the PriA molecule on a protruding domain and, in the absence of the high ADP concentration, exclusively engages the ssDNA (Figure 2.3)<sup>1,27,56-61,92</sup>. Photo-cross-linking data, describe here, unambiguously show that the strong DNA-binding subsite is located on the large helicase domain of the PriA protein<sup>92</sup>. Moreover, the fact that there is no indication of any radioactive band corresponding size to the small N-terminal domain (Figure 3.11b) indicates that, in the absence of the high ADP concentration, the N-terminal domain does not engage the nucleic acid<sup>92</sup>. This is in accord with thermodynamic analysis, which shows that the DNA-binding subsite on the N-terminal domain of PriA can efficiently engage the DNA only when the weak nucleotide-binding site of the helicase is associated with ADP<sup>27,59-61,92</sup>.

### **3.5.3 PriA Preferentially Binds to the dsDNA over the ssDNA.**

As it was indicated in Chapter 2, the PriA helicase may have a significant affinity for a dsDNA, however, the complex structure of the gapped DNA precluded quantitative determination of the intrinsic affinity of PriA for the dsDNA<sup>27,92</sup>. The results presented above (Chapter 3) indicate that this surprising prediction was correct and that, indeed, the PriA helicase has significantly higher intrinsic affinity for the dsDNA, as compared to its intrinsic affinity for the ssDNA<sup>27,56-59,92</sup>. The PriA protein shows a strong preference for the homo-pyrimidine ssDNAs, however, even in this case, the highest intrinsic binding constant for the homo-thymine nucleic acid is  $\sim 1.5 \times 10^6 \text{ M}^{-1}$ , as compared to  $\sim 1.6 \times 10^7$

$M^{-1}$  for the dsDNA (the difference in the salt conditions have been corrected with a use of a log - log plots so that the binding constants could be efficiently compared)<sup>92</sup>. This dramatic difference in the intrinsic binding constant is diminished in the presence of NTP analogs<sup>27,59-61,92</sup>. As a result, the strong DNA-binding subsite of the PriA protein seems to be better geared to accept the dsDNA than the ssDNA<sup>92</sup>. Importantly, when corrected for the difference in the salt concentrations in solution and the statistical effect, in the absence of the nucleotide cofactors, PriA - dsDNA affinity for the duplex determined here ( $\sim 1.6 \times 10^7 M^{-1}$ ) and the affinity of the enzyme for the dsDNA parts of the gapped DNA structures ( $\sim 2.0 \times 10^7 M^{-1}$ ), are very similar (Figure 2.13b)<sup>27,92</sup>. Moreover, in case of the direct interactions of PriA with dsDNA described here, the enzyme affinity for the dsDNA is additionally amplified by significant positive cooperative interactions<sup>92</sup>. Such a high affinity of the PriA helicase for dsDNA is rather unexpected<sup>92</sup>. Helicases, typically possess significantly higher intrinsic affinity for the ssDNA than for the dsDNA, particularly in the presence of NTPs<sup>22,27,61,92</sup>. However, in case of the PriA helicase, the high dsDNA affinity of the PriA protein may reflect complex role of the protein in the recognition of the damaged DNA and the primosome assembly site<sup>27,92</sup>.

#### **3.5.4 The PriA Helicase Binds dsDNA with Specific Orientation.**

A distinct feature the PriA - dsDNA interactions is the presence of significant positive cooperativity (Table 3.1)<sup>92</sup>. Interestingly, the interactions of the PriA helicase with the ssDNA, in the same solution conditions, are characterized by weak cooperative interactions<sup>56-59,92</sup>. This dramatic difference in the nature of enzyme interactions with ss and dsDNA indicates that PriA exists in a very different orientation when bound in each of these DNA complexes<sup>92</sup>. The intrinsic interactions and the cooperative interactions of the PriA - dsDNA complex are weakened by the increase of the salt concentration in

solution as shown in the Figure 3.5c<sup>92</sup>. The negative slope of the log - log plot, describing cooperativity parameter,  $\partial \log \omega / \partial \log [\text{NaCl}] = -1 \pm 0.3$ , shows that a net release of a single ion goes along with the engagement of the interacting areas of the bound protein molecules<sup>83,84,92</sup>. Yet again, this behavior is very different from the salt effect on the cooperative interactions of PriA with the ssDNA, where the increase of the values of  $\omega$  is observed at higher salt concentrations, indicating a net uptake of  $\sim 2.5$  ions<sup>57,83,84,92</sup>. Different thermodynamic response of cooperativity parameters to changes in the salt concentration highlights the notion that interactions of PriA with ssDNA and dsDNA are of a very different nature<sup>92</sup>. In other words, the engagement of different areas of the protein enables different PriA orientations observed in the complex with the dsDNA *versus* the ssDNA<sup>92</sup>.

### **3.5.5 The Effect of Temperature on the PriA – dsDNA Interactions Indicates Enzyme's Conformational Flexibility.**

The simplest thermodynamic model that describes observed nonlinear character of the van't Hoff plot, presented in Figure 3.6b, includes two conformations of the protein,  $P_L$  and  $P_H$ , with different temperature dependences of the intrinsic affinities for the dsDNA<sup>92</sup>. Above 15°C, the enzyme exists predominantly in the  $P_H$  conformation, whose apparent enthalpy of intrinsic interactions with the nucleic acid is strongly negative with the  $\Delta H_{10H} \approx -27$  kcal/mole, while below 10°C the helicase assumes the  $P_L$  conformation and the intrinsic interactions are characterized by a positive  $\Delta H_{10L} \approx 14$  kcal/mole<sup>92</sup>. The only explanation of such drastically different changes in the apparent enthalpy is a large conformational transition of the entire protein molecule<sup>92</sup>. This conclusion is also supported by the large and positive enthalpy of the  $P_L \leftrightarrow P_H$  transition,  $\Delta H_C \sim 60$  kcal/mol<sup>92</sup>. The strong temperature dependence of the dsDNA

affinities of two enzyme conformations indicates that the intrinsic PriA - dsDNA interaction is effectively enthalpy-driven process at temperatures above  $\sim 20^{\circ}\text{C}$  and entropy-driven process below  $\sim 10^{\circ}\text{C}$ <sup>92</sup>. This noteworthy behavior indicates that the PriA helicase is flexible and can exist in different conformations, which allow the protein to engage differently in the interactions with the dsDNA<sup>92</sup>.

### **3.5.6 Binding of ADP to the Strong – Nucleotide Binding Site of PriA Increases the Positive Cooperativity of the Enzyme for dsDNA.**

Interestingly, saturation of the strong nucleotide-binding site with ADP causes fairly small change in the value of the intrinsic affinity of the PriA helicase for the dsDNA, but has a dramatic effect on the cooperativity parameter,  $\omega$ , which increases from  $\sim 10$  to  $\sim 45$  (Table 3.1)<sup>92</sup>. This dramatic increase in the cooperativity parameter compensates for the diminished intrinsic affinity and, as a result, the enzyme preserves its overall high affinity for the dsDNA<sup>92</sup>. This high overall affinity is now achieved not through protein - nucleic acid but through protein - protein interactions, and it seems that the enzyme is able to form long clusters on the nucleic acid lattice<sup>81,92</sup>. The value of  $\Delta F_1$  remains similar to the value determined in the absence of ADP, indicating similar intrinsic interactions and similar orientation of a single enzyme molecule on the DNA (Table 3.1)<sup>92</sup>. However,  $\Delta F_{\text{max}}$  is lower than observed in the absence of ADP, indicating a changed orientation of the enzyme now engaged in strong cooperative interactions<sup>92</sup>.

### **3.5.7 Saturation of Both Nucleotide-Binding Sites with ADP Has a Dramatic Effect on Intrinsic Affinity and Cooperativity of PriA – dsDNA Interactions.**

When both, the strong and the weak, nucleotide binding sites of PriA are saturated with ADP, completely different situation is observed (Figure 3.7, Figure 3.8 and Table 3.1)<sup>92</sup>. In this case, the affinity of the PriA helicase for dsDNA increases dramatically<sup>92</sup>.

However, this high affinity is reached not through protein - protein but through the intrinsic protein - nucleic acid interactions<sup>92</sup>. Notice that the increased intrinsic affinity is reflected in the values of  $\Delta F_1$  and  $\Delta F_{\max}$ , which are considerably higher than those determined in the case where only the strong nucleotide-binding site is saturated with ADP or in the case without nucleotides (Table 3.1)<sup>92</sup>. Interestingly, the dependence of  $\Delta F$  upon the total average degree of binding value is biphasic, as observed in the absence of ADP indicating similar orientations of the bound enzyme molecules in the states characterized by weak cooperative interactions (Figure 3.1b and Figure 3.8b)<sup>92</sup>.

It was previously suggested by the Bujalowski's group that, when both nucleotide-binding sites are saturated with ADP, the PriA helicase engages in the interactions with additional fragment of the ssDNA<sup>27,59-61,92</sup>. Presumably, the engagement of the N-terminal domain of the PriA helicase in the interactions with the nucleic acid is a cause for this interesting discovery (Figure 2.3)<sup>27,59-61,92</sup>. The interactions of an isolated N-terminal domain of the PriA helicase with the nucleic acid, the effect of ADP on those interactions, as well as the change in the stoichiometry when saturated with ADP, directly demonstrating the engagement of an additional fragment of the PriA helicase in the interactions with ssDNA will be discussed, in detail, in Chapter 4. In the case of PriA – dsDNA interactions, the site-size of the PriA - dsDNA complex is not affected by the presence of ADP bound to both nucleotide - binding sites, strongly suggesting that different orientation of the enzyme on the dsDNA prevents the N-terminal domain of PriA engaging in the interactions with additional areas of DNA<sup>27,59-61,92</sup>.

### **3.5.8 Only the Intrinsic Affinity, Not the Cooperativity of PriA – dsDNA Interactions is Controlled by ATP[S].**

Association of ATP analog, ATP $\gamma$ S, affects only the intrinsic affinity of the

enzyme<sup>92</sup>. This behavior is very different from what is observed for the effect of ADP binding to both nucleotide-binding sites of the PriA helicase, where both intrinsic affinity and cooperativity parameter are affected by the nucleotide<sup>92</sup>. The difference is particularly dramatic in the case when both, strong and weak, nucleotide-binding sites are bound with the ATPγS<sup>92</sup>. The intrinsic affinity is ~ 2 and ~ 1 orders of magnitude lower than that observed for the analogous state in the presence of ADP, or in the absence of any cofactor, respectively (Table 3.1)<sup>92</sup>. Notice, the cooperativity parameter is within experimental accuracy the constant in these ligation states (Table 3.1)<sup>92</sup>.

### **3.5.9 Functional Implications.**

Surprisingly low site-size, mind-boggling strong affinity, and staggering changes cooperativity of the PriA helicase – dsDNA interactions described in this Chapter may be a very puzzling in the context of existing data on the PriA helicase, and the current thinking on the helicases, in general<sup>22,23,92</sup>. However, these interesting results can be understood in the context of the enzyme activities in the *E. coli* chromosomal DNA and plasmid replication<sup>5,11-17,27,54,92,99</sup>. It has been shown that PriA specifically recognizes the ssDNA gap in the process of restarting DNA replication at the damaged DNA sites<sup>5,11-17,27,92</sup>. In addition, the enzyme specifically recognizes the structure of the primosome assembly sites (PAS) in the formation process of the primosome, originally described for phage phiX174<sup>5,26,48,54,92,99</sup>. In order to do so, the PriA helicase must be able to specifically recognize the ssDNA gap, as well as the PAS-like structures, which consist of abundant stretches of the dsDNA<sup>27,92,99</sup>. In addition, the recognition processes should be geared for high affinity and efficiency, without involving mechanical translocation of the enzyme<sup>27,92,99</sup>. This can be achieved through the exclusive engagement of the strong DNA-binding subsite with the site-size of only  $5 \pm 1$  bps without affecting the site-size of

the complex, and through coordinated control of the intrinsic affinity and cooperativity by two nucleotide-binding sites of PriA without involving free energy transduction<sup>27,92,99</sup>.

In the Figure 3.11a, proposed recognition process of PAS-like DNA structure by PriA is presented<sup>92</sup>. Short stretches of the dsDNA (~ 3 - 10 bps), incorporated among small ssDNA loops and bulges make up PriA binding sites or are components of the binding sites for PriA<sup>92,99</sup>. The recognition process could be initiated by binding of ADP to the strong nucleotide-binding site, or hydrolysis of the bound ATP and release of ADP from the weak nucleotide-binding site, which would allow PriA to engage in significant positive cooperative interactions, reinforcing the overall affinity<sup>92</sup>. When both nucleotide-binding sites are saturated with ADP, the cooperativity is strongly diminished, but to compensate, the intrinsic affinity for the dsDNA is drastically increased, maintaining the specificity of the recognition of the PAS structures<sup>92</sup>. The size of the PAS-like DNA structure along with proposed dsDNA fragments as well as the data presented in this Chapter strongly suggest that more than one PriA molecule may participate in the initial recognition of the PAS, however, at the time this work was published, no clear-cut answer to the PriA – PAS stoichiometry could be found in literature (section 1.4)<sup>48,54,92</sup>. In Chapter 6, the initiation of the primosome formation on the primosome assembly site (PAS) is illustrated, providing the first quantitative study of the assembly process of this interesting macromolecular machine of DNA metabolism<sup>99</sup>.

In the recognition process of the damaged DNA structures by the PriA helicase, the gap is embedded between two dsDNA parts, as shown in the ssDNA gap structures in Figure 3.11b<sup>27,92</sup>. It was revealed, in Chapter 2, that the recognition site includes both the dsDNA and the ds-ss DNA junctions, but not the ssDNA of the gap by itself<sup>27,92</sup>. The PriA helicase, with both nucleotide-binding sites saturated with ADP, seems to be involved in the recognition process of gapped DNA structures, although the enzyme

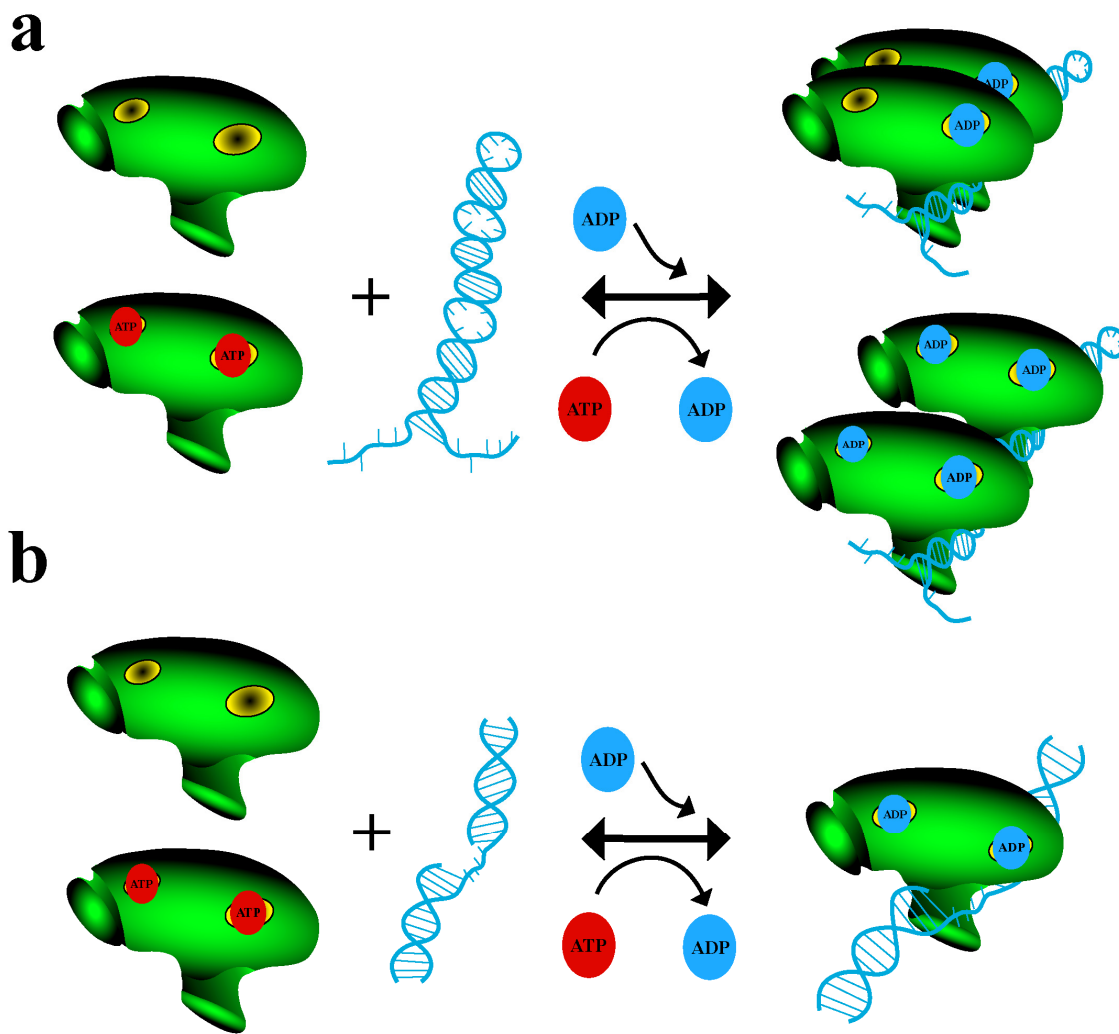


**Figure 3.12 Schematic, functional models of the PAS-like structure and the ssDNA gap recognition processes by the PriA helicase – nucleotide cofactor complexes. a.** In the case of the PAS-like structure recognition, binding of ADP to the strong nucleotide-binding site, or hydrolysis of the bound ATP and the release of ADP from the weak nucleotide-binding site, induces a significant positive cooperativity, which reinforces the enzyme affinity for the dsDNA of the PAS structure<sup>92</sup>. As a result, more than one PriA molecule may participate in the initial PAS recognition process<sup>92</sup>. **b.** In the case of the ssDNA gap at the damaged DNA site, the complex with both nucleotide-binding sites of the PriA protein saturated with ADP is involved<sup>92</sup>.



without nucleotide cofactors may also participate in the recognition process<sup>27,92</sup>. In this case, low cooperativity of the binding process indicates that a single PriA molecule participates in the ssDNA gap recognition<sup>27,92</sup>.

Notice that the recognition processes discussed above would not involve the PriA protein associated with ATP, as this cofactor only slightly affects the interactions with the dsDNA<sup>27,92</sup>. This results corroborate well with early biochemical studies which suggest that the initial steps of the primosome assembly don't require ATP or ATP hydrolysis<sup>15,40,92</sup>. The data presented here suggest that, in the presence of ATP, the ATP hydrolysis is only necessary to provide ADP, which controls the intrinsic affinity and the cooperativity<sup>92</sup>. Once the ssDNA gap in a damaged DNA is recognized, the protein must change its mode of interactions and engage the single-stranded conformation of the nucleic acid<sup>27,92</sup>. This intriguing transition process, possibly involving translocation or unwinding, will be a subject of further studies in the Bujalowski's laboratory (Chapter 7).

The presence of two nucleotide-binding sites on the PriA helicase, revealed by the Bujalowski's group, dramatically changed current thinking regarding the nature and the mechanism of interplay between the nucleotide cofactors and the conformation of the nucleic acid bound to the helicase<sup>59-61,92</sup>. In this Chapter, we presented yet another interesting discovery that will add our understanding of multiple roles of helicases in DNA metabolism, specifically in the assembly process of the primosome<sup>92,99</sup>. The PriA helicase binds the dsDNA with the affinity higher than the affinity of PriA for ssDNA<sup>27,92</sup>. The binding process is controlled by coordinated action of both nucleotide-binding sites different from the nucleotide effect on the enzyme - ssDNA interactions<sup>27,92</sup>. The difference probably reflects the separation between recognition processes, predominantly occurring in complexes with the dsDNA and/or the ds-ssDNA junctions, and mechanical translocation occurring in complexes with the ssDNA<sup>27,92</sup>.

**Table 3.1. Thermodynamic and spectroscopic parameters of the binding of the *E. coli* PriA helicase to the double-stranded DNA 10-mer, in buffer C505, and different concentrations of ADP, and ATP $\gamma$ S\*.**

Nucleotides	Stoichiometry	K <sub>10</sub>	$\omega$	$\Delta F_1$	$\Delta F_{\max}$
No Nucleotides	2	$(1.6 \pm 0.6) \times 10^7$	$10 \pm 3$	$0.12 \pm 0.03$	$0.41 \pm 0.03$
ADP $1 \times 10^{-3}$ M	2	$(8.0 \pm 2.5) \times 10^6$	$45 \pm 14$	$0.14 \pm 0.03$	$0.29 \pm 0.03$
ADP $3 \times 10^{-3}$ M	2	$(1.3 \pm 0.4) \times 10^8$	$2 \pm 0.6$	$0.21 \pm 0.03$	$0.93 \pm 0.03$
ATP $\gamma$ S $1 \times 10^{-4}$ M	2	$(5.8 \pm 1.4) \times 10^6$	$12 \pm 4$	$0.20 \pm 0.03$	$0.35 \pm 0.03$
ATP $\gamma$ S $3 \times 10^{-3}$ M	2	$(2.8 \pm 0.6) \times 10^6$	$16 \pm 6$	$0.15 \pm 0.03$	$0.40 \pm 0.03$

\*The errors are standard deviations determined using 3 - 4 independent titration experiments.

## CHAPTER 4

### THE *ESCHERICHIA COLI* PRIA HELICASE N-TERMINAL DOMAIN POSESSES BOTH DNA AND NUCLEOTIDE BINDING SITE<sup>100</sup>

#### 4.1 ABSRACT

Functional energetics of interactions of the *E. coli* PriA helicase 181aa N-terminal domain with the DNA and nucleotide cofactors has been studied, using the quantitative fluorescence titration, photo-cross-linking, and analytical ultracentrifugation methods<sup>100</sup>. Isolated 181aa N-terminal domain forms a stable dimer in solution<sup>100</sup>. Only one monomer of the domain dimer binds the DNA, *i.e.*, the dimer has one effective DNA-binding site<sup>100</sup>. Although the total site-size of the dimer - ssDNA complex is  $13 \pm 1$  nucleotides, the DNA-binding subsite engages in direct interactions  $5 \pm 1$  nucleotides<sup>100</sup>. Small number of directly interacting nucleotides indicates that the strong subsite on the helicase domain and the weak subsite on the 181aa N-terminal domain are spatially separated in the enzyme molecule<sup>100</sup>. The subsite located on 181aa N-terminal domain has only a slight preference for the 3'-end OH group of the DNA and lacks any significant base specificity, though it has a significant dsDNA affinity<sup>100</sup>. The 181aa N-terminal domain possesses a nucleotide-binding corresponding to the allosteric, weak nucleotide-binding site of the intact PriA<sup>100</sup>. The specific ADP effect on the domain DNA-binding subsite

---

<sup>100</sup> Reprinted with permission from Szymanski, M.R., Bujalowski, P.J., Jezewska, M.J., Gmyrek, A.M., Bujalowski, W. (2011). The N-Terminal Domain of the *Escherichia coli* PriA Helicase Contains Both the DNA- and Nucleotide-Binding Sites. Energetics of Domain-DNA Interactions and Allosteric Effect of the Nucleotide Cofactors. *Biochemistry* **50**(43), 9167-9183. Copyright 2011 American Chemical Society.

indicates that in the intact helicase, ADP not only opens the subsite but also increases its intrinsic DNA affinity<sup>100</sup>.

## 4.2 INTRODUCTION

The activities of helicases *in vivo* are related to the ability of the enzyme to interact with both the ss and the dsDNA, when during the dsDNA unwinding reaction, binding and/or hydrolysis of NTPs regulates the helicase activity and affinity toward different conformations of the DNA<sup>5,11,14-18,24-27,47,54,92,99,100,103</sup>. As it was presented earlier, in the introduction to Chapter 2, the quantitative thermodynamic analyses showed that in the complex with the ssDNA, the total DNA-binding site of the PriA helicase occludes ~ 20 nucleotides<sup>1,27,56-61,92,99,100</sup>. In addition, the total DNA-binding site is not homogenous and possesses a strong ssDNA-binding subsite, located on the helicase domain in the central part of the enzyme molecule, which engages in interactions with only ~ 6 nucleotides (Figure 2.3a)<sup>1,27,56-59,92,99,100</sup>. Further, it was shown, in Chapter 2 and Chapter 3, that in the process of ssDNA gap recognition of the damaged DNA structures as well as in the complex with dsDNA, the PriA helicase engages the nucleic acid using exclusively the strong DNA-binding subsite located on the helicase domain (Figure 3.11)<sup>27,92,99,100</sup>. As a result, the enzyme preferentially recognizes the ssDNA gap containing 5 nucleotides while the total site-size of the PriA - dsDNA complex is only ~ 5 base pairs<sup>27,92,100</sup>.

The characteristic feature of the PriA protein, so far not found in other monomeric helicases, is that the enzyme possesses not one but two nucleotide-binding sites, strong and weak, which profoundly differ in their affinities for the type of the cofactors and effects on the intrinsic affinity of the protein - DNA complexes<sup>1,27,59-61,92,99,100</sup>. Moreover, cooperative interactions between the two nucleotide-binding sites indicate

communication between them<sup>27,59-61,92,100</sup>. Saturation of both nucleotide binding sites of PriA with ADP was proposed to induce the engagement of the N-terminal domain of the enzyme in the interactions with the DNA<sup>27,59-61,92,100</sup>. This conclusion was reinforced by the fact that the ssDNA-binding activity of the isolated 181aa N-terminal domain has been detected, however, no quantitative data to support this suggestion were presented<sup>97,100</sup>. As a result, the enzyme possesses two DNA-binding subsites, one located on the helicase domain and the other one on the N-terminal domain<sup>92,100</sup>. The intricate, structure-function organizations of the PriA helicase - ssDNA - nucleotide complexes, based on these studies, are schematically depicted in Figure 2.3 and Figure 4.1a<sup>27,56-61,92,99,100</sup>.

Understanding the PriA helicase interactions with the DNA requires the elucidation of the functional role of its DNA-binding subsites and the effect of the nucleotide cofactor on both subsites<sup>27,56-61,92,99,100</sup>. Although the strong subsite - DNA interactions have been intensively examined, analogous interactions of the subsite located on the N-terminal domain are much less understood<sup>27,92,97,100,104</sup>. To date, there is no crystal structure of the full-length PriA helicase available<sup>100</sup>. However, the crystal structures of the truncated N-terminal domain containing 105 amino acid residues (105aa N-terminal subdomain) have been solved at 2.5 Å resolution (Figure 4.1b)<sup>100,104</sup>. In the crystal the protein forms an intervening dimer, where two monomers interact through their N-terminal fragments (Figure 4.1b)<sup>100,104</sup>. The 105aa N-terminal subdomain retains its ssDNA-binding activity in solution; nevertheless, quantitative analyses of interactions of the 105aa N-terminal subdomain and the complete 181aa N-terminal domain with the ssDNA have not been addressed<sup>100,104</sup>. In addition, available qualitative analyses of the domains – ssDNA interactions provide some contradicting results<sup>100,104</sup>. Nothing is known about the stoichiometries and intrinsic energetics of the complete 181aa N-

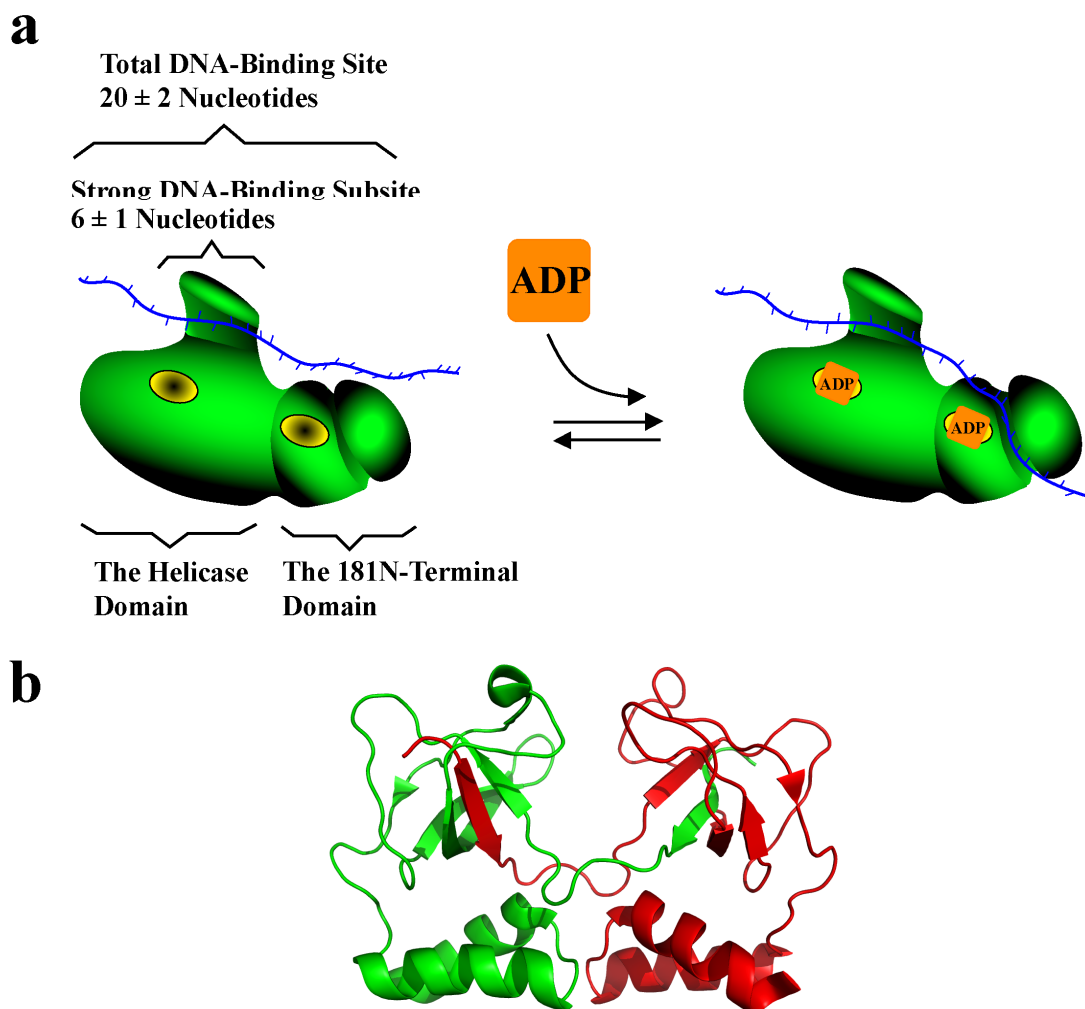


**Figure 4.1 Schematic model of the PriA helicase in the complex with the ssDNA and ADP.** **a.** The enzyme has two functional domains, two nucleic acid binding subsites, and two nucleotide-binding sites<sup>27,56-61,92,99,100</sup>. The yellow ovals symbolize the strong and weak nucleotide-binding sites of the helicase, although their location with respect to protein domains *prior* to this work was arbitrary assigned<sup>59-61,100</sup>. In the absence of nucleotide cofactors, only the strong subsite on the helicase domain engages the nucleic acid. Upon binding of ADP to both nucleotide-binding sites, the DNA-binding subsite of the helicase on the N-terminal domain opens and engages in interactions with the ssDNA<sup>27,59-61,92,99,100</sup>. **b.** Structure of the 105aa N-terminal subdomain dimer of the PriA helicase, based on crystallographic studies (PDB code 2D7E) using PyMOL. Each monomer of the dimer is marked with different color<sup>100,104</sup>.

terminal domain - ssDNA/dsDNA complexes<sup>100</sup>. Whether or not one of the PriA nucleotide-binding sites is located on the N-terminal domain is also unknown<sup>100</sup>. The role of the cofactors and the structure of their phosphate groups in the process of N-terminal domain - nucleic acid association, if any, have never been addressed<sup>100</sup>.

In this Chapter, quantitative studies of the interactions of the 181aa N-terminal domain of the PriA helicase with the ss and dsDNA, and the effect of the nucleotide cofactors on the recognition process are described<sup>100</sup>. The domain forms a dimer in solution<sup>100</sup>. Only one monomer of the dimer binds the ssDNA, engaging in direct interactions  $5 \pm 1$  nucleotides<sup>100</sup>. The DNA-binding subsite of isolated domain is in open conformation and has only a modest preference for the 3' end of the nucleic acid<sup>100</sup>. The discovery that the 181aa N-terminal domain possesses a nucleotide-binding site, which corresponds to the weak nucleotide-binding site of the intact PriA helicase, is also described<sup>100</sup>.

## **4.3 MATERIALS AND METHODS**

### **4.3.1 Buffers and Chemicals.**

All solutions used in experiments described in this Chapter were made with distilled and deionized >18 M $\Omega$  (Milli-Q Plus) water. The standard buffer was buffer C205 with 10 mM sodium cacodylate adjusted to pH 7.0 with HCl at 10°C, 1 mM DTT, 20 mM NaCl, 5 mM MgCl<sub>2</sub>, and 25% glycerol w/v<sup>100</sup>. The standard temperature in all the experiments described in this Chapter was 10°C. All experiments were carried out in the standard buffer C205 unless otherwise specified in the text. Polynucleotide Kinase was from Roche (Indianapolis, IN). Lysozyme, Phenylmethanesulfonylfluoride (PMSF), Sodium Deoxycholate, Polymin P, Ammonium sulfate, and Imidazole were from Sigma (Saint Louis, MI). All chemicals were reagent grade.

### 4.3.2 Water Activity of Buffering Solution.

Water activity “error term” of the standard buffer C205, used in this Chapter, had been calculated according to the values in the literature<sup>132,133</sup>. Due to the presence of the glycerol and salt, the water activity “error term” is less than 5%, and is contained within the experimental error of all the experiments presented here<sup>27,132,133</sup>.

### 4.3.3 Nucleotides and Nucleic Acids.

ATP $\gamma$ S and ADP, were from GE Healthcare (Piscataway, NJ). 2'(3')-O-(2,4,6-Trinitrophenyl)adenosine (TNP-ATP) and 2'(3')-O-(2,4,6-trinitrophenyl)adenosine-5'-diphosphate (TNP-ADP) were from Invitrogen (Eugene, OR)<sup>100</sup>. All nucleotides were of high purity as judged by thin layer chromatography (TLC). Unmodified nucleic acid oligomers were purchased from Midland Certified Reagents (Midland, TX)<sup>100</sup>. All nucleic acids were HPLC purified and at least >95% pure as judged by electrophoresis on polyacrylamide gel<sup>100</sup>.

To monitor binding, different length etheno-derivatives of adenosine oligomers were obtained by modification with chloroacetaldehyde<sup>90-92,100</sup>. The concentration of etheno-derivative of the nucleic acids was determined spectrophotometrically using following the extinction coefficients:  $\epsilon_{257} = 3700 \text{ cm}^{-1}\text{M}^{-1}$  (nucleotide) for  $\epsilon_A$ <sup>81,87,90-92,100</sup>.

The sequence of dsDNA substrate was ACGAGCCTGC. The concentration of unmodified oligomers were determined spectrophotometrically using the extinction coefficients:  $\epsilon_{260} = 10000 \text{ cm}^{-1}\text{M}^{-1}$  (nucleotide) for A,  $\epsilon_{260} = 8500 \text{ cm}^{-1}\text{M}^{-1}$  (nucleotide) for G,C and T<sup>27,62</sup>. dsDNA substrates were obtained by mixing ssDNA oligomers with complementary oligomers at appropriate concentration. The mixture was then warmed for 5 minutes at 95°C, and slowly cooled for a period of ~ 4 - 5 hours<sup>27,62,63,100</sup>.



The integrity of the dsDNA substrate have been checked by UV melting and analytical ultracentrifugation techniques<sup>27,62,63,92,100</sup>. The melting temperature of the examined dsDNA substrate was ~ 52°C in the studied solution conditions<sup>27,62,63,92,100</sup>.

#### **4.3.4 PriA 181aa N-terminal Domain Purification.**

The fragment of the *E. coli* PriA protein gene coding 181 amino acid residues from the N-terminus of the protein and the C-terminal His-Tag has been placed under T7 promoter in plasmid Pet30a<sup>100</sup>. The cells were grown at 37°C in Luria Broth (LB) induced by adding 1 mM IPTG and grown overnight at 18°C. The cells were collected by centrifugation, flash frozen, and stored in -80°C. All purification procedures were performed in 4°C cold room unless otherwise specified. Typically, ~ 35g of frozen cell pallet was thawed on ice and suspended in 200 ml of buffer A (50 mM Tris-HCl pH 7.5, 0.5 mM EDTA, 5 mM B-MeOH, 10% glycerol w/v) and stirred gently until the suspension was homogeneous. About 50 ml of buffer B (200 mM Tris-HCl pH 7.5, 1 M NaCl, 1.5M Ammonium sulfate, 100 mM Spermidine-HCl) was added for the final volume of 250 ml. Freshly prepared phenylmethanesulfonylfluoride (PMSF) was added to the final concentration of 0.2 mM. At this time the pH was adjusted to ~ 8.5 with 2 M Tris-Base. Next, the lysozyme was added, dropwise, to the final concentration of 400 µg/ml and the suspension was incubate with gentle stirring for 30 minutes on ice Next, sodium deoxycholate, to the final concentration of 0.04% was added and the suspension was stirred for additional for 30 minutes. After that the cell suspension was placed in centrifuge bottles and centrifuged for 30 min at 12000 rpm in Sorvall GSA rotor to collect soluble protein of interest. To the collected supernatant 0.8% of Polymyxin P, in 3 portions, over a period of 30 min, with gentle stirring, was added to precipitate nucleic acid. Again, the suspension was centrifuged for 30 min in GSA rotor at 12000 rpm and

white precipitation was removed. The supernatant was collected and ammonium sulfate to the concentration of 0.35 g/ml was added, in portions, while stirring gently for 30 min. The suspension was incubated for extra 30 min with stirring after ammonium sulfate was added. The suspension was then centrifuged at 12000 rpm for 30 min in GSA rotor. The protein of interest was in the pellet and was dissolved in buffer C1 (50 mM Tris-HCl pH 7.5, 5 mM B-MeOH, 300 mM NaCl, 10% glycerol w/v) and dialyzed against 1000 ml of buffer C1 for ~6 hours. The buffer was then exchanged and the sample was dialyzed overnight against 1000 ml of buffer C20 (50 mM Tris-HCl pH 7.5, 20 mM Imidazole, 5 mM B-MeOH, 300 mM NaCl, 10% glycerol w/v). Precipitation formed in the dialysis bags was removed by centrifugation at 12000 rpm for 30 min in GSA rotor and the supernatant was loaded onto the standard, hand packed, nickel column (GE Healthcare, Piscataway, NJ). The 181aa N-terminal domain of PriA was eluted with buffer C125 (50 mM Tris-HCl pH 7.5, 125 mM Imidazole, 5 mM B-MeOH, 300 mM NaCl, 10% glycerol w/v) and a large volume of the sample was ammonium sulfate precipitated (0.35 g/ml of ammonium sulfate was added in portions while stirring gently for 30 min). Additionally, the suspension was incubated for extra 30 min with stirring after ammonium sulfate was added. The suspension was then centrifuged at 12000 rpm for 30 min in GSA rotor. Again, the protein of interest was in the pellet and was dissolved in buffer D150 (50 mM Tris-HCl pH 7.5, 5 mM B-MeOH, 150 mM NaCl, 10% glycerol w/v) and dialyzed overnight against 1000 ml of the same buffer. After dialysis was stopped the sample was centrifuged at 12000 rpm for 30 min in GSA rotor. In the next step, the Heparin Sepharose CL-6B Column (GE Healthcare, Piscataway, NJ) was used. Bound 181aa N-terminal domain of PriA was eluted with buffer D300 (50 mM Tris-HCl pH 7.5, 5 mM B-MeOH, 300 mM NaCl, 10% glycerol w/v) and a large volume of the sample was ammonium sulfate precipitated to the concentration of 0.35 g/ml. Ammonium sulfate was

added in portions while stirring gently for 30 min. Additionally, the suspension was incubated for extra 30 min with stirring after ammonium sulfate was added. The suspension was then centrifuged at 12000 rpm for 30 min in GSA rotor. The protein of interest was in the pellet which was then dissolved in buffer D150 (50 mM Tris-HCl pH 7.5, 5 mM B-MeOH, 150 mM NaCl, 10% glycerol w/v) and dialyzed overnight against 1000 ml of the same buffer. After dialysis was stopped the sample was centrifuged at 12000 rpm for 30 min in GSA rotor. In the next step, the DEAE Sephacryl Column (GE Healthcare, Piscataway, NJ) was used. 181aa N-terminal domain of PriA doesn't bind to that column and comes out in large volume of flow through. This fraction was then ammonium sulfate precipitated to the concentration of 0.35 g/ml. Ammonium sulfate was added in portions while stirring gently for 30 min. Additionally, the suspension was incubated for extra 30 min with stirring after ammonium sulfate was added. The suspension was then centrifuged at 12000 rpm for 30 min in GSA rotor. The protein of interest was in the pellet and was dissolved in buffer D150 (50 mM Tris-HCl pH 7.5, 5 mM B-MeOH, 150 mM NaCl, 10% glycerol w/v) and dialyzed overnight against 1000 ml of the same buffer. Next, the pure protein sample was dialyzed overnight against 1000 ml of storage buffer (50 mM Tris-HCl pH 7.5, 5 mM B-MeOH, 150 mM NaCl, 50% glycerol w/v) and stored in -80°C. Typical yield of this purification protocol was ~ 120mg of pure 181aa N-terminal domain from ~ 35g of frozen cell pellet<sup>100</sup>.

Before each use, frozen 181aa N-terminal domain of PriA was allowed to thaw on ice, transferred to the dialysis bag, and dialyzed against ~ 150 ml of buffer C205 for 4-6 hours. After that time the buffer was exchanged and the dialysis was allowed to go overnight. The protein sample was then centrifuged at 15000 rpm for 20 minutes and the absorption spectrum of the protein was taken. In these solution conditions, the maximum solubility of 181aa N-terminal domain was about  $2.5 \times 10^{-4} \text{ M}$ <sup>100</sup>.

Untagged 181aa N-terminal domain was purified using the same protocol except of the nickel column step. The tagged domain has DNA-binding properties indistinguishable for the unmodified protein; therefore, in all experiments described here a tagged protein was used<sup>100</sup>.

#### **4.3.5 Determination of Extinction Coefficient of PriA 181 aa N-terminal Domain.**

The concentration of the protein was spectrophotometrically determined, with an extinction coefficient  $\epsilon_{280} = 6.946 \times 10^4 \text{ cm}^{-1}\text{M}^{-1}$  (dimer) obtained using an approach based on the Edelhoch's method<sup>27,56-61,64,65,81,92,99,100</sup>.

#### **4.3.6 Fluorescence Measurements.**

All steady-state fluorescence titrations were performed using the ISS PC-1 spectrofluorometer (Urbana, IL) as previously described<sup>27,56-63,81,92,99,100</sup>. The temperature of the cuvette holder was regulated by circulating water at  $10.0 \pm 0.1 \text{ }^{\circ}\text{C}$ <sup>100</sup>. The 181aa N-terminal domain binding was followed by monitoring the etheno-derivative fluorescence of the nucleic acids ( $\lambda_{\text{ex}} = 325 \text{ nm}$ ,  $\lambda_{\text{em}} = 410 \text{ nm}$ )<sup>100</sup>. In order to avoid possible artifacts, due to the fluorescence anisotropy of the sample, polarizers were placed in excitation and emission channels and set at  $90^{\circ}$  and  $55^{\circ}$  (magic angle), respectively<sup>27,56-63,81,92,99,100</sup>. The relative fluorescence increase,  $\Delta F_{\text{obs}}$ , of the DNA emission upon protein binding is defined as,  $\Delta F_{\text{obs}} = (F_i - F_o)/F_o$ , where  $F_i$  is the fluorescence of the sample at a given titration point “i” and  $F_o$  is the initial fluorescence of the same solution<sup>1,27,56-63,81,92,100</sup>. Binding of TNP-ATP and TNP-ADP to the 181aa N-terminal domain of PriA was examined using the quenching of the protein fluorescence induced by the cofactor<sup>1,56-63,92,100</sup>. Analogously, the relative fluorescence quenching is defined as,  $\Delta F = (F_o - F_i)/F_o$ <sup>1,27,56-63,81,92,100,101</sup>. In the case of titrations with nucleotide analog, TNP-ADP, the

fluorescence intensity of the sample,  $F_i$ , was corrected for the dilution and inner filter effect as<sup>1,59-61,92,100,101</sup>

$$F_i = (F_{ie} - B_i) \left( \frac{V_i}{V_o} \right) 10^{0.5b(A_{iex} + A_{iem})} \quad (4.1)$$

where  $F_{ie}$  is the experimentally measured fluorescence intensity,  $B_i$  is the background,  $V_i$  is the volume of the sample at a given titration point,  $V_o$  is the initial volume of the sample,  $b$  is the total length of the optical path in the cuvette expressed in cm,  $A_{iex}$  and  $A_{iem}$  are the absorbances of the sample at excitation and emission wavelengths, respectively<sup>1,59-61,92,100,101</sup>.

#### **4.3.7 Determination of Quantitative Binding Isotherm of the 181aa N-terminal Domain - DNA Associations or the Nucleotide Binding to the Domain.**

In this Chapter, the binding of the 181aa N-terminal domain of PriA helicase to the DNA oligomers was followed by monitoring the fluorescence increase,  $\Delta F$ , of etheno-derivative of the nucleic acid<sup>90-92,100</sup>. Quantitative estimates of the total average degree of binding,  $\Sigma\Theta_i$  (average number of bound 181aa N-terminal domain of PriA helicase molecules per DNA oligomer) and the free protein concentration,  $P_F$ , independent of any assumption about the relationship between the observed spectroscopic signal and  $\Sigma\Theta_i$ , were determined using the approach previously described in section 2.3.7<sup>1,56,57,82,87,92,100</sup>. Computer fits were performed using Mathematica (Wolfram, IL) and KaleidaGraph (Synergy Software, PA).

#### **4.3.8 Analytical Ultracentrifugation Measurements.**

All analytical ultracentrifugation experiments were performed with an Optima XL-A analytical ultracentrifuge (Beckman Inc., Palo Alto, CA), as we previously described in section 2.3.8<sup>27,66-69,72,76,82,92,100</sup>.

#### **4.3.9 Determination of the Partial Specific Volume of PriA 181aa N-terminal Domain.**

Partial specific volume of the 181aa N-terminal domain of PriA protein ( $v$ ) was calculated from the amino acid composition of the protein according to Lee and Timasheff and was 0.744 mL/g<sup>27,70,100</sup>.

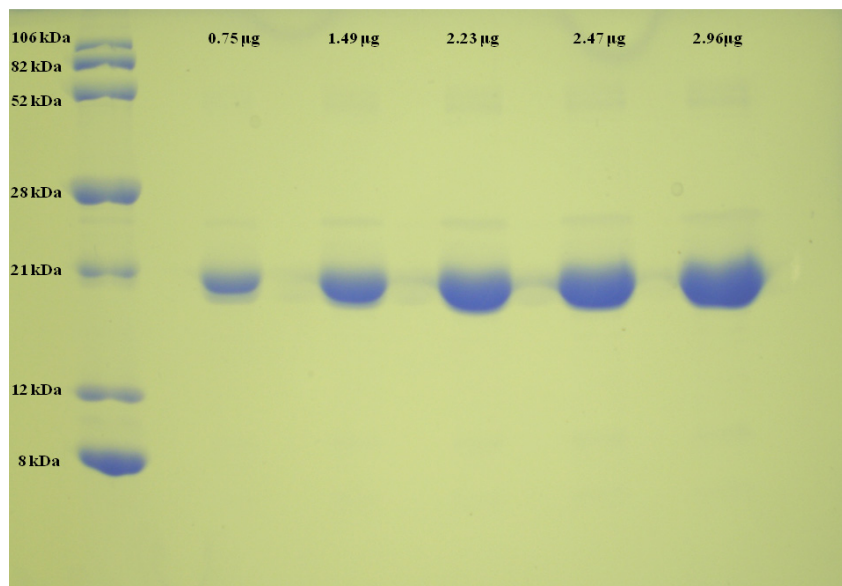
#### **4.3.10 Photo-Cross-Linking Experiments.**

Photo-cross-linking of the 181aa N-terminal domain - ssDNA complex has been performed in the same buffer as the binding experiments. The ssDNA oligomer, dT(pT)<sub>19</sub>, has been labeled at the 5' end with [<sup>32</sup>P], using polynucleotide kinase<sup>81,92,93,100,102</sup>. The samples (total volume 60  $\mu$ L) were placed on Parafilm, at  $\sim 10^{\circ}\text{C}$ , and irradiated for 20 minutes, at a distance of 11 cm, using a mineral lamp (model UVG-11) with a maximum output of 254 nm<sup>81,92,100</sup>. The controls were performed to determine the optimal time for cross-linking and to avoid possible degradation of the protein by prolonged exposure to UV light<sup>81,92,100</sup>. The samples collected at different protein concentrations were loaded on 15% SDS polyacrylamide gel and electrophoresis was performed at a constant voltage<sup>81,92,100</sup>. The gels were stained with Coomassie Brilliant Blue and scanned, using the phosphorimager SI (Molecular Dynamics, PA)<sup>81,92,93,100,102</sup>.

## 4.4 RESULTS

### 4.4.1 The 181aa N-Terminal Domain of the PriA Helicase.

The enzyme was > 99% pure as judged by polyacrylamide electrophoresis with Coomassie Brilliant Blue staining (Figure 4.2). The identity of the sample was confirmed by both mass spectrometry and N-terminal sequencing<sup>100</sup>.



**Figure 4.2** 15% SDS polyacrylamide gel of the final step of 181aa N-terminal Domain of PriA helicase purification. Serial dilution clearly shows that employed purification protocol yields 181aa N-terminal Domain of PriA of high purity<sup>27,56-61,92,99,100</sup>.

#### 4.4.2 The Hydrodynamic properties of the 181aa N-Terminal Domain of PriA Helicase.

Typical example of the sedimentation velocity profiles of the 181aa N-terminal domain of PriA performed at 60000 rpm, monitored at 280 nm, in the standard buffer C205 (section 4.3.1) are shown in Figure 4.3a<sup>72,76,78-80,100</sup>. The concentration of the PriA 181aa N-terminal domain is  $5.76 \times 10^{-6}$  M (dimer)<sup>100</sup>. The inspection of the profiles clearly shows that there is a single moving boundary<sup>72,76,78-80,100</sup>. The sedimentation coefficient of the PriA 181aa N-terminal domain has been obtained using the time-derivative approach and corrected for solvent viscosity and temperature to standard conditions<sup>27,66,67,69,100</sup>. The dependence of the sedimentation coefficient ( $s_{20,w}$ ) upon the protein concentration, is shown in Figure 4.3b<sup>72,100</sup>. Within experimental accuracy values of  $s_{20,w}$  are similar and show a very little dependence upon the examined protein concentration range<sup>27,72,76,100</sup>. The extrapolation of the plots to  $[\text{PriA}] = 0$  provides  $s^{\circ}_{20,w} = 3.28 \pm 0.13$  S in examined solution conditions (Figure 4.3b)<sup>27,72,76,100</sup>.

The primary structure of the 181aa N-terminal domain of the PriA helicase indicates that the molecular weight of the monomer is  $\sim 21,000$ <sup>54,55,92,97,100</sup>. The oligomeric state of the protein in solution has been addressed using the analytical ultracentrifugation method<sup>67,76,81,99,100</sup>. An example of the sedimentation equilibrium profile of the 181aa N-terminal domain recorded at the protein absorption band (280 nm) is shown in Figure 4.4<sup>67,76,81,100</sup>. The protein concentration is  $5.76 \times 10^{-6}$  M (dimer)<sup>100</sup>. The solid line is the nonlinear least-squares fit, using the single exponential function defined by equation 2.4 (section 2.3.8)<sup>66,67,64,76,100</sup>. The fit provides an excellent description of the experimental curve indicating the presence of a single species with the



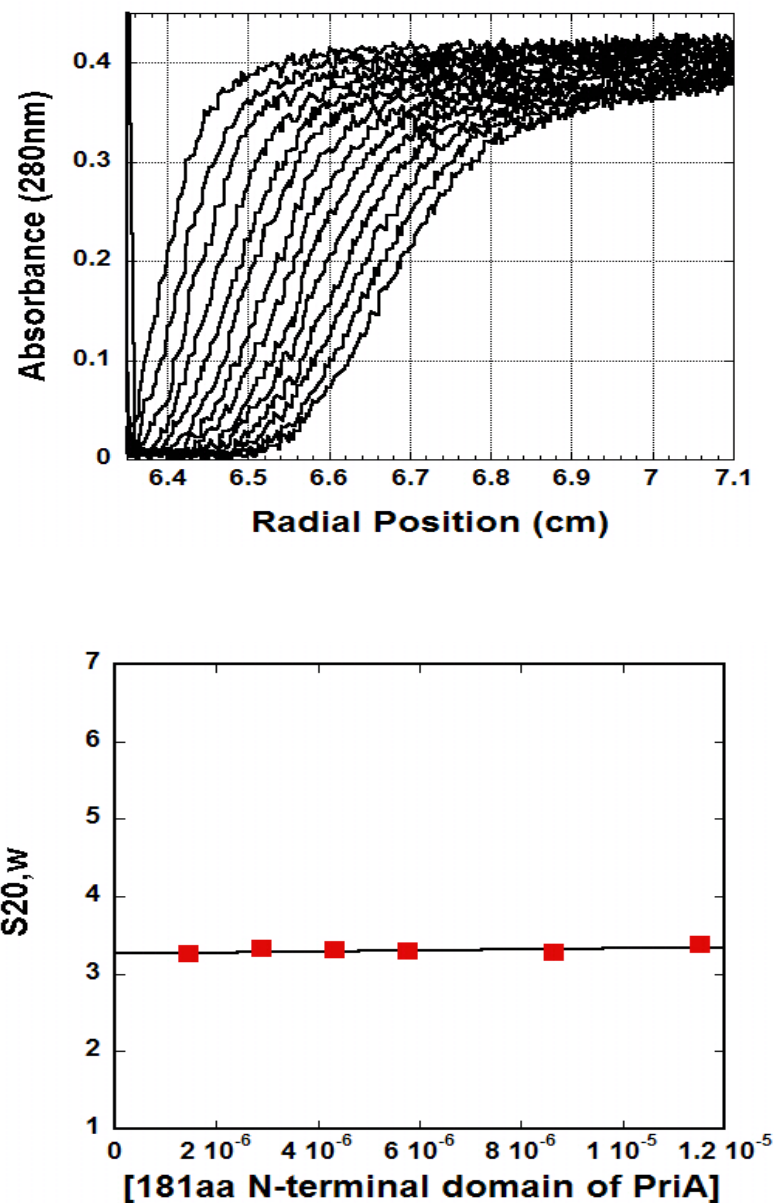


**Figure 4.3** 181aa N-terminal domain of PriA in solution sediments as a single homogenous species. **a.** Example of analytical sedimentation velocity profiles recorded at 280 nm and 60000 rpm for [ $5.76 \times 10^{-6}$  M (dimer)] of 181aa N-terminal domain of PriA<sup>100</sup>. **b.** The dependence of the sedimentation coefficient ( $s_{20,w}$ ) upon the 181aa N-terminal domain of PriA concentration<sup>100</sup>.

molecular weight of  $41,000 \pm 3000$ <sup>66,67,64,76,100</sup>. Adding additional exponents does not improve the statistics of the fit (data not shown)<sup>66,67,64,76,100</sup>.

The equilibrium sedimentation experiments have been performed at different protein concentrations and different rotational speeds, providing the molecular weight ranging from 38,000 to 43,000 (data not shown)<sup>100</sup>. These results indicate that, similar to the crystal structure of truncated 105aa N-terminal subdomain, the 181N-terminal domain exists, in solution, as a dimer in the protein concentration range studied in this work<sup>67,76,100,104</sup>.

#### **4.4.3 Maximum Stoichiometry of the 181aa N-terminal Domain – ssDNA Complexes.**

The studies described in this Chapter were facilitated by the fact that the formation of the 181aa N-terminal domain complex with the etheno-derivatives of the homo-adenosine oligomers causes a strong increase of the nucleic acid fluorescence, providing an excellent signal to perform high-resolution measurements of the protein - ssDNA complex formation (section 4.3.3 and section 4.3.6)<sup>1,56-59,81,87,94,95,100</sup>. The fundamental problem of the stoichiometry of the domain - ssDNA complex, as well as the functional structure of the nucleic acid binding site has been addressed using a series of ssDNA oligomers with different numbers of nucleotides<sup>1,27,56,57,81,100</sup>.

Fluorescence titrations of the ssDNA 12-mer, dεA(pεA)<sub>11</sub>, with the 181aa N-terminal domain at three different nucleic acid concentrations, in buffer C205 (section 4.3.1), are shown in Figure 4.5a<sup>1,56,81,100</sup>. The concentration of the domain is expressed as a dimer. The shift of the titration curve at a higher nucleic acid concentration, results from the fact that more protein is required to obtain the same total average degree of binding,  $\Sigma\Theta_i$ <sup>1,27,56,57,81,85,87,94,95,100</sup>. The selected nucleic acid concentrations provide

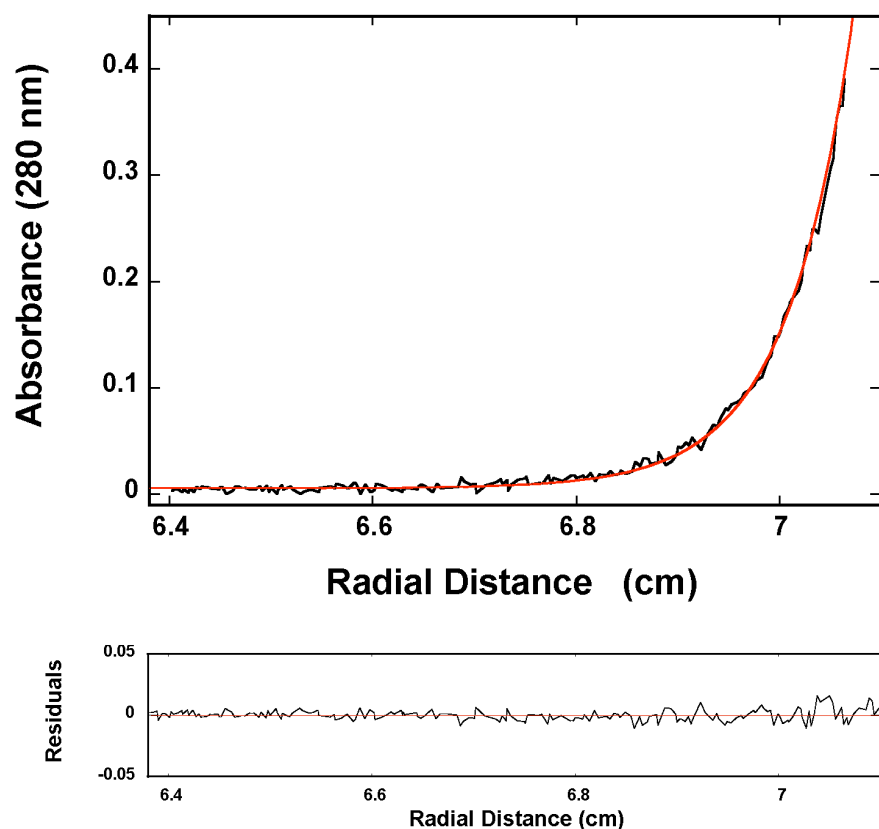


**Figure 4.4 Sedimentation equilibrium concentration profile of 181aa N-terminal domain of PriA helicase.** Example of a typical sedimentation equilibrium profile recorded at 24000 rpm and monitored at 280 nm<sup>72,76,100</sup>. The concentration of 181aa N-terminal domain of PriA was  $5.76 \times 10^{-6}$  M (dimer)<sup>100</sup>. The solid red line is the nonlinear least-squares fit, using the single exponential function defined by equation 2.4 with the molecular mass of 42103 Da<sup>72,76,100</sup>.

separation of the titration curves up to the relative fluorescence increase of  $\sim 1.5$ <sup>1,27,56,57,81,85,87,94,95,100</sup>. The values of  $\Sigma\Theta_i$  have been obtained using the quantitative approach outlined in section 2.3.6, section 4.3.6, and section 4.3.7<sup>1,81,85,87,94,95,100</sup>. Figure 4.5b shows the dependence of the relative fluorescence increase of the nucleic acid,  $\Delta F$ , as a function of  $\Sigma\Theta_i$  of the domain<sup>1,81,85,87,94,95,100</sup>. Extrapolation to the maximum fluorescence change,  $\Delta F_{\max} = 2.55 \pm 0.11$ , provides the stoichiometry of the complex  $0.98 \pm 0.09$ . Thus, a single 181aa N-terminal domain dimer binds to the ssDNA 12-mer<sup>100</sup>.

Analogous fluorescence titrations of the 24-mer, dεA(pεA)<sub>23</sub>, at three different nucleic acid concentrations, are shown in Figure 4.5c<sup>1,81,100</sup>. The maximum increase of the nucleic acid fluorescence at saturation is significantly lower than observed for the 12-mer, reaching the value of  $\sim 1.4$ . The dependence of the relative fluorescence increase of the nucleic acid,  $\Delta F$ , as a function of  $\Sigma\Theta_i$  is shown in Figure 4.5d<sup>1,81,85,87,94,95,100</sup>. Extrapolation to the maximum fluorescence change,  $\Delta F_{\max} = 1.41 \pm 0.08$ , provides the stoichiometry of the complex  $0.91 \pm 0.09$ <sup>100</sup>. In spite of the fact that the oligomer is twice as long as the 12-mer, only a single 181aa N-terminal domain dimer binds to the ssDNA 24-mer<sup>1,81,95,100</sup>.

On the other hand, increasing the length of the ssDNA oligomer only by further 2 nucleotides changes the maximum stoichiometry of the 181aa N-terminal domain - ssDNA complex<sup>1,81,100</sup>. Fluorescence titrations of the 26-mer, dεA(pεA)<sub>25</sub>, with the domain at three different oligomer concentrations, are shown in Figure 4.6a<sup>1,81,95,100</sup>. The dependence of the relative fluorescence increase of the 26-mer, as a function of  $\Sigma\Theta_i$  of the 181aa N-terminal domain on the oligomer, is shown in Figure 4.6b<sup>1,81,100</sup>. The plot is clearly nonlinear, indicating the presence of two binding phases<sup>1,27,56,57,81,85,87,94,95</sup>. Extrapolation of the second affinity phase to the maximum fluorescence increase  $\Delta F_{\max} =$

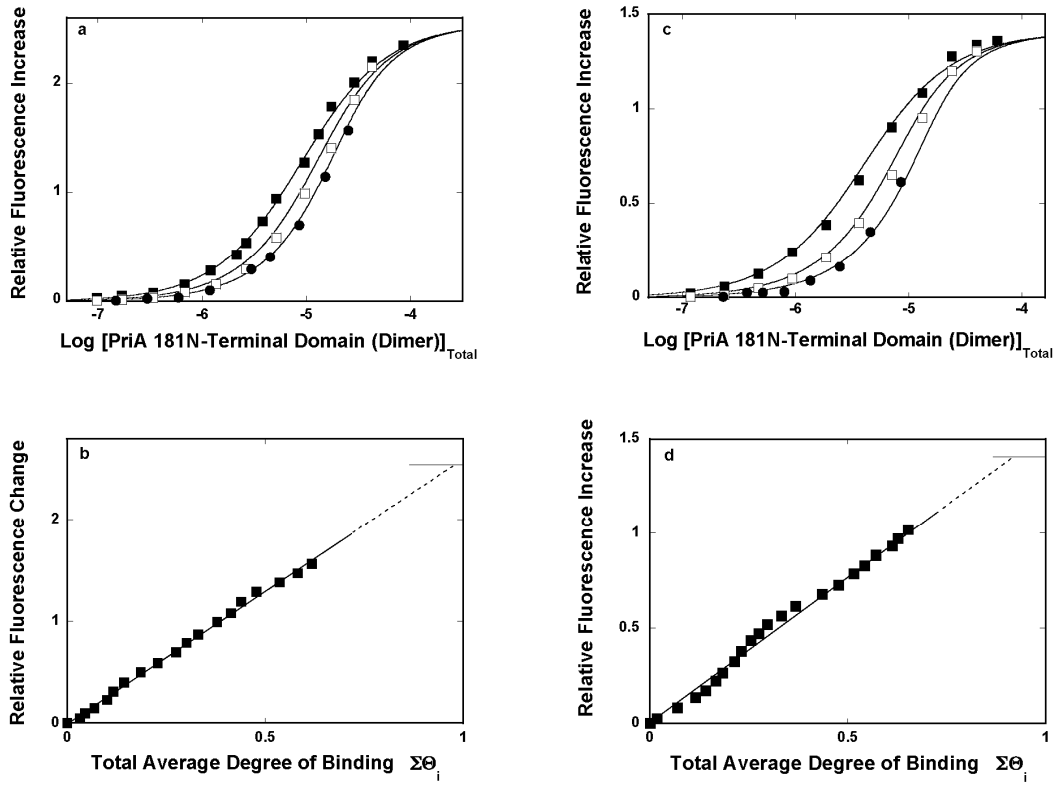


**Figure 4.5 Maximum Stoichiometry of the 181aa N-terminal Domain – ssDNA Complexes.** **a.** Fluorescence of the ssDNA 12-mer,  $\text{d}\epsilon\text{A}(\text{p}\epsilon\text{A})_{11}$ , with the 181aa N-terminal domain of the PriA helicase at three different concentrations of the nucleic acid:  $1.76 \times 10^{-6} \text{ M}$  ( $\blacksquare$ ),  $8.78 \times 10^{-6} \text{ M}$  ( $\square$ ), and  $1.76 \times 10^{-5} \text{ M}$  ( $\bullet$ ) (oligomer)<sup>1,81,95,100</sup>. The solid lines are nonlinear least-squares fits of the fluorescence titration curves according to the one-site binding model defined by equation 4.2. **b.** The dependence of the relative fluorescence increase,  $\Delta F$ , upon the total average degree of binding,  $\Sigma\Theta_i$ , of the 181aa N-terminal domain dimer – 12-mer complex<sup>1,81,95,100</sup>. The solid straight line follows the data points and does not have theoretical basis<sup>1,81,92,100</sup>. The dashed straight line is an extrapolation of the total average degree of binding to the maximum value of the observed fluorescence increase  $\Delta F_{\text{max}} = 2.54 \pm 0.1$ . **c.** Fluorescence titrations of the  $\text{d}\epsilon\text{A}(\text{p}\epsilon\text{A})_{23}$  substrate with the 181aa N-terminal domain of the PriA helicase at three different concentrations of the nucleic acid:  $1.5 \times 10^{-6} \text{ M}$  ( $\blacksquare$ ),  $7.5 \times 10^{-6} \text{ M}$  ( $\square$ ) and  $1.5 \times 10^{-6} \text{ M}$  ( $\bullet$ ) (oligomer)<sup>1,81,95,100</sup>. The solid lines are nonlinear least-squares fits of the fluorescence titration curves according to the one-site binding model defined by equation 4.2. **d.** The dependence of the relative fluorescence increase,  $\Delta F$ , upon  $\Sigma\Theta_i$  of the 181aa N-terminal domain dimer - 24-mer complex<sup>1,81,95,100</sup>.

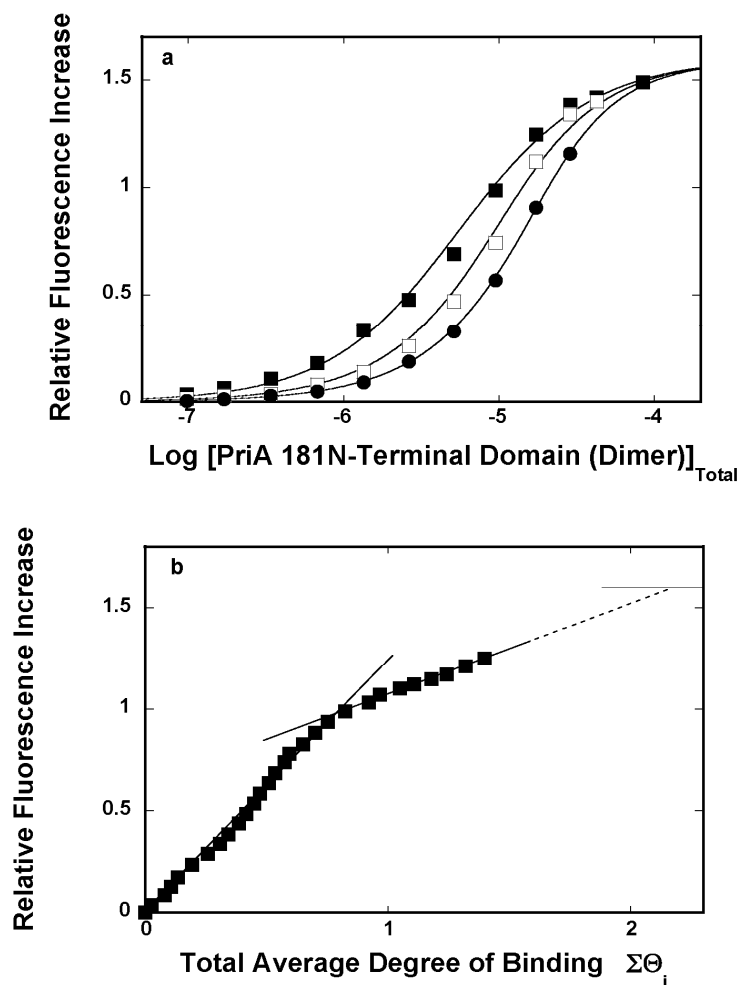


**Figure 4.6 181aa N-terminal domain – ssDNA interactions. Maximum stoichiometry.** **a.** Fluorescence titrations of the ssDNA 26-mer, dεA(pεA)<sub>25</sub>, with the 181aa N-terminal domain of the PriA helicase at three different concentrations of the nucleic acid: 1.76 x 10<sup>-6</sup> M (■), 8.78 x 10<sup>-6</sup> M (□), and 1.76 x 10<sup>-5</sup> M (●) (oligomer)<sup>1,100</sup>. The solid lines are nonlinear least-square fits of the fluorescence titration curves according to the two-sites binding model, defined by equations 4.5 – 4.8. **b.** The dependence of the relative fluorescence increase, ΔF, upon the total average degree of binding,  $\Sigma\Theta_i$ , of the 181aa N-terminal domain dimer - 26-mer complex<sup>1,100,127</sup>. The solid straight lines are the limiting slopes of the high and low-affinity binding phases<sup>1,27,81,100</sup>. The dashed straight line is an extrapolation of the low affinity phase part of the plot to the

maximum value of the observed fluorescence increase  $\Delta F_{\text{max}} = 1.6 \pm 0.1$  that provides the maximum stoichiometry of  $2.2 \pm 0.2$  of the domain dimer - 26-mer complex<sup>1,81,92,100</sup>.

$1.6 \pm 0.08$  provides  $\Sigma \Theta_i = 2.2 \pm 0.2^{1,81,94,95,100}$ . Thus, the 26-mer provides enough interaction space for the binding of two dimers of the 181aa N-terminal domain<sup>100</sup>.

#### **4.4.4 Number of Nucleotides Directly Engaged in the Interactions with the 181aa N-terminal Domain Dimer.**

Analogous quantitative analysis of the maximum stoichiometry of 181aa N-terminal - ssDNA complexes, as described above, has been performed for an entire series of ssDNA oligomers<sup>1,81,94,100,127</sup>. The dependence of the maximum number of the bound domain dimers per ssDNA oligomer upon the length of the oligomer is shown in Figure 4.7<sup>1,56,81,94,100,127</sup>. The selected ssDNA oligomers range from 8 to 33 nucleotides in length<sup>100</sup>. A single 181aa N-terminal dimer binds to the oligomers containing 8, 10, 12, 14, 16, 18, 20, and 24 nucleotides<sup>100</sup>. Sharp transition from a single dimer bound per ssDNA oligomer to two dimers bound per oligomer occurs between 24- and 26-mers (Figure 4.7)<sup>1,56,81,94,100,127</sup>. However, a further increase in the length of the oligomer, up to 33 nucleotides, does not lead to the increase of the number of the bound domain dimers<sup>1,27,56,81,85,87,100</sup>. These data indicate that a total site-size of the 181aa N-terminal domain dimer - ssDNA complex encompasses minimum  $13 \pm 1$  nucleotides per protein dimer<sup>1,27,56,57,81,85,87,94,95,100</sup>.

#### **4.4.5 Intrinsic Affinities of 181aa N-Terminal Domain – ssDNA Interactions.**

Binding of a single 181aa N-terminal domain dimer to 8-, 10-, 12-, 14-, 16-, 18-, 20-, and 24-mer can be analyzed using a single-site-binding isotherm described by

$$\Delta F = \Delta F_{\max} \left[ \frac{K_N P_F}{1 + K_N P_F} \right] \quad (4.2)$$



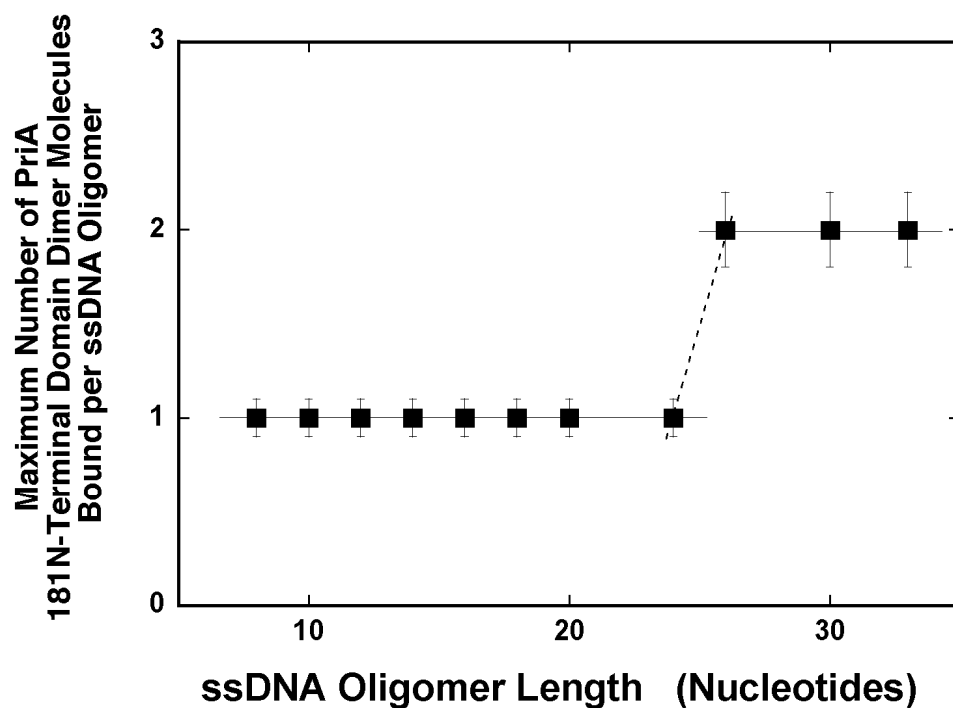


**Figure 4.7** The maximum stoichiometry of the 181aa N-terminal domain dimer on the ssDNA oligomer as a function of the length of the oligomer (nucleotides). The solid horizontal lines connect the points with the same maximum stoichiometry<sup>1,56,81,100,127</sup>. The dashed line marks the transition of the maximum stoichiometry from one dimer molecule to two dimer molecules per the ssDNA oligomer<sup>1,56,81,100,127</sup>.

where  $K_N$  is the macroscopic binding constant characterizing the affinity for a given ssDNA oligomer, containing  $N$  nucleotides, and  $\Delta F_{\max}$  is the maximum relative fluorescence increase<sup>1,27,56,81,85,87,100</sup>. The solid lines in Figure 4.5a and Figure 4.5c are nonlinear least-squares fits of the experimental titration curves using equation 4.2, with a single set of binding and spectroscopic parameters for corresponding oligomers. The values of  $K_N$  for all studied ssDNA oligomers, which can accept only a single domain dimer, are included in Table 4.1<sup>1,56,81,100,127</sup>.

Within experimental error, the value of  $K_N$  increases with the length of the ssDNA oligomers (Table 4.1)<sup>1,56,81,100,127</sup>. This behavior indicates the presence of a statistical factor hidden in  $K_N$ , resulting from the fact that the number of nucleotides engaged in direct interactions with the ssDNA-binding site of the domain dimer,  $p$ , must be less than the length of the examined ssDNA oligomers<sup>1,56,57,81,85,87,94,95,100</sup>. In other words, the 181aa N-terminal domain dimer experiences the presence of potential binding sites, with the direct intrinsic interactions characterized by the intrinsic binding constant,  $K_i$ . The determined macroscopic binding constant,  $K_N$ , is then defined as<sup>1,56,57,81,85,87,94,95,100</sup>

$$K_N = (N - p + 1) K_i \quad (4.3)$$

and

$$K_N = N K_i - (p - 1) K_i \quad (4.4)$$

Thus,  $K_N$  should be a linear function of  $N$  with the slope  $\partial K_N / \partial N = K_i$ . Moreover, for  $K_N = 0$ , the plot of  $K_N$ , as a function of the DNA length, will intercept the  $N$  axis at the value of  $N = p - 1$ <sup>1,56,57,81,85,87,94,95,100</sup>.

The dependence of the macroscopic equilibrium constant,  $K_N$ , for the 181aa N-terminal domain dimer binding to the ssDNA oligomers, which can accept only a single dimer, as functions of the ssDNA oligomer length, is shown in Figure 4.8<sup>1,56,81,100,127</sup>. The plot is strictly linear, as predicted by equations 4.3 and 4.4<sup>1,56,57,81,85,87,94,95,100</sup>. Extrapolation of the plot to zero value of  $K_N$  intercepts the DNA length axis at  $N = p - 1 = 4.2 \pm 1$ . Thus the obtained data show that the 181aa N-terminal domain dimer engages in direct interactions only  $p = 5 \pm 1$  nucleotides of the nucleic acid<sup>1,56,57,81,85,87,94,95,100</sup>. In the examined solution conditions, the slope of the plot in Figure 4.8 provides the intrinsic binding constant  $K_i = (1.6 \pm 0.3) \times 10^4 \text{ M}^{-1}$  (Table 4.1)<sup>100</sup>.

#### **4.4.6 Intrinsic Affinities and Cooperativities of the 181aa N-terminal Domain Binding to the ssDNA Oligomers Which Can Accept Two Dimer Molecules.**

For the ssDNA oligomers, 26-, 30-, and 33-mer, which can accept two 181aa N-terminal domain dimers the partition function,  $Z_N$ , must account for the potential overlap of the binding sites and the possible cooperative interactions between the bound dimer molecules<sup>1,56,57,81,85,87,94,95,100</sup>. Such a binding system can be directly treated by the exact combinatorial theory for large ligand binding to a finite linear, homogeneous lattice<sup>1,56,57,81,85,87-89,94,95,100</sup>. The partition function,  $Z_N$ , is defined as

$$Z_N = \sum_{k=0}^g \sum_{j=0}^{k-1} P_N(k, j) (K_i P_F)^k \omega^j \quad (4.5)$$

where  $g$  is the maximum number of ligand molecules which may bind to the finite

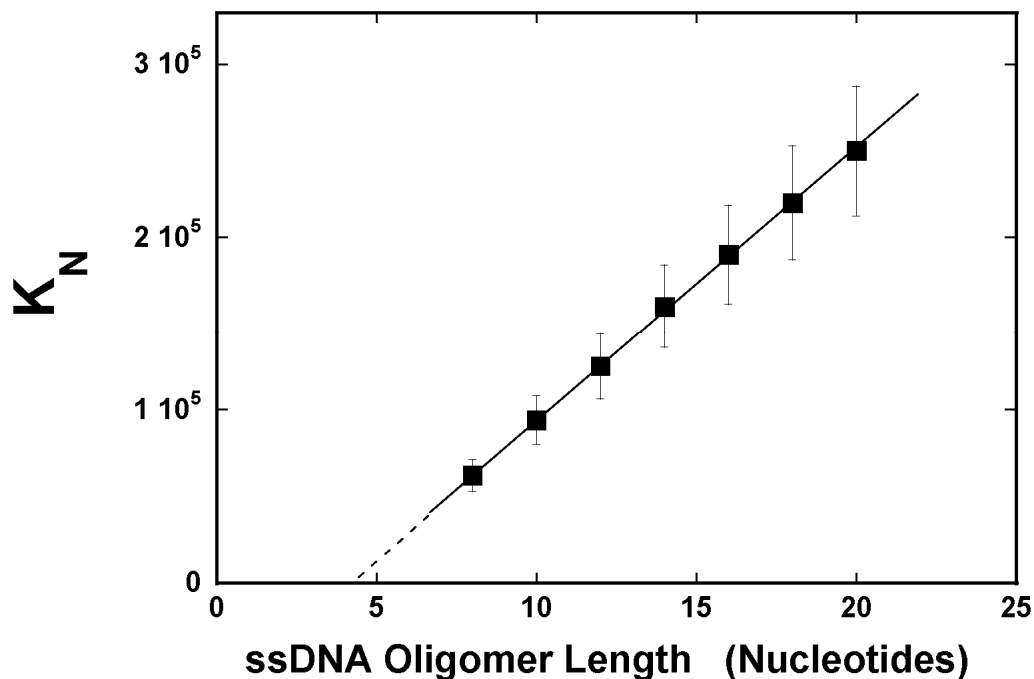


**Figure 4.8** The dependence of the macroscopic, equilibrium binding constant,  $K_N$ , characterizing the binding of the 181aa N-terminal domain dimer to different etheno-derivatives of the ssDNA oligomers, which accept only a single domain dimer, upon the length of the ssDNA oligomer (nucleotides)<sup>1,56,81,100,127</sup>. The solid line is the linear least-squares fit of the plot according to equations 4.3 and 4.4. The dashed line is the extrapolation of the plot to the zero value of the macroscopic equilibrium binding constant<sup>1,56,81,100,127</sup>.

nucleic acid lattice (for the nucleic acid lattice  $N$  residues long,  $g = N/n$ ),  $\omega$  is the cooperative interactions parameter,  $k$  is the number of ligand molecules bound, and  $j$  is the number of cooperative contacts between the  $k$  bound ligand molecules in a particular configuration on the lattice<sup>1,56,57,81,85,87-89,94,95,100</sup>. The combinatorial factor  $P_N(k, j)$  is the number of distinct ways that  $k$  ligands bind to a lattice, with  $j$  cooperative contacts, and is defined by<sup>1,56,57,81,85,87-89,94,95,100</sup>

$$P_N(k, j) = \frac{[(N - nk + 1)!(k - 1)!]}{[(N - nk + j + 1)!(k - j)!(k - j - 1)!]} \quad (4.6)$$

The total average degree of binding,  $\Sigma\Theta_i$ , is then

$$\Sigma\Theta_i = \frac{\sum_{k=1}^g \sum_{j=0}^{k-1} k P_N(k, j) (K_i P_F)^k \omega^j}{\sum_{k=0}^g \sum_{j=0}^{k-1} P_N(k, j) (K_i P_F)^k \omega^j} \quad (4.7)$$

The value of the relative fluorescence increase,  $F$ , at any titration point, is defined as

$$\Delta F = \Delta F_1 \left[ \frac{(N - n + 1) K_i P_F}{Z_N} \right] + \Delta F_{\max} \left[ \frac{\sum_{j=0}^{k-1} P_N(k, j) (K_i P_F)^k \omega^j}{Z_N} \right] \quad (4.8)$$

where  $\Delta F_1$  and  $\Delta F_{\max}$  are the relative molar fluorescence increases accompanying the binding of one and two domain dimers<sup>1,56,57,81,85,87-89,94,95,100</sup>. The values of the total site-size of the 181aa N-terminal domain - ssDNA complex,  $n = 13$ , is known. The value of

$\Delta F_1$  can be estimated for each particular ssDNA oligomer as  $\Delta F_1 = \partial \Delta F / \partial \Sigma \Theta_i$ , from the initial part of the plot of  $\Delta F$  as a function of  $\Sigma \Theta_i$ , as shown in Figure 4.6b for the 26-mer<sup>1,56,81,100,127</sup>. The value of  $\Delta F_{\max}$  is the maximum observed relative fluorescence increase and can be estimated from the parental fluorescence titration curves, as shown in Figure 4.6a<sup>1,56,81,100,127</sup>. Thus, two independent parameters,  $K_i$ , and  $\omega$  must be determined. The solid lines in Figure 4.6a are nonlinear least-squares fits of the titration curves using equations 4.5 – 4.8<sup>1,56,81,100,127</sup>. The obtained spectroscopic and binding parameters for all examined ssDNA oligomers, which can accommodate two domain dimers, are included in Table 4.1<sup>1,56,57,81,85,87-89,94,95,100</sup>.

The values of the intrinsic binding constants for the 26-, 30-, and 33-mer are similar to each other and to the values of  $K_i$ , obtained for the oligomers accommodating only a single dimer molecule<sup>1,56,81,100,127</sup>. Such similarity indicates that the same intrinsic binding process is observed, *i.e.*, the cooperative interactions do not affect the intrinsic affinity<sup>1,56,81,94,100,127</sup>. The value of the cooperativity parameter,  $\omega \approx 20 - 27$  is large, indicating the 181aa N domain dimer binds the ssDNA with significant positive cooperative interactions<sup>1,56,57,81,85,87-89,94,95,100</sup>. Interestingly, the value of  $\Delta F_1$ , which characterizes the binding of the first dimer, is lower than those observed for most of the ssDNA oligomers, which accept only a single dimer and it decreases with the length of the oligomer (Table 4.1)<sup>1,56,57,81,85,87-89,94,95,100</sup>.

#### **4.4.7 Only One Monomer of the 181aa N-Terminal Domain Dimer Can Effectively Engage in the Interactions with ssDNA. Photo-Cross-Linking Experiments.**

In the next step, we addressed the involvement of the monomers of the 181aa N-terminal domain dimer in interactions with the single-stranded nucleic acid using the UV

irradiation method<sup>81,92,100,102</sup>. UV irradiation produces covalent linkage between nucleic acid bases and amino acid residues, resulting in a "zero-length" cross-linking with minimal perturbation to the protein - nucleic acid complex<sup>81,92,100,102</sup>. Among the nucleic acid bases, thymine is the most reactive in the photo-crosslinking reactions<sup>81,92,100,102</sup>. Thus, parallel to the thermodynamic studies, we performed photo-cross-linking studies of the 181aa N-terminal domain complex with the radioactive [<sup>32</sup>P]-dT<sub>20</sub> (section 4.3.10)<sup>81,92,100,102</sup>. Recall, only a single 181N-terminal domain dimer can associate with the ssDNA 20-mer (Table 4.1)<sup>100</sup>.

Figure 4.9a shows the SDS polyacrylamide gel of the 181aa N-terminal domain alone (lane 6) and the 181N-terminal domain - 5'-[<sup>32</sup>P]-dT<sub>20</sub> complex, after irradiation, at different protein concentrations, stained with Coomassie Brilliant Blue (section 4.3.10)<sup>81,92,100,102</sup>. In the case of the protein - nucleic acid complex, at the highest protein concentration applied, the nucleic acid is completely saturated with the protein (data not shown)<sup>100</sup>. A single protein band at ~ 21,000 indicates the location of the 181aa N-terminal domain monomer<sup>81,92,100,102</sup>. Figure 4.9b shows the autoradiogram of the same SDS polyacrylamide gel of the 181aa N-terminal domain - 5'-[<sup>32</sup>P]-dT<sub>20</sub> complex<sup>100</sup>. A single predominant radioactive band appears on the gel, at the molecular weight of ~26,000, corresponding to the 181aa N-terminal monomer - 20-mer complex<sup>100</sup>. This band is undetectable on the Coomassie Brilliant Blue stained gel because of the very low efficiency of the photo-cross-linking reaction<sup>100</sup>. It is evident that only one monomer of the 181aa N-terminal domain dimer principally engages the ssDNA in interactions in the complex<sup>100</sup>. Nevertheless, a very slight radioactive band at the molecular weight of ~ 46,000, corresponding to the 181aa N- domain dimer, indicates that the DNA-binding subsite of the other monomer may engage the DNA, although at much lower efficiency<sup>81,92,100,102</sup>.

#### 4.4.8 Base Specificity of 181aa N-terminal Domain – ssDNA Interactions. Lattice Competition Titrations Using the MCT.

Quantitative determination of affinities of the 181N-terminal domain for unmodified ssDNAs, differing by the type of base, has been performed, using the macromolecular competition titration (MCT) method<sup>1,56,57,81,87,92,95,100</sup>. The approach is based on the same thermodynamic arguments as applied to quantitative titrations (see section 3.4.4)<sup>1,57,81,87,92,95,100,126,127</sup>. Shortly, in the presence of the competing unmodified ssDNA, the protein binds to two different nucleic acids that are present in the solution, while the observed signal originates only from the fluorescent "reference" nucleic acid<sup>1,57,81,87,92,95,100,126,127</sup>. In this work, as a reference lattice, the 20-mer, dεA(pεA)<sub>19</sub>, was used and the base specificity of the 181aa N-terminal domain has been examined using different 20-mers, dN(pN)<sub>19</sub><sup>100</sup>. At a given titration point, “i”, the total concentration of the bound protein, P<sub>b</sub>, is defined as

$$P_b = (\sum \Theta_i)_R M_{TS} + (\sum \Theta_i)_S M_{TS} \quad (4.9)$$

where  $(\sum \Theta_i)_R$  and  $(\sum \Theta_i)_S$  are the total average degree of binding of the domain on the reference dεA(pεA)<sub>19</sub> and the examined oligomer, dN(pN)<sub>19</sub>, respectively, M<sub>TR</sub> and M<sub>TS</sub> are the total concentrations of the reference and the unmodified 20-mer, respectively<sup>1,56,57,81,87,92,95,100,127</sup>. Using the corresponding macroscopic binding constant, K<sub>NR</sub> and K<sub>NS</sub>, the above expression is defined as

$$P_b = \left( \frac{K_{NR} P_F}{1 + K_{NR} P_F} \right) M_{TR} + \left( \frac{K_{NS} P_F}{1 + K_{NS} P_F} \right) M_{TS} \quad (4.10)$$



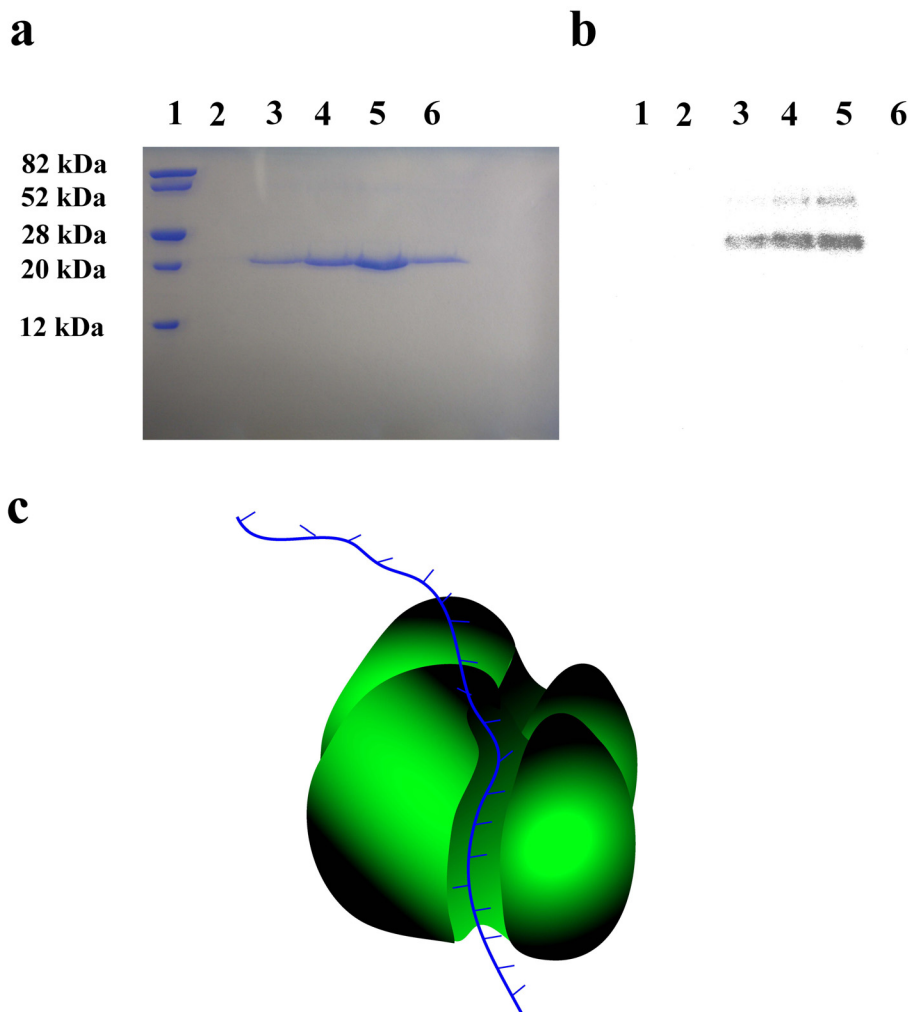


**Figure 4.9 Photo-cross-linking of PriA 181aa N-terminal domain to ssDNA 20-mer.** **a.** 15% SDS polyacrylamide gel of the 181aa N-terminal domain - 5' [ $^{32}$ P]-dT<sub>20</sub> complex after UV-mediated cross-linking at different concentration of the domain dimer stained with Coomassie Brilliant Blue<sup>81,92,100,102</sup>. The concentration of the 5' [ $^{32}$ P]-dT<sub>20</sub> is [ $3 \times 10^{-7}$  M] (oligomer)<sup>100</sup>. Lane 1 contains protein markers. Lane 2 contains 5' [ $^{32}$ P]-dT<sub>20</sub> alone<sup>100</sup>. Lanes 3 to 5 contain the constant concentration of the ssDNA 20-mer and the increasing concentration of the domain (dimer): lane 3,  $3 \times 10^{-6}$  M; lane 4,  $6 \times 10^{-6}$  M; and lane 5,  $9.0 \times 10^{-6}$  M<sup>100</sup>. Lane 6 contains only the 181aa N-terminal domain ( $3 \times 10^{-6}$  M (dimer)) in the absence of the 5' [ $^{32}$ P]-dT<sub>20</sub><sup>100</sup>. **b.** The autoradiogram of the same SDS polyacrylamide gel, as shown in panel a<sup>100</sup>. **c.** Schematic model of the 181aa N-terminal domain dimer - ssDNA complex<sup>100</sup>.

The concentration of the free protein,  $P_F$ , is then

$$P_F = P_T - P_b \quad (4.11)$$

where  $P_T$  is the known total concentration of the 181aa N-terminal domain dimer. The observed relative fluorescence increase,  $\Delta F$ , is then defined by equation 4.2<sup>1,56,57,81,87,92,95,100</sup>.

Fluorescence titrations of dεA(pεA)<sub>19</sub> with the 181N-terminal domain in buffer C205 in the presence of two different dA(pA)<sub>19</sub> concentrations, are shown in Figure 4.10a<sup>1,57,81,100,127</sup>. For comparison, the titration curve of dεA(pεA)<sub>19</sub> in the absence of the competing oligomer is also included<sup>1,57,81,100,127</sup>. The titration curve shifts, with increasing dA(pA)<sub>19</sub> concentration, indicating a significant competition between dεA(pεA)<sub>19</sub> and the unmodified 20-mer for the domain<sup>1,57,81,100,127</sup>. Because  $K_{NR} = 2.5 \times 10^5 \text{ M}^{-1}$  and  $\Delta F_{\max} = 1.15$  are known from independent titration experiments (Table 4.1), the solid lines in Figure 4.10a are nonlinear least-squares fits of the experimental titration curves, with a single fitting parameter,  $K_{NS}$ , using equations 4.9- 4.11<sup>100</sup>. The binding constants for all examined 20-mers, differing by the type of base, are included in Table 4.2<sup>1,56,57,81,87,92,95,100</sup>. The obtained value of  $K_{NS}$  are similar for dA(pA)<sub>19</sub> and dT(pT)<sub>19</sub>, respectively. Nevertheless, the domain show modest preference for dC(pC)<sub>19</sub>, with the intrinsic binding constant being higher by a factor of ~3 than the analogous parameter determined for the dA(pA)<sub>19</sub> and dT(pT)<sub>19</sub><sup>1,56,57,81,87,92,95,100</sup>.

#### **4.4.9 Conformational and 3' End Specificity of 181aa N-Terminal Domain – ssDNA Interactions.**

The specific binding to the 3'-OH end group of deoxyribose by the PriA N-

terminal domain, during the damaged DNA site recognition, has been invoked as the major feature, which allows the helicase to position itself on the nucleic substrate<sup>97,98,100,104</sup>. Therefore, the effect of the presence of the phosphate group at the 3'-OH group, which blocks the access to the 3' OH group of the terminal deoxyribose, on the 181aa N-terminal domain association with the ssDNA 20-mer, dC(pC)<sub>18</sub>pCp, has been addressed using the MCT method (see section 4.4.7)<sup>1,56,57,81,87,92,95,100</sup>. The homocytidine oligomer has been selected because of its highest affinity for the domain (Table 4.2)<sup>100</sup>. Fluorescence titrations of dεA(pεA)<sub>19</sub> with the 181aa N-terminal domain, in the absence of presence of two different concentrations of dC(pC)<sub>18</sub>pCp, are shown in Figure 4.10b<sup>57,81,100,127</sup>. As observed for dA(pA)<sub>19</sub> (Figure 4.10a), the titration curves significantly shift in the presence of dC(pC)<sub>18</sub>pCp, indicating efficient competition for the domain by the oligomer<sup>57,81,100,127</sup>. The solid lines in Figure 4.10b are nonlinear least-squares fits of the experimental titration curves, with a single fitting parameter,  $K_{NS}$ , using equations 4.9 – 4.11<sup>57,81,100,127</sup>. It is clear that the obtained value of  $K_{NS} = (1.6 \pm 0.3) \times 10^6 \text{ M}^{-1}$  is only by a factor of  $\sim 3$  lower than determined for the analogous dC(pC)<sub>19</sub> (Table 4.2)<sup>1,56,57,81,87,92,95,100</sup>. Thus, the presence of the phosphate group, which blocks access to the 3'-OH terminal group of the ssDNA oligomer, has rather a modest effect on the 181aa N-terminal domain association<sup>57,81,100,127</sup>. Finally, fluorescence titrations of dεA(pεA)<sub>19</sub> with the 181aa N-terminal domain, in the absence of presence of two different concentrations of the dsDNA 10-mer are shown in Figure 4.10c<sup>57,81,100,127</sup>. The solid lines in Figure 4.10c are nonlinear least-squares fits of the experimental titration curves, with a single fitting parameter,  $K_{NS}$ , using equations 4.9 - 4.11. Surprisingly, the obtained value of  $K_{NS} = (3.0 \pm 1.0) \times 10^7 \text{ M}^{-1}$  is higher by a factor of  $\sim 6$  than  $K_{NS}$  obtained for dC(pC)<sub>19</sub>, and more than an order of magnitude higher than the macroscopic affinity of dA(pA)<sub>19</sub>, and dT(pT)<sub>19</sub> (Table 4.2)<sup>1,56,57,81,87,92,95,100</sup>.

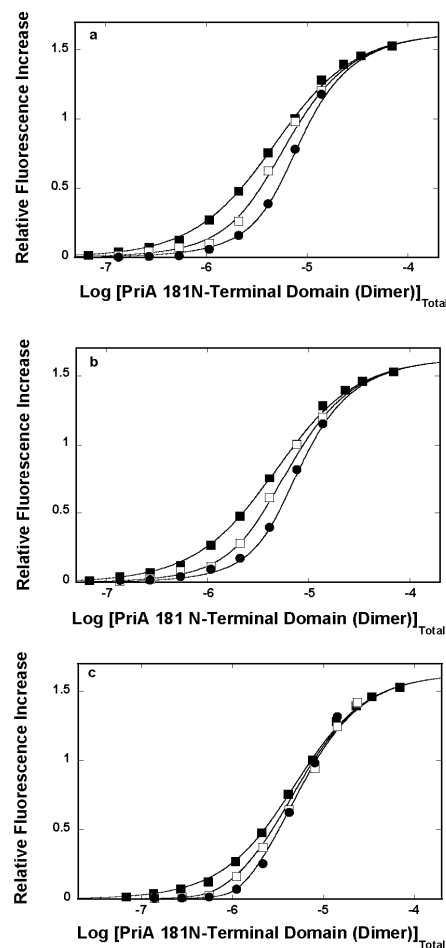


**Figure 4.10 Lattice Competition Titrations.** **a.** Fluorescence titrations of the ssDNA 20-mer, dεA(pεA)<sub>19</sub> [ $1.43 \times 10^{-6}$  M (oligomer) in all panels] with the 181aa N-terminal domain in the absence (■) and presence of two different concentrations of dT(pT)<sub>19</sub>,  $1.74 \times 10^{-6}$  M (□) and  $4.16 \times 10^{-6}$  M (●) (oligomer), respectively<sup>57,81,100,127</sup>. **b.** Fluorescence titrations of the ssDNA 20-mer, dεA(pεA)<sub>19</sub>, with the 181aa N-terminal domain in the absence (■) and presence of two different concentrations of dC(pC)<sub>18</sub>pCp,  $1.71 \times 10^{-6}$  M (□) and  $3.73 \times 10^{-6}$  M (●) (oligomer)<sup>57,81,100,127</sup>. **c.** Fluorescence titrations of the ssDNA 20-mer, dεA(pεA)<sub>19</sub>, with the 181aa N-terminal domain in the absence (■) and presence of two different concentrations of dsDNA 10-mer<sup>100</sup>. The concentrations of the dsDNA 10-mer are:  $5.0 \times 10^{-7}$  M (□) and  $1.0 \times 10^{-6}$  M (●) (oligomer), respectively<sup>57,81,100,127</sup>. The solid lines in all panels are nonlinear least-squares fits of the titration curves using equations 4.9 – 4.11, with the binding  $K_N = 1.7 \times 10^6 \text{ M}^{-1}$  and  $\Delta F_{\text{max}} = 1.18$  for dεA(pεA)<sub>19</sub>. The binding constants for the examined nucleic acids are included in Table 4.2<sup>57,81,100,127</sup>.

#### **4.4.10 The Salt Effect on the 181aa N-Terminal Domain of PriA – ssDNA Interactions.**

Fluorescence titrations of dεA(pεA)<sub>17</sub> with the 181aa N-terminal domain, in buffer C205 containing different NaCl concentrations, are shown in Figure 4.11a<sup>100</sup>. Increasing the salt concentration in solution clearly decreases the macroscopic affinity of the domain for the nucleic acid, as the titration curves shift toward higher protein concentrations range<sup>1,27,56,57,81,83,84,92,100</sup>. Also, there is a decline of the maximum fluorescence increase at saturation,  $\Delta F_{\max}$ , from  $\sim 1.9$  at 20 mM to  $\sim 1.2$  at 88.6 mM NaCl, indicating the changing structure of the nucleic acid in the complex<sup>1,27,56,57,81,83,84,92,100</sup>. The solid lines in Figures 4.11a are nonlinear least-squares fits to a single-site binding model with two fitting parameters,  $K_N$ , and the maximum relative fluorescence increase,  $\Delta F_{\max}$  (equation 4.2)<sup>100</sup>. Figure 4.11b shows the dependence of the logarithm of  $K_N$  upon the logarithm of NaCl concentration (log-log plots)<sup>1,27,56,57,81,83,84,92,100</sup>. Within experimental accuracy, the plot is linear in the examined salt concentration range and characterized by the slopes  $\partial \log K_N / \partial \log [\text{NaCl}] = -1.2 \pm 0.3$ <sup>100</sup>. The value of the slope indicates that there is a net release of  $\sim 1$  ion upon the complex formation<sup>1,56,57,81,83,84,92,100</sup>.

#### **4.4.11 The 181aa N-terminal Domain of PriA Helicase Binds Nucleotide Cofactors.**

As mentioned above, the intact PriA helicase has two nucleotide binding sites dramatically differing in their affinities, the strong and weak nucleotide binding sites<sup>27,59-61,92,99,100</sup>. However, the location of these sites with respect to the domain structure of the protein is unknown<sup>100</sup>. Surprisingly and similarly to the intact PriA molecule, the ADP analog, TNP-ADP, binds to the 181aa N-terminal domain of PriA<sup>59-61,100</sup>. Moreover, the

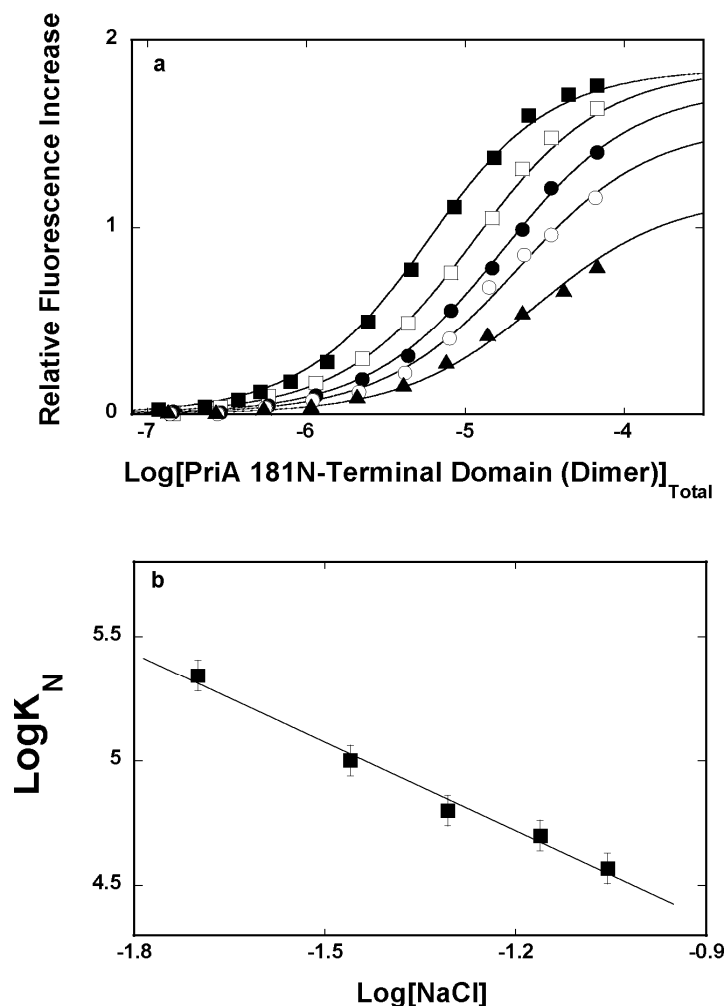


**Figure 4.11 The salt effect on the 181aa N-terminal domain – ssDNA interactions.**  
**a.** Fluorescence titrations of the ssDNA 18-mer, dεA(pεA)<sub>17</sub> [ $2.43 \times 10^{-6}$  M (oligomer)] with the 181aa N-terminal domain containing different NaCl concentrations: 20 mM (■); 34.7 mM (□); 49.4 mM (●); 69 mM (○), and 89 mM (▲)<sup>1,57,81,83,84,92,100</sup>. The solid lines are nonlinear least-squares fits of the titration curves, using equation 2.4, with  $\Delta F_{\max}$  and  $K_N$ :  $1.85, 2.2 \times 10^5 \text{ M}^{-1}$  (■);  $1.85, 1 \times 10^5 \text{ M}^{-1}$  (□);  $1.75, 6.3 \times 10^4 \text{ M}^{-1}$  (●);  $1.55, 5 \times 10^4 \text{ M}^{-1}$  (○);  $1.17, 3.7 \times 10^4 \text{ M}^{-1}$  (▲)<sup>100</sup>. **b.** The dependence of the logarithm of the binding constant,  $K_N$  upon the logarithm of [NaCl]<sup>1,57,81,83,84,92,100</sup>. The solid line is the linear least-squares fit, which provides the slope,  $\partial \text{Log}K_N / \partial \text{Log}[\text{NaCl}] = -1.2 \pm 0.3$ <sup>100</sup>.

association is accompanied by a very strong quenching of the protein fluorescence, providing an excellent signal to monitor the association process<sup>59-61,100</sup>. Fluorescence titrations of the 181aa N-terminal domain with TNP-ADP, at three different protein concentrations, in buffer C205, are shown in Figure 4.12a<sup>59-61,100,101,123</sup>. The maximum quenching of the protein fluorescence at saturation is  $1.0 \pm 0.05$ <sup>100</sup>. The selected protein concentrations provide separation of the titration curves up to a quenching value of  $\sim 0.65$ <sup>59-61,100</sup>.

Quantitative analysis of the titration data has been performed using the quantitative method, analogous to the approach applied in the nucleic acid binding studies and outlined in section 2.3.7, section 4.3.6, and section 4.3.7<sup>1,56-61,85-89,92,95,100,101,123</sup>. The dependence of the observed relative fluorescence quenching,  $\Delta F$ , upon the total average degree of binding,  $\Sigma\Theta_i$ , of TNP-ADP on the 181aa N-terminal domain dimer is shown in Figure 4.12b<sup>59-61,100,101,123</sup>. The separation of the titration curves allows us to obtain the values of  $\Sigma\Theta_i$  up to  $\sim 1.5$  TNP-ADP molecules per dimer<sup>100</sup>. The plot is, within experimental accuracy, linear<sup>100</sup>. Extrapolation to the maximum value of the quenching provides the stoichiometry of the complex as  $2.2 \pm 0.2$ <sup>100</sup>. Therefore, the data show that the 181N-terminal domain dimer binds two molecules of TNP-ADP, indicating that each monomer binds a single nucleotide cofactor molecule<sup>1,59-61,81,92,95,100,101</sup>.

#### **4.4.12 The Statistical Thermodynamic Model for the Nucleotide Cofactor Binding to the 181N-Terminal Domain Dimer.**

Because of the 181aa N-terminal domain dimer is built of two identical monomers, the two nucleotide-binding sites must be structurally identical, although they may be energetically different<sup>1,59,100,101,123</sup>. Therefore, the simplest statistical

thermodynamic model, *i.e.*, the model containing the fewest number of parameters, that can account for the observed binding process includes two nucleotide-binding sites, characterized by two different intrinsic affinities described by intrinsic binding constant,  $K_{C1}$  and  $K_{C2}$ , respectively, and possible cooperative interactions between the sites, accounted for by the cooperative interaction parameter,  $\sigma$ <sup>1,59,100,101,123</sup>. The partition function,  $Z$ , of the system is then defined as

$$Z=1+(K_{C1}+K_{C2})L_F+K_{C1}K_{C2}\sigma L_F^2 \quad (4.12)$$

where  $L_F$  is the free nucleotide cofactor concentration<sup>1,59,100,101,123</sup>. The total average degree of binding,  $\Sigma\Theta_i$ , is defined as

$$\Sigma\Theta_i = \frac{(K_{C1}+K_{C2})L_F+2K_{C1}K_{C2}\sigma L_F^2}{Z} \quad (4.13)$$

The linear character of the plot in Figure 4.12b indicates that binding of the first and second cofactor molecules is characterized by the same, relative partial quenching of the protein tryptophans<sup>1,85,94,95,100,101</sup>. Therefore, experimentally observed fluorescence quenching,  $\Delta F$ , expressed in terms of the binding parameters,  $K_C$  and  $\sigma$ , is then

$$\Delta F = \Delta F_{\max} \left( \frac{(K_{C1}+K_{C2})L_F+K_{C1}K_{C2}\sigma L_F^2}{Z} \right) \quad (4.14)$$

There are three unknown parameters,  $K_{C1}$ ,  $K_{C2}$ , and  $\sigma$  in equations. 4.12 – 4.14<sup>1,85,94,95,100,101</sup>. The solid lines in Figure 4.12a are the nonlinear least-squares fits of the titration curves using equations 4.12 – 4.14, with a single set of the spectroscopic and



binding parameters<sup>1,95,100,101</sup>. The fit provides excellent description of the binding process. The obtained intrinsic binding constants and cooperativity parameter are:  $K_{C1} = K_{C2} = (4.1 \pm 0.6) \times 10^4 \text{ M}^{-1}$  and  $\sigma = 1 \pm 0.2$ , respectively<sup>100</sup>. The same values of both intrinsic binding constants indicate that the nucleotide cofactor sites are not only structurally but also energetically identical<sup>100</sup>. Moreover, the value of  $\sigma \approx 1$  indicates that binding of the cofactor to two nucleotide-binding sites of the 181aa N-terminal dimer is not characterized by any cooperative interactions<sup>1,81,85,94,95,100,101</sup>.

It was shown by Lucius *et al.*, that the same solution conditions, TNP-ADP binds to the strong and weak nucleotide-binding sites of the intact PriA helicase with the intrinsic binding constants:  $K_S = (1.5 \pm 0.5) \times 10^6 \text{ M}^{-1}$ ,  $K_W = (1.9 \pm 0.6) \times 10^4 \text{ M}^{-1}$ , respectively, and the cooperativity parameter,  $\sigma = 1 \pm 0.3$ <sup>59-61,100</sup>. Thus, the intrinsic binding constants of the two sites of the intact enzyme differs by  $\sim 2$  orders of magnitude<sup>59-61,100</sup>. Such a dramatic difference between the affinities of the two nucleotide-binding sites of the intact PriA protein facilitates the assignment of the nucleotide-binding site of the 181aa N-terminal domain. Figure 4.12c shows the dependence of  $\Sigma\Theta_i$  of the TNP-ADP on the intact PriA helicase and the isolated 181aa N-terminal domain dimer as function of the free cofactor concentration<sup>59-61,100</sup>. The plots have been generated using the binding parameters for the intact enzyme and the 181aa N domain dimer as provided above<sup>59-61,100</sup>. The isotherm for the 181aa N-terminal domain is strongly shifted toward the higher nucleotide concentration range<sup>100</sup>. In other words, it reflects the cofactor association with the weak nucleotide-binding site of the intact PriA protein, as expressed by the value of  $K_C \approx 4.1 \times 10^4 \text{ M}^{-1}$ , being very close to the intrinsic binding constant  $K_S \approx 1.9 \times 10^4 \text{ M}^{-1}$ , of the weak nucleotide-binding site<sup>59-61,100</sup>. Therefore, obtained data indicate that the nucleotide-binding site located on the N-

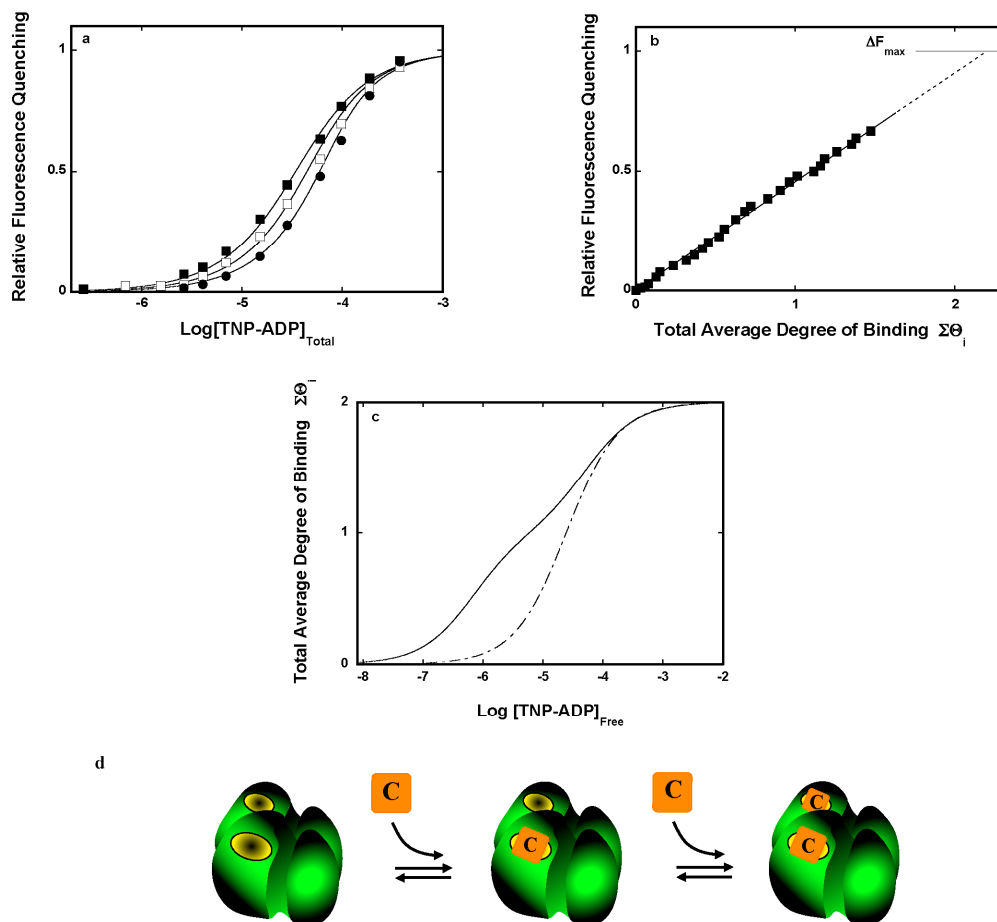


**Figure 4.12 The 181aa N-terminal Domain of the PriA helicase binds nucleotide cofactors.** **a.** Fluorescence titrations of the 181aa N-terminal domain with TNP-ADP at different protein concentrations (dimer):  $9.85 \times 10^{-6} \text{ M}$  (■),  $2.0 \times 10^{-5} \text{ M}$  (□),  $3.5 \times 10^{-5} \text{ M}$  (●)<sup>1,59,95,100,101</sup>. The solid lines are nonlinear least-squares fits of the titration curves, according to the model described by equations 4.12 – 4.14, using a single set of binding parameters:  $K_{C1} = K_{C2} = 4.1 \times 10^4 \text{ M}^{-1}$ ,  $\sigma = 1$ , and  $\Delta F_{\text{max}} = 1.0$ <sup>100</sup>. **b.** Dependence of the relative fluorescence quenching,  $\Delta F$ , upon the average degree of binding of TNP-ADP on the 181aa N-terminal domain dimer,  $\Sigma\Theta_i$ , (■)<sup>1,59,100,101,123</sup>. The solid line follows the experimental points and does not have a theoretical basis<sup>100</sup>. The dashed line is an extrapolation of  $\Sigma\Theta_i$  to the maximum value of the fluorescence quenching,  $\Delta F_{\text{max}}$ <sup>100</sup>. **c.** The dependence of the total average degree of binding of TNP-ADP on the intact PriA helicase (solid line) and on the 181aa N-terminal domain dimer as a function of the free cofactor concentration<sup>1,59,95,100,101</sup>. The plots were generated using the binding parameters for the intact enzyme and the for the domain dimer, respectively<sup>59-61,100</sup>. **d.** Schematic representation of the nucleotide cofactor binding to the 181N-terminal domain dimer<sup>100</sup>.

terminal domain of PriA corresponds to the weak nucleotide-binding site of the intact PriA helicase<sup>100</sup>.

#### **4.4.13 The 181aa N-Terminal Domain – ssDNA Interactions in the Presence of ADP or ATP $\gamma$ S.**

Characteristic feature of the nucleotide effect on the intact PriA helicase association with the ssDNA is that saturation of the weak nucleotide-binding site with ADP but not ATP analog, ATP $\gamma$ S, dramatically increases the enzyme affinity for the nucleic acid<sup>27,59-61,92,99,100</sup>. On the other hand, saturation of only the strong nucleotide-binding site with ADP or ATP $\gamma$ S has no effect on the enzyme ssDNA-affinity<sup>27,59-61,92,99,100</sup>. Fluorescence titrations of the ssDNA 18-mer, dεA(pεA)<sub>17</sub>, with the 181aa N-terminal domain in buffer C205, in the absence and presence of two different concentrations of ADP, are shown in Figure 4.13a<sup>100</sup>. The solid lines in Figure 4.13a are nonlinear least-squares fits of the titration curves, using the single-site binding isotherm (equation 4.2)<sup>59-61,100</sup>. The presence of [ADP] = 1 x 10<sup>-5</sup> M, which would fill the strong nucleotide-binding site of the intact enzyme slightly diminishes the 181aa N-terminal domain affinity for the ssDNA with  $K_N = (1.9 \pm 0.4) \times 10^5 \text{ M}^{-1}$  as compared to  $K_N = (2.2 \pm 0.4) \times 10^5 \text{ M}^{-1}$ , determined in absence of the cofactor<sup>59-61,100</sup>. However, at [ADP] = 3 x 10<sup>-3</sup> M, which saturates the 181aa N-terminal nucleotide binding site, as well as the weak nucleotide-binding site of the intact PriA, the affinity of the domain for the nucleic acid is increased by a factor of ~ 5 with a concomitant increase of  $\Delta F_{\text{max}}$ <sup>59-61,100</sup>.

Analogous fluorescence titrations of the ssDNA 18-mer, dεA(pεA)<sub>17</sub>, with the 181aa N-terminal domain in the absence and presence of ATP $\gamma$ S, at two different concentrations of the nucleotide cofactor, are shown in Figure 4.13b<sup>100</sup>. The effect of the nucleoside tri-phosphate is very different from the effect of ADP (Figure 4.13a)<sup>59-61,100</sup>.

At low concentration of ATP $\gamma$ S ( $1 \times 10^{-4}$  M), which would saturate the strong nucleotide-binding site of the intact PriA protein, the ssDNA affinity of the domain detectably decreases to  $K_N = (1.4 \pm 0.3) \times 10^5 \text{ M}^{-1}$  with no effect on the observed  $\Delta F_{\text{max}}^{59-61,100}$ . Similarly, at  $[\text{ATP}\gamma\text{S}] = 3 \times 10^{-3}$  M, which saturates both the strong and weak nucleotide-binding site of the intact enzyme and the nucleotide-binding sites of the 181aa N-terminal domain, the value of  $K_N$  is hardly affected by the cofactor ( $K_N = (1.8 \pm 0.4) \times 10^5 \text{ M}^{-1}$ ), as compared to the affinity obtained in the absence of ATP $\gamma$ S, although the value of the observed  $\Delta F_{\text{max}}$  is slightly decreased<sup>59-61,100</sup>.

## 4.5 DISCUSSION

### 4.5.1 The 181aa N-Terminal Domain Dimer Has Only One Effective ssDNA Binding Site.

The crystallographic analyses of the 105aa N-terminal subdomain dimer suggested that the dimer has two DNA-binding sites, though not necessarily energetically equivalent ones<sup>100,104</sup>. Similarly, 181aa N-terminal domain dimer should also be built of two identical monomers and possess two structurally identical and potential DNA-binding sites, each located on a different monomer<sup>100,104</sup>. On the contrary, thermodynamic and photo-cross-linking data show that, in solution, only a single monomer of the 181aa N-terminal domain predominantly engages the ssDNA (Figure 4.5, Figure 4.9, and Table 4.1)<sup>100</sup>. Notice, only a single domain dimer binds to the 20- or 24-mer, although the length of these oligomers is large enough to fully access to the DNA-binding site on the second monomer (Figure 4.8, Table 4.1)<sup>100</sup>. In fact, the photo-cross-linking data indicate that the second monomer of the 181aa N-terminal domain may very weakly engage the nucleic acid (Figure 4.9b)<sup>100</sup>. Nevertheless, the local concentration of these longer oligomers in the complex with the domain dimer is very high. Thus, the affinity of the second binding

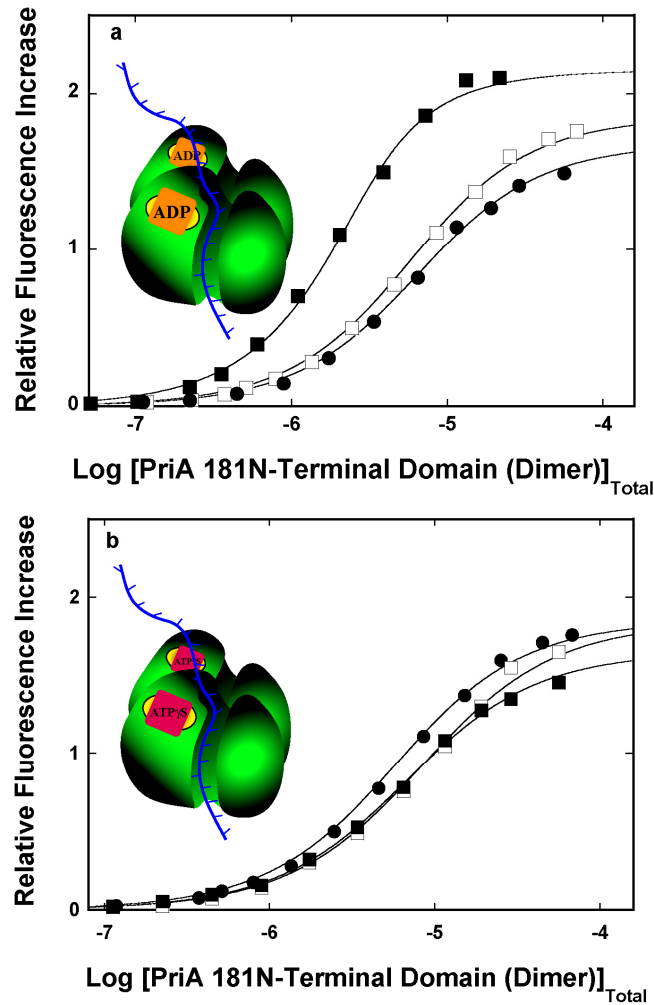


**Figure 4.13 The 181aa N-Terminal Domain – ssDNA Interactions in the Presence of ADP or ATP $\gamma$ S.** **a.** Fluorescence titrations of the ssDNA 18-mer, d $\epsilon$ A(p $\epsilon$ A)<sub>17</sub> [ $2.43 \times 10^{-6}$  M(oligomer)] with the 181aa N-terminal domain in the absence ( $\square$ ) and presence of different ADP concentrations:  $1 \times 10^{-5}$  M ( $\bullet$ );  $3 \times 10^{-3}$  M ( $\blacksquare$ )<sup>100</sup>. The concentration of the ssDNA 18-mer is  $2.43 \times 10^{-6}$  M (oligomer)<sup>100</sup>. The solid lines are nonlinear least-squares fits of the titration curves, using equation 4.2 with  $\Delta F_{\max}$  and  $K_N$ :  $1.85, 2.2 \times 10^5 \text{ M}^{-1}$  ( $\square$ );  $1.68, 1.9 \times 10^5 \text{ M}^{-1}$  ( $\bullet$ );  $2.15, 1.2 \times 10^6 \text{ M}^{-1}$  ( $\blacksquare$ )<sup>59-61,100</sup>. **b.** Fluorescence titrations of the ssDNA 18-mer, d $\epsilon$ A(p $\epsilon$ A)<sub>17</sub>, with the 181aa N-terminal domain in the absence ( $\bullet$ ) and presence of different ATP $\gamma$ S concentrations:  $1 \times 10^{-4}$  M ( $\square$ ) and  $3 \times 10^{-3}$  M ( $\blacksquare$ ), respectively<sup>100</sup>. The solid lines are nonlinear least-squares fits of the titration curves, using equation 4.2, with  $\Delta F_{\max}$  and  $K_N$ :  $1.85, 2.2 \times 10^5 \text{ M}^{-1}$  ( $\square$ );  $1.84, 1.4 \times 10^5 \text{ M}^{-1}$  ( $\bullet$ );  $1.65, 1.8 \times 10^6 \text{ M}^{-1}$  ( $\blacksquare$ )<sup>59-61,100</sup>. Inserts schematically show the final tertiary complexes of the examined association processes in the presence of saturating concentration of the corresponding nucleotide cofactor<sup>100</sup>.

site must be very low, or otherwise it would be easily accessed by the long oligomers and manifested in a large change in the total site-size of the complex, and the intrinsic affinity<sup>81,100</sup>. However, this is not experimentally observed (Figure 4.7 and Figure 4.8)<sup>100</sup>. The total site-size of the 181aa N-terminal dimer complexes with the longer oligomers is  $13 \pm 1$  nucleotides and the intrinsic affinity is, within experimental accuracy, the same as the corresponding affinity of the shorter oligomers (Table 4.1)<sup>100</sup>. The lack of any significant DNA-binding activity of the second monomer of the 181aa N-terminal domain dimer with ssDNA oligomer, which encompasses the site-size of  $\sim 5$  nucleotides of the DNA-binding subsite, most probably results from a steric hindrance induced by the active, binding competent, monomer (Figure 4.9)<sup>100</sup>.

#### **4.5.2 The Small Number of Nucleotides Engaged in Direct Interactions with the ssDNA Indicates That the DNA-Binding Subsites of Intact PriA Helicase are Spatially Separated.**

The binding site of the 181aa N-terminal domain engages in direct interactions only  $\sim 5$  nucleotides of the ssDNA (Figure 4.8). Such a small site-size provides indication that only one monomer of the dimer interacts with the nucleic acid<sup>81,100</sup>. Notice, the maximum relative fluorescence increase of the etheno-adenosine ssDNA oligomers,  $\Delta F_{\text{max}}$ , induced upon the domain binding, gradually decreases with the length of the oligomer (Table 4.1)<sup>100</sup>. This behavior can be explained by the fact that as the number of the nucleotides in the nucleic acid increases, the number of the nucleotides directly engaged in interactions with the protein ( $\sim 5$ ) remains unchanged<sup>100</sup>. Recall, the total site-size of the DNA-binding site of the intact PriA helicase is  $\sim 20$  nucleotides, while the site-size of the strong DNA-binding subsite on the helicase domain is only  $\sim 6$  nucleotides<sup>1,27,56-61,92,100</sup>. Thus, when both subsites interact with the nucleic acid, *e.g.*,

when both nucleotide-binding sites are saturated with ADP, the intact enzyme engages in direct interactions only ~ 10 - 11 nucleotides of the DNA<sup>1,27,56-61,92,100</sup>. These data suggest that the strong DNA-binding subsite on the helicase domain and the subsite on the N-terminal domain are spatially separated in the intact enzyme molecule by a distance corresponding to at least ~ 3 - 5 nucleotides of the ssDNA, *i.e.*, they do not form a structurally continuous entity<sup>1,27,56-61,81,92,100</sup>.

#### **4.5.3 The Ability of 181aa N-Terminal Domain to Bind to the ssDNA in the Absence of Nucleotide Cofactors Indicates the Presence of Allosteric Domain – Domain Motions in the Intact Enzyme.**

In the case of the intact PriA helicase, the DNA-binding subsite of the N-terminal domain becomes involved in interactions with the ssDNA only in the presence of ADP concentration, which is high enough to saturate the weak nucleotide-binding site<sup>27,59-61,92,100</sup>. As we previously proposed, the subsite on the N-terminal domain must be in “closed” conformation in the intact enzyme and transforms to the “open” conformation in the presence of high [ADP]<sup>27,56-61,92,100</sup>. On the other hand, the isolated domain is able to efficiently bind the nucleic acid in the absence of the cofactor, although with lower affinity (Table 4.1)<sup>100</sup>. If the DNA-binding subsite in the intact enzyme was in open conformation, the intrinsic ssDNA-affinity of the isolated 181aa N-terminal domain subsite, even in the absence of ADP, would be too high to prevent the subsite from engaging in the interactions with the ssDNA (Tables 4.1 and 4.2)<sup>100</sup>. The fact that the isolated domain associates with the nucleic acid even in the absence of ADP indicates the presence of a significant transition from the closed to open conformations in the intact PriA molecule<sup>27,56-61,92,100</sup>. This inter-domain movement, induced by ADP binding to the

week nucleotide binding site of PriA would allow the N-terminal domain to engage in the interactions with additional fragments of ssDNA<sup>27,56-61,92,100</sup>.

#### **4.5.4 The 181aa N-Terminal Domain DNA-Binding Subsite Has Only a Slight Preference for the 3' End of the Nucleic Acid.**

The specific binding of the N-terminal domain subsite of PriA helicase to the deoxyribose OH group at the 3' end of the nucleic acid has been proposed as important factor in the recognition of the damaged replication fork by PriA, even in the absence of the nucleotide cofactors<sup>97,100,104</sup>. However, quantitative thermodynamic and kinetic analyses of the enzyme binding to the ssDNA oligomers, previously reported by the Bujalowski's group, did not indicate the presence of any significant and specific affinity of the intact enzyme for the 3' end of the nucleic acid<sup>56-61,100</sup>. However, it was shown that the enzyme predominantly binds the ssDNA, gapped DNA substrates, and dsDNA using its strong DNA-binding subsite located on the helicase domain, not the weak subsite, which was proposed to be sited on the 181aa N-terminal domain of the protein (Chapter 2 and Chapter 3)<sup>27,56,92,100</sup>. In the case of the isolated 181aa N-terminal domain, blocking the 3'end OH group of the ssDNA by the phosphate group only slightly decreases, by a factor of ~ 3, the intrinsic affinity for examined oligomer (Table 4.2)<sup>100</sup>. To what extent this modest affinity difference plays a role in specific enzyme binding to the damaged DNA substrate, particularly, in the presence of large local concentrations of different DNA conformations, if any, is at present not clear<sup>100</sup>. The answer to that question could be provided by examining the effect of blocking the 3'end OH group of the ssDNA by the phosphate group in the presence of ADP<sup>100</sup>. Examining the effect ADP has on the intrinsic affinity of intact PriA – ssDNA-3'-OH interactions would give further insight to that interesting possibility (see Chapter 7)<sup>100</sup>.



#### **4.5.5 The 181aa N-Terminal Domain of PriA Helicase Has a Significant Affinity for dsDNA.**

A very surprising result is presented in the Figure 4.10c where PriA 181aa N-terminal domain exhibits very high affinity for the dsDNA (Table 4.2)<sup>100</sup>. If the site-size of the domain – dsDNA interactions is the same as determined for the ssDNA (~5 nucleotides or correspondingly ~5 base pairs), then the intrinsic affinity is by a factor of ~20 - 50 higher than determined for the ssDNA oligomers, including, dC(pC)<sub>18</sub>pCp and dC(pC)<sub>18</sub> (Table 4.2)<sup>100</sup>. It is possible that the dsDNA affinity, not the 3'end-OH group affinity, plays a role in the recognition of the damaged DNA by the N-terminal domain in the stalled replication fork<sup>100</sup>. Further quantitative studies are necessary to assess the role of the 3'end-OH group and the dsDNA affinity of the N-terminal domain, in specific recognition of the damaged replication fork by the PriA helicase<sup>100</sup>.

#### **4.5.6 The DNA-Binding Subsite of the 181aa N-Terminal Domain Lacks Significant Base Specificity in the Interactions with the ssDNA.**

The strong DNA-binding subsite of the intact PriA helicase shows a significant preference for the pyrimidine homo-oligomers, with the intrinsic binding constant being ~ 1 order of magnitude higher for the dT(pT)<sub>19</sub> and dC(pC)<sub>19</sub> than observed for dA(pA)<sub>19</sub> or dεA(pεA)<sub>19</sub><sup>57,100</sup>. On the other hand, the DNA-binding subsite located of the N-terminal domain has only a small preference for dC(pC)<sub>19</sub>, as compared to other unmodified oligomers (Figure 4.10, and Table 4.2)<sup>100</sup>. Interestingly, unlike the strong subsite on the helicase domain, the 181aa N-terminal domain subsite has pronouncedly lower affinity for the etheno-modified oligomers than for all other examined nucleic acids (Table 4.2)<sup>56,57,100</sup>. Moreover, in similar solution conditions, the 181aa N-terminal domain subsite has the intrinsic ssDNA-affinity lower by a factor of ~ 6 - 7 than the intrinsic

DNA affinity of the strong subsite<sup>56,57,100</sup>. These data indicates that these two DNA-binding subsites of the PriA helicase differ significantly in their nature of interactions with the ssDNA<sup>100</sup>. This difference is further indicated by the salt effect on the corresponding interactions<sup>100</sup>. While the DNA binding to the strong subsite is accompanied by the net release of ~ 3 - 4 ions, binding to the 181aa N-terminal domain subsite induces the net release of only ~ 1 ion (Figure 4.11)<sup>57,100</sup>.

#### **4.5.7 The Weak Nucleotide-Binding Site of the Intact PriA Helicase Is Located on the 181aa N-terminal Domain.**

As mentioned above, what differs the PriA protein from other well-studied monomeric helicases is the fact that the protein possesses two nucleotide-binding sites, strong and weak binding sites<sup>27,59-61,92,99,100</sup>. First, the discovery that the isolated 181aa N-terminal domain possesses a nucleotide-binding site firmly places one of these sites on the N-terminal domain of the intact PriA protein<sup>100</sup>. Moreover, the low intrinsic affinity, very similar to the affinity of the weak nucleotide-binding site of the intact enzyme, provides a clear indication that the site located on the N-terminal domain corresponds to the weak nucleotide-binding site of the intact PriA helicase (section 4.4.10 and section 4.4.11)<sup>100</sup>. As a result, the strong nucleotide-binding site must be located on the helicase domain of the enzyme<sup>57,59-61,92,99,100</sup>.

Another indication that the nucleotide-binding site on the N-terminal domain corresponds to the weak site of the intact enzyme comes from the effect of the cofactors on the binding process of the nucleic acid<sup>59-61,100</sup>. Only when the nucleotide-binding site is saturated with ADP, the ssDNA affinity of the DNA-binding subsite of the domain strongly increases (Figure 4.13a), while saturation of the site with the ATP nonhydrolyzable analog, ATP $\gamma$ S, leads to slightly diminished affinity for the nucleic acid

(Figure 4.13b)<sup>59-61,100</sup>. This is exactly the behavior, which is observed in the case of the weak nucleotide-binding site of the intact PriA helicase<sup>27,59-61,92,99,100</sup>. The weak nucleotide-binding site acts as an allosteric site, which controls the engagement of the N-terminal domain into the interactions with the DNA<sup>27,59-61,92,99,100</sup>.

The presence of two nucleotide-binding sites on the domain dimer indicates that each monomer of the dimer binds a single cofactor molecule<sup>100</sup>. Thus, unlike the ssDNA-binding subsites, both nucleotide-binding sites are accessible on the domain dimer and the binding process is independent<sup>100</sup>. Notice, binding of TNP-ADP induces ~ 100% quenching of the 181aa N-terminal tryptophan fluorescence (Figure 4.12a)<sup>100,101,123</sup>. Moreover, the quenching is the same for each binding site<sup>100</sup>. Although TNP moiety is an excellent fluorescence energy transfer acceptor from tryptophans, it is rather unlikely that the cofactor would bind at close proximity to all 5 tryptophan residues of each monomer of the dimer<sup>100,101</sup>. Such a large quenching must result from a significant conformational transition of the domain induced by the cofactor binding, leading to an additional quenching of the protein tryptophans<sup>100,101</sup>.

#### **4.5.8 ADP Increases the Intrinsic Affinity of the 181aa N-Terminal Domain - ssDNA Interactions.**

The finding that saturation of the nucleotide-binding site of the 181aa N-terminal domain of PriA with ADP increases the affinity of the DNA-binding subsite corroborates the conclusion that the nucleotide cofactor induces a major conformational transition of the domain<sup>27,59-61,92,99,100</sup>. Nevertheless, the process is different from the analogous effect in the case of the intact enzyme, where the DNA-binding subsite is in closed conformation in the absence of high [ADP] and does not manifest any DNA-binding activity<sup>27,59-61,92,99,100</sup>. In the isolated domain, the DNA-binding subsite is already open

and has a substantial DNA affinity in the absence of ADP<sup>100</sup>. These data indicate that the allosteric effect of ADP in the weak nucleotide-binding site of the intact enzyme, on the DNA-binding subsite of the N-terminal domain, not only opens the subsite and enables the nucleic acid to enter, but also affects the intrinsic DNA affinity of the subsite<sup>27,59-61,92,99,100</sup>.

#### **4.5.9 Comparison with Other Works.**

The crystallographic data on the truncated 105aa N-terminal subdomain dimer of PriA indicate that the DNA-binding subsite of the complete 181aa N-terminal domain is located on the 105aa N-terminal subdomain, *i.e.*, further away from the helicase domain and corroborating our conclusion that the DNA subsites of the intact enzyme are spatially separated<sup>27,59-61,92,99,100,104</sup>. However, the same data also indicate that the 105aa N-terminal subdomain dimer can bind two nucleic acid molecules, while thermodynamic data and photo-cross-linking experiments discussed in this Chapter show the presence of only one effective DNA-binding subsite<sup>100,104</sup>. However, the examined crystallographic complexes of the 105aa N-terminal subdomain had a very high concentrations of short di- and tri-nucleotides, which may not reflect the interactions with the longer nucleic acids<sup>97,100,104</sup>. The truncated subdomain may have a different conformation causing the difference in the access of the DNA to the binding site<sup>100</sup>. It should be pointed out that the conserved motif (W83, Y87, Y88), previously proposed to be involved in the DNA binding to the N-terminal domain is not present in the proximity of the determined DNA-binding site in the crystal structure<sup>97,100,104</sup>.

Another puzzling result, previously published by Sasaki *et al.*, showed that the 105N-terminal subdomain dimer showed the highest macroscopic affinity for the short oligomers (~ 4 nucleotides) and its macroscopic DNA-affinity decreases with the length

of the nucleic acid<sup>100,104</sup>. As it was discussed above, unlike the intrinsic affinity, the macroscopic affinity is affected by the length of the ssDNA, because of the presence of the statistical factor, which increases with the length of the nucleic acid and positively contributes to the determined free energy of binding (equations 4.3 and 4.4)<sup>1,56,81,95,100</sup>. In other words, macroscopic affinity is not a parameter, which provides clear estimate of the preferential association<sup>1,56,81,95,100,127</sup>. Moreover, a factor of  $\sim 6$  lower affinity of the 105aa N-terminal subdomain, for oligomers with the 3' end-OH group blocked by the phosphate group was also reported, as compared to the factor of  $\sim 3$  found in this work<sup>100,104</sup>. We cannot to explain all the differences<sup>100</sup>. Nevertheless, in these previous studies, neither the intrinsic affinity nor the stoichiometries have been determined<sup>100,104</sup>. The reported titration curves do not have plateaus, which prevents any quantitative analyses<sup>1,100,104,127</sup>. The macroscopic affinity estimates were based on qualitative comparisons of apparent translational diffusion coefficients of the complexes, with large inherent error of the applied method, and with the values of the diffusion parameter being, within experimental accuracy, the same for the ssDNAs containing from 2 to 7 nucleotides<sup>100,104</sup>. Moreover, the reported lower value of the diffusion parameter for the wild-type protein at higher protein concentration in different sets of data is inconsistent, as a higher value of the parameter at a higher protein concentration should be observed<sup>100,104</sup>.

#### **4.5.10 Further Functional Implications.**

The large differences between the two DNA-binding subsites of the *E. coli* PriA helicase in their affinities, base specificities, and nucleotide effects must reflect the differences in functional roles of both sites in the PriA activities<sup>27,59-61,92,99,100</sup>. A significant preference of the strong DNA-binding subsite on the helicase domain for homo-pyrimidine oligomers coincides with overwhelming preference of the PriB protein

for homo-thymine ssDNAs<sup>81,100</sup>. The PriA - PriB complex is an initial complex of one of two major restart pathways, PriA-dependent pathway, of the chromosomal DNA replication in *E. coli* at the damaged DNA site (Figure 2.1, section 2.2.1)<sup>11-14,35,43,100</sup>. The preference for pyrimidine stretches of both proteins strongly suggests that the sequence of the nucleic acid around the damaged DNA site may play an important role in the damage DNA recognition process, and in selection of the pathway to restart the replication fork<sup>100</sup>. Moreover, stopped-flow kinetic data showed that the strong subsite on the PriA helicase domain is the area, which makes the first contact with the nucleic acid in the enzyme association reaction<sup>58,100</sup>. Furthermore, the strong subsite plays a major role in the recognition of the ss-ds junctions in the gapped DNA substrates, specifically matching the size of the ssDNA gap with 5 nucleotides<sup>27,100</sup>.

In all these activities of the intact enzyme, the subsite on the N-terminal domain is absent, or its role is secondary<sup>27,59-61,92,99,100</sup>. Its decisive presence appears only when the weak nucleotide-binding site of the PriA protein is saturated with ADP<sup>27,59-61,92,99,100</sup>. The ssDNA affinity of the N-terminal domain subsite is dramatically controlled by the nucleotide cofactors, while the control of the DNA affinity of the strong subsite is, if any, very modest<sup>27,59-61,92,99,100</sup>. Moreover, the 181aa N-terminal domain DNA-binding subsite has very low base specificity (Table 4.2)<sup>100</sup>. These differences point out to the strong subsite as the major recognition site of the DNA structures and/or conformations, while the N-terminal subsite predominantly becomes involved during the mechanical translocation and the dsDNA unwinding, where the nucleotide control of the nucleic acid affinity is crucial and the base/sequence specificity is not necessary<sup>2,100</sup>. As a result, the subsite on the 181aa N-terminal domain would be the DNA-binding subsite of the PriA protein essential for efficient energy transduction process<sup>2,100</sup>.

**Table 4.1. Thermodynamic and spectroscopic parameters characterizing the binding of the *E. coli* PriA helicase 181aa N-terminal domain to etheno-derivatives of ssDNA oligomers in buffer C205\*.**

	8-mer	10-mer	12-mer	14-mer	16-mer	18-mer	20-mer	24-mer	26-mer	30-mer	33-mer
n	1 ± 0.1	1 ± 0.1	1 ± 0.1	1 ± 0.1	2 ± 0.2	2 ± 0.2	1 ± 0.2	1 ± 0.2	2 ± 0.2	2 ± 0.2	2 ± 0.2
p	5	5	5	5	5	5	5	5	13	13	13
K <sub>N</sub> (M <sup>-1</sup> )	(6.2 ± 0.9) × 10 <sup>4</sup>	(9.4 ± 1.7) × 10 <sup>4</sup>	(1.3 ± 0.2) × 10 <sup>5</sup>	(1.6 ± 0.3) × 10 <sup>5</sup>	(1.9 ± 0.3) × 10 <sup>5</sup>	(2.2 ± 0.4) × 10 <sup>5</sup>	(2.5 ± 0.4) × 10 <sup>5</sup>	(3.1 ± 0.5) × 10 <sup>5</sup>	-	-	-
K <sub>i</sub> (M <sup>-1</sup> )	(1.6 ± 0.3) × 10 <sup>4</sup>	(1.6 ± 0.3) × 10 <sup>4</sup>	(1.9 ± 0.3) × 10 <sup>4</sup>	(1.6 ± 0.3) × 10 <sup>4</sup>	(1.6 ± 0.3) × 10 <sup>4</sup>	(1.6 ± 0.3) × 10 <sup>4</sup>	(1.6 ± 0.3) × 10 <sup>4</sup>	(1.6 ± 0.3) × 10 <sup>4</sup>	(2.0 ± 0.4) × 10 <sup>4</sup>	(2.0 ± 0.4) × 10 <sup>4</sup>	(1.5 ± 0.3) × 10 <sup>4</sup>
w	-	-	-	-	-	-	-	-	27 ± 8	28 ± 9	20 ± 7
ΔF <sub>i</sub>	-	-	-	-	-	-	-	-	1.25 ± 0.05	0.80 ± 0.05	0.65 ± 0.05
ΔF <sub>max</sub>	3.10 ± 0.10	2.33 ± 0.05	2.55 ± 0.05	1.95 ± 0.05	1.23 ± 0.05	1.83 ± 0.05	1.15 ± 0.05	1.41 ± 0.05	1.60 ± 0.05	1.45 ± 0.05	1.33 ± 0.05

\*The errors are standard deviations determined using 3 - 4 independent titration experiments.

**Table 4.2. Macroscopic and intrinsic binding constants,  $K_N$  and  $K_{in}$ , and the site-size,  $n$ , characterizing the binding of the PriA helicase 181N-terminal domain to different ssDNA homo-oligomers, dN(pN)<sub>19</sub>, homo-oligomer, dC(pC)<sub>18</sub>pCp, containing phosphate group; at the 3' end, and the dsDNA 10-mer, in buffer C205. The values of the binding constants for the unmodified nucleic acids have been determined using the MCT Method\*.**

	dεA(pεA) <sub>19</sub>	dA(pA) <sub>19</sub>	dT(pT) <sub>19</sub>	dC(pC) <sub>19</sub>	dC(pC) <sub>18</sub> pCp	dsDNA 10-mer
$K_N (M^{-1})$	$(2.5 \pm 0.4) \times 10^5$	$(1.3 \pm 0.4) \times 10^6$	$(1.5 \pm 0.4) \times 10^6$	$(4.5 \pm 0.8) \times 10^6$	$(1.6 \pm 0.3) \times 10^6$	$(3.0 \pm 1.0) \times 10^7$
$K_{in} (M^{-1})$	$(1.6 \pm 0.3) \times 10^4$	$(8.1 \pm 0.2) \times 10^4$	$(9.4 \pm 0.2) \times 10^4$	$(2.8 \pm 0.5) \times 10^5$	$(1.0 \pm 0.2) \times 10^5$	-
$p^{**}$	5	5	5	5	5	-

\*Errors are standard deviations determined using 3-4 independent titration experiments.

\*\* The site-size of the strong DNA-binding subsite (details in text).



## CHAPTER 5

### INTERACTIONS OF THE *ESCHERICHIA COLI* PRIMOSOMAL PRIB PROTEIN WITH THE DNA<sup>81</sup>

#### 5.1 ABSTRACT

Quantitative analysis of the interactions of the *Escherichia coli* primosomal PriB protein with a single-stranded DNA was accomplished using quantitative fluorescence titration, photo-cross-linking, and analytical ultracentrifugation techniques<sup>81</sup>. Stoichiometry studies were performed with a series of etheno-derivatives of single-stranded (ss) DNA oligomers<sup>81</sup>. Interactions with the unmodified nucleic acids were studied, using the macromolecular competition titration (MCT) method<sup>81</sup>. The total site-size of the PriB dimer - ssDNA complex, *i.e.*, the maximum number of nucleotides occluded by the PriB dimer in the complex, is  $12 \pm 1$ <sup>81</sup>. The protein has a single DNA binding site, which is located centrally within the dimer and has a functionally homogeneous structure<sup>81</sup>. The stoichiometry and photo-cross-linking data show that only a single monomer of the PriB dimer engages in interactions with the nucleic acid<sup>81</sup>. The analysis of the PriB binding to long oligomers was done using a statistical thermodynamic model that takes into account the overlap of potential binding sites and cooperative interactions<sup>81</sup>. The PriB dimer binds the ssDNA with strong positive cooperativity<sup>81</sup>. Both the intrinsic affinity and cooperative interactions are accompanied by a net ion release, with anions participating in the ion exchange process<sup>81</sup>. The intrinsic

---

<sup>81</sup> This research was originally published in Journal of Molecular Biology. Szymanski, M. R., Jezewska, M.J. & Bujalowski, W. (2010). Interactions of the *Escherichia coli* primosomal PriB protein with the single-stranded DNA. Stoichiometries, intrinsic affinities, cooperativities, and base specificities. *J Mol Biol* 398, 8-25. Reproduced with permission.

binding process is an entropy-driven reaction, suggesting strongly that the DNA association induces a large conformational change in the protein<sup>81</sup>. The PriB protein shows a dramatically strong preference for the homo-pyrimidine oligomers with an intrinsic affinity higher by about three orders of magnitude, as compared to the homo-purine oligomers<sup>81</sup>.

## 5.2 INTRODUCTION

As mentioned in Chapter 1 and section 2.2.1, the priming of the DNA strand during the replication process is catalyzed by a multiple-protein complex called the primosome<sup>11-18,24,25,47,48,81,99,105-109</sup>. This macromolecular machine synthesizes short oligoribonucleotide primers, which are used to initiate synthesis of the complementary DNA strand<sup>11-18,24,25,47,48,105-109</sup>. Current data show that the assembly of the primosome is a fundamental step in the restart of the stalled replication fork at the damaged DNA sites and that the PriB protein is an essential replication protein in *Escherichia coli* that plays a fundamental role in the ordered formation of the primosome<sup>11-18,24,81,99,109</sup>. The assembly process of the primosome is initiated by recognition of the PAS sequence or damaged DNA site by the PriA protein<sup>11-18,24,81,99,109</sup>. The next step includes the association of the PriB protein with the PriA - DNA complex, followed by binding of the DnaT and the PriC protein<sup>11-18,24,81,99,109</sup>. This complex constitutes a scaffold recognized by the DnaB helicase - DnaC protein complex and, subsequently, by the primase resulting in a functional primosome<sup>11-18,24,81,99,109</sup>. The PriB protein was originally discovered to be an essential factor during synthesis of the complementary DNA strand of phage phiX174 DNA<sup>47,81,105</sup>. The gene encoding the PriB protein with the molecular weight of ~ 11.4 kDa has been cloned, and the native protein is a homo-dimer in solution<sup>25,81,106-108</sup>. Multiple crystal structures of the apo PriB dimer and its complex with the ssDNA

oligomer have been solved to a resolution of 2 - 2.7 Å<sup>16,81,110-113</sup>. The structure of the PriB dimer alone is depicted in Figure 5.1a<sup>81,110-112</sup>. The structure of the PriB dimer - ssDNA complex, with the proposed engagement of the nucleic acid in interactions with the protein, based on crystallographic analyses, is shown in Figure 5.1b<sup>81,113</sup>.

In the last two decades it has been shown, by different groups, that the PriB protein displays multiple activities<sup>15,16,24,81,106,114</sup>. It was proposed that PriB specifically interacts with the PriA protein as well as the PriA - ssDNA complex<sup>15,16,24,81,106,114</sup>. This interaction is considered the major biological function of the PriB protein and crucial in the PriA-dependent pathway of the assembly process of the primosome<sup>15,16,24,81,106,114</sup>. It was also indicated that PriB can specifically interact with the DnaT protein, which in turn is considered to be a next key step in the primosome assembly process allowing subsequent recruitment of the DnaB – DnaC complex to the primosome<sup>15,16,18,24,81,114</sup>. Also, nonspecific binding to the ssDNA, which is proposed to be crucial for recognition of the PriA - ssDNA complex and recruiting the DnaT protein to the primosome has been indicated<sup>15,16,18,24,81</sup>. In addition, it was demonstrated that PriB can bind to SSB protein and, in addition, strongly interact with ssDNA coated with the SSB protein<sup>15,16,18,24,81</sup>.

It is evident that most of the functions of the PriB protein reflect the ability of the protein to interact with the ssDNA and ssDNA-protein complexes<sup>15,16,18,24,81,112,113</sup>. In the crystal structure, the ssDNA-binding pocket of each monomer of PriB dimer bears a resemblance to that of the *E. coli* single-stranded binding protein (SSB), suggesting a similar mode of engaging the DNA by both proteins<sup>81,110-113</sup>. Although the importance of understanding the PriB protein - ssDNA interactions has been recognized, quantitative aspects of these interactions remain obscure<sup>15,16,18,24,81,112,113</sup>. Fundamental quantities as the stoichiometry (site-size) of the PriB - ssDNA complex, *i.e.*, the number of nucleotides

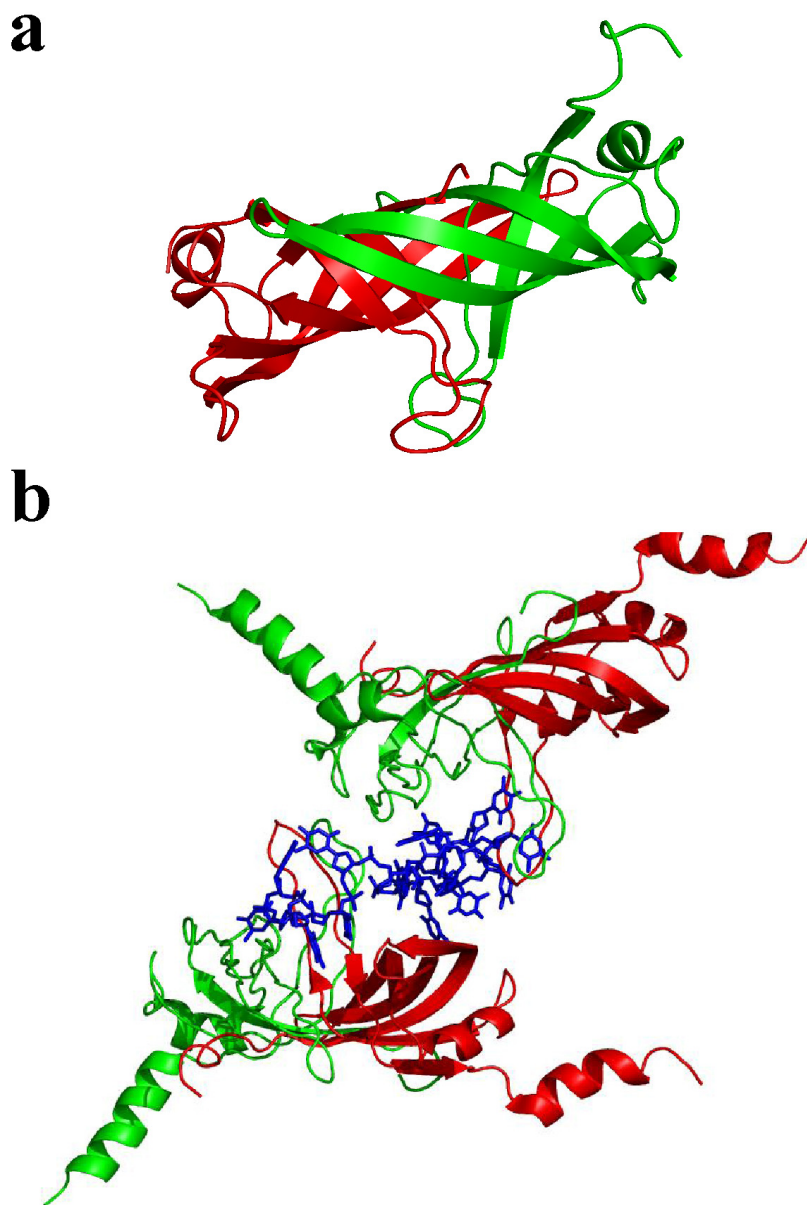


**Figure 5.1 The PriB protein structures.** **a.** Structure of the PriB protein dimer (PDB 1V1Q) based on crystallographic studies<sup>81,110</sup>. Two monomers in the PriB dimer are marked with different colors. **b.** Proposed structure of the PriB dimer complex with a single ssDNA 15-mer, dT15 (blue), obtained in crystallographic studies (PDB 2CCZ)<sup>81,113</sup>. Two different monomers of PriB dimer make contacts with the nucleic acid, as marked with different colors<sup>81,113</sup>. The structures have been generated using PyMOL.

occluded by the protein in the complex, the number of the ssDNA-binding sites on the PriB dimer, are unknown<sup>81</sup>. Computer modeling of the crystal structure inferred that both monomers of the dimer can engage in interactions with the ssDNA, *i.e.*, the presence of two ssDNA-binding sites on the PriB dimer, as depicted in Figure 5.1b<sup>81,113</sup>. However, this has never been experimentally established in solution<sup>81</sup>. Little is known about the energetics of the PriB protein - DNA complexes<sup>16,81,110,113</sup>. No quantitative data is available on the intrinsic affinities and cooperativities of the PriB protein - ssDNA interactions, and the effects of solution conditions, salt and type of salt on the complex formation<sup>16,81,110,113</sup>.

Knowledge of the energetics and mechanisms of the PriB - ssDNA complex formation is important for understanding the activities of this essential protein in DNA metabolism, especially in the primosome formation<sup>11-18,24,25,47,48,81,99,105-113</sup>. In order to be able to quantitatively assemble the primosome complex, which is a long term goal of this project, the interactions of PriB with different conformations of DNA, in solution, must be elucidated<sup>81</sup>. Therefore, in this Chapter, the quantitative analyses of the PriB interactions with the ssDNA were described<sup>81</sup>. It was established that, in solution, the PriB dimer occludes  $12 \pm 1$  nucleotides in the complex using a single, functionally homogeneous, ssDNA-binding site<sup>81</sup>. Moreover, only one monomer of the dimer engages in interactions with the nucleic acid<sup>81</sup>. The PriB dimer binds the ssDNA with strong positive cooperativity<sup>81</sup>. The protein shows a very strong preference for the homopyrimidine oligomers, as compared to the homopurine ssDNA<sup>81</sup>.

## 5.3 MATERIALS AND METHODS

### 5.3.1 Buffers and Chemicals.

All solutions used in experiments described in this chapter were made with

distilled and deionized >18 M $\Omega$  (Milli-Q Plus) water. The standard buffer was buffer C100 with 10 mM sodium cacodylate adjusted to pH 7.0 with HCl at 10°C, 1 mM DTT, 100 mM NaCl, and 25% glycerol w/v<sup>81</sup>. The standard temperature in all the experiments described herein was 10°C. All experiments were carried out in the standard buffer C100 unless otherwise specified in the text. Polynucleotide Kinase was from Roche (Indianapolis, IN). Lysozyme, Phenylmethanesulfonylfluoride (PMSF), Sodium Deoxycholate, Polymyxin B, Ammonium sulfate, Imidazole were from Sigma (Saint Louis, MI). All chemicals were reagent grade.

### **5.3.2 Water Activity of Buffering Solution.**

Water activity “error term” of the standard buffer C100, used in this Chapter, had been calculated according to the values in the literature<sup>132,133</sup>. Due to the presence of the glycerol and salt, the water activity “error term” is less than 5%, and is contained within the experimental error of all the experiments presented here<sup>27,132,133</sup>.

### **5.3.3 Nucleic Acids.**

Unmodified nucleic acid oligomers, dA(pA)<sub>13</sub>, dA(pA)<sub>15</sub>, dA(pA)<sub>17</sub>, dA(pA)<sub>19</sub>, dA(pA)<sub>23</sub>, dA(pA)<sub>30</sub>, dA(pA)<sub>34</sub>, dC(pC)<sub>19</sub>, dT(pT)<sub>19</sub>, and fluorescein-labeled ssDNA oligomers were purchased from Midland Certified Reagents (Midland, TX)<sup>81</sup>. The modified ssDNA oligomers contain a fluorescent label, fluorescein (Fl), attached to the 5' through phosphoramidate chemistry and are referred to as 21-mer, 5'Fl-dT(pT)<sub>19</sub> and 27-mer, 5'Fl-dT(pT)<sub>25</sub>, respectively<sup>81</sup>. All nucleic acids were HPLC purified and at least >95% pure as judged by electrophoresis on polyacrylamide gel.

To monitor binding, different length etheno-derivatives of adenosine oligomers were obtained by modification with chloroacetaldehyde<sup>81,90-92</sup>. The concentration of

etheno-derivative of the nucleic acids was determined spectrophotometrically using following the extinction coefficients:  $\epsilon_{257} = 3700 \text{ cm}^{-1}\text{M}^{-1}$  (nucleotide) for  $\epsilon\text{A}$ <sup>56,57,81,87,90-92</sup>.

The concentration of dC(pC)<sub>19</sub>, dT(pT)<sub>19</sub>, and dA(pA)<sub>19</sub> were determined using extinction coefficients:  $\epsilon_{270} = 7200 \text{ cm}^{-1}\text{M}^{-1}$ (nucleotide),  $\epsilon_{260} = 8100 \text{ cm}^{-1}\text{M}^{-1}$ (nucleotide), and  $\epsilon_{260} = 10000 \text{ cm}^{-1}\text{M}^{-1}$ (nucleotide)<sup>27,62,81,115,116</sup>. Concentrations of the fluorescein-labeled ssDNA oligomers have been spectrophotometrically determined as previously described<sup>27,81,99,116</sup>.

### 5.3.4 The PriB Protein Purification.

The gene of the *E. coli* PriB protein has been directly isolated from the *E. coli* K12 strain<sup>81</sup>. The isolated gene of the PriB protein with and without in-frame C-terminal histidine-tag has been placed in pET30a plasmid (Novagen)<sup>81</sup>. The cells were grown at 37°C in Luria Broth (LB) induced by adding 1 mM IPTG and grown overnight at 18°C. The cells were collected by centrifugation, flash frozen, and stored in -80°C. All purification procedures were at performed in 4°C cold room unless otherwise specified. Typically, ~20g of frozen cell pallet was thawed on ice and suspended in 125 ml of buffer A (50 mM Tris-HCl pH 7.5, 0.5 mM EDTA, 5 mM B-MeOH, 10% glycerol w/v) and stirred gently until the suspension was homogeneous. About 25ml of buffer B (200 mM Tris-HCl pH 7.5, 1 M NaCl, 1.5 M ammonium sulfate, 100 mM Spermidyne-HCl) was added for the final volume of ~ 150 ml. Freshly prepared phenylmethanesulfonylfluoride (PMSF) was added to the final concentration of 0.2 mM and the pH was adjusted to ~ 8.5 with 2 M Tris-Base. Next, the lysozyme was added to the final concentration of 400 µg/ml and the suspension was incubate with gentle stirring for 30 minutes on ice Next, sodium deoxycholate, to the final concentration of 0.04% was added, and the suspension was stirred for additional for 30 minutes. After that the cell

suspension was placed in centrifuge bottles and centrifuge, for 30 min, at 12000 rpm in Sorvall GSA rotor to collect soluble protein of interest in the supernatant. 0.5% of Polymin P, in 3 portions, over a period of 30 min, with gentle stirring, was added to the supernatant in order to precipitate the nucleic acid. Again, the suspension was centrifuged for 30 min in GSA rotor at 12000 rpm to remove white precipitation and the supernatant was collected. To the supernatant ammonium sulfate to the concentration of 0.30 g/ml was added, in portions, while stirring gently for 30 min. Additionally, the suspension was incubated for extra 30 min with stirring after ammonium sulfate was added. The suspension was centrifuged at 12000 rpm, for 30 min, in GSA rotor. The protein of interest was in the pellet which was then dissolved in ~ 75 ml of buffer B1 (50 mM Tris-HCl pH 7.1, 1 mM DTT, 300 mM NaCl, 10% glycerol w/v) and dialyzed against 1000 ml of buffer B1 overnight. Precipitation formed in the dialysis bags was removed by centrifugation at 12000 rpm, for 30 min, in GSA rotor and the supernatant was loaded onto the standard, hand packed, nickel column (GE Healthcare, Piscataway, NJ). PriB was eluted with buffer C200 (50 mM Tris-HCl pH 7.1, 200 mM Imidazole, 1 mM DTT, 300 mM NaCl, 10% glycerol w/v) and a large volume of the sample was ammonium sulfate precipitated to the concentration of 0.30 g/ml. Ammonium sulfate was added in portions, while stirring for 30 min. Additionally, the suspension was incubated for extra 30 min, with stirring, after ammonium sulfate was added. The suspension was centrifuged at 12000 rpm, for 30 min, in GSA rotor. The protein of interest was in the pellet which was dissolved in buffer CC300 (50 mM Tris-HCl pH 7.1, 1 mM DTT, 300 mM NaCl, 10% glycerol w/v) and dialyzed overnight against 1000 ml of the same buffer. After dialysis was stopped the sample was centrifuged at 12000 rpm for 30 min in GSA rotor. Next, the pure protein sample was dialyzed overnight against 1000 ml of storage buffer (50 mM Tris-HCl pH 7.1, 1 mM DTT, 300 mM NaCl, 50% glycerol w/v) and



stored in -80°C. Typical yield of this purification protocol for His-Tagged PriB protein was ~ 160 mg of pure protein from ~ 20 g of frozen cell pellet.

Untagged PriB purification protocol was also developed. Heparin Sepharose CL-6B Column (GE Healthcare, Piscataway, NJ) and DEAE Sephacryl Column (GE Healthcare, Piscataway, NJ) were used to purify the PriB protein without the Histag. Typically, ~ 35 g of frozen cell pellet was thawed on ice and suspended in 200 ml of buffer A (50 mM Tris-HCl pH 7.5, 0.5 mM EDTA, 5 mM B-MeOH, 10% glycerol w/v) and stirred gently until the suspension was homogeneous. About 50 ml of buffer B (200 mM Tris-HCl pH 7.5, 1 M NaCl, 1.5M ammonium sulfate, 100 mM Spermidine-HCl) was added for the final volume of ~ 250 ml. Freshly prepared phenylmethanesulfonylfluoride (PMSF) was added to the final concentration of 0.2 mM and the pH was adjusted to ~ 8.5 with 2 M Tris-Base. Next, the lysozyme was added to the final concentration of 400 µg/ml and the suspension was incubated with gentle stirring for 30 minutes on ice. Next, sodium deoxycholate to the final concentration of 0.04% was added and the suspension was stirred for additional 30 minutes. After that the cell suspension was placed in centrifuge bottles and centrifuged, for 30 min, at 12000 rpm in Sorvall GSA rotor to collect soluble protein of interest in the supernatant. 0.5% of Polymyxin B, in 3 portions, over a period of 30 min, with gentle stirring, was added to precipitate the nucleic acid. Again, the supernatant was centrifuged to remove white precipitation for 30 min in GSA rotor at 12000 rpm and the supernatant was collected. To the supernatant ammonium sulfate was added, in portions, while stirring gently for 30 min, to the concentration of 0.30 g/ml. Additionally, the suspension was incubated for extra 30 min with stirring after ammonium sulfate was added. The suspension was centrifuged at 12000 rpm, for 30 min, in GSA rotor. The protein of interest was in the pellet which was then dissolved in ~50 ml of buffer B1 (50 mM Tris-HCl pH 7.1, 1 mM

DTT, 100 mM NaCl, 20% glycerol w/v) and dialyzed against 1000 ml of buffer B1 overnight. Precipitation formed in the dialysis bags and was removed by centrifugation at 12000 rpm, for 30 min, in GSA rotor and the supernatant was loaded onto the standard, Heparin Sepharose CL-6B Column. Bound PriB was eluted with buffer B500 (50 mM Tris-HCl pH 7.1, 1 mM DTT, 500 mM NaCl, 20% glycerol w/v) and a large volume of the sample was ammonium sulfate precipitated to the concentration of 0.3 g/ml. Ammonium sulfate was added in portions while stirring gently for 30 min. Additionally, the suspension was incubated for extra 30 min with stirring after ammonium sulfate was added. The suspension was centrifuged at 12000 rpm, for 30 min, in GSA rotor. The protein of interest was in the pellet which was then dissolved in buffer B1 (50 mM Tris-HCl pH 7.1, 1 mM DTT, 100 mM NaCl, 20% glycerol w/v) and dialyzed overnight against 1000 ml of the same buffer. After dialysis was stopped the sample was centrifuged at 12000 rpm, for 30 min, in GSA rotor. In the next step the DEAE Sephacryl Column was used. PriB doesn't bind to that column and comes out in large volume of flow through which was then ammonium sulfate precipitated to the concentration of 0.30 g/ml. Ammonium sulfate was added in portions, while stirring gently for 30 min. Additionally, the suspension was incubated for extra 30 min with stirring after ammonium sulfate was added. The suspension was centrifuged at 12000 rpm, for 30 min, in GSA rotor. The protein of interest was in the pellet which was then dissolved in buffer B1 (50 mM Tris-HCl pH 7.1, 1 mM DTT, 100 mM NaCl, 20% glycerol w/v) and dialyzed overnight against 1000 ml of the same buffer. Next, the pure protein sample is dialyzed overnight against 1000 ml of storage buffer (50 mM Tris-HCl pH 7.1, 1 mM DTT, 300 mM NaCl, 50% glycerol w/v) and stored in -80°C. Typical yield of this purification protocol for untagged PriB was ~ 90 mg of pure protein from ~ 35 g of frozen cell pellet.

The tagged PriB has DNA-binding properties indistinguishable for the unmodified protein; therefore, in all experiments described in this Chapter a tagged PriB protein was used.

Before each use frozen PriB sample was allowed to thaw on ice, transferred to the dialysis bag, and dialyzed against ~ 150 ml of buffer C100 for 4-6 hours. After that time, the buffer was exchanged and the dialysis was allowed to go overnight. The protein sample was then centrifuged at 15000 rpm for 20 minutes and the absorption spectrum of the PriB protein was taken. In these solution conditions, the maximum solubility of the PriB protein was about  $1.1 \times 10^{-4}$  M.

### 5.3.5 Determination of Extinction Coefficient of the PriB Protein.

The concentration of the protein was spectrophotometrically determined, with an extinction coefficient  $\epsilon_{280} = 1.0776 \times 10^4 \text{ cm}^{-1}\text{M}^{-1}$  (dimer) obtained using an approach based on the Edelhoch's method<sup>27,56-61,64,65,81,92,99</sup>.

### 5.3.6 Fluorescence Measurements.

All steady-state fluorescence titrations were performed using the ISS PC-1 spectrofluorometer (Urbana, IL) as previously described<sup>27,56-63,81,92,99</sup>. The temperature of the cuvette holder was regulated by circulating water at  $10.0 \pm 0.1$  °C. The PriB protein - ssDNA binding was followed by monitoring the etheno-derivative fluorescence of the nucleic acids ( $\lambda_{\text{ex}} = 325$  nm,  $\lambda_{\text{em}} = 410$  nm). In order to avoid possible artifacts, due to the fluorescence anisotropy of the sample, polarizers were placed in excitation and emission channels and set at 90° and 55° (magic angle), respectively<sup>27,56-63,81,92,99</sup>. The relative fluorescence increase,  $\Delta F_{\text{obs}}$ , of the DNA emission upon protein binding is defined as,  $\Delta F_{\text{obs}} = (F_i - F_o)/F_o$ , where  $F_i$  is the fluorescence of the sample at a given titration point “i” and  $F_o$  is the initial fluorescence of the same solution<sup>1,27,56-63,81,92</sup>.

### **5.3.7 Determination of Thermodynamically Quantitative Binding Isotherms of the PriB Protein - ssDNA Complexes.**

In this Chapter, the binding of PriB protein to the DNA oligomers was followed by monitoring the fluorescence increase,  $\Delta F$ , of etheno-derivative of the nucleic acid<sup>90-92</sup>. Quantitative estimates of the total average degree of binding,  $\Sigma\Theta_i$  (average number of bound PriB dimers per DNA oligomer) and the free protein concentration,  $P_F$ , independent of any assumption about the relationship between the observed spectroscopic signal and  $\Sigma\Theta_i$ , were determined using the approach previously described in section 2.3.7<sup>1,56,57,82,87,92</sup>. Computer fits were performed using Mathematica (Wolfram, IL) and KaleidaGraph (Synergy Software, PA).

### **5.3.8 Analytical Ultracentrifugation Measurements.**

All analytical ultracentrifugation experiments were performed with an Optima XL-A analytical ultracentrifuge (Beckman Inc., Palo Alto, CA), as was previously described in section 2.3.8<sup>27,66-69,72,76,81,82,92</sup>.

### **5.3.9 Determination of PriB Partial Specific Volume.**

Partial specific volume of the PriB protein ( $v$ ) was calculated from the amino acid composition of the protein according to Lee and Timasheff and was 0.733 mL/g<sup>27,70,81</sup>.

### **5.3.10 Photo-Cross-Linking Experiments.**

Photo-cross-linking of the PriB - ssDNA complex has been performed in the same buffer as the binding experiments<sup>81</sup>. The ssDNA oligomer, dT(pT)<sub>19</sub>, has been labeled at the 5' end with [<sup>32</sup>P], using polynucleotide kinase<sup>81,92,93,102</sup>. The samples (total volume 100  $\mu$ L) were placed on Parafilm, in  $\sim 10^\circ\text{C}$  water bath, and irradiated for 20 minutes, at a

distance of 11 cm, using a mineral lamp (model UVG-11) with a maximum output of 254 nm<sup>81,92</sup>. The controls were performed to determine the optimal time for cross-linking and to avoid possible degradation of the protein by prolonged exposure to UV light<sup>81,92</sup>. The samples collected at different protein concentrations were loaded on 15% SDS polyacrylamide gel and electrophoresis was performed at a constant voltage<sup>81,92</sup>. The gels were stained with Coomassie Brilliant Blue and scanned, using the phosphorimager SI (Molecular Dynamics, PA)<sup>81,92,93,102</sup>.

## **5.4 RESULTS**

### **5.4.1 The PriB Protein.**

The enzyme was > 98% pure as judged by polyacrylamide electrophoresis with Coomassie Brilliant Blue staining (Figure 5.2). The identity of the sample was confirmed by both mass spectrometry and N-terminal sequencing.

### **5.4.2 The Hydrodynamic Properties of the PriB Protein.**

Typical sedimentation velocity profiles of the PriB protein performed at 60000 rpm, monitored at 280 nm, in the standard buffer C100 are shown in Figure 5.3a. The concentration of the PriB protein is  $6.03 \times 10^{-5} \text{M}$  (dimer)<sup>72,76,78-81</sup>. Inspection of the profiles clearly shows that there is a single moving boundary<sup>72,74,76</sup>. The sedimentation coefficient of the PriB protein has been obtained using the time-derivative approach and corrected for solvent viscosity and temperature to standard conditions<sup>66,67,69,72,76</sup>. The dependence of the sedimentation coefficient ( $s_{20,w}$ ) upon the protein concentration, is shown in Figure 5.3b<sup>72,76</sup>. Within experimental accuracy values of  $s_{20,w}$  are similar and show a very little dependence upon the examined protein concentration range<sup>72,74,76</sup>. The

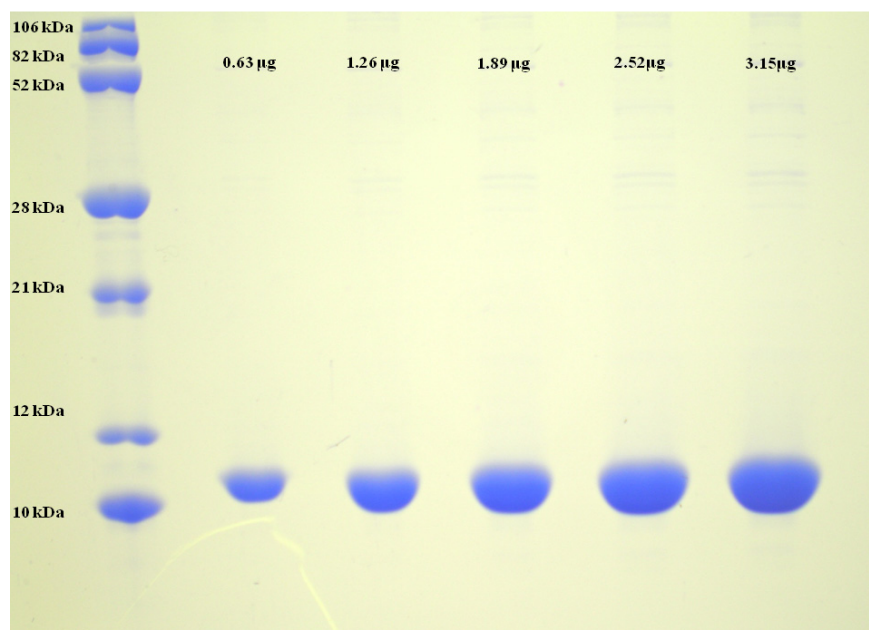


**Figure 5.2 15% SDS polyacrylamide gel of the final step of the PriB protein purification.** Serial dilution clearly shows that employed purification protocol yields the PriB protein of high purity<sup>27,56-61,92,99</sup>.

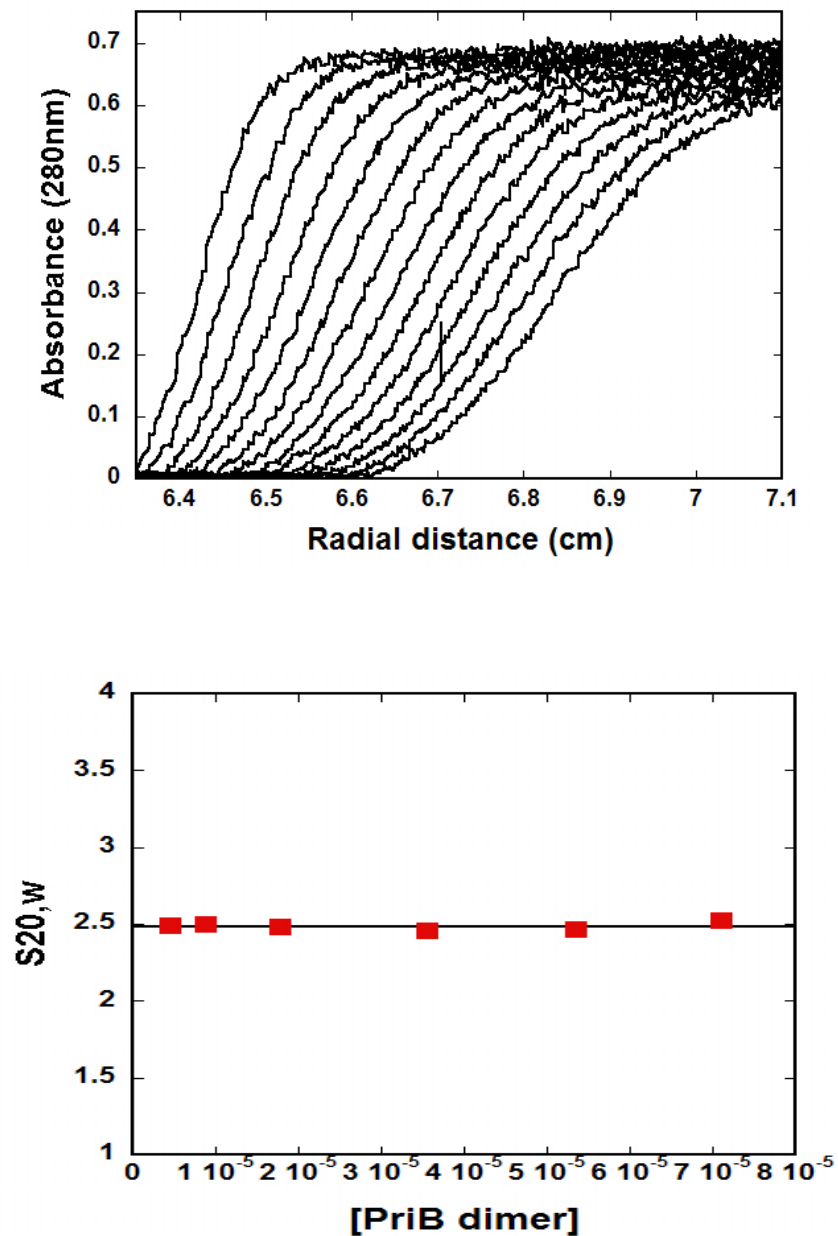


**Figure 5.3** PriB in solution sediments as a single homogenous species. **a.** Example of typical analytical sedimentation velocity profiles recorded at 280 nm and 60000 rpm for  $[6.03 \times 10^{-5} \text{ M (dimer)}]$  of PriB<sup>72,74,76</sup>. **b.** The dependence of the sedimentation coefficient ( $s_{20,w}$ ) upon the PriB concentration<sup>72,74,76,81</sup>.

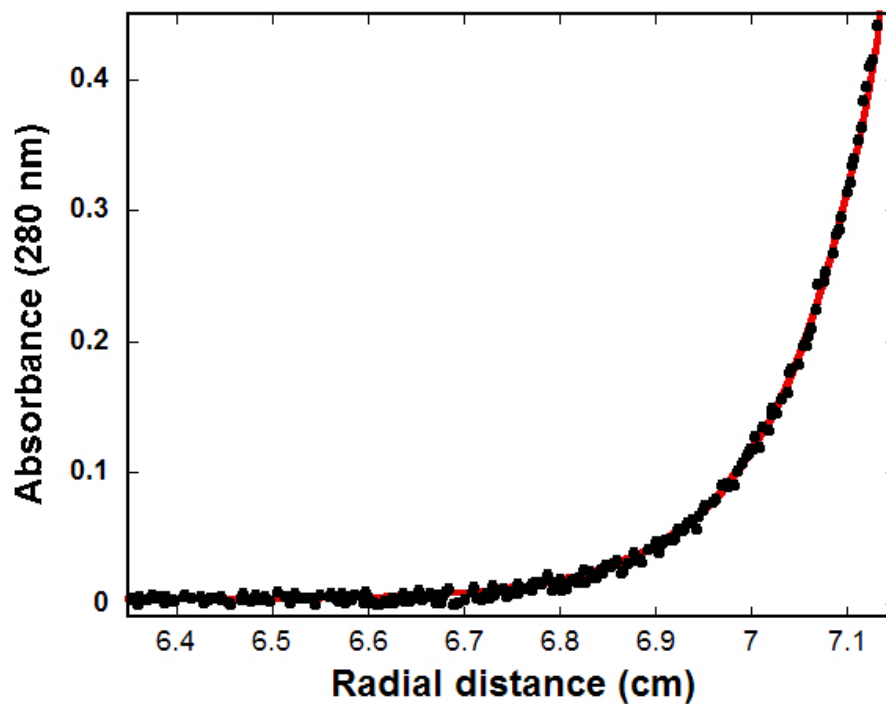


**Figure 5.4 Sedimentation equilibrium concentration profile of PriB.** Example of a typical sedimentation equilibrium profile recorded at 26000 rpm and monitored at 280 nm<sup>66-69,81</sup>. The concentration of PriB was  $5.76 \times 10^{-6}$  M (dimer). The solid red line is the nonlinear least-squares fit, using the single exponential function defined by equation 2.4 with the molecular mass of 24001 Da<sup>66-69,81</sup>.



extrapolation of the plots to  $[\text{PriB}] = 0$  provides  $s_{20,w}^{\circ} = 2.48 \pm 0.1$  S in examined solution conditions (Figure 5.3b)<sup>66,68,72,76</sup>.

The primary structure of the PriB protein indicates that the molecular weight of the monomer is  $\sim 11,400$  kDa. The oligomeric state of the protein in solution has been addressed using the analytical ultracentrifugation method<sup>66-69,76,81</sup>. An example of the sedimentation equilibrium profile of PriB [ $8.89 \times 10^{-6}$  M (dimer)] recorded at the protein absorption band (280 nm) is shown in Figure 5.4<sup>66-69,76,81</sup>. The solid line is the nonlinear least-squares fit, using the single exponential function defined by equation 2.4 (section 2.3.8)<sup>66-69,76,81</sup>. The fit provides an excellent description of the experimental curve indicating the presence of a single species with the molecular weight of  $23,000 \pm 3000$ <sup>66-69,76,81</sup>. Adding additional exponents does not improve the statistics of the fit (data not shown)<sup>66-69,76,81</sup>. The equilibrium sedimentation experiments have been performed at different protein concentrations and different rotational speeds, providing the molecular weight ranging from 20,000 to 26,000 (data not shown)<sup>66-69,76,81</sup>. These results indicate that PriB exists in solution as a stable dimer in the protein concentration range studied in this work<sup>81</sup>.

#### **5.4.3 The Total Site-Size of the PriB – ssDNA Complex.**

It was shown that the PriB protein binding to the ssDNA homopolymers is accompanied by a very modest change in the protein fluorescence emission (data not shown)<sup>81,111</sup>. This small change in the protein tryptophan's fluorescence could limit the quality of the quantitative studies. The resolution of the binding studies described in this Chapter was significantly increased by the finding that the binding of PriB dimer to the etheno-derivative of the adenosine oligomers causes a strong nucleic acid fluorescence increase<sup>1,7,8,27,56,81</sup>. This excellent signal was used to perform the high-resolution

measurements of the stoichiometry and elucidation of the mechanism of the protein - ssDNA complex formation<sup>81</sup>. To address the fundamental problem of the stoichiometry of the PriB - ssDNA complex, we performed a series of quantitative studies using several ssDNA oligomers with different numbers of nucleotides<sup>1,7,27,56-58,81,92,99,117</sup>.

Fluorescence titrations of the 20-mer, dεA(pεA)<sub>19</sub>, with the PriB protein at two different nucleic acid concentrations, in buffer C100, are shown in Figure 5.5a<sup>81</sup>. The shift of the titration curve at a higher nucleic acid concentration, results from the fact that more protein is required to obtain the same total average degree of binding,  $\Sigma\Theta_i$ <sup>1,27,56,57,81,92,99</sup>. The selected nucleic acid concentrations provide separation of the binding isotherms up to the relative fluorescence increase of  $\sim 0.8$ <sup>81</sup>. To obtain thermodynamic binding parameters, independent of any assumption about the relationship between the observed signal and the total average degree of binding,  $\Sigma\Theta_i$  the fluorescence titration curves, shown in Figure 5.5a, have been analyzed, using the quantitative approach outlined in section 2.3.6, section 5.3.6, and section 5.3.7<sup>1,81,85,87,94,95</sup>. Figure 5.5b shows the dependence of the relative fluorescence increase of the 20-mer,  $\Delta F$ , as a function of the total average degree of binding,  $\Sigma\Theta_i$  of the PriB protein<sup>81</sup>. Extrapolation to the maximum fluorescence change,  $\Delta F_{\max} = 1.18 \pm 0.03$ , provides the stoichiometry of the complex  $0.93 \pm 0.15$ ; as a result, a single PriB dimer binds to the ssDNA 20-mer<sup>81</sup>.

The maximum stoichiometry of the PriB - ssDNA oligomer dramatically changes for the 26-mer, dεA(pεA)<sub>25</sub>, even though this oligomer is only 6 nucleotides longer than the 20-mer<sup>81</sup>. Fluorescence titrations of the dεA(pεA)<sub>25</sub> with the PriB protein at two different oligomer concentrations, in buffer C100, are shown in Figure 5.5c<sup>81</sup>. Separation of the titration curves allowed us to determine the total average degree of binding,  $\Sigma\Theta_i$ ,

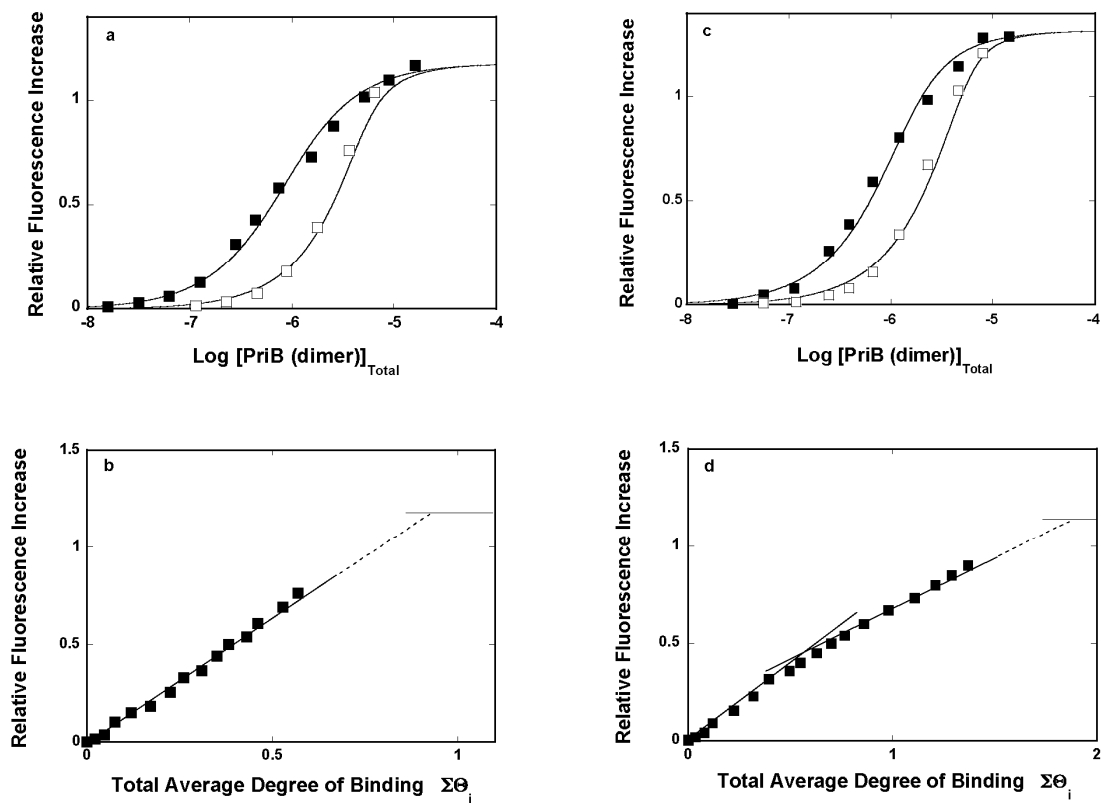


**Figure 5.5 Total site-size of the PriB – ssDNA complex.** **a.** Fluorescence titrations of the ssDNA 20-mer, dεA(pεA)<sub>19</sub>, with the PriB protein at two different nucleic acid concentrations:  $4.8 \times 10^{-7}$  M (■) and  $4.8 \times 10^{-6}$  M (□) (oligomer)<sup>1,56,81,94</sup>. The continuous lines are nonlinear least-squares fits of the titration curves, using the single-site binding isotherm described by equation 5.1<sup>1,56,81,94</sup>. **b.** Dependence of the relative fluorescence increase, ΔF, of dεA(pεA)<sub>19</sub>, upon the total average degree of binding of the PriB dimer, ΣΘ<sub>i</sub> (■)<sup>1,56,81,94</sup>. The continuous line follows the experimental points and has no theoretical basis. The broken line is the extrapolation of ΔF to its maximum value, ΔF<sub>max</sub>.<sup>1,56,81,94</sup> **c.** Fluorescence titrations of the ssDNA 26-mer, dεA(pεA)<sub>25</sub>, with the PriB protein at two different nucleic acid concentrations:  $6.0 \times 10^{-7}$  M (■) and  $2.75 \times 10^{-6}$  M (□) (oligomer)<sup>1,56,81,94</sup>. The continuous lines are nonlinear least-squares fits of the titration curves, using the statistical thermodynamic model, described by equations 5.4 – 5.7<sup>1,56,81,94</sup>. **d.** Dependence of ΔF, of dεA(pεA)<sub>25</sub>, upon the total average degree of binding of the PriB dimer, ΣΘ<sub>i</sub> (■)<sup>1,56,81,94</sup>. The continuous lines indicate the slopes of the high and low-affinity phases of the plot. The broken line is the extrapolation of ΔF to its maximum value, ΔF<sub>max</sub><sup>1,56,81,94</sup>. The continuous line is the computer simulation of the dependence of ΔF upon ΣΘ<sub>i</sub> using equations 5.4 – 5.7 and the binding parameters obtained<sup>1,56,81,94</sup>.

up to  $\sim 1.4$ <sup>81</sup>. The dependence of the relative fluorescence increase of the 26-mer, as a function of  $\Sigma\Theta_i$  of the PriB protein on the oligomer, is shown in Figure 5.5d<sup>81</sup>. The plot is nonlinear, indicating the presence of two, high and low affinity binding phases<sup>1,81,85,87,94,95</sup>. Extrapolation of the weak affinity phase to the maximum fluorescence increase  $\Delta F_{\max} = 1.32 \pm 0.03$  provides  $\Sigma\Theta_i = 1.9 \pm 0.2$ <sup>81</sup>. Consequently, the 26-mer provides enough interaction space for the binding of two PriB dimers<sup>81</sup>.

Interestingly, additional increase of the nucleic acid length by as much as 9 nucleotides does not influence the maximum stoichiometry and throughout two PriB dimers bound per ssDNA oligomer<sup>81</sup>. For example, fluorescence titrations of the 35-mer, dεA(pεA)<sub>34</sub>, with the PriB protein at two different nucleic acid concentrations, in buffer C100 are shown in Figure 5.6a<sup>81</sup>. The dependence of the relative fluorescence increase of the 35-mer, as a function of the total average degree of binding of the PriB protein on the oligomer, is shown in Figure 5.6b<sup>81</sup>. Extrapolation of the plot to the maximum fluorescence increase  $\Delta F_{\max} = 2.0 \pm 0.05$  provides  $\Sigma\Theta_i = 2.1 \pm 0.2$ <sup>81</sup>. Notice, maximum increase of the nucleic acid fluorescence is significantly higher than that observed for the 20- and 26-mer and the plot is, within experimental accuracy, linear<sup>81</sup>.

#### **5.4.4 Maximum Stoichiometry of the PriB Dimer – ssDNA Complex Determined by Sedimentation Equilibrium Method.**

Further studies of the PriB - ssDNA stoichiometry has been performed using the independent sedimentation equilibrium technique<sup>27,67,72,76-81,92</sup>. In this approach, we utilize the 21- and 27-mer containing fluorescein at its 5' end, 5'-Fl-dT(pT)<sub>19</sub> and 5'-Fl-dT(pT)<sub>25</sub> and the fact that the sedimentation equilibrium profile of the ssDNA oligomer can be exclusively monitored at the fluorescein absorption band, without any interference of the protein absorbance (section, 2.3.8 and section 5.3.3)<sup>27,67,72,76-81,92</sup>. The experiments,

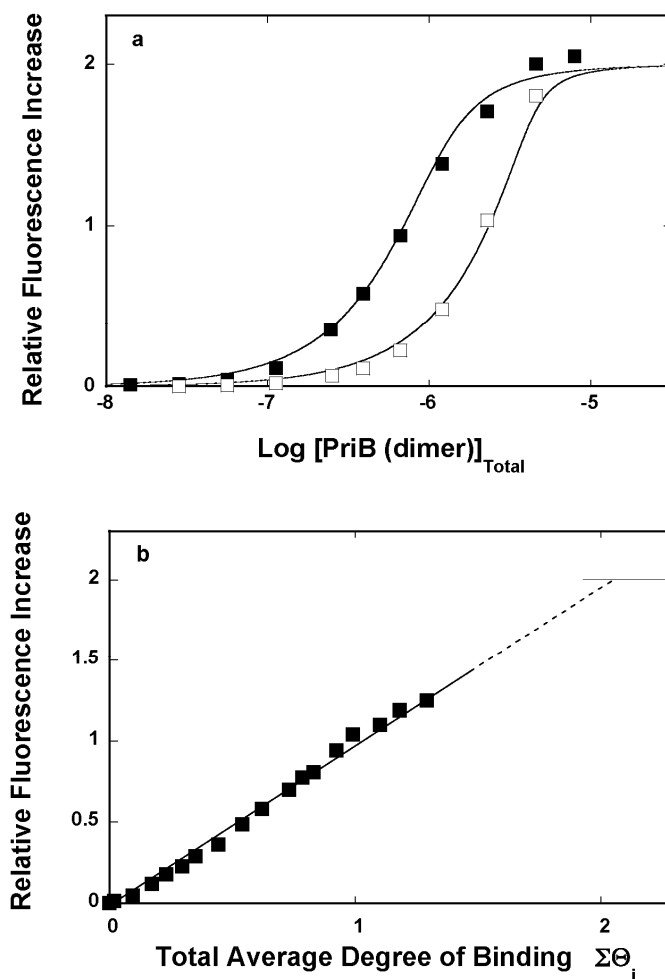


**Figure 5.6 Interactions of PriB – 35-mer ssDNA.** **a.** Fluorescence titrations of the ssDNA 35-mer, dεA(pεA)<sub>34</sub>, with the PriB protein at two different nucleic acid concentrations:  $4.0 \times 10^{-7}$  M (■) and  $2.0 \times 10^{-6}$  M (□) (oligomer)<sup>81</sup>. The continuous lines are nonlinear least-squares fits of the titration curves, using the statistical thermodynamic model described by equations 5.4 – 5.7<sup>81</sup>. **b.** Dependence of the relative fluorescence increase  $\Delta F$ , of dεA(pεA)<sub>34</sub>, upon the total average degree of binding of the PriB dimer,  $\Sigma\Theta_i$  (■)<sup>81</sup>. The continuous line follows the experimental points and has no theoretical basis<sup>81</sup>. The broken line is the extrapolation of  $\Delta F$  to its maximum value,  $\Delta F_{\max} = 2.0$ <sup>81</sup>.

described here, have been performed at the large excess of the PriB protein to assure full saturation of the nucleic acid over the entire equilibrium profile<sup>27,67,72,76-81,92</sup>. Because the molecular weights of the 21- or 27-mer are relatively small,  $\sim 6700$  and  $\sim 8600$ , respectively, the formation of the complex between the oligomer and the PriB dimer, with a molecular weight of  $\sim 23,000$ , will be manifested by a large increase of the molecular weight of the nucleic acid (section 2.3.8 and section 5.4.2)<sup>27,67,72,76-81,92</sup>.

Sedimentation equilibrium profiles of the ssDNA 21-mer, 5'-Fl-dT(pT)<sub>19</sub>, in the presence of the PriB dimer, recorded at the fluorescein absorption band (495 nm) is shown in Figure 5.7a<sup>81</sup>. PriB and the nucleic acid concentrations are  $1.86 \times 10^{-5}$  M (dimer) and  $1.56 \times 10^{-6}$  M (oligomer), respectively<sup>81</sup>. The solid line is the nonlinear least squares fit, using the single exponential function defined equation 2.4 (section 2.3.8)<sup>27,67,72,76-81,92</sup>. Adding additional exponents does not improve the statistics of the fit (data not shown)<sup>81</sup>. The fit provides an excellent description of the experimental curve indicating the presence of a single species with the molecular weight of  $27200 \pm 2900$ ; therefore, the data show that a single PriB dimer binds to the ssDNA 21-mer<sup>81</sup>.

Analogous sedimentation equilibrium profiles of the ssDNA 27-mer, 5'-Fl-dT(pT)<sub>25</sub>, in the presence of the PriB dimer, is shown in Figure 5.7b<sup>81</sup>. The protein and the nucleic acid concentrations are  $1 \times 10^{-5}$  M (dimer) and  $1.58 \times 10^{-6}$  M (oligomer), respectively<sup>81</sup>. The solid line is the nonlinear least squares fit, using the single exponential function defined by equation 2.4, which indicates the presence of a single species with the molecular weight of  $51300 \pm 5100$  (section 2.3.8)<sup>27,67,72,76-81,92</sup>. Therefore, the results of the sedimentation equilibrium experiments unambiguously show that two PriB dimers bind to the 27-mer, which is in accord with the fluorescence titration data (Figure 5.6 and Figure 5.7)<sup>81</sup>.

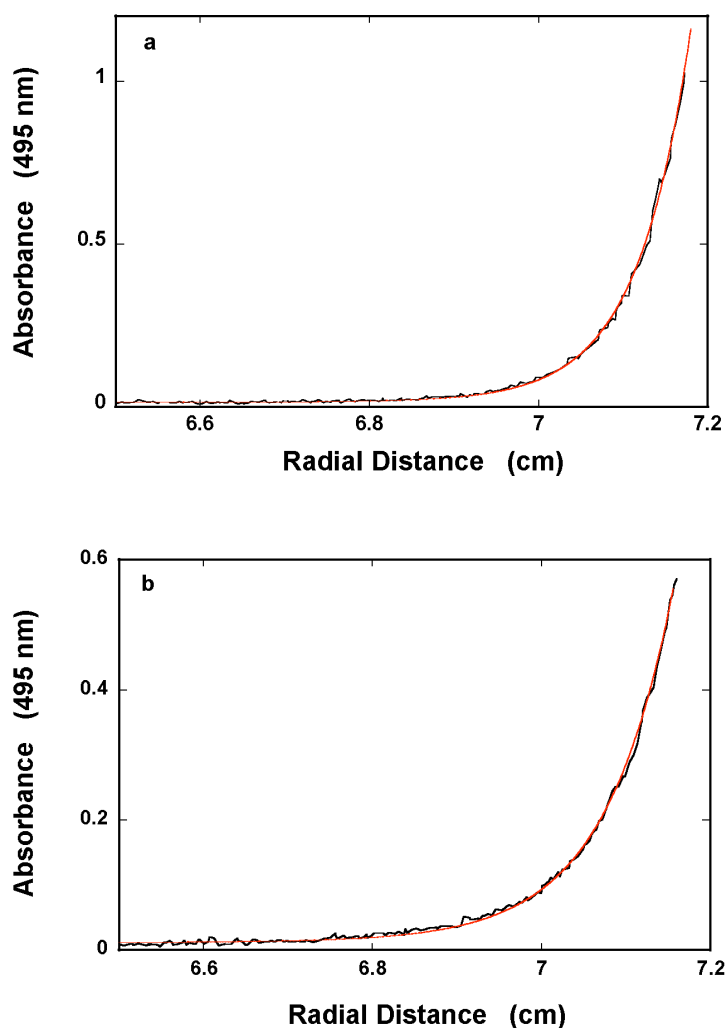


**Figure 5.7 Sedimentation equilibrium studies of PriB – ssDNA complexes. a.** Sedimentation equilibrium concentration profile of the ssDNA 21-mer, 5'-Fl-dT(pT)<sub>19</sub> [ $1.56 \times 10^{-6}$  M (oligomer)] in the presence of PriB protein [ $1.86 \times 10^{-5}$  M (dimer)]<sup>81</sup>. The profile has been recorded at 495 nm and at 28,000 rpm<sup>81</sup>. The continuous line is the nonlinear least squares fit to a single exponential function (equation 2.4) with single species having a molecular mass of  $27,200 \pm 2900$  Da<sup>81</sup>. **b.** Sedimentation equilibrium concentration profile of the ssDNA 27-mer, 5'-Fl-dT(pT)<sub>25</sub> [ $1.58 \times 10^{-6}$  M (oligomer)] in the presence of the PriB protein [ $1 \times 10^{-5}$  M]<sup>81</sup>. The profile has been recorded at 495 nm and at 18,000 rpm<sup>81</sup>. The continuous line is the nonlinear least-squares fit to a single exponential function (equation 2.4) with a single species having a molecular mass of  $51,300 \pm 5000$  Da<sup>81</sup>.

### 5.4.5 Determination of the Site-Size of the PriB Dimer – ssDNA Interactions.

Analogous quantitative analysis of the maximum stoichiometry of PriB – ssDNA complexes, as described for 20- and 26 - mer in section 5.4.3 and section 5.4.4, have been performed for a series of ssDNA oligomers ranging from 14 to 35 nucleotides in length<sup>1,7,27,56-59,81,117</sup>. The dependence of the maximum number of bound PriB dimers per ssDNA oligomer upon the length of the oligomer is shown in Figure 5.8<sup>81</sup>. It is evident that a single PriB dimer binds to the oligomers containing 14, 16, 18, and 20 nucleotides<sup>81</sup>. A sharp transition from a single PriB dimer bound per ssDNA oligomer to two PriB dimers bound per oligomer occurs between 20- and 24-mers (Figure 5.8)<sup>81</sup>. Further increase in the length of the oligomer up to 35 nucleotides, does not lead to the increase in the number of bound PriB dimers<sup>81</sup>. As a result, the total site-size of the PriB - ssDNA complex must contain at least 11 but less than 18 nucleotides per protein dimer<sup>81</sup>.

### 5.4.6 Intrinsic Affinity of the PriB protein – ssDNA Interactions.

Binding of a single PriB dimer to 14-, 16-, 18-, and 20-mer can be analyzed using a single-site-binding isotherm described by

$$\Delta F = \Delta F_{\max} \left[ \frac{K_N P_F}{1 + K_N P_F} \right] \quad (5.1)$$

where  $K_N$  is the macroscopic binding constant characterizing the affinity for a given ssDNA oligomer, containing  $N$  nucleotides, and  $\Delta F_{\max}$  is the maximum relative fluorescence increase<sup>1,7,56,81,85,87</sup>. The solid lines in Figures 5.5a are nonlinear least squares fits of the experimental titration curve for the PriB - 20-mer complex using equation 5.1, and a single set of binding and spectroscopic parameters<sup>1,56,81</sup>. The values of



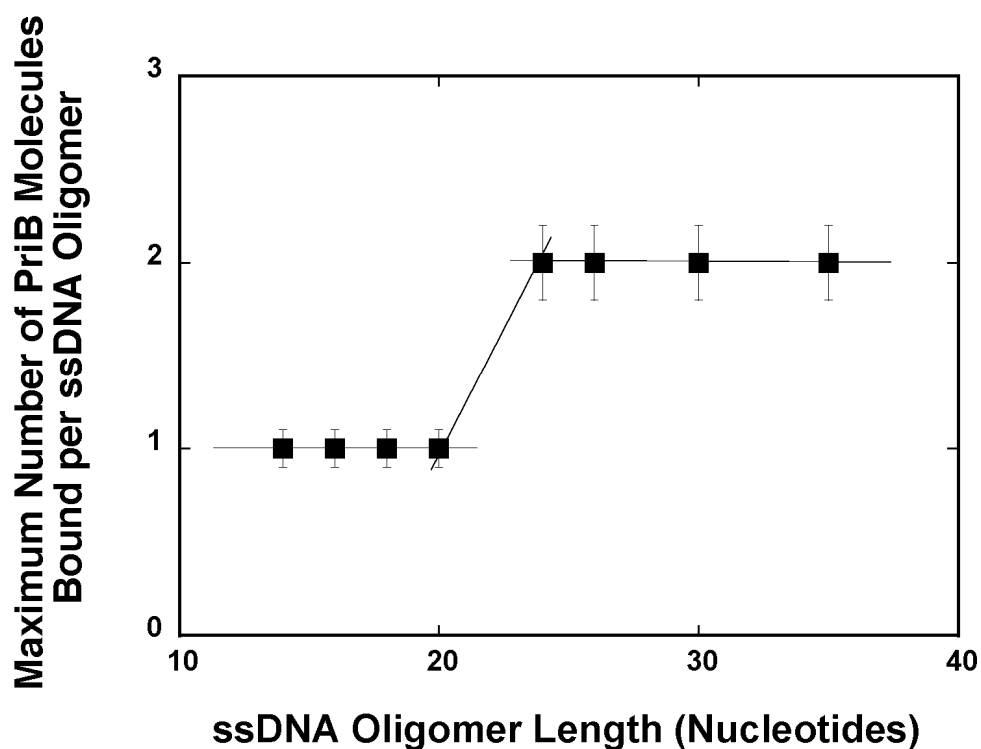


**Figure 5.8 The site-size of the PriB dimer – ssDNA interactions a.** The maximum number of the PriB protein dimers bound per ssDNA oligomer, as a function of the length of the nucleic acid<sup>81</sup>. The continuous lines follow the experimental points and have no theoretical basis<sup>81</sup>. The number of the bound PriB protein dimers has been determined using the quantitative approach described in section 5.4.6 and section 5.4.7<sup>81</sup>.

$K_N$ , for all studied ssDNA oligomers described in this Chapter, which can accept only a single PriB dimer, are included in Table 5.1<sup>81</sup>.

Notice that the value of  $K_N$ , within experimental error, increases as the length of the ssDNA oligomers increases<sup>1,56,81</sup>. This behavior is an indication that there is a statistical factor hidden in  $K_N$ <sup>81</sup>. This is a consequence of the fact that the number of nucleotides engaged in direct interactions with the ssDNA-binding site of the PriB dimer must be less than the length of the examined ssDNA oligomers<sup>1,56,81,86,88,89</sup>. These direct intrinsic interactions can be characterized by the intrinsic binding constant,  $K_i$ <sup>1,56,81,86,88,89</sup>. Using  $K_i$ , the expression describing the binding of the PriB dimer to the ssDNA oligomers, which can accommodate only a single dimer molecule, is defined as

$$\Delta F = \Delta F_{\max} \left( \frac{(N - n + 1) K_i P_F}{1 + (N - n + 1) K_i P_F} \right) \quad (5.2)$$

where  $n$  is the number of nucleotides engaged in direct interactions with the DNA-binding site of the protein<sup>1,56,81,86,88,89</sup>. Thus, expression 5.2 takes into account the overlap of the potential binding sites<sup>1,56,81,86,88,89</sup>. The determined macroscopic binding constant,  $K_N$ , may be then defined as

$$K_N = (N - n + 1) K_i \quad (5.3a)$$

and

$$K_N = N K_i - (n - 1) K_i \quad (5.3b)$$

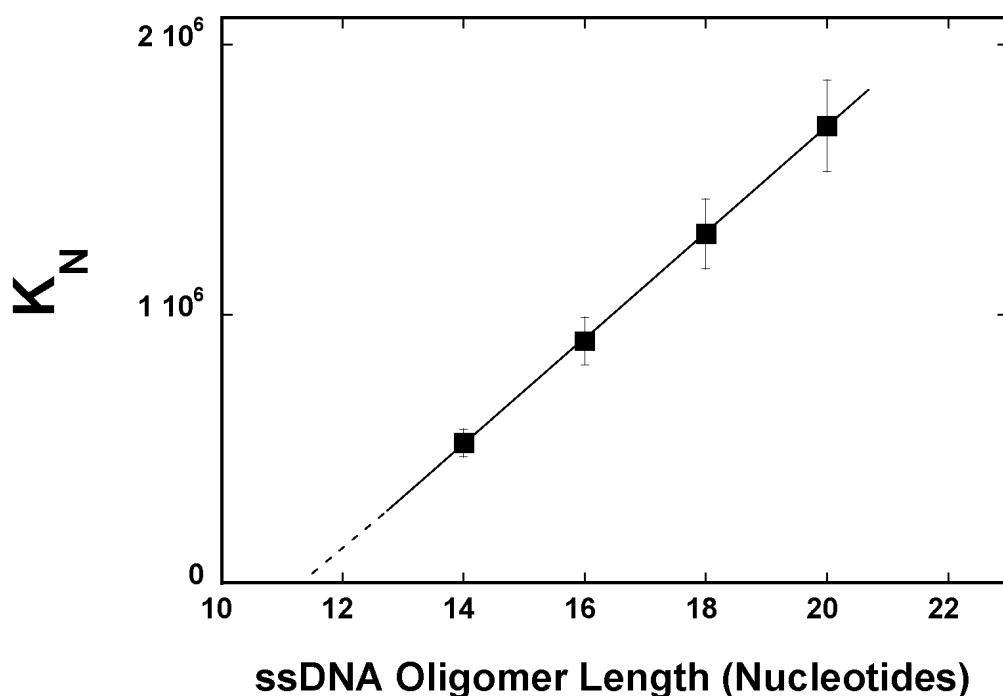


**Figure 5.9 The site - size of PriB – ssDNA is  $12 \pm 1$  nucleotides.** The dependence of the macroscopic equilibrium binding constant,  $K_N$ , characterizing the binding of the PriB protein dimer to different etheno-derivatives of the ssDNA oligomers, upon the length of the ssDNA oligomer (nucleotides)<sup>81</sup>. The continuous line is the linear least-squares fit of the plot according to equations 5.3a and 5.3b<sup>81</sup>. The broken line is the extrapolation of the plot to the zero value of the equilibrium binding constant<sup>81</sup>.

As a result,  $K_N$  should be a linear function of  $N$  with the slope  $\partial K_N / \partial N = K_i$  and, if this is the case, for  $K_N = 0$ , the plot of  $K_N$ , as a function of the nucleic acid length, will intercept the  $N$  axis at the value of  $N = n - 1$ <sup>1,56,81,86,88,89</sup>. The dependence of the macroscopic equilibrium constant,  $K_N$ , for the PriB dimer binding to the ssDNA oligomers, big enough to accept only a single dimer, as functions of the ssDNA oligomer length, is shown in Figure 5.9<sup>81</sup>. As evident from the figure, the plot is strictly linear<sup>81</sup>. Such behavior of  $K_N$  is a very strong indication of the existence of several potential binding sites on the ssDNA oligomers<sup>1,56,81,86,88,89</sup>. Extrapolation of the plot to zero value of the macroscopic equilibrium constant intercepts the DNA length axis at  $N = n - 1 = 11.3 \pm 1$  and provides the site-size of the PriB dimer - ssDNA complex of  $n = 12 \pm 1$  nucleotides (Figure 5.9)<sup>1,56,81,86,88,89</sup>.

#### **5.4.7 Intrinsic Affinities and Cooperativities of the PriB protein – ssDNA Interactions.**

Since the quantitative analysis of the PriB dimer binding to the 24-, 26-, 30-, and 35-mer is much more complex, the partition function,  $Z_N$ , for these systems must account for the potential overlap of the binding sites and the possible cooperative interactions between the bound protein molecules<sup>1,56,81,86,88,89</sup>. Such a binding system can be directly treated by the exact combinatorial theory for large ligand binding to a finite linear, homogeneous lattice<sup>1,56,81,88</sup>. The partition function,  $Z_N$ , of the system is defined as

$$Z_N = \sum_{k=0}^g \sum_{j=0}^{k-1} P_N(k, j) (K_i P_F)^k \omega^j \quad (5.4)$$

where  $g$  is the maximum number of ligand molecules which may bind to the finite nucleic acid lattice (for the nucleic acid lattice  $N$  residues long,  $g = N/n$ ),  $\omega$  is the cooperative interactions parameter,  $k$  is the number of ligand molecules bound, and  $j$  is the number of cooperative contacts between the  $k$  bound ligand molecules in a particular configuration on the lattice<sup>1,56,81,86,88,89</sup>. The combinatorial factor  $P_N(k, j)$  is the number of distinct ways that  $k$  ligands bind to a lattice, with  $j$  cooperative contacts, and is defined by<sup>1,56,81,86,88,89</sup>

$$P_N(k, j) = \frac{[(N - nk + 1)!(k - 1)!]}{[(N - nk + j + 1)!(k - j)!(k - j - 1)!]} \quad (5.5)$$

The total average degree of binding,  $\Sigma\Theta_i$ , is then<sup>1,56,81,86,88,89</sup>

$$\Sigma\Theta_i = \frac{\sum_{k=1}^g \sum_{j=0}^{k-1} k P_N(k, j) (K_i P_F)^k \omega^j}{\sum_{k=0}^g \sum_{j=0}^{k-1} P_N(k, j) (K_i P_F)^k \omega^j} \quad (5.6)$$

The value of the relative fluorescence increase,  $\Delta F$ , at any titration point, is defined as<sup>1,56,81,86,88,89</sup>

$$\Delta F = \Delta F_1 \left[ \frac{(N - n + 1) K_i P_F}{Z_N} \right] + \Delta F_{\max} \left[ \frac{\sum_{j=0}^{k-1} P_N(k, j) (K_i P_F)^k \omega^j}{Z_N} \right] \quad (5.7)$$

where  $\Delta F_1$  and  $\Delta F_{\max}$  are the relative molar fluorescence increases accompanying the binding of one and two PriB dimers<sup>81</sup>. Since the values of the total site-size of the PriB - ssDNA complex,  $n = 12$ , was just determined above, in section 5.4.6, the value of  $\Delta F_1$  can be estimated for each ssDNA oligomer as  $\Delta F_1 = \partial \Delta F / \partial \Sigma \Theta_i$ , from the initial part of the plot of  $\Delta F$  as a function of  $\Sigma \Theta_i$ , as shown in Figure 5.5d and Figure 5.6b, and the value of the maximum observed relative fluorescence increase ( $\Delta F_{\max}$ ) can be estimated from the parental fluorescence titration curves, as shown in Figure 5.5c and Figure 5.6a, only two independent parameters,  $K_i$ , and  $\omega$  must be determined<sup>1,56,81,88</sup>. The solid lines in Figure 5.5c and Figure 5.6a are nonlinear least squares fits of the titration curves using equations 5.4 – 5.7, which provide an excellent description of the experimental data providing spectroscopic and binding parameters for all etheno-derivatives of the ssDNA oligomers, which can accommodate two PriB dimers (Table 5.1)<sup>1,56,81,86,88,89</sup>.

Inspection of the values of the intrinsic binding constants for the 24-, 26-, 30-, and 35-mer shows that they are very similar to each other and to the values of  $K_i$ , obtained for the oligomers, which can accommodate only a single dimer molecule (Table 5.1)<sup>1,56,81</sup>. Such similarity indicates that the same intrinsic binding process is observed<sup>1,56,81</sup>. The value of the cooperativity parameter is very large,  $\omega \approx 45 - 50$ , indicating the PriB dimer binds the ssDNA with strong positive cooperative interactions could form long clusters on the nucleic acid lattice<sup>1,56,81,88,92</sup>. Yet again, within experimental accuracy,  $\omega$  for the 24-, 26-, 30-, and 35-mer is the same indicating that the nature of the cooperative interactions in complex with different oligomers is similar<sup>1,56,81,88,92</sup>. Interestingly, the value of  $\Delta F_1$ , describing binding of the first PriB dimer to the ssDNA is lower than the value observed for the ssDNA oligomers which accept only a single PriB dimer (Table 5.1)<sup>1,56,81</sup>. This behavior may reflect the fact that a single PriB dimer exerts less pronounced effect on the nucleic acid structure in the case of the longer oligomer, where

large part of the nucleic acid is not engaged in interactions with the protein<sup>1,56,81</sup>. Nevertheless, with the exception of the 35-mer, the value of  $\Delta F_{\max}$  is similar to the analogous parameter obtained for shorter oligomers, indicating similar nucleic acid structure in the examined complexes (Table 5.1)<sup>1,56,81</sup>.

#### 5.4.8 The Effect of Salt on the Intrinsic PriB – ssDNA Interactions.

Fluorescence titrations of dεA(pεA)<sub>19</sub> with the PriB protein, in buffer C100 containing different NaCl concentrations, are shown in Figure 5.10a<sup>81</sup>. Parallel studies have been performed in the presence of NaBr (data not shown)<sup>81</sup>. As the salt concentration increases, there is a modest decrease of the maximum fluorescence increase at saturation,  $\Delta F_{\max}$ , from  $\sim 1.2$  at 100 mM to  $\sim 1.0$  at 154 mM NaCl, indicating the similar structure of the nucleic acid in the complex<sup>1,56,81</sup>. The solid lines in Figures 5.10a are nonlinear least squares fits to a single-site binding model with two fitting parameters,  $K_{20}$ , and the maximum relative fluorescence increase,  $\Delta F_{\max}$  as described above in section 5.4.6 (equation 5.1)<sup>1,56,81</sup>. Figure 5.10b shows the dependence of the logarithm of  $K_{20}$  upon the logarithm of NaCl and NaBr concentrations (log-log plots)<sup>1,27,56,57,81,83,84,92</sup>. The plots are linear in the examined salt concentration range and are characterized by the slopes  $\partial \log K_{20} / \partial \log [\text{NaCl}] = -5.7 \pm 0.5$  and  $\partial \log K_{20} / \partial \log [\text{NaBr}] = -5.4 \pm 0.5$ , respectively<sup>1,27,56,57,81,83,84,92</sup>. The values of the slopes indicate that there is a net release of  $\sim 5 - 6$  ions upon the complex formation, with an indication of a clear anion effect on the interactions reflected in the value of the binding constant, which is lower in the presence of NaBr, as compared to  $K_{20}$  in the analogous NaCl concentrations<sup>1,27,56,57,81,83,84,92</sup>.

#### **5.4.9 The Effect of Magnesium on the Intrinsic Interactions of PriB – ssDNA.**

A series of fluorescence titrations of dεA(pεA)<sub>19</sub> with the PriB protein, in buffer C100, containing different MgCl<sub>2</sub> concentrations, are shown in Figure 5.10c<sup>1,27,56,81,83</sup>. Again, both macroscopic affinity and  $\Delta F_{\text{max}}$  decrease as a result of the magnesium



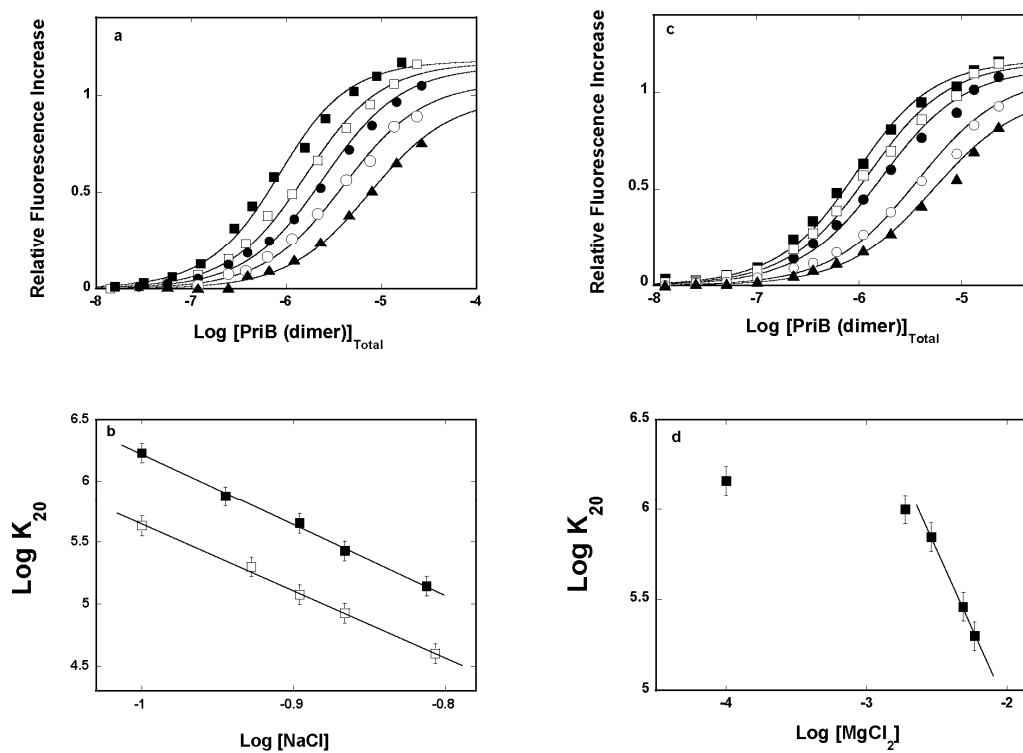


**Figure 5.10 The salt effect on the intrinsic PriB – ssDNA interactions.** **a.** Fluorescence titrations of the ssDNA 20-mer, dεA(pεA)<sub>19</sub> [ $4.8 \times 10^{-7}$  M (oligomer)] with the PriB protein at different NaCl concentrations: 100 mM (■); 113.5 mM (□); 127 mM (●); 136 mM (○); 154 mM (▲)<sup>81</sup>. The continuous lines are nonlinear least-squares fits of the titration curves, using the single-site binding isotherm described by equation 5.1 with  $\Delta F_{\max}$ ,  $K_{20}$ : 1.18,  $1.7 \times 10^6$  M<sup>-1</sup> (■); 1.17,  $7.5 \times 10^5$  M<sup>-1</sup> (□); 1.15,  $4.5 \times 10^5$  M<sup>-1</sup> (●); 1.07,  $2.7 \times 10^5$  M<sup>-1</sup> (○); 0.99,  $1.4 \times 10^5$  M<sup>-1</sup> (▲)<sup>81</sup>. **b.** The dependence of the logarithm of  $K_{20}$  upon the logarithm of the concentration of NaCl (■) and NaBr (□), respectively<sup>81</sup>. The continuous lines are linear least-squares fits, which provide the slope  $\partial \log K_{20} / \partial \log [\text{NaCl}] = -5.7 \pm 0.6$  and  $\partial \log K_{20} / \partial \log [\text{NaBr}] = -5.4 \pm 0.6$ <sup>81</sup>. **c.** Fluorescence titrations of the ssDNA 20-mer, dεA(pεA)<sub>19</sub>, with the PriB protein containing 0.1 mM EDTA and different concentrations of  $MgCl_2$ : 0 mM (■); 1.9 mM (□); 2.9 mM (●); 4.9 mM (○); 5.9 mM (▲)<sup>81</sup>. The continuous lines are nonlinear least-squares fits of the titration curves, using the single-site isotherm described by equation 5.1 with  $\Delta F_{\max}$ ,  $K_{20}$ : 1.17,  $1.45 \times 10^6$  M<sup>-1</sup> (■); 1.16,  $1.0 \times 10^6$  M<sup>-1</sup> (□); 1.13,  $7.0 \times 10^5$  M<sup>-1</sup> (●); 1.09,  $2.9 \times 10^5$  M<sup>-1</sup> (○); 1.0,  $2.0 \times 10^5$  M<sup>-1</sup> (▲)<sup>81</sup>. **d.** The dependence of the logarithm of  $K_{20}$  upon the logarithm of  $[MgCl_2]$  (■)<sup>81</sup>. The continuous line is the linear least-squares fit of the plot in the high  $[MgCl_2]$  range, which provides the slope  $\partial \log K_{20} / \partial \log [MgCl_2] = -1.8 \pm 0.4$ <sup>81</sup>.

concentration increase<sup>1,56,81</sup>. As described above, the solid lines in Figure 5.10c are nonlinear least squares fits to a single-site-binding model, with two fitting parameters, intrinsic binding constant,  $K_{20}$ , and  $\Delta F_{\max}$  (equation 5.1)<sup>1,56,81</sup>. Figure 5.10d shows the dependence of the logarithm of  $K_{20}$  upon the logarithm of  $[\text{MgCl}_2]$  (log-log plot)<sup>1,27,56,81,83,84</sup>. Contrary to the behavior depicted in the presence of different concentrations of NaCl or NaBr, the plot is evidently nonlinear<sup>1,56,81</sup>. At low magnesium concentrations, the slope,  $\partial \log K_{20} / \partial \log [\text{MgCl}_2] = \sim 0 \pm 0.2$ . Beyond  $\sim 1$  mM  $\text{MgCl}_2$  the affinity dramatically decreases, indicating that the intrinsic binding process is accompanied by a net ion release with  $\partial \log K_{20} / \partial \log [\text{MgCl}_2] = -1.8 \pm 0.4$ <sup>1,27,56,81,83,84,92</sup>.

#### **5.4.10 The Effect of Salt on the Intrinsic Affinity and Cooperativity of PriB Dimer – ssDNA Interactions.**

To address the effect salt on the intrinsic affinity and cooperativity of the PriB protein binding to the ssDNA, 26-mer was used, which can accept two PriB dimer molecules (Table 5.1)<sup>81</sup>. Fluorescence titrations of dεA(pεA)<sub>25</sub>, with the PriB protein in buffer C100, containing different NaCl concentrations, are shown in Figure 5.11a<sup>81</sup>. Analysis of the titration curves has been performed, as described above in section 5.4.7, and the solid lines in Figure 5.11a are nonlinear least squares fits using equations 5.4 – 5.7<sup>1,27,56,81,83,84,92</sup>. The dependence of the logarithm of the intrinsic binding constant,  $K_i$ , upon the logarithm of NaCl concentration is shown in Figure 5.11b<sup>1,81,83,84</sup>. The plot is linear in the studied salt concentration range and is characterized by the slope  $\partial \log K_i / \partial \log [\text{NaCl}] = -5.3 \pm 0.6$ , which is very interesting<sup>1,27,56,81,83,84</sup>. The value of this slope is within experimental accuracy the same as observed for the 20-mer, which can accommodate only one PriB dimer<sup>81</sup>. As a result, the intrinsic interactions between the PriB dimer and the 26-mer are accompanied by the release of  $\sim 5 - 6$  ions<sup>1,56,81,83,84</sup>. The

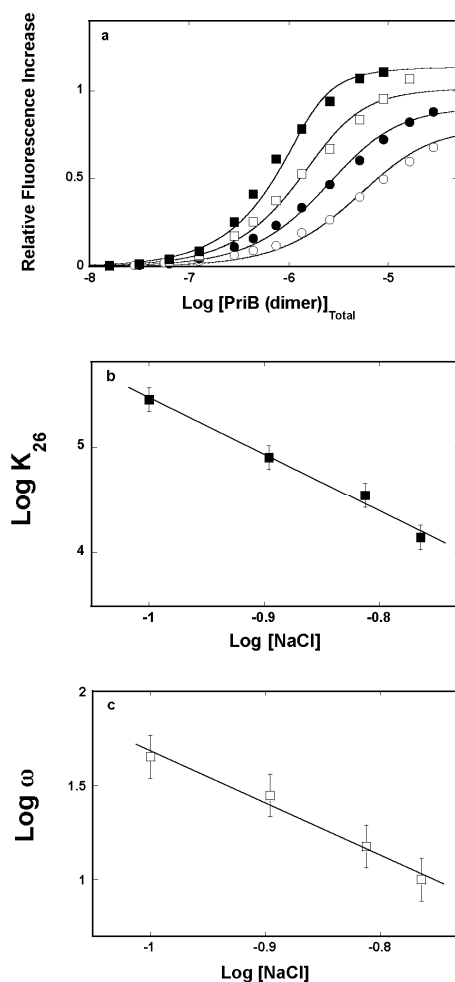


**Figure 5.11 The salt effect on the intrinsic affinity and cooperativity of PriB – ssDNA interactions.** **a.** Fluorescence titrations of the ssDNA 26-mer, dεA(pεA)<sub>25</sub> [ $6 \times 10^{-7}$  M (oligomer)] with the PriB protein at different NaCl concentrations: 100 mM (■); 127 mM (□); 154 mM (●); 172 mM (○)<sup>81</sup>. The continuous lines are nonlinear least-squares fits of the titration curves, using the statistical thermodynamic model described by equations 5.4 – 5.7 with  $\Delta F_1$ ,  $\Delta F_{\max}$ ,  $K_i$ ,  $\omega$ : 0.8, 1.08,  $2.8 \times 10^5$  M<sup>-1</sup>, 45 (■); 0.8, 1.02,  $8 \times 10^4$  M<sup>-1</sup>, 28 (□); 0.8, 0.91,  $3.5 \times 10^4$  M<sup>-1</sup>, 15 (●); 0.77, 0.78,  $1.4 \times 10^4$  M<sup>-1</sup>, 10 (○)<sup>81</sup>. **b.** The dependence of the logarithm of the intrinsic binding constant  $K_i$  upon the logarithm of [NaCl]<sup>81</sup>. The continuous line is the linear least-squares fit, which provides the slope  $\partial \log K_i / \partial \log [\text{NaCl}] = -5.3 \pm 0.6$ <sup>81</sup>. **c.** The dependence of the logarithm of the cooperativity parameter,  $\omega$ , upon the logarithm of [NaCl]<sup>81</sup>. The continuous line is the linear least-squares fit, which provides the slope  $\partial \log \omega / \partial \log [\text{NaCl}] = -2.8 \pm 0.6$ <sup>81</sup>.

dependence of the logarithm of the cooperative interactions parameter,  $\omega$ , upon the logarithm of  $[\text{NaCl}]$ , is shown in Figure 5.11c<sup>56,81,83,84</sup>. The value of  $\omega$  strongly decreases with increasing NaCl concentration, indicating that positive cooperative interactions are weakened by high salt concentrations<sup>1,56,81,83,84,92</sup>. The salt effect on the free energy of cooperative interactions between the two bound PriB molecules is characterized by the negative slope,  $\partial \log \omega / \partial \log [\text{NaCl}] = -2.8 \pm 0.6$ , therefore, cooperative interactions between the bound protein molecules are accompanied by the net release of  $\sim 3$  ions<sup>56,81,83,84</sup>.

#### 5.4.11 The Effect of Temperature on the Intrinsic PriB – ssDNA Interactions.

In a next step, the nature of the intrinsic interactions in the PriB - ssDNA complex was addressed by examining the temperature effect on the protein binding to the ssDNA 20-mer, dεA(pεA)<sub>19</sub><sup>81</sup>. Figure 5.12 shows a very unusual results of fluorescence titrations of dεA(pεA)<sub>19</sub> with the PriB protein performed at different temperatures<sup>81</sup>. It is clear that in the range from 5°C to 20°C, neither the intrinsic affinity nor the values of  $\Delta F_{\text{max}}$  are affected by temperature<sup>81</sup>. The solid line in Figure 5.12 is the nonlinear least squares fit of the experimental titration curve, obtained at 10°C, using  $K_i = 1.9 \times 10^5 \text{ M}^{-1}$  and  $\Delta F_{\text{max}} = 1.18$  (Table 5.1)<sup>81</sup>. Within experimental accuracy, the fit provides remarkably adequate description for titration curves obtained at all examined temperatures<sup>81</sup>. As a result, the PriB - ssDNA interactions must be characterized by the apparent enthalpy change of  $\Delta H^\circ \approx 0$ <sup>81</sup>. In other words, the intrinsic interactions are completely driven by the apparent entropy change,  $\Delta S^\circ$ <sup>81</sup>. Using the standard thermodynamic formulas,  $\Delta G^\circ = -RT \ln K_i$ , and  $\Delta S^\circ = (-\Delta G^\circ + \Delta H^\circ)/T$ , one obtains the free energy of binding at 10°C,  $\Delta G^\circ \approx -6.8$  kcal/mole, which provides  $\Delta S^\circ \approx 24 \text{ cal/mol deg}$ <sup>81</sup>.

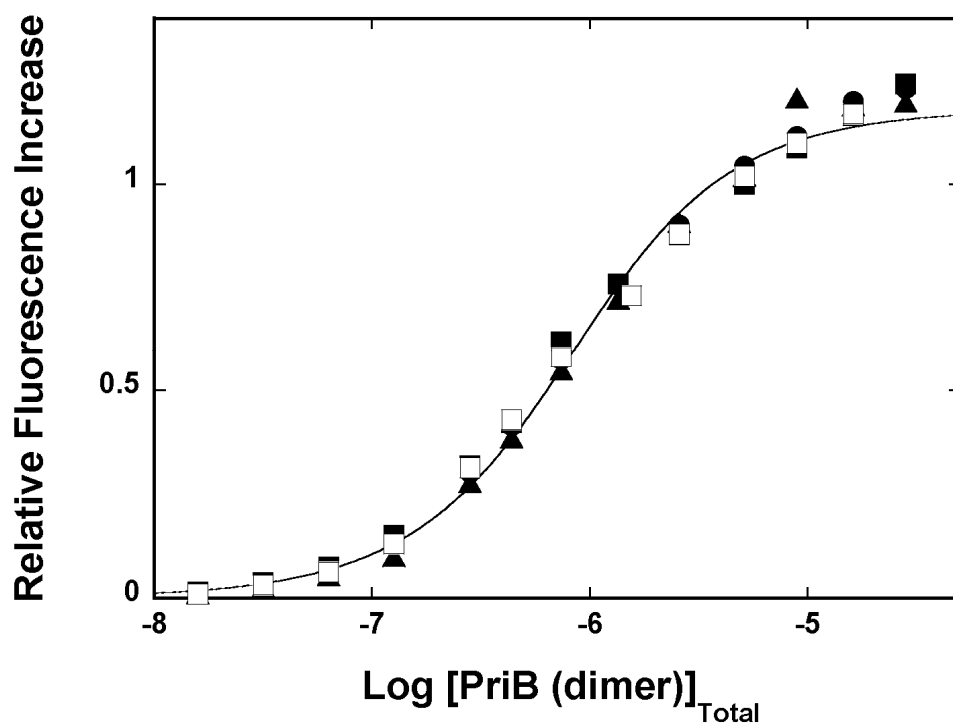


**Figure 5.12 The temperature effect on the PriB - ssDNA interactions.** Fluorescence titrations of the ssDNA 20-mer, dεA(pεA)<sub>19</sub> [ $4.8 \times 10^{-7}$  M (oligomer)] with the PriB protein at different temperatures: 5°C (■), 10°C (□), 15°C (●), 20°C (▲)<sup>81</sup>. The continuous line is the nonlinear least-squares fit of the titration curve, obtained at 10 °C, using the single-site binding isotherm defined by equation 5.1 with  $K_{20} = 1.7 \times 10^6 \text{ M}^{-1}$  and  $\Delta F_{\text{max}} = 1.18$ , respectively<sup>81</sup>.

#### 5.4.12 The Base Specificity of PriB – ssDNA Interactions.

Quantitative determination of affinities of the PriB protein for unmodified ssDNAs, differing by the type of base, has been performed using the macromolecular competition titration (MCT) as described in Chapter 4, section 4.4.7<sup>1,57,81,87,116</sup>. In accord with the base specificity studies described for 181aa N-terminal domain of PriA, in experiments described in this Chapter, the 20-mer, dεA(pεA)<sub>19</sub> was used as a reference lattice, and the base specificity of the PriB protein has been examined using different 20-mers, dN(pN)<sub>19</sub><sup>1,57,81</sup>.

Fluorescence titrations of dεA(pεA)<sub>19</sub> with the PriB protein in buffer C100 in the absence and presence of two different dT(pT)<sub>19</sub> concentrations, are shown in Figure 5.13a<sup>81</sup>. The titration curve dramatically shifts, with increasing dT(pT)<sub>19</sub> concentration, indicating a strong competition between dεA(pεA)<sub>19</sub> and dT(pT)<sub>19</sub> for the PriB protein<sup>1,57,81,87,116</sup>.  $K_{20R} = 1.7 \times 10^6 \text{ M}^{-1}$  and  $\Delta F_{\max} = 1.18$  are known from independent titration experiments (Figure 5.5a)<sup>81</sup>. Parallel fluorescence titrations of dεA(pεA)<sub>19</sub> with the PriB protein alone and in the presence of dA(pA)<sub>19</sub> and dC(pC)<sub>19</sub>, at the same concentration of both ssDNA oligomers, are shown in Figure 5.13b. As observed for dT(pT)<sub>19</sub>, the titration curve significantly shifts in the presence of dC(pC)<sub>19</sub>, while it is barely affected by the same concentration of dA(pA)<sub>19</sub><sup>1,57,81</sup>. The solid lines in Figure 5.13a and Figure 5.13b are nonlinear least squares fits of the experimental titration curves, with a single fitting parameter,  $K_{20S}$ , using equations 4.9 and 4.10 in section 4.4.7<sup>1,57,81,116</sup>. The values of the binding constants,  $K_{20S}$ , obtained for pyrimidine oligomers dT(pT)<sub>19</sub> and dC(pC)<sub>19</sub> are  $\sim 3$  and  $\sim 2$  of magnitude higher than the analogous parameter determined for the homo-purine oligomer, dA(pA)<sub>19</sub> (Table 5.2)<sup>81</sup>.

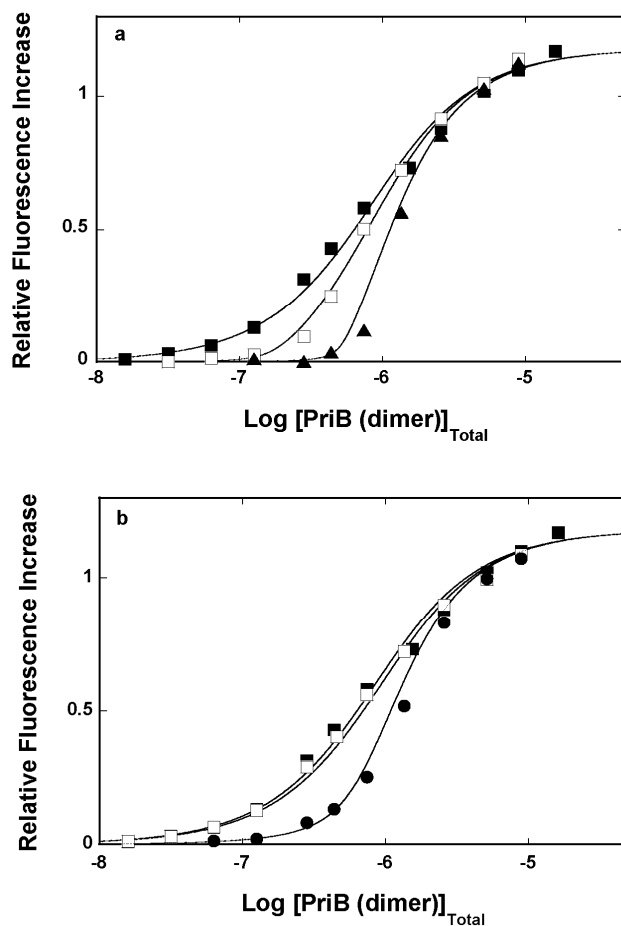


**Figure 5.13 The base specificity of PriB – ssDNA interactions.** **a.** Fluorescence titrations of the ssDNA 20-mer, dεA(pεA)<sub>19</sub> [ $4.8 \times 10^{-7}$  M (oligomer)] with the PriB protein in the absence (■) and in the presence of two different concentrations of dT(pT)<sub>19</sub>:  $1.5 \times 10^{-7}$  M (○) and  $5 \times 10^{-7}$  M (▲)<sup>81</sup>. The continuous lines are nonlinear least-squares fits of the binding titration curves, using equations 4.9 and 4.10, with the binding constant for dεA(pεA)<sub>19</sub>,  $K_{20} = 1.7 \times 10^6 \text{ M}^{-1}$  and  $\Delta F_{\text{max}} = 1.18$ , and the intrinsic binding constant  $K_{20S} = 3 \times 10^8 \text{ M}^{-1}$  for dT(pT)<sub>19</sub><sup>81</sup>. **b.** Fluorescence titrations of the ssDNA 20-mer, dεA(pεA)<sub>19</sub> [ $4.8 \times 10^{-7}$  M (oligomer)] with the PriB protein in the absence (■) and in the presence of dA(pA)<sub>19</sub> (□) and dC(pC)<sub>19</sub> (●)<sup>81</sup>. The concentration of dA(pA)<sub>19</sub> and dC(pC)<sub>19</sub> is  $5 \times 10^{-7}$  M (oligomer)<sup>81</sup>. The continuous lines are nonlinear least-squares fits of the binding titration curves using equations 4.9 and 4.10, with the binding constant  $K_{20} = 1.7 \times 10^6 \text{ M}^{-1}$ ,  $\Delta F_{\text{max}} = 1.18$  for dεA(pεA)<sub>19</sub> and the binding constant  $K_{20S} = 3.5 \times 10^5 \text{ M}^{-1}$  for dA(pA)<sub>19</sub> and  $K_{20S} = 2.5 \times 10^7 \text{ M}^{-1}$  for dC(pC)<sub>19</sub><sup>81</sup>.

#### **5.4.13 Photo-Cross-Linking of the PriB Dimer To the ssDNA.**

The involvement of the monomers of the PriB dimer in the interactions with the ssDNA, has been addressed using the UV irradiation<sup>81,92,102,116</sup>. UV irradiation generates covalent linkage between nucleic acid bases and amino acid residues through free-radical mechanisms between photo-excited nucleic acid bases and the amino acid residues in very close proximity, resulting in a "zero-length" cross-linking with minimal perturbation to the protein - nucleic acid complex<sup>81,92,102,116</sup>. Thymine is the most reactive base, therefore, it was used here in the photo-cross-linking reaction<sup>81,92,102,116</sup>. Thus, parallel to our thermodynamic binding studies, we performed photo-cross-linking experiments of the PriB dimer - dT(pT)<sub>19</sub> complex<sup>81,92,102,116</sup>. The nucleic acid has been labeled at the 5' end with [<sup>32</sup>P], using polynucleotide kinase<sup>81,92,93,102,116</sup>. Figure 5.14a shows the autoradiogram of the SDS polyacrylamide gel of the PriB - dT(pT)<sub>20</sub> complex, after irradiation, at different protein concentrations<sup>81</sup>. At the highest protein concentration applied, the nucleic acid is completely saturated with the protein and only a single radioactive band appears on the gel, at the molecular weight of ~ 17,000, corresponding to the PriB monomer - 20-mer complex<sup>81</sup>. The same gel but stained with Coomassie Brilliant Blue is shown in Figure 5.14b where a single protein band at ~ 12,000 indicates the location of the PriB monomer<sup>81</sup>. The same location of the PriB monomer band is observed for the non-irradiated complex and the PriB protein alone (Figure 5.14b). As a result, only one monomer of the PriB dimer is engaged in interactions with ssDNA in the complex, independent of the protein concentration<sup>81</sup>.



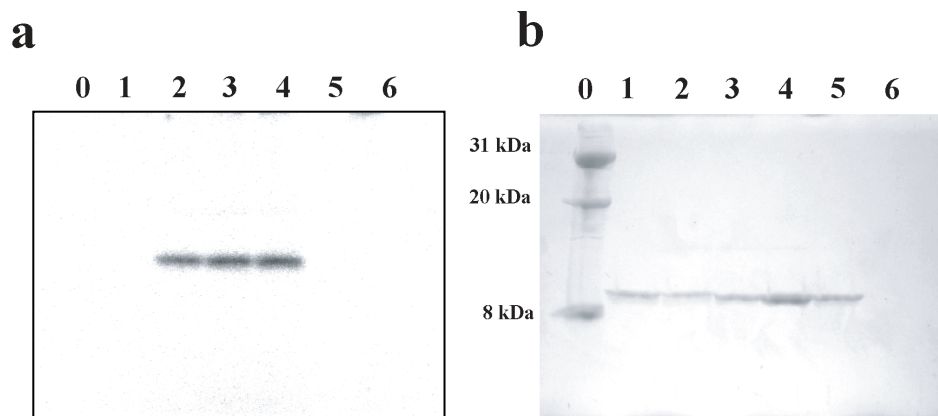


**Figure 5.14 Photo-cross-linking of PriB to ssDNA.** **a.** An autoradiogram of the 15% SDS polyacrylamide gel of the PriB – 5'-[<sup>32</sup>P]dT<sub>20</sub> complex, after UV-mediated cross-linking of the protein to the DNA, formed at different concentrations of the PriB dimer<sup>81</sup>. The concentration of the 5'-[<sup>32</sup>P]dT<sub>20</sub> is 5 x 10<sup>-6</sup> M (oligomer). Lane 0 contains protein molecular markers. Lane 1 contains the control sample, which is the PriB – dT<sub>20</sub> complex not subjected to UV irradiation. Lanes 2 – 4, a constant concentration of the ssDNA 20-mer and increasing concentrations of the PriB protein (dimer): lane 2, 5 x 10<sup>-6</sup> M; 3, 8 x 10<sup>-6</sup> M; and 4, 1.3 x 10<sup>-5</sup> M. Lane 5 contains only the PriB protein (5 x 10<sup>-6</sup> M (dimer) in the absence of the 5'-[<sup>32</sup>P]dT<sub>20</sub>. Lane 6 contains the 5'-[<sup>32</sup>P]dT<sub>20</sub> alone. **(b)** The same gel as shown in panel a, but stained with Coomassie Brilliant Blue<sup>81</sup>.

## 5.5 DISCUSSION

### 5.5.1 The Total Site-Size of the PriB Dimer – ssDNA Complex Is $12 \pm 1$ Nucleotides.

The total site-size of a large protein ligand - DNA complex corresponds to the portion of the DNA occluded by a bound protein and, in addition, includes nucleotides prevented from interacting with another protein molecules by the protruding protein matrix of the bound protein<sup>1,81,86,88,89,95,116</sup>. This elementary quantity has to be determined in any quantitative analysis of the energetics and dynamics of the protein - DNA complex, and is vital if any conclusions about the physiological activities of the protein are proposed<sup>1,81,86,88,89,95,116</sup>. The strategy applied in this Chapter relies on the examination of the maximum stoichiometry and macroscopic affinity of the PriB - ssDNA complexes with the ssDNA oligomers, which can accommodate one or two PriB dimers<sup>1,7,56,57,81,95,116,117</sup>. The strictly linear dependence of the macroscopic binding constant for the oligomers, which can accommodate only a single PriB dimer, upon the length of the ssDNA oligomer (Figure 5.10) indicates that the minimum length of the nucleic acid, which forms all necessary contacts with the binding site on the protein, is  $12 \pm 1$  nucleotides<sup>81</sup>.

The change of the maximum stoichiometry from one to two bound PriB dimers takes place between the 20 and 24 mer, indicating that a stretch of 24 nucleotides is long enough for the second PriB dimer to associate with the ssDNA (Figure 5.9)<sup>81</sup>. In addition, only two PriB dimers bind to the 35-mer, which is only possible if the total site-size is 12 nucleotides<sup>81</sup>. Moreover, these data indicate that the ssDNA-binding site must be centrally located, with respect to the dimer molecule<sup>81</sup>. As pointed out above, very similar

intrinsic affinities determined for the all oligomers, which can accept one PriB dimer or two dimers, indicate that the same intrinsic binding process, that is, the association with the same number of 12 nucleotides is observed (Table 5.1)<sup>81</sup>.

### **5.5.2 PriB Possesses Only One DNA-Binding Site Located on a Single Monomer of the PriB Dimer.**

Depicted in Figure 5.1b is the model of the PriB dimer – ssDNA interactions, based on crystallographic studies<sup>81,113</sup>. According to that model, both protein monomers are able to engage the ssDNA 15-mer using assumed DNA-binding pockets, although located on two different dimers (Figure 5.1b)<sup>81,113</sup>. In other words, one PriB dimer has two possible DNA-binding sites, and two PriB dimers can bind to the ssDNA 15-mer<sup>81,113</sup>. However, this is not experimentally observed in solution<sup>81</sup>. First, as shown in section 5.4.6, the total site-size of the protein – ssDNA interactions is only  $12 \pm 1$  nucleotides<sup>81</sup>. This is just enough to fill a single DNA-binding pocket of one monomer but not long enough to wrap the nucleic acid around the protein dimer<sup>81</sup>. Second, it is evident from Figure 5.5 that even 10 fold increase in the oligomer concentration does not change 1:1 stoichiometry of the PriB – 20mer complex<sup>81</sup>. The same is true for binding of the PriB protein to 14-, 16-, 18-mer<sup>81</sup>. These results provide strong thermodynamic evidence that the dimer has a single ssDNA-binding site, and if there was another binding site, its affinity must be  $\sim 2$  orders of magnitude lower than the affinity of the strong site<sup>81</sup>. Third, the oligomers large enough to fully access the presumed second DNA-binding site on another monomer, *i.e.*, 26-, 30-, and 35-mers, still bind only two PriB dimers (Figure 5.5d and Figure 5.6b)<sup>81</sup>. Notice that the local concentration of these longer oligomers in the complex with the PriB dimer is very high and if there was a second binding site, with detectable affinity, it would be accessed by the long oligomers

and manifested in the large change of the total site-size of the complex, and the intrinsic affinity<sup>81</sup>. This is not experimentally observed<sup>81</sup>. Lastly, the results of photo-cross-linking experiment clearly show that only a single monomer engages the ssDNA in the complex, independent of the protein concentration (Figures 5.14)<sup>81</sup>. It stands to reason that the model of the PriB dimers – ssDNA interactions, proposed on the basis of crystallographic studies, is a result of the crystal packing forces, rather than reflecting functional interactions of the PriB dimer with the ssDNA in solution<sup>81</sup>.

In addition, the data presented in this Chapter indicate that the PriB dimer behaves like a protein with half-site reactivity, where only one monomer of the dimer can engage in interactions with the nucleic acid<sup>81,118</sup>. This is a well-known phenomenon in enzymology, where only half of protomers of the multi-subunit enzyme engages in its activity<sup>81,118</sup>. Nevertheless, the functional significance of such a behavior, in the case of the PriB dimer, is not known<sup>81</sup>. Also, it is unknown whether or not the PriB dimer exists in solution in a pre-equilibrium between two conformational states<sup>81</sup>. If so, only one state could be selected by the nucleic acid. It is also possible that upon ssDNA binding the PriB dimer structure changes such that the other, free monomer of the dimer, is unable to bind anymore<sup>81</sup>. All these possibilities are very interesting not only in the context of PriB – ssDNA interactions but also in the context of the formation of the primosome and possible role of PriB in the assembly process<sup>81</sup>.

### **5.5.3 The PriB Dimer ssDNA-Binding Site Has Functionally Homogenous Structure.**

Even though the total site-size of the protein - DNA complex includes nucleotides inaccessible for the binding of another protein molecule, it may have a heterogeneous structure and contain an area, which is directly involved in interactions with the nucleic

acid, like the strong DNA-binding subsite, as well as the nucleotides not engaged in direct interactions, but occluded by the protruding protein matrix<sup>1,56,81</sup>. Such a pronounced heterogeneous structure of the total DNA-binding site plays a significant functional role in activities of different enzymes and has been found for the *E. coli* PriA and DnaB helicases, plasmid RSF1010 Rep helicase, rat and human pol  $\beta$ , as well as polymerase X of the African Swine Fever virus<sup>1,7,8,56-59,81,117</sup>. In the case of PriB, the transition from a single PriB dimer bound per ssDNA oligomer to two bound dimers occurs between 20- and 24-mers, indicating that the DNA-binding site, which occludes the total site-size of  $\sim 12$  nucleotides, is fully engaged in the protein - nucleic acid interactions<sup>1,81</sup>. In other words, the DNA-binding site of the PriB dimer is, in its entirety, the functional DNA-binding site, or it has a functionally homogeneous structure<sup>1,81</sup>.

#### **5.5.4 The PriB Dimer Binds the ssDNA With Significant Positive Cooperativity.**

The cooperative binding of the PriB dimer to ssDNA has been previously inferred on the basis of the Hill coefficient<sup>1,81,113</sup>. In these studies, the values of the Hill coefficient significantly higher than 1, have been determined for the ssDNA oligomers containing 15 nucleotides, which bind only a single PriB dimer, and as a result, the cooperative interactions cannot transpire<sup>1,81,113</sup>. In addition, the search of PriB related literature shows that the apparent affinities of the PriB protein for the ssDNA oligomers have also been obtained assuming a noncooperative binding process<sup>1,16,81</sup>. On the contrary, the statistical thermodynamic approach, applied in the studies described here, allows to quantitatively extract both the intrinsic affinities and the cooperative interactions parameter,  $\omega$ , characterizing the interactions between the bound PriB dimers<sup>1,81,86,88,89</sup>. The obtained value of  $\omega \sim 45 - 50$  indicates that PriB dimer engages in

strong positive cooperative interactions when associated with the ssDNA and the protein could form long clusters on the nucleic acid lattice (Table 5.1)<sup>81</sup>. Interestingly, the number of PriB dimers participating in the primosome assembly is still not completely clear with some reports indicated the presence of at least two PriB dimers in the primosome<sup>15,81,99</sup>. The finding of strong positive cooperativity in the PriB protein binding to the ssDNA indicates that, indeed, multiple PriB dimers may participate in the initial stages of the primosome assembly<sup>15,81,99</sup>. This interesting possibility will be examined in Chapter 6<sup>99</sup>.

#### **5.5.5 The Salt Effect on the Intrinsic Affinity of the PriB Dimer –DNA Interactions Indicates Engagement of the Entire Total Binding Site of the Protein.**

The results presented above clearly show that the entire total DNA-binding site of the PriB dimer engages in direct interactions with the nucleic acid<sup>81</sup>. The salt effect on the intrinsic affinity of the protein strongly supports that conclusion<sup>81</sup>. The slopes,  $\partial \log K_{20} / \partial \log [\text{NaCl}] = -5.7 \pm 0.5$  and  $\partial \log K_{20} / \partial \log [\text{NaBr}] = -5.4 \pm 0.5$  indicate a net release of 5 - 6 ions accompanied the engagement in intrinsic interactions (Figure 5.10b)<sup>81</sup>. Notice, the protein affinity is lower in the presence of bromide than in the presence of the chloride ions<sup>81</sup>. It is well established, however, that bromide anions,  $\text{Br}^-$ , have significantly higher affinity for protein amine groups than  $\text{Cl}^-$ , thus, explaining observed difference in the affinity<sup>81,119</sup>. The apparent independence of the slope of the log - log plot upon the type of anion most probably results from the fact that in the studied salt concentration range (>100 mM) all anion-binding sites are fully saturated with  $\text{Br}^-$ , or  $\text{Cl}^-$ <sup>81,83,84,119</sup>.

Crystallographic studies have identified the DNA-binding pocket of PriB dimer containing Arg13, Lys18, Arg34, Lys84, Lys88, and Lys89 residues in close contact with

the bound nucleic acid<sup>81,113</sup>. The number of possible ionic contacts in the DNA-binding site corroborates very well the net number of ions released at the protein - nucleic acid interface, determined in solution, and described in this Chapter<sup>81,113</sup>. Moreover, the arginine and lysine residues are spread over the entire DNA-binding site of the PriB protein providing another indication that the DNA binding site is homogenous<sup>81,113</sup>. In order to engage all these basic residues, as indicated from the log - log plots, the entire total DNA-binding site must participate in interactions with the nucleic acid<sup>81,83,84,113</sup>. Contrary to monovalent salts, the log-log plot, in the presence MgCl<sub>2</sub> is clearly nonlinear and the linear part at the high MgCl<sub>2</sub> concentration range indicate that ~2 ions are released upon formation of the complex (Figure 5.10d). The lower absolute value of the slope of the linear part of the plot, as compared to NaCl or NaBr, is expected because of the lower value of the thermodynamic binding for magnesium cations to the nucleic acid<sup>83,84</sup>. Because the thermodynamic degree of Mg<sup>+2</sup> binding on the 20-mer changes in the studied salt concentration ranges, the nonlinear behavior of the log-log plot suggests that the released ions may originate predominantly from the nucleic acid<sup>81</sup>. It should be mentioned that, due to the presence of multiple components in solution, the studied system is extremely complex<sup>81</sup>. Nevertheless, a strong decrease of the intrinsic binding constant of the PriB protein - 20-mer complex, occurs around 1 mM MgCl<sub>2</sub> and suggests that the ions are released from the binding sites are characterized by the least 500 M<sup>-1</sup> affinity constant<sup>81</sup>.

#### **5.5.6 The PriB Dimer Shows a Very Strong Preference For the Homo-Pyrimidine ssDNA.**

The difference in the intrinsic affinity of the PriB protein for the ssDNA, differing by the type of base is dramatic and is particularly pronounced for dT(pT)<sub>19</sub> and dA(pA)<sub>19</sub>

with the intrinsic binding constant is  $\sim 3.3 \times 10^7 \text{ M}^{-1}$  and  $\sim 3.9 \times 10^4 \text{ M}^{-1}$ , respectively (Table 5.2)<sup>81</sup>. The  $\sim 3$  orders of magnitude difference in the intrinsic affinity between dT(pT)<sub>19</sub> and dA(pA)<sub>19</sub> indicates significant contribution of the base in ssDNA binding, which is not obvious in the crystal structure of the complex<sup>81,113</sup>. What is obvious from the crystal structure is, that in spite of the low sequence homology (only 11% identity and 27% similarity), the structure of the DNA binding pocket of the PriB dimer is very similar to the structure of the DNA-binding site of the *E. coli* SSB protein, which shows exceptionally high affinity for thymine polymers<sup>81,113,120</sup>. In this context, the lack of temperature effect on the PriB dimer interactions with the ssDNA is perplexing (Figure 5.12). Such a high intrinsic binding constant of PriB – dT<sub>20</sub> interaction ( $\sim 3.3 \times 10^7 \text{ M}^{-1}$ ) should involve a significant participation of nucleic acid bases in interactions with the protein<sup>81,113</sup>. This would, in turn, suggest a large enthalpy contribution to the free energy of binding but this is not what is observed experimentally<sup>81</sup>. Exclusively, apparent entropy-driven binding reaction strongly suggests large conformational change of the protein upon the association reaction, whose enthalpy change would compensate the enthalpy change of the intrinsic, DNA binding process<sup>81</sup>.

Interestingly, estimated concentration of the PriB dimer in the *E. coli* cell is  $\sim 6 \times 10^{-8} \text{ M}$ , which suggests that, at this concentration, the protein predominantly associates with the stretches of thymine nucleotides on the DNA<sup>81,106</sup>. It should be mentioned that the *E. coli* PriA helicase also shows significantly higher intrinsic affinity for homo-pyrimidine over homo-purine oligomers ( $\sim 1$  order of magnitude in similar solution conditions)<sup>57,81</sup>. The physiological significance of the strong preference of both proteins for the homo-pyrimidine ssDNA is still unknown; however, it may be important the context of the stalled replication fork recognition, and primosome assembly process<sup>11-17,25,27,57,81,99</sup>. The PriA - PriB complex, is one of two major pathways of the restart of the



chromosomal DNA replication in *E. coli* at the damaged DNA site and the key pathway in formation of the primosome at the primosome assembly site<sup>11-17,25,27,57,81,99</sup>. The details the molecular mechanism of recognition, assembly and repair are still unclear<sup>22,27,81,99</sup>. Nevertheless, it invokes the recognition of the specific structure of the ssDNA gap of the damaged DNA at the stalled replication fork, as proposed in Chapter 2. Similarly, in case of the primosome assembly, the specific hairpin structure of the primosome assembly site must be recognized (Chapter 6)<sup>81,99</sup>. The finding of a very strong preference of PriB for homo-thymine ssDNAs and a significant preference of the PriA for the same pyrimidine stretches strongly suggests that the sequence of the nucleic acid around the damaged site, as well as the primosome assembly site, may play an important role in the assembly process and the pathway selection during the restart of the replication fork<sup>81</sup>.

**Table 5.1. Thermodynamic and spectroscopic parameters characterizing the binding of the *E. coli* PriB protein to etheno-derivatives of ssDNA oligomers in buffer C100\*.**

	14-mer	16-mer	18-mer	20-mer	24-mer	26-mer	30-mer	35-mer
	dεA(pεA) <sub>13</sub>	dεA(pεA) <sub>15</sub>	dεA(pεA) <sub>17</sub>	dεA(pεA) <sub>19</sub>	dεA(pεA) <sub>23</sub>	dεA(pεA) <sub>25</sub>	dεA(pεA) <sub>29</sub>	dεA(pεA) <sub>34</sub>
Stoichiometry	1 ± 0.1	1 ± 0.1	1 ± 0.1	1 ± 0.1	2 ± 0.2	2 ± 0.2	2 ± 0.2	2 ± 0.2
Site-size p	12	12	12	12	12	12	12	12
K <sub>N</sub> (M <sup>-1</sup> )	(5.2 ± 0.7) × 10 <sup>5</sup>	(9.0 ± 1.3) × 10 <sup>5</sup>	(1.3 ± 0.2) × 10 <sup>6</sup>	(1.7 ± 0.2) × 10 <sup>6</sup>	-	-	-	-
K <sub>i</sub> (M <sup>-1</sup> )	(1.7 ± 0.2) × 10 <sup>5</sup>	(1.8 ± 0.3) × 10 <sup>5</sup>	(1.9 ± 0.3) × 10 <sup>5</sup>	(1.9 ± 0.3) × 10 <sup>5</sup>	(2.5 ± 0.4) × 10 <sup>5</sup>	(2.8 ± 0.5) × 10 <sup>5</sup>	(2.8 ± 0.5) × 10 <sup>5</sup>	(1.5 ± 0.3) × 10 <sup>5</sup>
ω	-	-	-	-	50 ± 10	45 ± 10	45 ± 10	45 ± 10
ΔF <sub>1</sub>	-	-	-	-	0.90 ± 0.03	0.80 ± 0.03	0.70 ± 0.03	0.9 ± 0.03
ΔF <sub>max</sub>	0.77 ± 0.03	1.04 ± 0.03	1.19 ± 0.03	1.18 ± 0.03	1.32 ± 0.2	1.14 ± 0.03	1.22 ± 0.03	2.0 ± 0.05

\*The errors are standard deviations determined using 3 - 4 independent titration experiments.

**Table 5.2. Macroscopic and intrinsic binding constants,  $K_{20}$  and  $K_{in}$ , and the site-size,  $n$ , characterizing the binding of the PriB protein to different ssDNA homo-oligomers,  $dN(pN)_{19}$ , in buffer C100. The values of  $K_{20}$  for the unmodified 20-mers have been determined using the MCT Method (details in text). \***

	$d\epsilon A(p\epsilon A)_{19}$	$dA(pA)_{19}$	$dT(pT)_{19}$	$dC(pC)_{19}$
$K_{20} (M^{-1})$	$(1.7 \pm 0.4) \times 10^6$	$(3.5 \pm 0.8) \times 10^5$	$(3.0 \pm 0.7) \times 10^8$	$(2.5 \pm 0.4) \times 10^7$
$K_{in} (M^{-1})$	$(1.9 \pm 0.5) \times 10^5$	$(3.9 \pm 0.8) \times 10^4$	$(3.3 \pm 0.7) \times 10^7$	$(2.8 \pm 0.4) \times 10^6$
$n$	12	12	12	12

\*Errors are standard deviations determined using 3-4 independent titration experiments.

## CHAPTER 6

### **BINDING OF TWO PRIA - PRIB COMPLEXES TO THE PRIMOSOMAL ASSEMBLY SITE INITIATES THE PRIMOSOME FORMATION<sup>99</sup>**

#### **6.1 ABSTRACT**

Direct quantitative analysis of the initial steps in the primosome assembly, involving the PriA and PriB proteins and the minimal primosome assembly site (PAS) of phage phiX174, has been performed using fluorescence intensity and anisotropy titration, and fluorescence resonance energy transfer techniques<sup>99</sup>. Two PriA molecules bind to the PAS, at both the strong and the weak binding sites on the DNA, respectively, without detectable cooperative interactions<sup>99</sup>. Binding of the PriB dimer to the PriA - PAS complex dramatically increases the PriA affinity for the strong site, but only slightly affects the affinity for the weak site<sup>99</sup>. Associations to the strong and the weak site are driven by apparent entropy changes with the binding to the strong site accompanied by a large unfavorable enthalpy change<sup>99</sup>. The PriA - PriB complex, formed independently of the DNA, is able to directly recognize the PAS, without the prior binding of PriA to the PAS<sup>99</sup>. Thus, the high affinity state of PriA for PAS is generated through PriA - PriB interactions<sup>99</sup>. The PriB effect is specific for the PriA - PAS binding but not for the PriA - dsDNA, or the PriA - ssDNA interactions<sup>99</sup>. Only complexes containing two PriA

---

<sup>99</sup>This research was originally published in Journal of Molecular Biology. Szymanski, M.R., Jezewska, M.J., Bujalowski, W. Binding of Two PriA-PriB Complexes to the Primosome Assembly Site Initiates the Primosome Formation. *J Mol Biol* **411**(1), 123-42.Reproduced with permission.

molecules can generate profound change of the PAS structure, in the presence of ATP<sup>99</sup>. The obtained results provide a quantitative framework for elucidation of further steps in the primosome assembly and for quantitative analyses of other molecular machines of cellular metabolism<sup>99</sup>.

## 6.2 INTRODUCTION

The primosome is a multiple-protein-DNA complex, a prototype of a molecular machine involved in DNA metabolism, which can mechanically translocate along the DNA, while catalyzing synthesis of oligoribonucleotide primers<sup>5,11,14-18,24,48,54,99,103,121</sup>. It was originally discovered in the analysis of phage phiX174 DNA replication, where it assembles at the specific Primosome Assembly Site (PAS)<sup>5,24,48,99,103</sup>. The primosome formation is an essential step in recombination and repair processes in initiating the restart of the stalled replication fork at the damaged DNA sites but the molecular mechanism governing the assembly process is not well understood (section 1.3 in Chapter 1)<sup>11,14,33,99,122</sup>. As mentioned above the pre-primosome contains six proteins, PriA, PriB, DnaT, PriC, DnaB, and DnaC and is capable of mechanical translocation, due to the presence of two helicases, the PriA and the DnaB<sup>5,15,24-26,99</sup>. Transient association of the primase, the DnaG protein, with the pre-primosome results in the primosome capable of mechanical translocation and synthesis of RNA primers<sup>5,15,24-26,99</sup>.

Several similar and a number of contradictory, models of the primosome assembly has been proposed up to date; none of them comprehensive<sup>5,14-18,24-26,99</sup>. Therefore, the fundamental information about the primosome assembly process is remain elusive<sup>5,14-18,24-26,99</sup>. Currently accepted model of the initial steps of the primosome/pre-primosome formation is that the sequence/structure of the PAS, or the damaged-DNA site, are specifically recognized by the ~ 81.7 kDa monomeric PriA

protein, followed by binding of the PriB protein dimer of ~ 23 kDa to the PriA - DNA complex<sup>5,14-16,99</sup>. In further assembly steps, the DnaT, PriC and the DnaB - DnaC complex are proposed to associate in an orderly fashion with the formed PriA - PriB - DNA scaffold<sup>5,14-16,99</sup>. Nevertheless, in spite of intensive studies of the primosome structure and function over last two decades, many basic aspects of the primosome assembly process and its structure remain unclear<sup>5,15,24,99</sup>. The numbers of the individual protein components in the primosome are still uncertain with different and confusing results coming from different groups (Figure 1.2)<sup>5,15,24-26,99</sup>. For instance, it is not clear how many PriA monomers and PriB protein dimers participate in the initiation of the primosome assembly process<sup>5,15,24-26,99</sup>. Reported numbers range from 1 to ~ 3.5 for PriA and from 1 to ~ 2.4 for the PriB dimer, respectively<sup>5,15,24-26,99</sup>. The intrinsic affinities at different stages of the primosome assembly process are unknown beyond the qualitative or semi-qualitative data<sup>5,15,24-26,99</sup>. Quantitative analysis of possible cooperative interactions between the primosome components and mutual engagements among different primosome components has never been addressed<sup>5,15,24-26,99</sup>.

Although the importance of physiological activities of the primosome are well recognized, the lack of rigorous quantitative analyses of the different steps of the primosome assembly hinders any mechanistic elucidation of this fundamental complex of DNA metabolism<sup>5,15,24-26,99</sup>. In this Chapter, the first quantitative studies of the initial steps of the primosome assembly process on the PAS substrate are described<sup>99</sup>. It will be shown that two PriA molecules bind to the PAS, at both the strong and the weak binding sites, respectively, without cooperative interactions<sup>99</sup>. The PriB protein dramatically increases the PriA affinity for the strong site, but only slightly affects the affinity for the weak site<sup>99</sup>. The PriA - PriB complex, formed independently of the DNA, is able to

directly recognize the PAS<sup>99</sup>. Only complexes containing two PriA molecules can generate profound unwinding of the PAS structure in the presence of ATP<sup>99</sup>.

## **6.3 MATERIALS AND METHODS**

### **6.3.1 Buffers and Chemicals.**

All solutions used in experiments described in this chapter were made with distilled and deionized >18 MΩ (Milli-Q Plus) water. The standard buffer C1005 with 10 mM sodium cacodylate adjusted to pH 7.0 with HCl at 10°C, 1 mM DTT, 100 mM NaCl, 5 mM MgCl<sub>2</sub>, and 25% glycerol w/v<sup>99</sup>. The standard temperature in all the experiments described herein was 10°C. All experiments described herein were carried out in the standard buffer C1005 unless otherwise specified in the text. Fluorescein 5-maleimide and 7-diethylamino-3-(4'-maleimidyl-phenyl)-4-methylcoumarin (CPM) were from Molecular Probes (Eugene, OR) and all chemicals were reagent grade.

### **6.3.2 Water Activity of Buffering Solution.**

Water activity “error term” of the standard buffer C1005, used in this Chapter, had been calculated according to the values in the literature<sup>132,133</sup>. Due to the presence of the glycerol and salt, the water activity “error term” is less than 5%, and is contained within the experimental error of all the experiments presented here<sup>27,132,133</sup>.

### **6.3.3 Nucleotides and Nucleic Acids.**

ATPγS and ADP were from GE Healthcare (Piscataway, NJ). ATPγS and ADP were of high purity as judged by thin layer chromatography (TLC). Unmodified nucleic acid oligomers, etheno-derivatives, and fluorescein-labeled ssDNA oligomers and were

purchased from Midland Certified Reagents (Midland, TX). All nucleic acids were HPLC purified and at least >95% pure as judged by electrophoresis on polyacrylamide gel<sup>99</sup>.

To monitor binding, modified PAS substrate was used<sup>99</sup>. It contains a fluorescent label, fluorescein (Fl), attached through phosphoramidate chemistry<sup>99</sup>. In case of FRET studies the PAS substrate contains fluorescein (Fl) and/or the 7 – diethylaminocoumarin – 3 - carboxylic acid, coumarin derivative (CP) attached through the six-carbon linker<sup>99</sup>. Concentrations of all ssDNA oligomers have been spectrophotometrically determined<sup>27,62,63,81,92,99</sup>. The degree of labeling was determined by absorbance, using the extinction coefficients:  $\epsilon_{494} = 76000 \text{ cm}^{-1}\text{M}^{-1}$  for fluorescein and  $\epsilon_{436} = 44000 \text{ cm}^{-1}\text{M}^{-1}$  for coumarin<sup>27,62,63,99</sup>. All PAS substrates were warmed for 5 minutes at 95°C, and fast cooled on ice<sup>99</sup>.

To monitor binding, in competition experiments, etheno-derivative of the adenosine oligomers were used<sup>27,62,63,81,92,99</sup>. The etheno-derivative, of the ssDNA 20-mer, dεA(pεA)<sub>19</sub> was obtained by modification with chloroacetaldehyde<sup>90-92,99</sup>. The concentration of etheno-derivative of the nucleic acids was determined spectrophotometrically using following the extinction coefficients:  $\epsilon_{257} = 3700 \text{ cm}^{-1}\text{M}^{-1}$  (nucleotide) for εA<sup>56,57,81,87,90-92,99</sup>.

The dsDNA 10 bp substrate was build from components of unmodified and modified ssDNA oligomers<sup>99</sup>. Modified component contained a fluorescent label, fluorescein (Fl), attached to the 5' through phosphoramidate chemistry<sup>92,99</sup>. The sequence of the labeled oligomer was: Fl-CTGACGTGCG. The concentration labeled of the nucleic acids was determined spectrophotometrically<sup>27,62,63,81,92,99</sup>. The concentration of unmodified oligomers were determined spectrophotometrically using the extinction coefficients:  $\epsilon_{260} = 10000 \text{ cm}^{-1}\text{M}^{-1}$  (nucleotide) for A,  $\epsilon_{260} = 8500 \text{ cm}^{-1}\text{M}^{-1}$  (nucleotide) for G,C and T<sup>27,62,99</sup>. The degree of labeling was determined by absorbance, using the



extinction coefficients:  $\epsilon_{494} = 76000 \text{ cm}^{-1}\text{M}^{-1}$  for fluorescein<sup>27,62,63,99</sup>. 5'-Fl labeled dsDNA substrates were obtained by mixing labeled ssDNA oligomers with complementary unmodified oligomers at appropriate concentration<sup>27,62,63,81,92,99</sup>. The mixture was then warmed for 5 minutes at 95°C, and slowly cooled for a period of ~4 – 5<sup>99</sup>. The integrity of the PAS substrates was checked by UV melting and analytical ultracentrifugation techniques (see section 6.4.2)<sup>27,62,63,92,99</sup>.

#### **6.3.4 The UV Melting of the PAS Structure.**

The experiments have been performed in the standard binding buffer C1005 using 1 ml samples on Cary 5000 spectrophotometer (Varian), with the temperature probe inside the sample, equipped with specialized software to record the absorption as a function of the temperature<sup>99</sup>. The temperature increment was 0.1 deg/minute.

#### **6.3.5 The PriA and PriB Protein Purification.**

The PriA helicase and PriB protein purification was carried out as described in section 2.3.4, Chapter 2 and section 5.3.4, Chapter 5. Protein concentrations were spectrophotometrically determined with the extinction coefficient obtained using an approach based on the Edelhoch's method as described in section 2.3.5 and section 5.3.5 for PriA and PriB respectively<sup>27,56-61,64,65,81,92,99</sup>.

#### **6.3.6 Labeling of the PriA and PriB Protein with Fluorescent Markers.**

Labeling of the cysteine residues of the PriA helicase with coumarin derivative, 7-diethylamino-3-(4'-maleimidyl-phenyl)-4-methylcoumarin (CPM) and the PriB protein with fluorescein 5-maleimide was performed in H buffer [50 mM Hepes-HCl (pH 8.1), 100 mM NaCl, 5 mM MgCl<sub>2</sub>, 0.1 mM DTT and 10% glycerol w/v] at 4 °C<sup>8,99,123</sup>. The fluorescent label was added from the stock solution to a dye/protein molar ratio of ~ 25.

The mixture was incubated in dark for 4 h, with gentle mixing. After incubation, the PriA protein was precipitated with ammonium sulfate and dialyzed overnight against buffer D100 (50 mM Tris-HCl pH 8.1, 1 mM DTT, 100 mM NaCl, 25% glycerol w/v) in case of and buffer B1 (50 mM Tris-HCl pH 7.1, 1 mM DTT, 100 mM NaCl, 20% glycerol w/v) in case of PriB (section 5.3.4)<sup>81,99</sup>. Unbound dye was removed from the modified protein by applying the sample to a DEAE Sephacryl Column (GE Healthcare, Piscataway, NJ)<sup>81,99</sup>. The degree of labeling,  $q$ , was determined by the absorbance of a fluorescent marker using an extinction coefficient of  $\epsilon_{394} = 2.7 \times 10^4 \text{ M}^{-1}\text{cm}^{-1}$  for CPM – PriA and  $\epsilon_{494} = 7.8 \times 10^4 \text{ M}^{-1}\text{cm}^{-1}$  for Fl-PriB<sup>8,99,123</sup>.

### 6.3.7 Fluorescence Measurements.

All steady-state fluorescence titrations were performed using the ISS PC-1 spectrofluorometer (Urbana, IL) as previously described<sup>27,56-63,81,92,99</sup>. The temperature of the cuvette holder was regulated by circulating water at  $10.0 \pm 0.1$  °C. In competition experiments the binding was followed by monitoring the etheno-derivative fluorescence of the nucleic acids ( $\lambda_{\text{ex}} = 325 \text{ nm}$ ,  $\lambda_{\text{em}} = 410 \text{ nm}$ )<sup>99</sup>. The PriA protein binding to PAS was followed by monitoring the emission of the fluorescein-labeled nucleic acid ( $\lambda_{\text{ex}} = 480 \text{ nm}$ ,  $\lambda_{\text{em}} = 520 \text{ nm}$ )<sup>99</sup>. In order to avoid possible artifacts, due to the fluorescence anisotropy of the sample, polarizers were placed in excitation and emission channels and set at 90° and 55° (magic angle), respectively<sup>27,56-63,81,92,99</sup>. The relative fluorescence increase,  $\Delta F_{\text{obs}}$ , of the DNA emission upon protein binding is defined as,  $\Delta F_{\text{obs}} = (F_i - F_o)/F_o$ , where  $F_i$  is the fluorescence of the sample at a given titration point “i” and  $F_o$  is the initial fluorescence of the same solution<sup>1,27,56-63,81,92,99</sup>.

### 6.3.8 Quantitative Determination of Binding Isotherms and Stoichiometries of the PriA - PAS Complexes.

In this Chapter, we followed the binding of the PriA helicase to the PAS structure DNA by monitoring the fluorescence increase,  $\Delta F$ , of the FI-labeled PAS<sup>99</sup>. In case of the competition experiments etheno-derivative fluorescence of the nucleic acid was monitored<sup>92,99</sup>. In case of PriA – PriB interactions fluorescence anisotropy of FI-PriB was used to monitor the complex formation. To obtain quantitative estimates of the total average degree of binding,  $\Sigma\Theta_i$  (average number of bound PriA molecules per DNA oligomer) and the free protein concentration,  $P_F$ , independent of any assumption about the relationship between the observed spectroscopic signal and  $\Sigma\Theta_i$ , we applied an approach previously described in section 2.3.7<sup>1,56,57,82,87,92,99</sup>. Computer fits were performed using Mathematica (Wolfram, IL) and KaleidaGraph (Synergy Software, PA)<sup>92,99</sup>.

### 6.3.9 Fluorescence Resonance Energy Transfer (FRET) Measurements.

The apparent fluorescence energy transfer efficiency,  $E_D$ , obtained from the quenching of the donor fluorescence is defined as<sup>8,63,99,123-125</sup>

$$E_D = \left( \frac{1}{v_D} \right) \left( \frac{F_D - F_{DA}}{F_D} \right) \quad (6.1)$$

where  $F_D$  and  $F_{DA}$  are the fluorescence of the donor in the absence and presence of the acceptor, respectively,  $v_D$  is the fraction of the donor in the complex with the acceptor<sup>8,63,99,123-125</sup>.

The apparent fluorescence transfer efficiency,  $E_A$ , has been determined, using the sensitized acceptor fluorescence, by measuring the fluorescence intensity of the acceptor excited at a wavelength where the donor predominantly absorbs, in the absence and presence of the donor. The fluorescence intensities of the acceptor in the absence,  $F_A$ , and presence,  $F_{AD}$ , of the donor are defined as<sup>8,63,99,123-125</sup>

$$F_A = I_0 \varepsilon_A C_{AT} \phi_F^A \quad (6.2a)$$

and

$$F_{AD} = (1 - v_A)F_A + I_0 \varepsilon_A v_A C_{AT} \phi_B^A + I_0 \varepsilon_D C_{DT} v_D \phi_B^A E_A \quad (6.2b)$$

where  $I_0$  is the intensity of incident light,  $C_{AT}$  and  $C_{DT}$  are the total concentrations of the acceptor and the donor,  $v_A$  is the fraction of acceptors in the complex with donors,  $\varepsilon_A$  and  $\varepsilon_D$  are the molar absorption coefficients of the acceptor and the donor at the excitation wavelength, respectively,  $\phi_F^A$  and  $\phi_B^A$  are the quantum yields of the free and bound acceptor<sup>8,63,99,123-125</sup>. All quantities in equations 6.2a and 6.2b can be experimentally determined. Dividing equation 6.2a by equation 6.2b and rearranging provides  $E_A$ , as<sup>8,63,99,123-125</sup>

$$E_A = \left[ \frac{1}{v_D} \left( \frac{\varepsilon_A C_{AT}}{\varepsilon_D C_{DT}} \right) \right] \left\{ \left( \frac{\phi_F^A}{\phi_B^A} \right) \left[ \left( \frac{F_{AD}}{F_A} \right) + v_A - 1 \right] - v_A \right\} \quad (6.3)$$

The Förster energy transfer efficiency,  $E$ , is related to  $E_D$  and  $E_A$ , by<sup>8,63,99,123-125</sup>

$$E = \frac{E_A}{(1 - E_D + E_A)} \quad (6.4)$$

The Förster FRET efficiency between the donor and the acceptor dipoles,  $E$ , is related to the average distance,  $R$ , separating the acceptor and donor dipoles by<sup>8,63,99,123-125</sup>

$$R = R_0 \left[ \frac{(1-E)}{E} \right]^{\frac{1}{6}} \quad (6.5)$$

where,  $R_0 = 9790(\kappa^2 n^{-4} \phi_d J)^{1/6}$  is the so called Förster critical distance (in angstroms), the distance at which the transfer efficiency is 50%,  $\kappa^2$  is the orientation factor,  $\phi_d$  is the donor quantum yield in the absence of the acceptor, and  $n$  is the refractive index of the medium ( $n = 1.4$ ), the overlap integral,  $J$ , characterizes the resonance between the donor and acceptor dipoles<sup>8,63,99,123-125</sup>. The Förster critical distances,  $R_0 = 52 \text{ Å}$  and  $R_0 = 54 \text{ Å}$ , for fluorescein and coumarin derivatives (Fl and CPM, respectively) have been previously determined by the Bujalowski's group<sup>8,63,99,123-125</sup>.

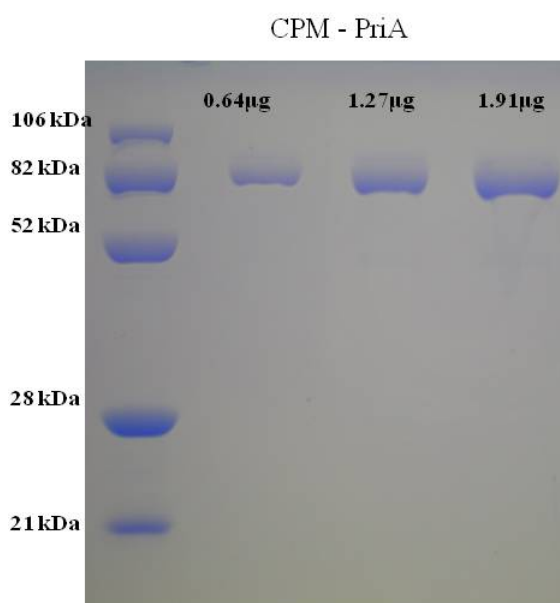
## 6.4 RESULTS

### 6.4.1 The Modified PriA and PriB protein.

The modified enzymes were  $> 99\%$  pure as judged by polyacrylamide electrophoresis with Coomassie Brilliant Blue staining (Figure 6.1)<sup>99</sup>. Both enzymes behaved similarly, within experimental error, to unlabeled enzymes as shown by analytical ultracentrifugation and binding studies<sup>99</sup>.

The degree of labeling  $q$  of the PriA protein with CPM has been determined by the absorbance of the fluorescent probe and mass spectrometry analysis and was  $0.36 \pm$

**a.**



**b.**

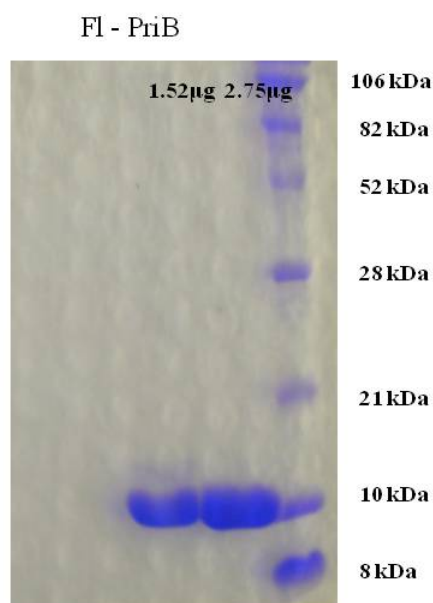


**Figure 6.1** Modified enzymes were > 99% pure as judged by polyacrylamide electrophoresis with Coomassie Brilliant Blue staining. **a.** 10% SDS polyacrylamide gel of the serial dilution after the final step of modification of the PriA protein with Coumarin (CPM)<sup>99</sup>. **b.** 15% SDS polyacrylamide gel of the serial dilution after the final step of modification of the PriB protein with Fluorescein (Fl)<sup>99</sup>.

0.1 (section 6.3.6)<sup>7,63,99,123</sup>. The PriA protein has 11 cysteine residues, 8 of which are proposed to be involved in the zinc finger structure, therefore, three “free” cystines are available for modification<sup>49,50,99</sup>. Since, the degree of labeling is  $q = 0.36 \pm 0.1$ , CPM labeled PriA protein population must be dominated by the species with a single modified cysteine residue<sup>99</sup>.

The degree of labeling  $q$  of the PriB protein with fluorescein maleimide has been determined using the absorbance of the fluorescent probe and mass spectrometry analysis<sup>7,63,99,123</sup>. The PriB protein dimer has 8 cysteine residues, 4 of which are involved in disulfide bond formation leaving 4 free cysteine residues available for modification with the fluorescent marker<sup>81,99,106-108</sup>. While the degree of labeling is  $q = 1.5 \pm 0.1$ , indicating that on average only  $\sim 1 - 2$  cysteine residues of the PriB dimer efficiently react with the fluorescein derivative<sup>99</sup>.

#### 6.4.2 The UV Melting of the PAS Substrate.

Based on thermodynamic calculations, selected phiX174 PAS substrate, containing 55 nucleotides, folds to form the structure shown in Figure 6.2a<sup>99,103</sup>. This hairpin structure, contains a small four-nucleotide loop, two dsDNA stretches, with six A-T base pairs, and five predominantly G-C base pairs, followed by two bulges separated by two and three base pairs fragments<sup>99,103</sup>. The UV melting curve of the PAS substrate is included in Figure 6.2a<sup>99</sup>. The concentration of the nucleic acid is  $2.37 \times 10^{-7}$  M (PAS). There are two transition regions in the plot strongly differing in their melting stabilities and induced hyperchromism<sup>99</sup>. The plot has been analyzed using the two-step, conformational-transition model as defined by



The observed absorbance of the sample as a function of the temperature is defined by

$$A_{\text{obs}} = [A_{D1} + C_{D1}(T - T_R)] \left( \frac{1}{Z_N} \right) + [A_{D2} + C_{D2}(T - T_R)] \left( \frac{\exp\left[\frac{(-\Delta H_1 + T\Delta S_1)}{RT}\right]}{Z_N} \right) + [A_{D3} + C_{D3}(T - T_R)] \left( \frac{\exp\left[\frac{(-\Delta H_1 + T\Delta S_1)}{RT}\right] \exp\left[\frac{(-\Delta H_2 + T\Delta S_2)}{RT}\right]}{Z_N} \right) \quad (6.7)$$

where,  $T_R$  is the reference temperature (20°C),  $A_{D1}$ ,  $A_{D2}$ , and  $A_{D3}$  are the absorbance of the states,  $D_1$ ,  $D_2$ , and  $D_3$ , at the reference temperature (20°C),  $C_{D1}$ ,  $C_{D2}$ ,  $C_{D3}$  are the optical constants characterizing the dependence of the absorbance of the states  $D_1$ ,  $D_2$ , and  $D_3$  upon the temperature,  $\Delta H_1$ ,  $\Delta H_2$ ,  $\Delta S_1$ , and  $\Delta S_2$  are enthalpies and entropies characterizing transitions,  $D_1 \leftrightarrow D_2$ , and  $D_2 \leftrightarrow D_3$ , respectively<sup>99</sup>. The partition function,  $Z_N$ , of the system is defined as

$$Z_N = 1 + \exp\left[\frac{(-\Delta H_1 + T\Delta S_1)}{RT}\right] + \exp\left[\frac{(-\Delta H_1 + T\Delta S_1)}{RT}\right] \exp\left[\frac{(-\Delta H_2 + T\Delta S_2)}{RT}\right] \quad (6.8)$$

Parameters,  $A_{D1}$ ,  $A_{D3}$ ,  $C_{D1}$ , and  $C_{D3}$  can be estimated from the experimental melting curve<sup>99</sup>. The well-defined melting temperature,  $T_m$ , of the final transition provides the relationship,  $T_m = \Delta H_2/\Delta S_2$ <sup>99</sup>. The solid black line is the nonlinear least-squares fit of the experimental curve to equation 6.7 with  $\Delta H_1$ ,  $\Delta S_1$ ,  $\Delta H_2$ ,  $A_{D2}$ , and  $C_{D2}$  as fitting parameters<sup>99</sup>. The obtained values of the enthalpy and entropy of the transitions are:  $\Delta H_1 = 6.5 \pm 0.7$  kcal/mol,  $\Delta S_1 = 190 \pm 5$  cal/mol deg,  $\Delta H_2 = 8.8 \pm 1.1$  kcal/mol, and  $\Delta S_2 = 248 \pm 10$  cal/mol deg<sup>99</sup>. The fit for the model, which includes a single transition,



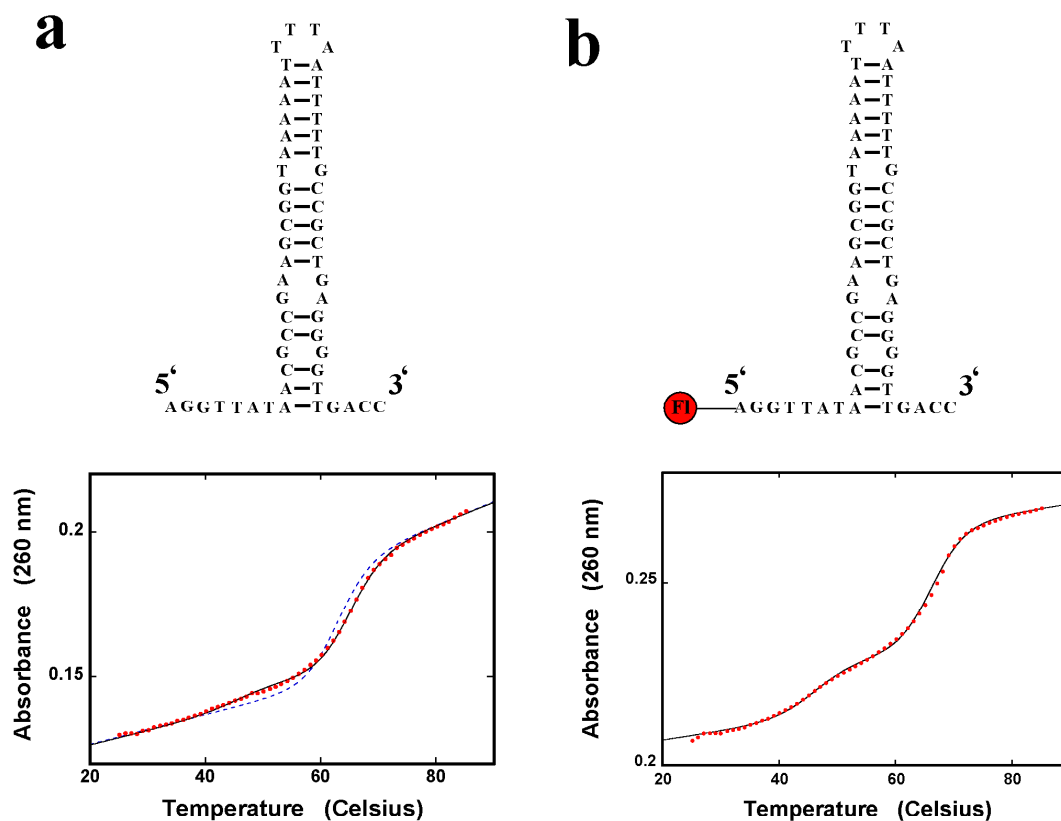


**Figure 6.2 The UV melting studies.** **a.** Proposed structure of phiX174 PAS substrate and a UV melting curve of the same substrate [ $2.37 \times 10^{-7}$  M (PAS)]<sup>99</sup>. The solid black line is the nonlinear least-squares fit of the experimental curve to equation 6.7 with  $\Delta H_1$ ,  $\Delta S_1$ ,  $\Delta H_2$ ,  $A_{D2}$ , and  $C_{D2}$  as fitting parameters<sup>99</sup>. Dashed blue line is a fit for the model, which includes only a single transition,  $D_1 \leftrightarrow D_2$ <sup>99</sup>. **b.** 5'-Fluorescein labeled phiX174 PAS substrate and a UV melting curve of that substrate [ $4.12 \times 10^{-7}$  M (PAS)]<sup>99</sup>. The solid line is the nonlinear least-squares fit of the experimental curve to equation 6.7 with  $\Delta H_1$ ,  $\Delta S_1$ ,  $\Delta H_2$ ,  $A_{D2}$ , and  $C_{D2}$  as fitting parameters<sup>99</sup>.

$D_1 \leftrightarrow D_2$ , is also shown in supplementary Figure 6.2 (dashed blue line). It is evident that it does not provide an adequate description of the observed melting curve<sup>99</sup>.

Figure 6.2b shows the phiX174 PAS substrate labeled with the fluorescent marker (fluorescein) at its 5' end (5'-FI-PAS)<sup>99</sup>. The UV melting curve of the 5'-FI-PAS is included in Figure 6.2b and analysis of the melting curve was performed as for unmodified PAS (Figure 6.2a)<sup>99</sup>. The concentration of the nucleic acid is  $4.12 \times 10^{-7}$  M (PAS)<sup>99</sup>. Observed two transition regions in the plot are visibly more pronounced than that shown for the unmodified PAS, in Figure 6.2a, indicating that the presence of the marker affects the hypochromism of the PAS to a greater extent, especially in the low-temperature melting transition<sup>99</sup>. The solid line is the nonlinear least-squares fit of the experimental curve to equation 6.7 with  $\Delta H_1$ ,  $\Delta S_1$ ,  $\Delta H_2$ ,  $A_{D2}$ , and  $C_{D2}$  as fitting parameters<sup>99</sup>. The obtained values of the enthalpy and entropy of the transitions are:  $\Delta H_1 = 6.45 \pm 0.70$  kcal/mol,  $\Delta S_1 = 190 \pm 5$  cal/mol deg,  $\Delta H_2 = 8.8 \pm 1.1$  kcal/mol, and  $\Delta S_2 = 245 \pm 10$  cal/mol deg<sup>99</sup>. These parameters are, within experimental accuracy, identical to the corresponding parameters obtained for the unmodified PAS indicating that, although the marker affects the hypochromism, it does not change the stability of the nucleic acid<sup>99</sup>.

#### **6.4.3 Binding of the PriA Helicase to the Fluorescein Labeled PAS Substrate.**

To address the initiation of the primosome formation, we examined the recognition process of the minimal PAS sequence of 55 nucleotides of the phage phiX174 DNA by the PriA protein, in the absence and presence of the PriB protein<sup>24,99,103</sup>. The nucleic acid contains the fluorescent marker (fluorescein) at the 5' end, which provides an excellent signal to monitor the binding process (Figure 6.2b and Figure 6.3)<sup>99</sup>.

Fluorescence titrations of the PAS, labeled at its 5' end with fluorescein (5'-Fl-PAS), with the PriA protein at three different nucleic acid concentrations, are shown in Figure 6.3a<sup>99</sup>. The dependence of the relative fluorescence quenching,  $\Delta F_{\text{obs}}$ , as a function of the total average degree of binding,  $\Sigma \Theta_i$  of the PriA protein on the PAS, is shown in Figure 6.3b<sup>1,85,87,92,94,99</sup>. The plot is clearly nonlinear and characterized by two binding phases, not immediately obvious in the original titration curves, with a single PriA molecule binding in the high-affinity phase (Figure 6.3b)<sup>1,27,81,99,126,127</sup>. Short extrapolation of the low-affinity phase of the plot to the maximum value of  $\Delta F_{\text{obs}}$  ( $\Delta F_{\text{max}}$ ) gives the maximum stoichiometry of the complex of  $2.1 \pm 0.2$ , showing that two PriA molecules associate with the examined PAS<sup>1,27,81,99,126,127</sup>.

#### **6.4.4 Statistical Thermodynamic Model of the PriA Helicase Binding to the PAS Structure.**

The most probable structure of the PAS is shown in the Figure 6.2a and indicates the presence of the hairpin loop and fragments of the duplex conformation separated by the unpaired ssDNA regions<sup>99,103,122</sup>. The results of PAS structure UV melting in section 6.4.2 are in accord with predicted structure of PAS indicating the presence of at least two dsDNA regions. In the context of structurally irregular PAS structure, it should be pointed out that the PriA helicase has very different stoichiometries and affinities for the ss and dsDNA conformations<sup>1,27,56-59,81,99</sup>. While the site-size of the protein on the ssDNA is  $\sim 20$  nucleotides, the site-size of the PriA - dsDNA complex is only  $\sim 5$  base pairs (Chapter 2 and Chapter 3)<sup>27,56,92,99</sup>. Moreover, the affinity of PriA for the dsDNA is  $\sim 1 - 2$  orders of magnitude higher than the affinity for the ss DNAs<sup>27,56,92,99</sup>.

Therefore, the simplest statistical thermodynamic model, which describes the binding of two PriA molecules to the PAS, containing mixed ss and duplex

conformations, includes two different binding sites characterized by intrinsic binding constants,  $K_1$  and  $K_2$ , respectively, and possible cooperative interactions between the bound protein molecules, described by the cooperativity parameter,  $\omega$ <sup>1,27,85,89,99,115</sup>. The partition function,  $Z_{PAS}$ , for the system is

$$Z_{PAS} = 1 + K_1 P_F + K_2 P_F + K_1 K_2 \omega P_F^2 \quad (6.9)$$

The total average degree of binding,  $\Sigma\Theta_i$ , is then<sup>1,27,85,89,99,115</sup>

$$\Sigma\Theta_i = \frac{K_1 P_F + K_2 P_F + 2K_1 K_2 \omega P_F^2}{Z_{PAS}} \quad (6.10)$$

The observed relative fluorescence quenching,  $\Delta F_{obs}$ , is defined as<sup>1,27,85,89,99,115</sup>

$$\Delta F_{obs} = \Delta F_1 \frac{K_1 P_F + K_2 P_F}{Z_{PAS}} + \Delta F_{max} \frac{K_1 K_2 \omega P_F^2}{Z_{PAS}} \quad (6.11)$$

where  $\Delta F_1$  and  $\Delta F_{max}$  are the relative molar fluorescence increases accompanying the binding of one and two PriA molecules<sup>1,27,85,89,99,115</sup>. In the case where there are no cooperative interactions,  $\omega = 1$ , and equation 6.11 reduces to

$$\Delta F_{obs} = \Delta F_1 \frac{K_1 P_F + K_2 P_F}{Z_{PAS}} + \Delta F_{max} \frac{K_1 K_2 P_F^2}{Z_{PAS}} \quad (6.12)$$

The value of  $\Delta F_1$  can be estimated as  $\Delta F_1 = \partial\Delta F / \partial\Sigma\Theta_i$ , from the initial part of the plot of  $\Delta F$  as a function of  $\Sigma\Theta_i$ , as shown in Figure 6.3b, which provides  $\Delta F_1 = 0.3 \pm 0.03$ <sup>99</sup>. The value of  $\Delta F_{max}$  is the maximum observed relative fluorescence increase and can be

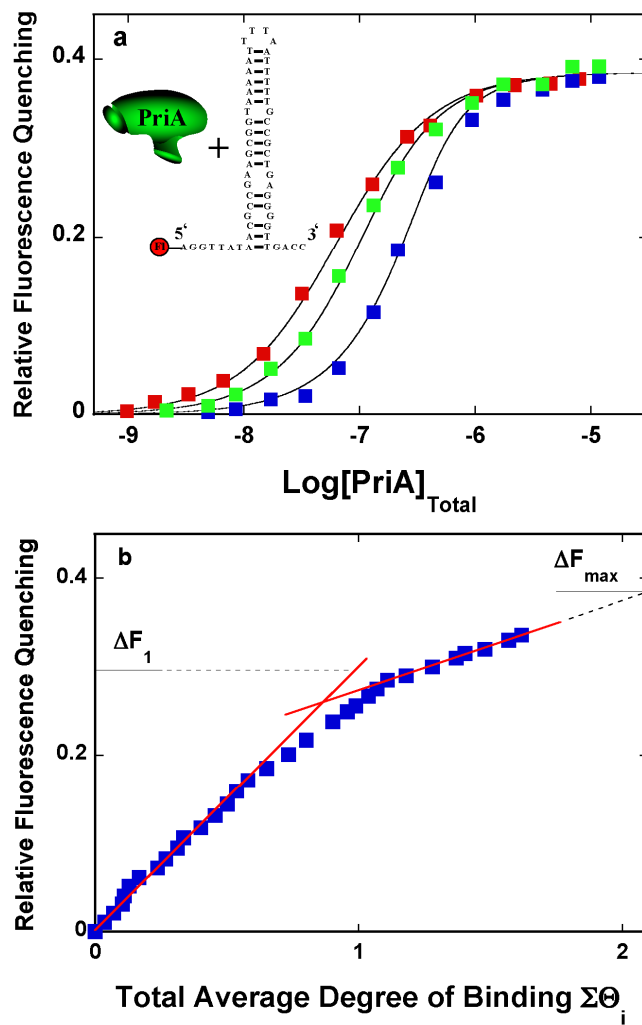


**Figure 6.3 Two molecules of the PriA helicase bind to the fluorescein labeled PAS substrate.** **a.** Fluorescence titrations of 5'-Fl-PAS substrate with PriA at three different concentrations of the nucleic acid:  $1.25 \times 10^{-8} \text{ M}$  (■),  $6.36 \times 10^{-8} \text{ M}$  (■), and  $2.56 \times 10^{-7} \text{ M}$  (■)<sup>99</sup>. The continuous lines represent nonlinear least-squares fits, using the binding model of two discrete binding sites, with the binding constants  $K_1$  and  $K_2$  and with the cooperative interaction parameter  $\omega$  as independent fitting parameters described by equations 6.9 – 6.12<sup>99</sup>. **b.** The dependence of the relative fluorescence quenching  $\Delta F_{\text{obs}}$  on the total average degree of binding  $\Sigma\Theta_i$  of PriA on the PAS<sup>99</sup>. The continuous red lines mark the slopes of the two binding phases and have no theoretical basis<sup>99</sup>. The broken line indicates extrapolation of the maximum value of  $\Delta F_{\text{obs}}$  ( $\Delta F_{\text{max}}$ ) marked by the horizontal line<sup>99</sup>. The value of  $\Delta F_{\text{obs}}$ , induced by the binding of the first PriA molecule  $\Delta F_1$ , is included in the panel<sup>99</sup>.

estimated from the parental fluorescence titration curves, as shown in Figures 6.3a ( $\Delta F_{\max} = 0.39 \pm 0.03$ )<sup>1,27,85,89,99,115</sup>. Thus, three independent parameters,  $K_1$ ,  $K_2$ , and  $\omega$  must be determined<sup>1,27,85,89,99,115</sup>. The solid lines in Figures 6.3a are nonlinear least-squares fits of the titration curves using equations 6.9 – 6.12, which provide  $K_1 = (2.0 \pm 0.7) \times 10^7 \text{ M}^{-1}$ ,  $K_2 = (4.5 \pm 0.8) \times 10^6 \text{ M}^{-1}$ , and the cooperativity parameter,  $\omega = 1 \pm 0.2$ <sup>99</sup>. As a result, in the examined solution conditions, the affinity of the PriA protein for the strong site is by a factor of  $\sim 4.5$  higher than the protein affinity for the weak site<sup>99</sup>. Furthermore, there is no detectable cooperativity between the bound PriA molecules; hence, the value of  $\omega$  is 1<sup>95,99,127</sup>.

#### **6.4.5 Fluorescence Resonance Energy Transfer (FRET) Results Yield the Location of the Strong PriA Binding Site On the PAS Structure.**

To determine where the strong PriA-binding site on the PAS substrate is located, *i.e.*, the position where the first PriA molecule binds to PAS structure, the fluorescence resonance energy transfer method was applied<sup>7,63,99,123-125</sup>. In this approach, the fluorescence donor (coumarin derivative, CPM) has been placed on the PriA protein (CPM-PriA) (section 6.4.1)<sup>99</sup>. The fluorescein moiety located at the 5' end of the PAS structure serves as the fluorescence acceptor (Figure 6.2b and Figure 6.4a)<sup>99</sup>.

Figure 6.4a shows the emission spectrum ( $\lambda_{\text{ex}} = 390 \text{ nm}$ ) of the CPM-PriA (green) in the presence of the unmodified PAS structure, the spectrum of the 5'-Fl-PAS (orange) in the presence of the unmodified PriA, the spectrum of the CPM-PriA - 5'-Fl-PAS complex (red), and the spectrum of the CPM-PriA normalized to the maximum of the CPM emission in the CPM-PriA - 5'-Fl-PAS complex (magenta)<sup>99</sup>. The sensitized emission spectrum of the 5'-Fl-PAS has been obtained by subtracting the normalized spectrum of the CPM-PriA from the spectrum of the CPM-PriA - 5'-Fl-PAS complex

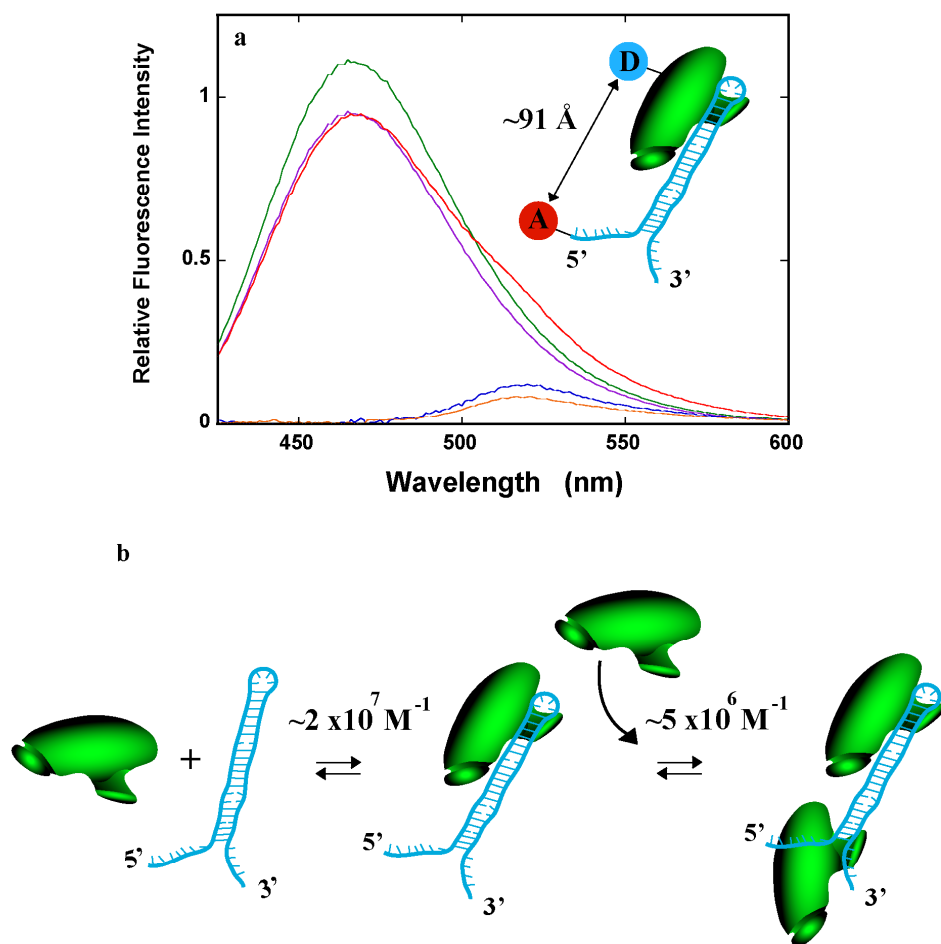


**Figure 6.4 The location of the strong PriA binding site on the PAS structure. a.** The emission spectrum ( $\lambda_{\text{ex}} = 390 \text{ nm}$ ) of CPM-PriA (green) in the presence of the unmodified PAS, the spectrum of 5'-Fl-PAS (orange) in the presence of unmodified PriA, the spectrum of the CPM-PriA – 5'-Fl-PAS complex (red), the spectrum of the CPM-PriA normalized to the maximum of the CPM emission in the CPM-PriA -5'-Fl-PAS complex (magenta), and the sensitized emission spectrum of 5'-Fl-PAS (blue)<sup>99</sup>. The concentrations of the PriA protein and the PAS are  $6.6 \times 10^{-8} \text{ M}$  and  $1.27 \times 10^{-8} \text{ M}$  (oligomer), respectively<sup>99</sup>. The figure shows the schematic representation of the average distance between the fluorescence donor (CPM), located on the PriA protein, and the fluorescence acceptor (Fl), located at the 5' end of the PAS<sup>99</sup>. **b.** Complete binding of the PriA protein to the examined PAS substrate, with intrinsic affinities and locations of both the strong and the weak binding sites included in the figure<sup>99</sup>.

(blue)<sup>99</sup>. At these selected concentrations of the protein and the DNA, only the strong binding site is saturated with the PriA protein<sup>99</sup>. The intensities of the donor and the acceptor have been obtained by integrating the corresponding areas under the spectra (Figure 6.4a)<sup>99</sup>. The obtained values of the apparent fluorescence energy transfer efficiencies are:  $E_D = 0.26 \pm 0.03$ ,  $E_A = 0.025 \pm 0.005$ , and the Förster FRET efficiency,  $E = 0.033 \pm 0.005$  (section 6.3.9)<sup>7,99,123</sup>. Because limiting anisotropies of all labeled components of the examined system are below  $\sim 0.23$  (data not shown), the orientation factor,  $\kappa^2$ , does not affect the discussed FRET measurements<sup>7,99,123</sup>. The value of  $E$  indicates that the average distance between CPM-PriA and the fluorescein moiety at the 5' end of the PAS is  $R = 91 \pm 5 \text{ \AA}$ <sup>7,99,123</sup>. It should be noted that although the exact location of the coumarin donor on the PriA protein is unknown, rather large distance of  $\sim 91 \text{ \AA}$  excludes the possibility that PriA is bound in the vicinity of the 5' end of the PAS<sup>99</sup>. Therefore, the strong binding site for PriA on PAS must be located near the hairpin loop of the PAS structure (Figure 6.2b and Figure 6.4a)<sup>99</sup>. Moreover, because of the lack of any cooperative interactions between bound PriA molecules, one could argue that the weak site should be located at a significant distance from the strong site, most probably near the 3' end of the examined PAS molecule (Figure 6.4b)<sup>99</sup>.

#### **6.4.6 Fluorescent Marker on the PAS Structure Does Not Affect the PriA – 5'-FI-PAS Interactions. Lattice Competition Titrations.**

Quantitative analysis of the PriA helicase binding to the unmodified PAS has been performed using the Macromolecular Competition Titration method (MCT) described in details in section 4.4.7 of Chapter 4<sup>1,81,87,92,99,126</sup>. As a reference fluorescent nucleic acid, the etheno derivative of the ssDNA 20-mer,  $d\epsilon A(p\epsilon A)_{19}$ , whose interactions with the PriA helicase have been extensively studied by the Bujalowski's group, was



used<sup>1,27,56-61,87,92,99,126</sup>. For the unmodified PAS, the partition function,  $Z_{PAS}$ , is described by equation 6.9 in section 6.4.4<sup>99</sup>. The partition function for the reference ssDNA 20-mer is

$$Z_{20} = 1 + K_R P_F \quad (6.13)$$

where  $K_R$  is the macroscopic binding constant of the PriA protein - dεA(pεA)<sub>19</sub> complex<sup>1,27,56-61,87,92,99,126</sup>. The concentration of the PriA protein, bound to the reference nucleic acid and the unmodified PAS,  $P_b$ , at their total concentrations,  $M_{TR}$  and  $M_{TS}$ , respectively, is then

$$P_b = (\Sigma \Theta_i)_R M_{TR} + (\Sigma \Theta_i)_S M_{TS} \quad (6.14)$$

and

$$P_b = \left[ \frac{K_R P_F}{Z_{20}} \right] M_{TR} + \left[ \frac{K_1 P_F + K_2 P_F + 2K_1 K_2 \omega P_F^2}{Z_{PAS}} \right] M_{TS} \quad (6.15)$$

where  $(\Sigma \Theta_i)_R$  and  $(\Sigma \Theta_i)_S$  are the total average degree of binding of the protein on the reference 20-mer and the examined unmodified PAS, respectively<sup>1,81,92,99,126</sup>. The observed relative fluorescence increase of the reference nucleic acid,  $\Delta F_{obs}$ , is then

$$\Delta F_{obs} = \Delta F_{max} \left[ \frac{K_R P_F}{1 + K_R P_F} \right] \quad (6.16)$$

where

$$P_F = P_T - P_b \quad (6.17)$$

and  $P_T$  is the total concentration of the PriA protein. Both,  $K_R = (1.6 \pm 0.3) \times 10^6 \text{ M}^{-1}$  and  $\Delta F_{\max} = 1.5 \pm 0.05$ , are known from the independent fluorescence titrations of  $d\epsilon A(p\epsilon A)_{19}$ , in the absence of the unmodified PAS<sup>27,56,81,92,99</sup>.

Fluorescence titrations of  $d\epsilon A(p\epsilon A)_{19}$  with the PriA protein, in buffer C505 in the absence and presence of three different concentrations of the unmodified PAS, are shown in Figure 6.5a. The lower salt concentration was applied to obtain a complete titration curve for the ssDNA 20-mer in the protein concentration range, which avoids the precipitation of the sample<sup>56,81,92,99</sup>. A significant shift of the binding isotherm, in the presence of the PAS, indicates efficient competition of the PAS with  $d\epsilon A(p\epsilon A)_{19}$  for the PriA protein<sup>56,81,92,99</sup>. The solid lines in Figure 6.5a are nonlinear least-squares fits of the experimental titrations with  $K_1$ ,  $K_2$ , and  $\omega$ , as independent fitting parameters, using equations 6.14 – 6.17<sup>56,81,92,99</sup>. The obtained binding parameters  $K_1 = (2.5 \pm 0.7) \times 10^7 \text{ M}^{-1}$ ,  $K_2 = (4.5 \pm 0.8) \times 10^6 \text{ M}^{-1}$ , and  $\omega = 1 \pm 0.2$ <sup>56,92,99</sup>. Obtained parameters are very similar to the parameters describing the PriA binding to the fluorescein-labeled PAS, in the same solution conditions (data not shown)<sup>99</sup>. In other words, the presence of the fluorescein marker does not affect the PriA protein interactions with the Fl-labeled PAS<sup>99</sup>.

#### **6.4.7 Binding of the PriA Helicase to PAS in the Presence of ADP and ATP $\gamma$ S.**

As mentioned above, in section 2.2.3, the PriA protein has two nucleotide-binding sites, which dramatically increase the protein affinity for the ssDNA and, to a lesser

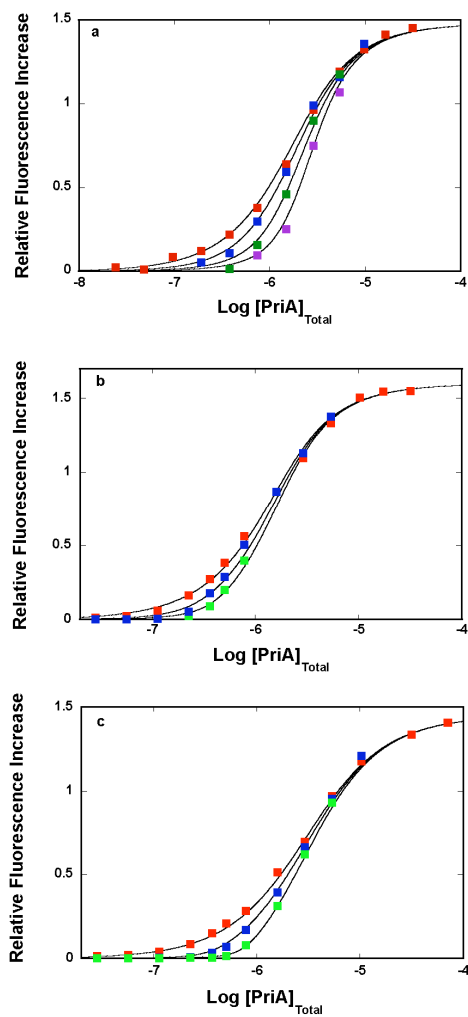


**Figure 6.5 Binding of PriA to unmodified PAS substrate.** **a.** Fluorescence titrations of  $d\epsilon A(p\epsilon A)_{19}$  [ $1.34 \times 10^{-6}$  M (oligomer)] with the PriA protein in the absence (■) and in the presence of three different concentrations of the unmodified PAS:  $1.48 \times 10^{-7}$  M (■),  $3.69 \times 10^{-7}$  M (■), and  $6.65 \times 10^{-7}$  M (■) (PAS)<sup>99</sup>. **b.** Fluorescence titrations of  $d\epsilon A(p\epsilon A)_{19}$  [ $1.34 \times 10^{-6}$  M (oligomer)] with the PriA protein, containing 1 mM ADP, in the absence (■) and in the presence of two different concentrations of the unmodified PAS:  $7.39 \times 10^{-8}$  M (■) and  $1.85 \times 10^{-7}$  M (■) (PAS)<sup>99</sup>. **c.** Analogous fluorescence titrations of  $d\epsilon A(p\epsilon A)_{19}$  [ $1.34 \times 10^{-6}$  M (oligomer)] with the PriA protein, in the absence (■) and in the presence of two different concentrations of the unmodified PAS:  $1.85 \times 10^{-7}$  M (■) and  $3.33 \times 10^{-7}$  M (■) (PAS)<sup>99</sup>. The continuous lines in all three panels represent nonlinear least-squares fits of the experimental titrations, with  $K_1$ ,  $K_2$ , and  $\omega$  as independent fitting parameters, using equations 6.13 – 6.17<sup>99</sup>.

extent, the affinity for the dsDNA (Figure 2.3)<sup>27,59-61,92,99</sup>. This specific nucleotide effect is particularly pronounced when the weak nucleotide-binding site is saturated with ADP<sup>27,59-61,92,99</sup>. Here, the Macromolecular Competition Titration method (MCT) has been used to examine the PriA protein binding to the unmodified PAS in the presence of the nucleotide cofactors<sup>27,59-61,92,99</sup>. As discussed above, in these studies we use, as a reference fluorescent nucleic acid, the etheno-derivative of the ssDNA 20-mer, dεA(peA)<sub>19</sub><sup>27,59-61,92,99</sup>. In examined solution conditions, the values of  $K_R = (4.3 \pm 0.5) \times 10^5 \text{ M}^{-1}$  and  $\Delta F_{\text{max}} = 1.45 \pm 0.05$ , for the solution containing ATPγS and  $K_R = (1.6 \pm 0.3) \times 10^6 \text{ M}^{-1}$  and  $\Delta F_{\text{max}} = 1.6 \pm 0.05$ , in the presence of ADP have been obtained in independent titration experiments<sup>81,99</sup>.

Fluorescence titrations of dεA(peA)<sub>19</sub> with the PriA protein, in buffer C505 and 1 mM ADP, and in the absence and presence of two different concentrations of the unmodified PAS, are shown in Figure 6.5b<sup>99</sup>. Due to the precipitation of the system at higher PriA concentrations, only part of the titration curve at the higher PAS concentration is included<sup>99</sup>. The solid lines in Figure 6.5b are nonlinear least-squares fits of the experimental titrations with  $K_1$ ,  $K_2$ , and  $\omega$ , as independent fitting parameters, using equations 6.14 – 6.17<sup>99</sup>. The obtained binding parameters are:  $K_1 = (6 \pm 1.1) \times 10^7 \text{ M}^{-1}$ ,  $K_2 = (6.0 \pm 1.1) \times 10^7 \text{ M}^{-1}$ , and  $\omega = 1 \pm 0.2$ <sup>99</sup>. Analogous fluorescence titrations of dεA(peA)<sub>19</sub> with the PriA protein, in buffer C505 and 1 mM ATPγS, in the absence and presence of two different concentrations of the unmodified PAS, are shown in Figure 6.5c<sup>99</sup>. The obtained binding parameters:  $K_1 = (6 \pm 1.1) \times 10^7 \text{ M}^{-1}$ ,  $K_2 = (6.0 \pm 1.1) \times 10^7 \text{ M}^{-1}$ , and  $\omega = 1 \pm 0.2$ , are virtually the same as obtained for the solution containing ADP (Figure 6.5b)<sup>99</sup>. The data indicate that the presence of the nucleotide cofactors has only a moderate effect on the PriA affinity for the strong site on the PAS, while the affinity for the weak site increases by ~ 1 order of magnitude<sup>99</sup>. It should be mentioned that the

affinities determined for both binding sites on PAS structure are very similar to the PriA affinity for the dsDNA in the same solution conditions<sup>27,92,99</sup>.

#### 6.4.8 The PriA Helicase Interacts with PriB Independent of PAS.

It has been reported that the PriA helicase and PriB can interact with one another only in the presence of the nucleic acid and the hand-off mechanism of PriA-PriB-DNA interactions was proposed<sup>16,99</sup>. Although this possibility is conceptually sound the experiments performed to arrive to this conclusion were somewhat inconsistent<sup>16,99</sup>. Therefore, the ability of PriA-PriB complex formation in solution was examined in the absence of the PAS<sup>99</sup>. The association of the PriB protein with PriA has been addressed using the fluorescence anisotropy titration using the fluorescein-labeled PriB protein (Fl-PriB) and the complex formation has been monitored by the increase of the anisotropy of the Fl-PriB protein<sup>99</sup>. The signal from the Fl-PriB protein was used because PriB is much smaller than PriA and one can expect a significantly larger change of its fluorescence anisotropy, as a result of the complex formation, than in the case of the labeled PriA<sup>99</sup>.

Fluorescence anisotropy titration ( $\lambda_{\text{ex}} = 480 \text{ nm}$ ,  $\lambda_{\text{em}} = 520 \text{ nm}$ ) of the Fl-PriB with the PriA protein, in buffer C1005 is shown in Figure 6.6<sup>99</sup>. The system has a tendency to precipitate at higher concentrations of both proteins, which preclude titrations at a higher concentration of Fl-PriB. The solid lines in Figure 6.6 are the nonlinear least-squares fit of the experimental titration curve to a single-site isotherm

$$\Delta A = \Delta A_{\text{PriB}} + \Delta A_{\text{max}} \left[ \frac{K_{\text{PP}} [\text{PriA}]_{\text{Free}}}{1 + K_{\text{PP}} [\text{PriA}]_{\text{Free}}} \right] \quad (6.18)$$

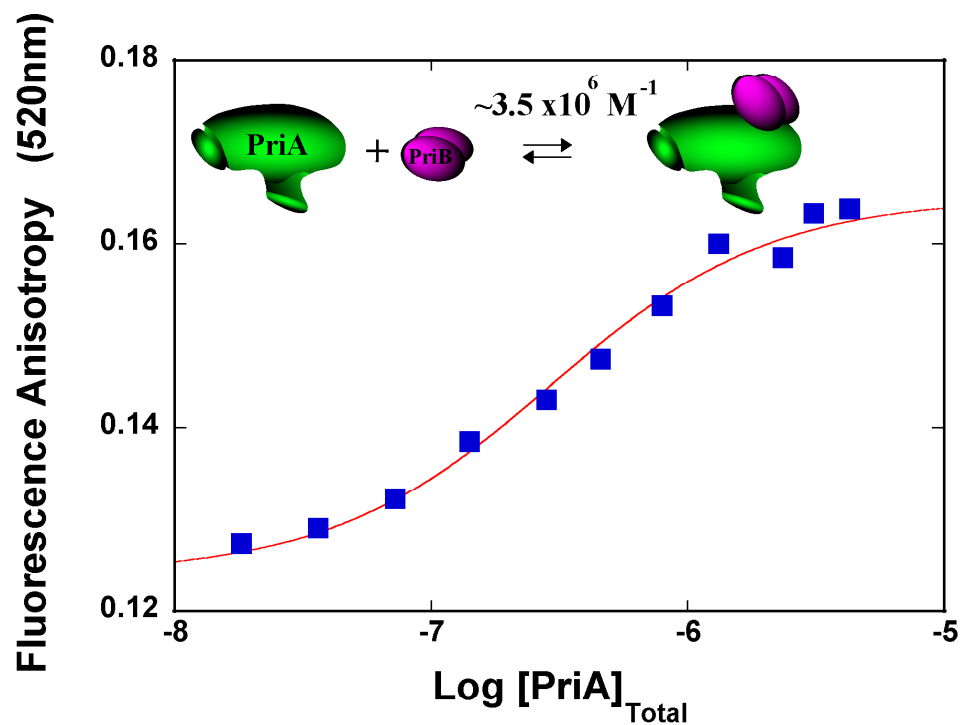


**Figure 6.6 The PriA helicase interacts with PriB in solution independent of PAS.** Fluorescence anisotropy titration of Fl-PriB [ $1.16 \times 10^{-8} \text{ M}$  (dimer)] with the PriA protein<sup>99</sup>. The continuous line represents the nonlinear least-squares fit of the experimental titration curve, with  $K_{pp}$  and  $\Delta A_{\max}$  as independent fitting parameters, using equation 6.18<sup>99</sup>.

where  $\Delta A_{\text{PriB}}$ ,  $\Delta A_{\text{max}}$ , and  $K_{\text{PP}}$  are the initial anisotropy of the free PriB protein, the maximum increase of the observed anisotropy, and the association constant of the PriA - PriB complex<sup>99</sup>. The value of  $\Delta A_{\text{PriB}}$  for the free PriB protein is obtained experimentally in the absence of PriA and is  $0.124 \pm 0.001$ <sup>99</sup>. The fit provides an excellent description of the experimental titration curve, indicating that a single PriB molecule associates with the PriA protein<sup>99</sup>. The obtained values of the binding constant,  $K_{\text{PP}}$  and the maximum increase of the fluorescence anisotropy of the PriB protein,  $\Delta A_{\text{max}}$ , in the examined solution conditions, are:  $(3.5 \pm 0.8) \times 10^6 \text{ M}^{-1}$  and  $0.041 \pm 0.001$ , respectively<sup>99</sup>.

#### **6.4.9 The PriB Protein Binding to PAS is Negligible.**

Although the PriB protein has a significant affinity for the ssDNA, its affinity for the dsDNA, which constitutes the major part of the PAS structure, is very low<sup>81,99</sup>. Nevertheless, to address the possibility that, in examined solution conditions, the PriB protein may associate with the PAS sequence/structure *prior* to the binding of the PriA protein, binding of PriB to the PAS was examined using the fluorescence titration method<sup>99</sup>. The process of PriB-PAS complex formation has been monitored by the fluorescence intensity of the 5'-FI-PAS, analogously to studies with the PriA protein described in section 6.4.3 and 6.4.4<sup>99</sup>. Fluorescence titration ( $\lambda_{\text{ex}} = 480 \text{ nm}$ ,  $\lambda_{\text{em}} = 520 \text{ nm}$ ) of  $5 \times 10^{-7} \text{ M}$  5'-FI-PAS with the PriB protein, in buffer C1005 is shown in Figure 6.7<sup>99</sup>. The inspection of the titration curve shows that the association becomes detectable only when PriB concentration exceeds  $\sim 3 \times 10^{-7} \text{ M}$  (dimer)<sup>99</sup>. In addition, it looks like the association process is cooperative, as shown by the span of less than 2 orders of magnitude between 10% and 90% of the titration curve<sup>99</sup>. The simplest partition function that could describe examined behavior of the system is

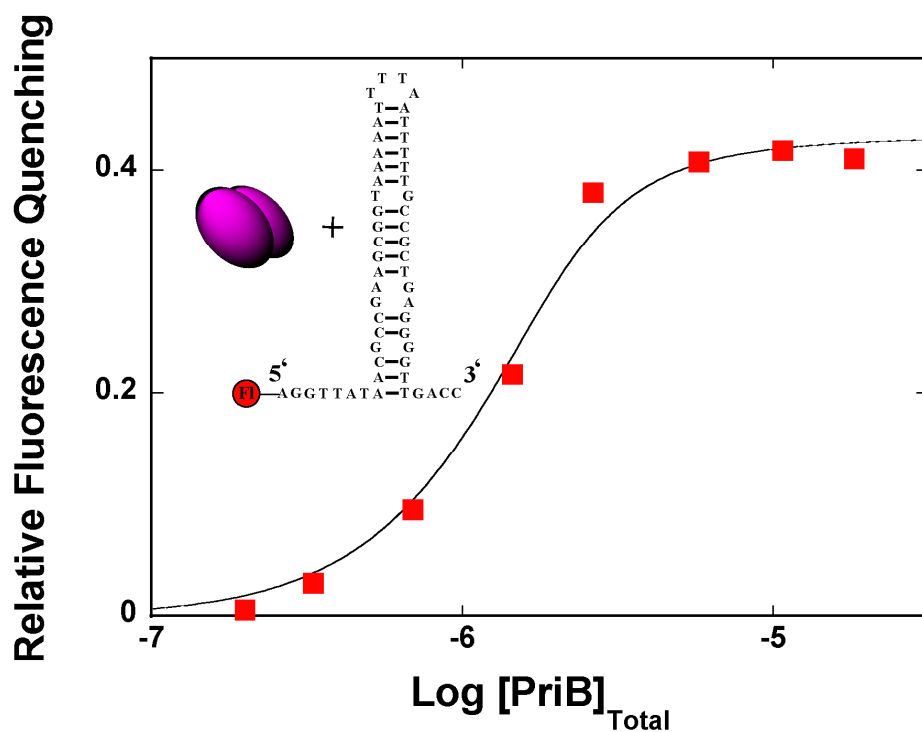


**Figure 6.7 The PriB protein binds to PAS structure with low affinity.** Fluorescence titration of 5'-Fl-PAS substrate [ $5 \times 10^{-7}$  M] with the PriB protein<sup>99</sup>. The solid line is the nonlinear least-squares fit of the experimental titration to equation 6.20 with  $K_{B1} = K_{B1} (2.3 \pm 0.8) \times 10^5 \text{ M}^{-1}$ ,  $\Delta F_1 = 0.05 \pm 0.01$ ,  $\Delta F_{\text{max}} = 0.43 \pm 0.03$ , and  $\omega = 40 \pm 8$ <sup>99</sup>.



$$Z_B = 1 + K_{B1}P_F + K_{B2}P_F + K_{1B}K_{2B}\omega P_F^2 \quad (6.19)$$

The observed relative fluorescence quenching,  $\Delta F_{\text{obs}}$ , is then

$$\Delta F_{\text{obs}} = \Delta F_1 \frac{K_{B1}P_F + K_{B2}P_F}{Z_B} + \Delta F_{\text{max}} \frac{K_{1B}K_{2B}\omega P_F^2}{Z_B} \quad (6.20)$$

where  $K_{B1}$  and  $K_{B2}$  are the binding constants for the association of the one and two PriB molecules with the PAS, respectively, the parameter,  $\omega$ , characterizes cooperative interactions,  $\Delta F_1$  is the relative fluorescence quenching accompanying the binding of the single PriB molecule to the PAS, and  $\Delta F_{\text{max}}$  is the maximum observed fluorescence quenching<sup>99</sup>. The solid line in Figure 6.7 is the nonlinear least-squares fit of the experimental titration to equation 6.20, which provides  $K_{B1} = K_{B1} (2.3 \pm 0.8) \times 10^5 \text{ M}^{-1}$ ,  $\Delta F_1 = 0.05 \pm 0.01$ ,  $\Delta F_{\text{max}} = 0.43 \pm 0.03$ , and  $\omega = 40 \pm 8$ <sup>99</sup>. Clearly, the PriB protein affinity for the PAS is at least  $\sim 2$  orders of magnitude lower than the corresponding affinity of the PriA protein and, as a result, in the examined concentration range of the PriB protein ( $< 1.3 \times 10^{-7} \text{ M}$  (dimer)), the association of the protein with the PAS is negligible<sup>99</sup>.

#### 6.4.10 The Effect of PriB in Solution on the Binding of PriA to PAS.

Fluorescence titrations of the 5'-FI-PAS with the PriA protein, in the presence of  $1.15 \times 10^{-7} \text{ M}^{-1}$  (dimer) of the PriB protein at three different nucleic acid concentrations, are shown in Figure 6.8a<sup>99</sup>. As shown above, in section 6.4.9, at the selected concentration, the PriB protein alone does not detectably bind to the PAS<sup>81,99</sup>. In addition, the value of  $K_{PP}$  characterizing the PriA – PriB interactions, independent of the DNA,

indicates that the PriA – PriB complex formation is also minimal at the applied protein concentrations (section 6.4.8)<sup>81,99</sup>. The biphasic character of the PriA binding to the PAS is now strongly pronounced, particularly at the low PAS concentration, where the free PriA protein concentration approaches its total concentration<sup>1,81,89,95,99,126</sup>. The dependence of relative fluorescence quenching,  $\Delta F_{\text{obs}}$ , as a function of  $\Sigma \Theta_i$  of the PriA protein on the PAS, is shown in Figure 6.8b<sup>1,81,89,95,99,126</sup>.

Surprisingly, the plot shows only slightly pronounced nonlinearity, due to the similar values of the induced fluorescence quenching, which accompanies the binding of the first and second PriA molecule<sup>1,27,81,92,99,127</sup>. Extrapolation of the plot to the maximum value of  $\Delta F_{\text{obs}}$  gives the maximum stoichiometry of  $2.2 \pm 0.2$ , showing that, still, two PriA molecules associate with the PAS structure and the presence of PriB protein does not change the maximum stoichiometry of the PriA - PAS complex<sup>99</sup>. The analysis of the titration curves in Figure 6.8a has been performed as described above for Figure 6.3a<sup>99</sup>. The solid lines in Figures 6.8a are nonlinear least-squares fits to equations 6.9 – 6.12 where  $K_1$  and  $K_2$  have been replaced by  $K_{1\text{ov}}$  and  $K_{2\text{ov}}$ , respectively, providing the overall binding constants of PriA for the PAS in the presence of PriB,  $K_{1\text{ov}} = (6 \pm 0.3) \times 10^8 \text{ M}^{-1}$  and  $K_{2\text{ov}} = (7.0 \pm 1.1) \times 10^6 \text{ M}^{-1}$ , respectively<sup>99</sup>. Thus, in the presence of the selected PriB concentration, the affinity of PriA for the strong site is increased by a factor of  $\sim 30$ , while the affinity for the weak site is only increased by a factor of  $\sim 2$  (section 6.4.4)<sup>99</sup>.

Fluorescence titrations of the 5'-Fl-PAS with PriA, in the presence of several selected PriB concentrations, are shown in Figure 6.9a<sup>99</sup>. Even at the lowest PriB concentration ( $1.27 \times 10^{-9} \text{ M}$  (dimer)) pronounced effect of PriB on the PriA affinity for the strong binding site is evident<sup>99</sup>. The solid lines in Figures 6.9a are nonlinear least-squares fits of the titration curves to equations 6.9 - 6.12 with  $K_{1\text{ov}}$  and  $K_{2\text{ov}}$  as the fitting parameters<sup>99</sup>. Because the value of the PriA - PriB association constant in the absence of

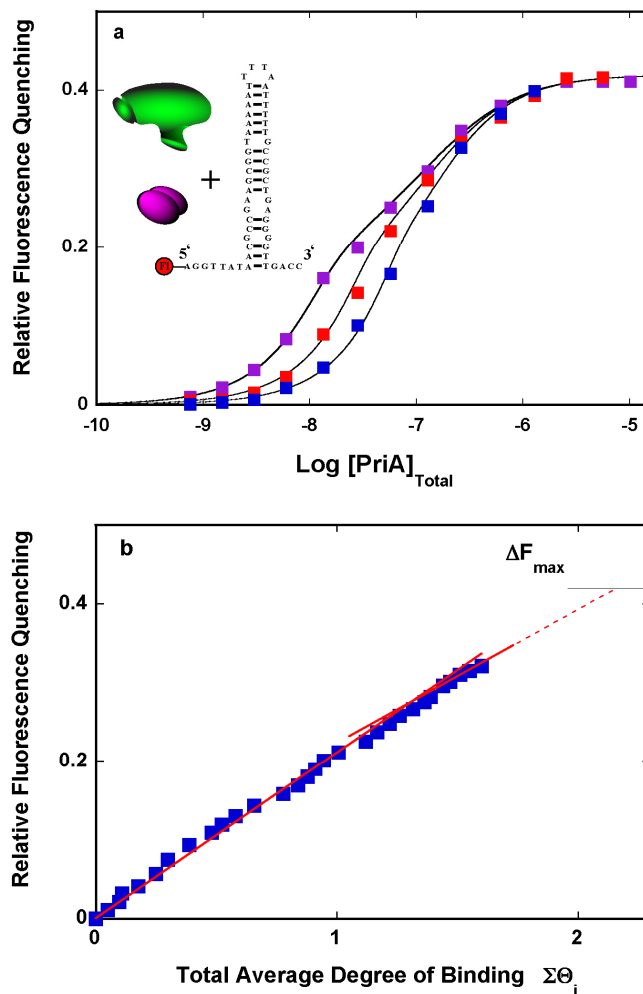
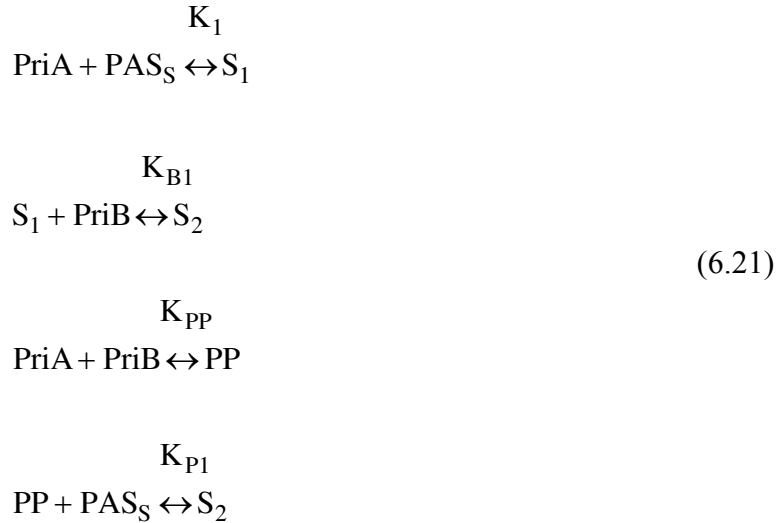


**Figure 6.8** The presence of PriB in solution has a dramatic effect on the binding of PriA to the PAS structure. **a.** Fluorescence titrations of 5'-Fl-PAS with PriA at three different concentrations of the nucleic acid  $1.25 \times 10^{-8}$  M (■),  $6.36 \times 10^{-8}$  M (■), and  $2.56 \times 10^{-7}$  M (■) in the presence of the PriB protein at the concentration of  $1.15 \times 10^{-7}$  M (dimer). The continuous lines represent nonlinear least-squares fits, using the binding model of the two discrete sites, with  $K_1$ ,  $K_2$ , and  $\omega$  as independent fitting parameters equations 6.9 -6.12. **b.** The dependence of the relative fluorescence quenching  $\Delta F_{\text{obs}}$  on the total average degree of binding  $\Sigma\Theta_i$  of PriA on the PAS in the presence of the PriB protein. The continuous red lines mark the slopes of the two binding phases and have no theoretical basis. The broken line indicates extrapolation of the maximum value of  $\Delta F_{\text{obs}}$  ( $\Delta F_{\text{max}}$ ) marked by the horizontal line<sup>99</sup>.

the DNA,  $K_{PP}$ , is known the concentration of free PriB ( $[PriB]_{Free}$ ) could be estimated<sup>99</sup>. The dependence of  $K_{1ov}$  upon  $[PriB]_{Free}$  is shown in Figure 6.9b<sup>99</sup>. It is obvious that the plot is hyperbolic, indicating that the PriB effect on  $K_{1ov}$  saturates at higher protein concentrations<sup>99</sup>. The linear character of the initial part of the plot indicates that a single PriB binds to the PriA - strong binding site complex<sup>99</sup>. Analogous dependence of  $K_{2ov}$  upon  $[PriB]_{Free}$  is shown in Figure 6.9c<sup>99</sup>.

#### 6.4.11 The Model of the PriB Effect On the PriA – PAS Interactions.

The fact that the PriB protein binds to the PriA protein in the absence of the DNA and the characteristic dependence of  $K_{1ov}$  and  $K_{2ov}$  upon the PriB protein concentration indicate that the PriB protein binds to the PriA protein associated with the strong and weak binding sites on the PAS, with a single PriB molecule engaging in interactions at each site<sup>99</sup>. First, consider the PriB effect on the PriA-PAS complex at the strong site,  $PAS_S$ <sup>99</sup>. The simplest binding model, which describes the examined system, is



where  $S_1$  is the strong site associated with PriA alone,  $S_2$  is the strong site associated with

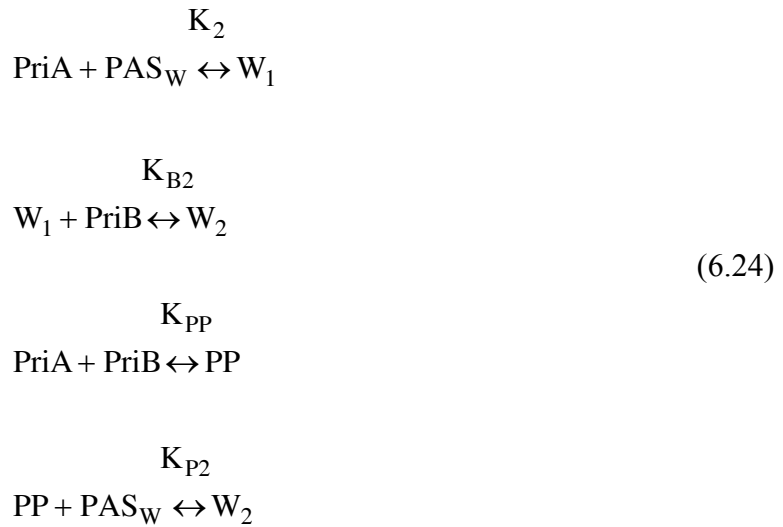
the PriA-PriB complex, PP is the PriA-PriB complex formed in solution independent of the DNA,  $K_{B1}$  is the PriB binding constant for the PriA-strong binding site complex, and  $K_{P1}$  is the binding constant of the PriA-PriB complex to the strong site<sup>99</sup>. The values of  $K_1$  and  $K_{pp}$  have been determined experimentally<sup>99</sup>. Thus, the overall binding constant, for the PriA binding to the strong site, in the presence of the PriB protein,  $K_{1ov}$ , expressed using the binding constant for the PriB protein to the PriA-strong site complex, is<sup>99</sup>

$$K_{1ov} = \frac{[S_1]_{Free} + [S_2]_{Free}}{([PriA]_{Free} + [PP])[PAS]_{Free}} \quad (6.22)$$

and

$$K_{1ov} = \frac{K_1 + K_1 K_{B1} [PriB]_{Free}}{1 + K_{pp} [PriB]_{Free}} \quad (6.23)$$

Thus,  $K_{1ov}$  includes binding of the PriA protein alone to the PAS and in the complex with the PriB protein dimer<sup>99</sup>. Analogous model for the weak binding site,  $PAS_w$ , is



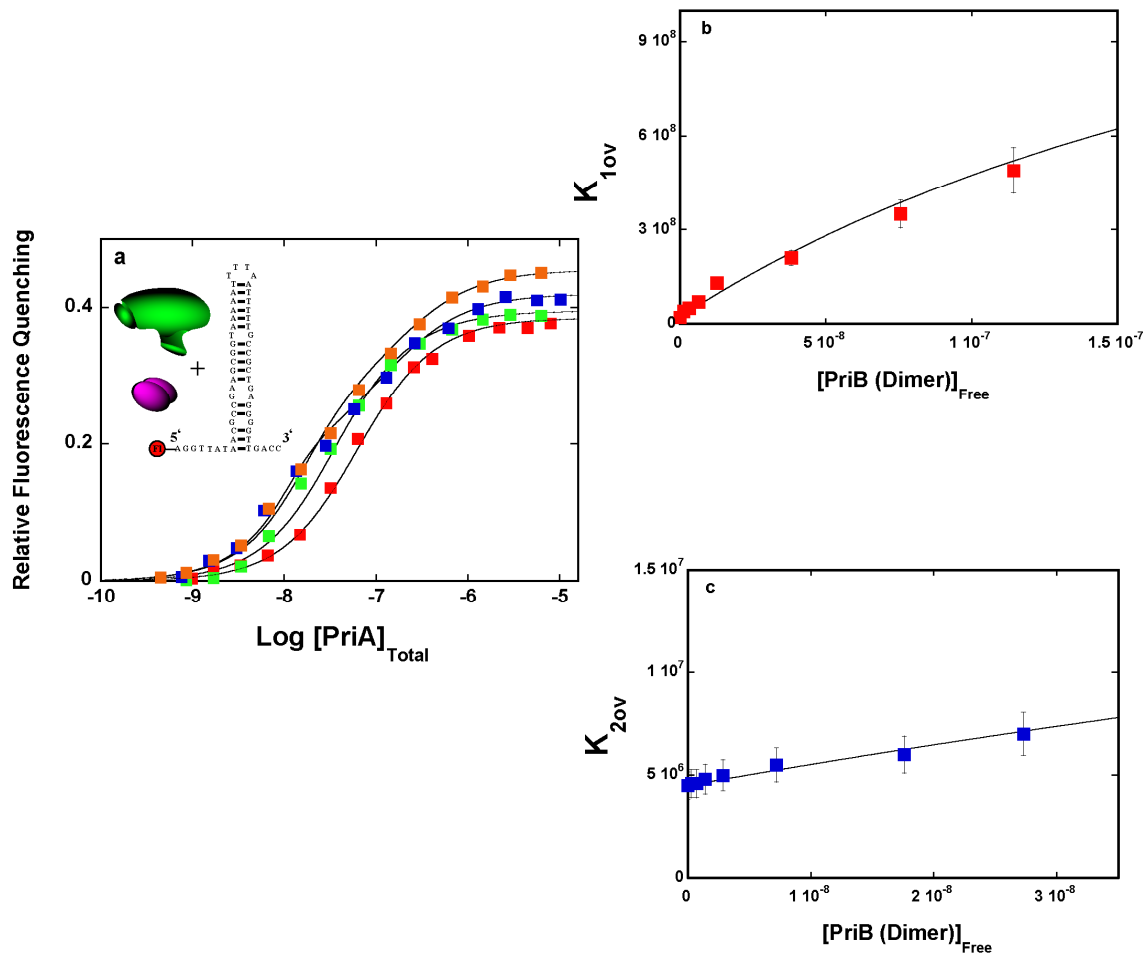


**Figure 6.9 The effect of PriB on PriA - PAS structure interactions. The plausible model.** **a.** Fluorescence titrations of 5'-FI-PAS [ $1.25 \times 10^{-8}$  M (PAS)] with PriA at different concentrations of the PriB protein (dimer): 0 (■),  $1.27 \times 10^{-9}$  M (■),  $1.27 \times 10^{-8}$  M (■), and  $1.15 \times 10^{-7}$  M (■)<sup>99</sup>. The continuous lines represent nonlinear least-squares fits, using the binding model of the two discrete sites, with  $K_1$ ,  $K_2$ , and  $\omega$  as independent fitting parameters using equations 6.9 - 6.12<sup>99</sup>. **b.** The dependence of the overall binding constant  $K_{1ov}$  on [PriB]<sub>Free</sub>. The continuous line represents the nonlinear least-squares fit of  $K_{1ov}$  to the thermodynamic model, where the PriA protein or the PriA - PriB complex binds to the strong site on the PAS (equation 6.23)<sup>99</sup>. **c.** The dependence of the overall binding constant  $K_{2ov}$  on [PriB]<sub>Free</sub>. The continuous line represents the nonlinear least-squares fit of  $K_{2ov}$  to the thermodynamic model, where the PriA protein or the PriA-PriB complex binds to the weak site on the PAS (equation 6.24)<sup>99</sup>.

and the expression for the overall binding constant, for the PriA binding to the weak site in the presence of the PriB protein,  $K_{2ov}$ , is<sup>99</sup>

$$K_{2ov} = \frac{K_2 + K_2 K_{B2} [PriB]_{Free}}{1 + K_{PP} [PriB]_{Free}} \quad (6.25)$$

The solid line in Figure 6.9b is the nonlinear least-squares fit of the data to the proposed model, equation 6.23, which provides the association constant of the PriB protein with the PriA - strong site complex,  $K_{B1} = (3.1 \pm 0.8) \times 10^8 \text{ M}^{-1}$ <sup>99</sup>. Analogously, the solid line in Figure 6.9c is the nonlinear least-squares fit of the data to the corresponding expression for  $K_{2ov}$ , equation 6.25, which provides the association constant of the PriB protein with the PriA - weak binding site complex,  $K_{B2} = (2.7 \pm 1.1) \times 10^7 \text{ M}^{-1}$ <sup>99</sup>. This large difference in the affinities indicates that PriB forms a very different complex with the PriA protein at the strong site, as compared to the weak site<sup>99</sup>.

#### **6.4.12 The Effect of PriB Protein on the PriA – ssDNA and PriA - dsDNA Interactions.**

To examine whether or not the effect of the PriB protein on PriA – PAS interactions is specific, the effect of PriB on the PriA interactions with the dsDNA was evaluated<sup>99</sup>. The binding of the PriA protein to the dsDNA 10-mer in the presence of PriB, was followed using the fluorescein label at the 5' end of one of ssDNA strands (section 6.3.3)<sup>92,99</sup>. PriA – 5'Fl-dsDNA interactions have been described in Chapter 3<sup>92,99</sup>. Recall, the dsDNA 10-mer accommodates two PriA molecules with the site-size  $n = 5 \pm 1$  base pairs and the binding process is characterized by a single intrinsic binding constant,  $K_{DS}$ , and positive cooperativity, characterized by the cooperativity parameter,  $\omega$  (section 3.4.3)<sup>92,99</sup>. The partition function,  $Z_{10}$ , of the PriA - dsDNA 10-mer system is<sup>92,99</sup>

$$Z_{10} = 1 + 6K_{DS}[P_F] + \omega (K_{DS}[P_F])^2 \quad (6.26)$$

The observed relative change of the nucleic acid fluorescence is defined by<sup>92,99</sup>

$$\Delta F = \Delta F_1 \left[ \frac{6K_{DS} P_F}{Z_{10}} \right] + \Delta F_{\max} \left[ \frac{\omega (K_{DS} P_F)^2}{Z_{10}} \right] \quad (6.27)$$

Fluorescence titrations ( $\lambda_{\text{ex}} = 480 \text{ nm}$ ,  $\lambda_{\text{em}} = 520 \text{ nm}$ ) of the 5'-Fl-dsDNA 10-mer with the PriA protein, in the absence and presence of the PriB protein ( $1.145 \times 10^{-7} \text{ M}$  (dimer)) are shown in Figure 6.10a<sup>99</sup>. The effect of PriB is very small as the addition of the protein only slightly shifts the titration curve. In the absence of the PriB protein,  $\Delta F_1 = 0.12$ ,  $\Delta F_{\max} = 0.41$ ,  $K_{DS} = (7.3 \pm 0.9) \times 10^6 \text{ M}^{-1}$ , and  $\omega = 1.5 \pm 0.3$ <sup>1,92,99,126,127</sup>. The solid lines in Figure 6.10a are nonlinear least-squares fits of the experimental titrations with  $K_{DS}$  and  $\omega$ , in the presence of the PriB protein, as independent fitting parameters and provide  $K_{DS} = (9.3 \pm 1.5) \times 10^6 \text{ M}^{-1}$  and the cooperativity parameter,  $\omega = 1.5 \pm 0.3$ <sup>1,92,99,126,127</sup>.

Analogously, the effect of PriB on the PriA – ssDNA interactions has been examined<sup>56,92,99</sup>. The binding of the PriA protein to the ssDNA 20-mer, was followed using the signal from etheno-derivative of the 20-mer, dεA(pεA)<sub>19</sub><sup>1,57,92,99,127</sup>. The fluorescence titrations ( $\lambda_{\text{ex}} = 325 \text{ nm}$ ,  $\lambda_{\text{em}} = 410 \text{ nm}$ ) of the dεA(pεA)<sub>19</sub>, with the PriA protein, in the absence and presence of two PriB protein concentrations, [ $7.39 \times 10^{-8} \text{ M}$  (dimer)] and [ $1.145 \times 10^{-7} \text{ M}$  (dimer)], respectively, are shown in Figure 6.10b<sup>99</sup>. The solid lines in Figure 6.10b are nonlinear least-squares fits of the experimental titrations to a single-site isotherm:



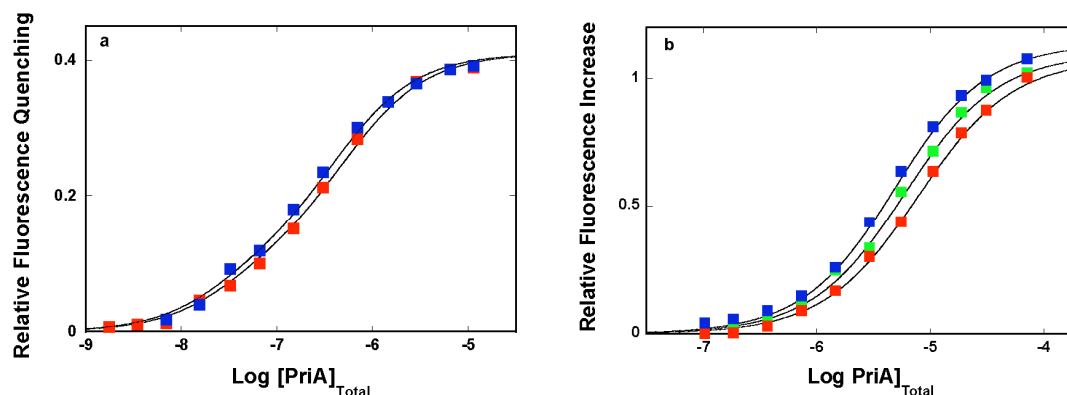


**Figure 6.10 The PriB protein has virtually no effect on the PriA – ssDNA and dsDNA interactions.** **a.** Fluorescence titrations of the dsDNA 10-mer [ $1.0 \times 10^{-8}$  M (oligomer)] with the PriA protein, in the absence (■) and in the presence of the PriB protein [ $1.145 \times 10^{-7}$  M (dimer)] (■)<sup>99</sup>. The continuous lines represent nonlinear least-squares fits of the experimental titrations in the presence of the PriB protein, with  $K_{DS}$  and  $\omega$  as independent fitting parameters (equations 6.26 and 6.27)<sup>99</sup>. **b.** Analogous fluorescence titrations of the ssDNA 20-mer dεA(pεA)<sub>19</sub> [ $1.34 \times 10^{-6}$  M (oligomer)] with the PriA protein, in the absence (■) and in the presence of two PriB protein concentrations:  $7.39 \times 10^{-8}$  M (dimer) (■) and  $1.145 \times 10^{-7}$  M (dimer) (■), respectively<sup>99</sup>. The continuous lines represent nonlinear least-squares fits of the experimental titrations to a single-site isotherm (equation 6.28)<sup>99</sup>.

$$\Delta F = \Delta F_{\max} \left[ \frac{K_{20} P_F}{1 + K_{20} P_F} \right] \quad (6.28)$$

with  $K_{20}$ , and  $\Delta F_{\max}$  as independent fitting parameters<sup>99</sup>. In the absence of the PriB protein,  $K_{20} = (1.4 \pm 1.5) \times 10^5 \text{ M}^{-1}$  and  $\Delta F_{\max} = 1.08 \pm 0.05^{1,57,92,99}$ . Corresponding values are:  $K_{20} = (1.9 \pm 1.5) \times 10^5 \text{ M}^{-1}$ ,  $\Delta F_{\max} = 1.10 \pm 0.05$  and  $K_{20} = (2.4 \pm 1.5) \times 10^5 \text{ M}^{-1}$ ,  $\Delta F_{\max} = 1.14 \pm 0.05$ , in the presence of  $7.39 \times 10^{-8} \text{ M}$  and  $1.145 \times 10^{-7} \text{ M}$  concentrations of the PriB protein (dimer), respectively<sup>99</sup>. It is obvious that the presence of the PriB protein, at the concentrations which dramatically influence the PriA interactions with the strong PAS binding site, has hardly noticeable effect on the enzyme binding to the dsDNA or the ssDNA<sup>99</sup>.

#### **6.4.13 The PriA and PriA - PriB – PAS Interactions. The Thermodynamic Cycle.**

Having determined the thermodynamic characteristics of the PriA binding to the strong and weak binding sites on the PAS, the association constant characterizing the PriA and PriB complex formation, as well as the association constants for the PriB binding to the PriA-PAS complexes, the affinities of the PriA-PriB complex, formed in solution independent of the PAS, for both the strong and the weak binding sites can be addressed<sup>99</sup>. Figure 6.11a and Figure 6.11b show the thermodynamic cycles for binding of PriA and PriB to the strong- and weak-binding sites, including alternative pathway, where the PriA - PriB complex, formed independent of the DNA, binds to the PAS<sup>99</sup>. Using the cycle in Figure 6.11a, the binding constant for the PriA - PriB complex formation at the strong binding site on the PAS,  $K_{P1}$ , is determined to be  $(1.7 \pm 0.5) \times 10^9 \text{ M}^{-1}$ <sup>99</sup>. The corresponding value of the binding constant for the weak binding site is,

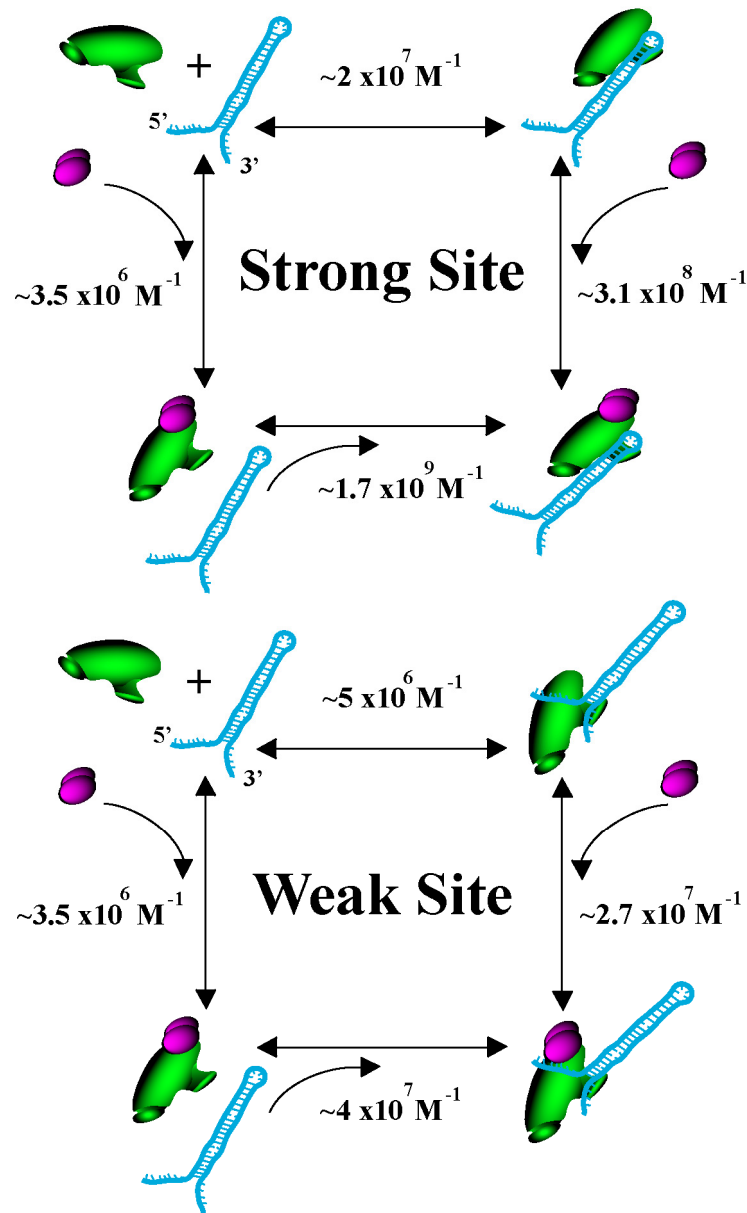


**Figure 6.11** Thermodynamic cycles of PriA – PAS, PriA – PAS – PriB, PriA – PriB and PriA – PriB - PAS interactions proposed in the recognition of the strong and weak binding sites on the PAS. The affinity of the PriA – PriB complex for the strong,  $K_{P1}$ , and weak binding sites,  $K_{P2}$ , has been obtained from the relationships  $K_{P1} = (K_1 K_{B1})/K_{PP}$  and  $K_{P2} = (K_2 K_{B2})/K_{PP}$ , respectively<sup>99</sup>.

$K_{P2} = (4.0 \pm 1.5) \times 10^7 \text{ M}^{-1}$  (Figure 6.11b)<sup>99</sup>.

#### 6.4.14 The Effect of Temperature on the PriA-PAS or PriA-PriB-PAS Complex Formation.

In order to further address the nature of complexes formed at the strong and weak binding sites of the PAS, the temperature effect on the energetics of the association reactions was examined<sup>99</sup>. Fluorescence titrations of the 5'-Fl-PAS with PriA alone, or in the presence of the PriB protein ( $1.15 \times 10^{-7} \text{ M}$ , dimer), have been performed at several different temperatures (data not shown) and Figure 6.12a shows the dependence of the natural logarithm of the binding constants,  $K_1$  and  $K_2$ , upon the reciprocal of the temperature (Kelvin)<sup>81,92,99</sup>. Corresponding plots for the overall binding constants,  $K_{1ov}$  and  $K_{2ov}$ , obtained in the presence of PriB, are shown in Figure 6.12b<sup>99</sup>. Within experimental accuracy, both plots are linear in the examined temperature range<sup>99</sup>. The temperature dependence of the given binding constant,  $K_i$ , is described by van't Hoff's equation<sup>81,92,96,99</sup>

$$\frac{\partial \ln K_i}{\partial \left(\frac{1}{T}\right)} = -\frac{\Delta H_i^\circ}{R} \quad (6.29)$$

where  $\Delta H_i$  is the enthalpy change accompanying a given intrinsic binding process<sup>99</sup>. Binding of the PriA protein alone to the strong and weak sites is characterized by the apparent enthalpy changes,  $\Delta H_1^\circ = 22.9 \pm 3 \text{ kcal/mol}$  and  $\Delta H_2^\circ = 0 \pm 3 \text{ kcal/mol}$ , respectively<sup>99</sup>. Such a large difference between the values of the thermodynamic functions indicates that very different binding processes occur at the strong and the weak

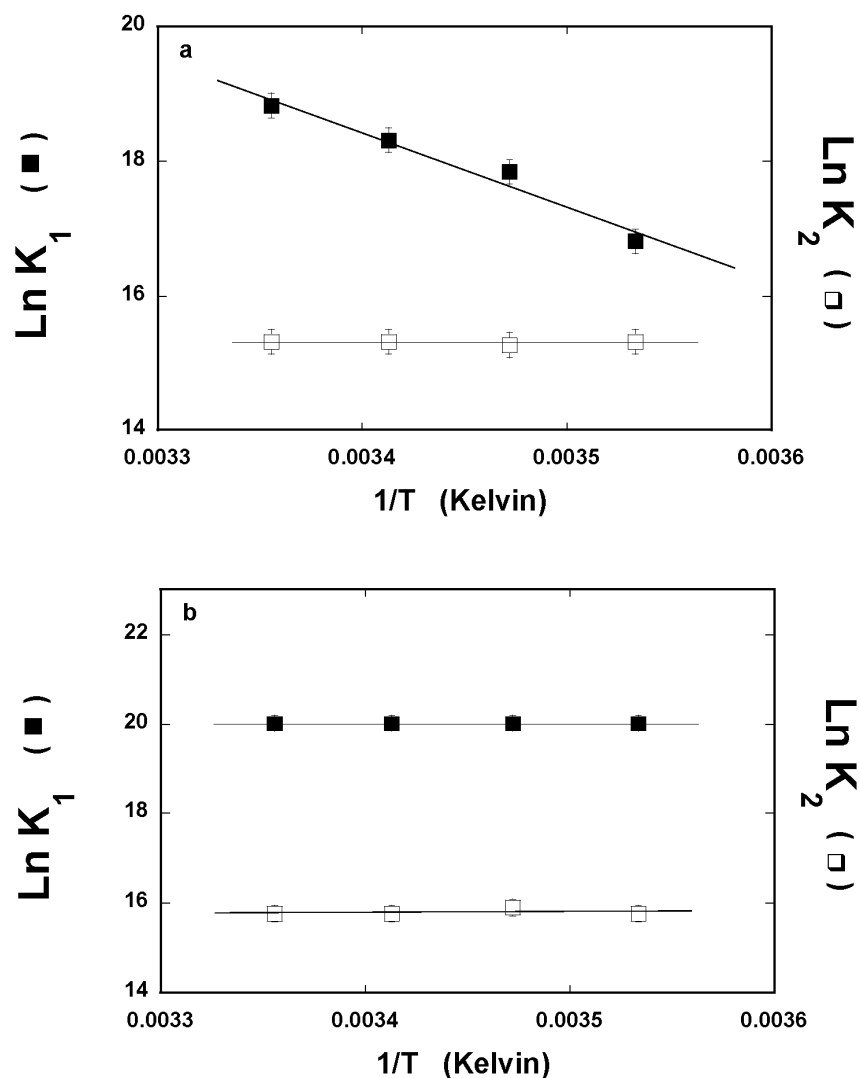


**Figure 6.12 Temperature effect on the PriA – PAS and PriA – PriB – PAS interactions.** a. The dependence of the natural logarithm of the binding constants  $K_1$  (■) and  $K_2$  (□), determined for the binding of the PriA protein alone to the strong and weak binding sites on the PAS, on the reciprocal of the temperature (in Kelvin) (van't Hoff plots)<sup>81,96,99</sup>. (b) The dependence of the natural logarithm of the overall binding constants  $K_{1ov}$  (■) and  $K_{2ov}$  (□), obtained for the binding of PriA to the strong and weak binding sites on the PAS in the presence of the PriB protein  $[1.15 \times 10^{-7} \text{ M (dimer)}]$ <sup>99</sup>. The continuous lines in both panels represent linear least-squares fits to equation 6.29<sup>99</sup>.

binding sites<sup>99</sup>. Using the thermodynamic relationship,  $\Delta G^\circ = -RT \ln K_i$ , the corresponding apparent entropy changes of the binding as,  $\Delta S_1^\circ = 114 \pm 25$  cal/mol deg and  $\Delta S_2^\circ = 30 \pm 6$  cal/mol deg, can be obtained<sup>81,92,99</sup>. In the presence of the PriB protein,  $\Delta H_1^\circ = 0 \pm 3$  kcal/mol and  $\Delta H_2^\circ = 0 \pm 3$  kcal/mol, respectively, and the corresponding apparent entropy changes are:  $\Delta S_1^\circ = 40 \pm 9$  cal/mol deg and  $\Delta S_2^\circ = 31 \pm 6$  cal/mol deg<sup>99</sup>. Thus, the PriB protein dramatically changes the thermodynamic characteristics of the PriA binding to the strong site, while it has no effect on the PriA protein binding to the weak site<sup>99</sup>.

#### **6.4.15 Changes to the PAS Structure Exerted by the PriA and PriA – PriB Binding in the Presence of ATP. FRET Experiments.**

In the final set of experiments, we examined the effect of the PriA helicase and PriA-PriB complex on the structure of the PAS substrate using the FRET method (section 6.3.9)<sup>8,63,99,123-125</sup>. Figure 6.13a shows used PAS substrate with the locations of the fluorescence acceptor (fluorescein) at the 5' end of the DNA (5'-FI-PAS) and the fluorescence donor, coumarin derivative (CP), at the 3' end of the nucleic acid (5'-FI-PAS-3'-CP)<sup>8,63,99,123-125</sup>. In the approach used in this experiments the nucleic acid is labeled with only the acceptor, 5'-FI-PAS, or only with the donor, PAS-3'-CP, or with both the acceptor and the donor, 5'-FI-PAS-3'-CP<sup>8,63,99,123-125</sup>. The Förster efficiency of the fluorescence energy transfer,  $E$ , from the acceptor to the donor and the average distance between the acceptor and the donor,  $R$ , have been determined using two apparent fluorescence energy transfer efficiencies.  $E_D$ , and  $E_A$  (section 6.3.9)<sup>8,63,99,123-125</sup>. Since PriA is a helicase, in the presence of ATP, the change of the PAS structure, most probably due to unwinding of its dsDNA parts, should lead to the spatial separation of the

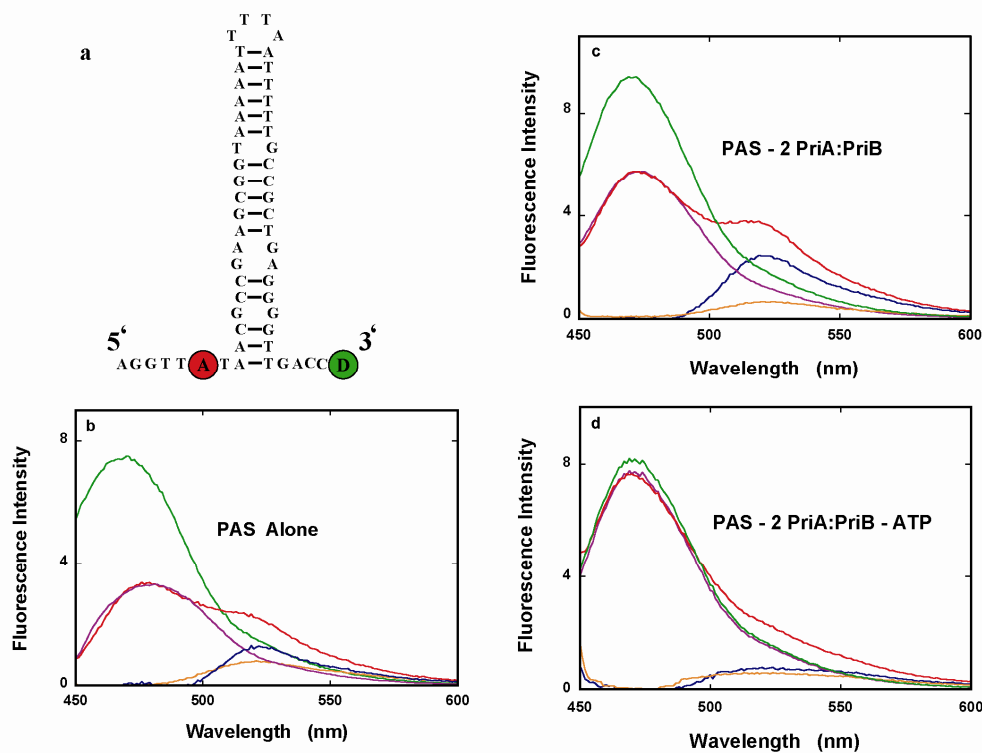


**Figure 6.13 The structural effect of the PriA helicase binding to the PAS. a.** The structure of the 5'-FI-PAS-3'-CP substrate. The fluorescence acceptor, A, Fluorescein, is located at the 5' end side of the DNA and with the fluorescence donor, D, coumarin derivative, CP, is located at the 3' end of the DNA<sup>99</sup>. **b.** The emission spectrum ( $\lambda_{\text{ex}} = 425$  nm) of PAS-3'-CP (green), the spectrum of 5'-FI-PAS (orange), the spectrum of 5'-FI-PAS-3'-CP (red), the spectrum of PAS-3'-CP normalized to the maximum of the coumarin emission in 5'-FI-PAS-3'-CP (magenta), and the sensitized emission spectrum of 5'-FI-PAS (blue). The concentration of the PAS substrate is  $1.25 \times 10^{-8}$  M (oligomer)<sup>99</sup>. **c.** The emission spectrum ( $\lambda_{\text{ex}} = 425$  nm) of PAS-3'-CP (green), the spectrum of 5'-FI-PAS (orange), the spectrum of 5'-FI-PAS-3'-CP (red), the spectrum of PAS-3'-CP normalized to the maximum of the coumarin emission in 5'-FI-PAS-3'-CP (magenta), and the sensitized emission spectrum of 5'-FI-PAS (blue), in the presence of PriA and PriB. The concentrations of the PriA and PriB proteins are  $8 \times 10^{-7}$  M and  $1.15 \times 10^{-7}$  M (oligomer)<sup>99</sup>. **d.** The emission spectrum ( $\lambda_{\text{ex}} = 425$  nm) of PAS-3'-CP (green), the spectrum of 5'-FI-PAS (orange), the spectrum of 5'-FI-PAS-3'-CP (red), the spectrum of PAS-3'-CP normalized to the maximum of the coumarin emission in 5'-FI-PAS-3'-CP (magenta), and the sensitized emission spectrum of 5'-FI-PAS (blue), in the presence of PriA helicase and PriB protein, and 1 mM ATP. The concentrations of the PriA and PriB proteins are  $8.0 \times 10^{-7}$  M and  $1.15 \times 10^{-7}$  M (oligomer)<sup>99</sup>.

acceptor and the donor and to the decrease of the values of  $E$ , and, in turn, to the increased average distances between the donor and the acceptor<sup>8,55-57,63,99,123-125</sup>.

Figure 6.13b shows the emission spectrum ( $\lambda_{\text{ex}} = 425 \text{ nm}$ ) of the PAS-3'-CP (green), the spectrum of the 5'-Fl-PAS (orange), the spectrum of the 5'-Fl-PAS-3'-CP (red), the spectrum of the PAS-3'-CP normalized to the maximum of the coumarin emission in the 5'-Fl-PAS-3'-CP, (magenta), and the sensitized emission spectrum of the 5'-Fl-PAS (blue)<sup>99,123-125</sup>. The intensities of the donor and the acceptor have been obtained by integrating the corresponding areas under the spectra and obtained values of the FRET efficiencies are:  $E_D = 0.53 \pm 0.03$ ,  $E_A = 0.23 \pm 0.03$ , and  $E = 0.32 \pm 0.03$ <sup>8,63,99,123-125</sup>. The value of  $E \approx 0.32$  indicates that the average distance between coumarin and fluorescein on the PAS in the absence of the PriA and/or PriB protein, is  $R = 58.5 \pm 3.0 \text{ \AA}$  (Table 6.1)<sup>99</sup>.

Corresponding emission spectrum ( $\lambda_{\text{ex}} = 425 \text{ nm}$ ) of the PAS-3'-CP (green), the spectrum of the 5'-Fl-PAS (orange), the spectrum of the 5'-Fl-PAS-3'-CP (red), the spectrum of the PAS-3'-CP normalized to the maximum of the coumarin emission in the 5'-Fl-PAS-3'-CP, (magenta), and the sensitized emission spectrum of the 5'-Fl-PAS (blue), in the presence of the PriA helicase and the PriB protein, in the absence of ATP, are shown in Figure 6.13c<sup>99</sup>. Concentrations of the PriA protein and the PriB protein are:  $8.0 \times 10^{-7} \text{ M}$  and  $1.15 \times 10^{-7} \text{ M}$  (oligomer), respectively. In these conditions two PriA molecules, with associated PriB proteins, are bound to the PAS<sup>99</sup>. The spectra are similar to the corresponding spectra recorded for the PAS substrate alone as expressed by very similar values of energy transfer efficiencies and the average distance between the acceptor and the donor (Table 6.1)<sup>99</sup>. It is evident that the presence of the PriA molecules, associated with the PriB protein, at the strong and weak binding sites on the PAS, does not affect that structure of the nucleic acid<sup>99</sup>. A similar lack of the effect of the PriA



protein, in the presence or absence of PriB on the PAS structure, is observed for the single enzyme molecule associated only with the strong binding site (Table 6.1)<sup>99</sup>.

The situation is different in the presence of ATP<sup>99</sup>. The protein - DNA complex has been mixed and incubated for 10 minutes<sup>99</sup>. Subsequently ATP was added, and the system was allowed to equilibrate for another 10 minutes, and the spectra were recorded<sup>99</sup>. Interestingly, the PriA protein alone, or of the PriA - PriB complex, associated only with the strong binding site, is capable of inducing a moderate change in the PAS structure, with  $R$  increasing from  $\sim 58.5$  Å to  $\sim 66 - 68$  Å (Table 6.1)<sup>99</sup>. This newly established complex could not be reached in the presence of ADP alone, where the average distance  $R \approx 60$  Å (data not shown)<sup>99</sup>. Thus, it is safe to say that the observed complex must be a result of the helicase activity of the enzyme accompanied by the ATP hydrolysis<sup>99</sup>.

The most dramatic difference is observed for the complex involving two PriA molecules bound to the strong and weak binding sites, alone, or associated with the PriB protein<sup>99</sup>. Figure 6.13d shows the emission spectrum ( $\lambda_{\text{ex}} = 425$  nm) of the PAS-3'-CP (green), the spectrum of the 5'-Fl-PAS (orange), the spectrum of the 5'-Fl-PAS-3'-CP (red), the spectrum of the PAS-3'-CP normalized to the maximum of the coumarin emission in the 5'-Fl-PAS-3'-CP, (magenta), and the sensitized emission spectrum of the 5'-Fl-PAS (blue), in the presence of the PriA helicase, the PriB protein, and ATP<sup>99</sup>. Concentrations of the PriA and PriB proteins are the same as in Figure 6.13c, *i.e.*, two PriA molecules, with associated PriB proteins, are bound to the PAS<sup>99</sup>. The spectra are very different from the corresponding spectra recorded for the PAS substrate alone (Figure 6.13b), or for the same system in the absence of ATP (Figure 6.13c)<sup>99</sup>. The emission intensity of the donor is only slightly diminished and the sensitized emission intensity is only very moderately larger than the emission of the acceptor alone<sup>99</sup>. The

obtained values of the FRET efficiencies are:  $E_D = 0.05 \pm 0.01$  and  $E_A = 0.09 \pm 0.02$ , and  $E = 0.08 \pm 0.02$  indicates that the average distance between CP and fluorescein on the PAS is  $R = 77.4 \pm 4.1 \text{ \AA}$  (Table 6.1)<sup>99</sup>. Thus, the spatial separation of the acceptor and the donor is  $\sim 19 \text{ \AA}$  much larger than observed for the PAS alone<sup>99</sup>. Comparable, but lower separation of the acceptor and the donor is observed in the case of the two PriA bound to the PAS in the absence of the PriB protein, with  $R \approx 75.5 \text{ \AA}$  (Table 6.1)<sup>99</sup>.

## 6.5 DISCUSSION

### 6.5.1 Binding of Two PriA Molecules to Two Discrete Binding Sites on the PAS Structure Initiates the Primosome Formation.

For almost two decades the exact numbers of components of the primosome complex, participating at each stage of the assembly process, remained elusive<sup>5,15,16,25,26,99</sup>. Application of the quantitative fluorescence titration method described in this Chapter allowed, for the first time, to unambiguously determine the stoichiometries of the initial steps of the primosome formation, involving the PriA and PriB proteins<sup>1,95,99,126,127</sup>. Presented data clearly show that the minimal phiX174 PAS substrate possesses two discrete binding sites to which two PriA molecules bind<sup>99</sup>. Moreover, the binding sites dramatically differ in their thermodynamic properties, the effect of the nucleotide cofactors, and the effect of the PriB protein<sup>99</sup>.

Taking into account the size of PriA ( $\sim 82 \text{ kDa}$ ) it is rather surprising that 55 nucleotides PAS substrate can accommodate up to two PriA monomers<sup>27,49,50,56,92,99</sup>. However, the stoichiometry of the PriA-PAS complex can be understood in the context of known properties of the PriA helicase and its ability to binding the ss and dsDNAs<sup>1,27,56,92,99</sup>. The PriA protein possesses a DNA-binding site, located on the

helicase domain, which protrudes from the rest of the protein matrix<sup>1,27,56,92,99</sup>. This unique structure enables the enzyme to associate with small fragments of the DNA, as clearly seen in the kinetics studies, and adjust its site-size to the conformation of the nucleic acid<sup>1,27,56,59,92,99</sup>. Thus, the site-size of the PriA-ssDNA complex is  $\sim 20$  nucleotides, while the site-size of the protein dsDNA is only  $\sim 5$  base pairs long<sup>1,27,56,59,92,99</sup>. Even so, such a large difference between the site-sizes of the PriA - ssDNA and the PriA - dsDNA complexes is confounding<sup>27,56,59,92,99</sup>. Moreover, while the binding of the enzyme to the ssDNA lacks any cooperativity, the association with the dsDNA is characterized by positive cooperativity<sup>27,56,92,99</sup>. This means that the PriA protein must be able to assume very different orientations in complexes with different DNA conformations<sup>27,56,59,92,99</sup>. PriA seems to take advantage of this ability when binding to the PAS structure containing dsDNA segments separated by loops and ssDNA bulges (Figure 6.2a)<sup>99,103,122</sup>. In the absence of the PriB protein, the affinity of the strong binding site is similar to the PriA protein affinity for the dsDNA<sup>92,99</sup>. These data indicate that the strong binding site includes one of the dsDNA fragments of the PAS and the protein binds in an orientation similar to the orientation in the complex with the duplex DNA, *i.e.*, without engaging the N-terminal domain in interactions with the nucleic acid<sup>92,99</sup>. Moreover, the separation of the protein bound at the strong site by  $\sim 9.1$  Å from the 5' end of the nucleic acid places the strong binding site close to the ssDNA loop of the PAS structure (Figure 6.4a)<sup>99</sup>.

On the other hand, the affinity of the weak site is close to the PriA protein affinity for the ssDNA<sup>19,22,24</sup>. Recall, the nucleotide cofactors, mostly ADP, profoundly affect only the PriA affinity for the ssDNA, leading to the engagement of the N-terminal domain in interactions with the DNA, while the same cofactors have only a modest effect on the protein dsDNA affinity<sup>27,59-61,92,99</sup>. The effect of the nucleotide cofactors on the

PriA binding to the strong and weak binding sites reflects similar behavior (Figure 6.5b and Figure 6.5c)<sup>92,99</sup>. These results, and the lack of any cooperative interactions between the PriA molecules associated with the strong site, indicate that the weak binding site must be located at the opening of the hairpin-like PAS structure and include ssDNA fragment of the PAS close to the 3' end of the nucleic acid<sup>92,99</sup>. Furthermore, the lack of cooperative interactions in the complex with the PAS strongly suggest that the PriA protein is associated in a different orientation and/or structural state in the strong site, as compared to the orientation and/or structure of the bound protein in the weak binding site<sup>92,99</sup>.

These conclusions are further corroborated by different thermodynamic characteristics of the PriA binding to the strong and weak binding sites on PAS<sup>99</sup>. While the association with both sites is driven by the apparent entropy changes, the association with the strong site is characterized by a very unfavorable apparent enthalpy change ( $\Delta H_1^\circ \approx 22$  kcal/mol), as compared to  $\Delta H_2^\circ \approx 0$  (Figure 6.12)<sup>99</sup>. Notice, this very peculiar thermodynamic response *i.e.*, a large enthalpy change, indicates profound structural transformation as a result of the PriA protein binding to the strong binding site of the PAS<sup>99</sup>. Interestingly, such a change is absent in the association process of the protein with the weak site<sup>99</sup>.

### **6.5.2 The PriB Protein Specifically Binds to the PriA Associated with the Strong Binding Site on the PAS Structure.**

As presented above, the difference between the effect of the PriB protein on the PriA association with the strong and weak binding sites is dramatic<sup>99</sup>. The overall binding constant of the PriA protein for the strong site increases by a factor of  $\sim 30$ , while the overall affinity of the weak site increases only by a factor of  $\sim 2$  (Figure 6.8 and Figure

6.9)<sup>99</sup>. The data presented in Figure 6.9 as well as the thermodynamic cycles in Figure 6.11 show that the PriB protein binds to the PriA protein at the strong site with the affinity more than an order of magnitude higher than to the PriA associated with the weak site<sup>99</sup>. This profound effect cannot be due to the PriB intrinsic affinity for the DNA<sup>81,99</sup>. First, as shown in the Figure 6.10, the PriB protein does not affect the PriA binding to the ssDNA or the dsDNA<sup>99</sup>. Second, the protein shows strong preference for the ssDNA and has very low intrinsic affinity for the PAS (Figure 6.7)<sup>81,99</sup>. These results clearly indicate that the PriB effect on PriA – PAS interaction is explicit and that the protein is able to specifically induce/recognize the conformational state of the PriA protein associated with the strong binding site on the PAS<sup>99</sup>.

### **6.5.3 The PriB Protein Induces Conformational Changes in the PriA Protein In the Absence of the DNA Which Specifically Increase the PriA Affinity for the Strong Binding Site On the PAS.**

In the context of presented data and the discussion in section above, the thermodynamic cycles in Figure 6.11 show that the affinity of the PriA-PriB complex, formed in the absence of the PAS, for the strong binding site is by a factor of  $\sim 100$  higher than the affinity of the PriA protein alone for the site<sup>99</sup>. Parallel increase in the affinity of the PriA-PriB complex for the weak site is by a factor of  $\sim 10$ <sup>99</sup>. These results point out that the PriB effect, seen in the overall binding constant of the PriA association with the strong site on the PAS, is induced on the level of PriA - PriB interactions and is independent of whether or not the PriA protein is associated with the PAS<sup>99</sup>. Moreover, the effect is specific for strong binding site on the PAS not for the ssDNA or dsDNA<sup>99</sup>. This further supports the fact that the PriB protein forms a very different complex with the PriA protein at the strong site, as compared to the weak site<sup>99</sup>. Notice, although the

PriA protein alone, in the absence or presence of the nucleotide cofactors, will preferably bind to the PAS in the presence of the competing ssDNA, the protein alone is not able to efficiently distinguish the PAS from any surrounding dsDNA<sup>99</sup>. Only the engagement of the PriB protein leads to the specific and efficient recognition of the PAS by the PriA helicase<sup>99</sup>.

#### **6.5.4 The PriA-PriB Complex Can Recognize the PAS Without Prior Binding of PriA to the DNA.**

The current model of the primosome assembly process is that the PriA protein first associates with the nucleic acid *prior* to the engagement of the PriB protein in the complex<sup>5,16,24,25,99</sup>. However, the data presented in this Chapter indicate that the PriA-PriB complex is formed independently of the PAS and is capable to recognize the PAS without the preceding PriA binding to the DNA (Figures 6.11)<sup>99</sup>. Even though the value of  $K_{PP}$ , characterizing the PriA-PriB complex formation in solution, indicates that, at the physiological concentrations of both proteins ( $\sim 5 \times 10^{-8}$  M), the PriA-PriB complex may constitute only  $\sim 10\%$  of the PriA population, the high affinity of the PriA-PriB complex could offset the low efficiency of its formation<sup>54,55,99,103</sup>. In this context, the temperature effect on the PriA and the PriA-PriB complex association with the PAS is very interesting<sup>99</sup>. The data indicate that at higher temperatures the PriA affinity for the strong site approaches the affinity of the PriA-PriB complex, while the affinity of the PriA-PriB complex remains unaffected by the temperature (Figure 6.12b)<sup>99</sup>. In the context of this results, the PriB protein seems to control the affinity of the PriA helicase for the strong site on the PAS by holding the corresponding binding constant at a specific value of  $\sim 5 \times 10^8 \text{ M}^{-1}$ <sup>99</sup>.

### **6.5.5 Only Moderate Conformational Changes in the PAS Structure are Induced by PriA and PriA-PriB Complex in the Presence of ATP.**

The helicase activity of the PriA protein or the PriA-PriB complex, associated with the strong site, should disrupt the dsDNA fragments of the PAS structure<sup>99</sup>. This ATP fuelled process only moderately increases the acceptor - donor distance from  $R \approx 58$  Å to  $R \approx 66 - 68$  Å (Table 6.1). Possible re-annealing of the PAS structure could be a reason for this small distance increase<sup>99</sup>. It should be noted, however, that such re-annealing process would return  $R$  to the initial value of  $\sim 58$  Å, which is not observed<sup>99</sup>. Thus, the data indicate that, as a consequence of the specific orientation and/or conformation in the strong binding site, the PriA helicase and the PriA-PriB complex have a strongly diminished capability to disrupt the duplex parts of the PAS substrate, resulting in a new protein-PAS complex with only partially affected nucleic acid structure<sup>99</sup>. This conclusion is further supported by the fact that the PriA protein, and particularly the PriA - PriB complex, retain the high-affinity state for the strong site in the presence of ADP<sup>99</sup>.

Different situation is observed when the PriA helicase or its complex with the PriB protein is associated with the strong and weak binding sites<sup>99</sup>. In the presence of the ATP, the acceptor - donor distance increases from  $\sim 58$  Å to  $\sim 77$  Å, indicating that the PriA protein and the PriA - PriB complex associated with the weak site can stimulate a significantly more pronounced change in the PAS structure, than the corresponding complexes exclusively bound to the strong site (Figure 6.13d and Table 6.1)<sup>99</sup>. Nevertheless, the distance of  $\sim 77$  Å is still shorter than the distance of  $\sim 140$  Å between the acceptor and the donor expected for the completely unwound ssDNA oligomer (Figure 6.10a), indicating that, as result of the PriA binding and activity, a specific and

stable protein-nucleic acid complex is reached, which is different from the initial complex formed in the absence of ATP<sup>99</sup>.

#### **6.5.6 Further Functional Implications.**

The role of two binding sites on the PAS, so different in their properties, can be understood in the context of the physiological role of the PriA protein, which serves as the recognition beacon of the PAS and as an auxiliary helicase<sup>5,11,24,25,55,99,128</sup>. Due to its very high affinity, the PriA-PriB complex, in the strong site, should serve as the major recognition complex of the PAS, while both complexes in the strong and weak sites are necessary for any subsequent assembly steps<sup>99</sup>. The PriA helicase activity of the strong complex is suppressed by the very high affinity of the site, as the complex only modestly unwinds the PAS structure in the presence of ATP (Table 6.1)<sup>99</sup>. On the other hand, the weak PriA-PAS complex lacks the significant stabilizing effect of the PriB protein and is strongly affected by the nucleotide cofactors<sup>99</sup>. In this property, the PriA protein in the weak site should be able to engage in helicase activity, as indicated by the fact that a profound unwinding of the PAS structure in the presence of ATP is observed only with both binding sites engaged in interactions with the PriA protein (Figure 6.13d and Table 6.1). Thus, the presence of two sites separates two different physiological roles of the same protein in a single molecular machine<sup>99</sup>.

Based on the results described in this Chapter, Figure 6.14 shows the schematic representation of initial recognition of the PAS by the PriA and PriB proteins in the context of the pre-primosome assembly process<sup>5,17,24,25,99</sup>. Two PriA-PriB complexes initiate the recognition of the PAS<sup>99</sup>. In the absence of ATP, the nonproductive pre-primosome assembles through the recognition of the specific PriA-PriB complex at the strong binding site. Notice that ATP is not necessary to initiate the primosome assembly



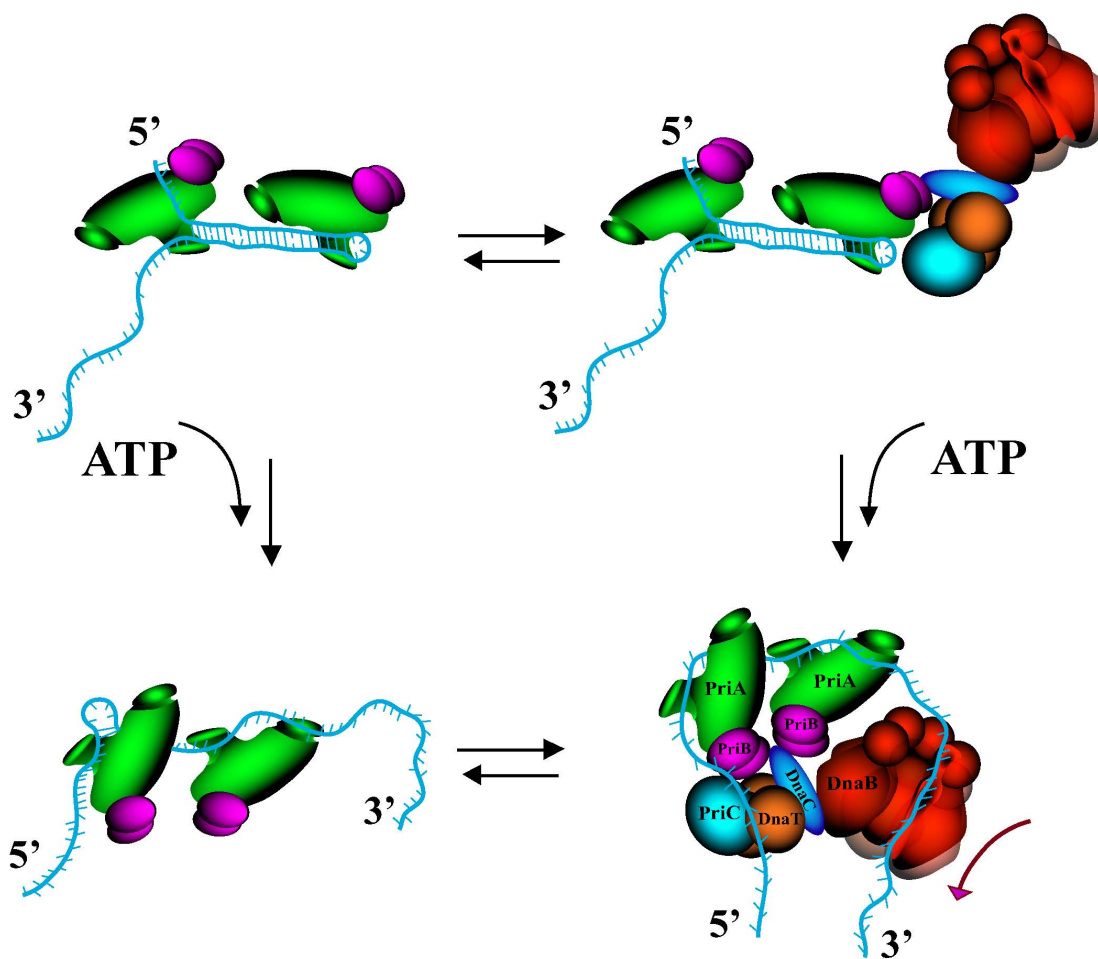


**Figure 6.14** Pictorial representation of the initial recognition of the PAS by the PriA and PriB proteins in the context of the pre-primosome assembly process, based on the results obtained in this work. By binding to the PAS structure two PriA-PriB complexes commence the assembly process<sup>99</sup>. In the absence of ATP, the nonproductive pre-primosome is formed through the recognition of the specific PriA-PriB complex at the strong binding site<sup>99</sup>. In the presence of ATP, the two PriA-PriB complexes convert the initial complex due to helicase activity, mostly of the PriA molecule associated with the weak site<sup>99</sup>. As a result, this is the most optimal entity recognized in the subsequent steps of the productive pre-primosome assembly process, which can then move in the 5'→3' direction on the nucleic acid lattice<sup>99</sup>.

reaction, but the process is optimized in the presence of the cofactor<sup>18,25,99</sup>. Thus, in the presence of ATP, the two PriA-PriB complexes transform the initial complex due the helicase activity, mostly of the PriA molecule associated with the weak site<sup>99</sup>. The resulting protein-PAS complex, containing two PriA and two PriB proteins, would then be the most optimal entity recognized in subsequent steps of the assembly process of the primosome<sup>99</sup>.

**Table 6.1. Fluorescence energy transfer efficiencies,  $E_D$ ,  $E_A$ ,  $E$ , and the distances,  $R$  (Å), between the donor and the acceptor located in the vicinity of the 5' and 3' ends of the PAS substrate (Figure 6.13a), associated with different numbers of the PriA molecules, in the absence and presence of the PriB protein and/or ATP.**

Parameter	PAS Alone	PAS 1 PriA	PAS 1 PriA ATP	PAS 1 PriA-PriB	PAS 1 PriA-PriB ATP	PAS 2 PriA	PAS 2 PriA ATP	PAS 2 PriA-PriB	PAS
$E_D$	$0.53 \pm 0.03$	$0.43 \pm 0.03$	$0.25 \pm 0.03$	$0.42 \pm 0.03$	$0.12 \pm 0.02$	$0.43 \pm 0.03$	$0.27 \pm 0.01$	$0.37 \pm 0.03$	$0.05 \pm 0.01$
$E_A$	$0.23 \pm 0.03$	$0.36 \pm 0.03$	$0.18 \pm 0.02$	$0.41 \pm 0.03$	$0.17 \pm 0.02$	$0.40 \pm 0.03$	$0.08 \pm 0.01$	$0.37 \pm 0.03$	$0.09 \pm 0.01$
$E$	$0.33 \pm 0.03$	$0.38 \pm 0.03$	$0.20 \pm 0.02$	$0.41 \pm 0.03$	$0.16 \pm 0.02$	$0.41 \pm 0.03$	$0.10 \pm 0.02$	$0.37 \pm 0.03$	$0.08 \pm 0.02$
$R$ (Å)	$58.5 \pm 3.0$	$56.3 \pm 3.0$	$65.7 \pm 3.0$	$55.1 \pm 3.0$	$68.6 \pm 3.0$	$55.1 \pm 3.0$	$75.5 \pm 4.1$	$56.8 \pm 3.0$	$77.4 \pm 4.1$

## CHAPTER 7

### CONCLUSIONS AND FUTURE DIRECTIONS

#### 7.1 CONCLUSIONS

DNA replication, recombination and repair are tightly synchronized, fundamental processes in the transmission of genetic information from one cell generation to the next<sup>3-5,11-18,32</sup>. These essential processes are carried out by variety of multiple protein complexes including the primosome and the replisome<sup>2-5,11-18,32</sup>. Deregulation of one or more of these processes has been shown to be responsible for various diseases such as cancer and human genetic disorders<sup>19-21,32-77</sup>. In order to understand and cure these serious, often lethal diseases, the mechanistic details of the ordered assembly of these essential molecular machines of DNA and RNA metabolism must be understood<sup>19-21</sup>.

Helicases are a class of ubiquitous enzymes identified in a variety of viruses, bacteriophages, prokaryotes, and eukaryotes, responsible for virtually all aspects of the DNA and RNA metabolism<sup>2-5,22,23</sup>. Numerous human genetic diseases such as Xeroderma pigmentosum, Cockayne's syndrome, Bloom, and Werner syndromes as well as different types of cancer involve defects in proteins that engage in the helicase activity<sup>19-23</sup>. Nevertheless, the mechanistic details on how helicases accomplish their functions are still unknown<sup>2,22,23</sup>.

Helicases are involved in the formation of the replisome, a multiple enzyme complex responsible for DNA replication, as well as in the assembly of the primosome, a large protein complex containing the primase, which catalyzes the DNA priming reaction<sup>2-5,11-25</sup>. The integrity of the replisome and primosome is constantly compromised

due to environmental factors and cellular metabolism that induce damages to the genomic DNA<sup>11-25</sup>. Different organisms employ elaborated pathways to restart DNA replication independent of *oriC* and it is now established that the restart of the replication fork, through the primosome assembly, occurs more often than previously thought<sup>11-25</sup>. It is believed that in *E. Coli*, in the PriA-dependent restart pathway, the PriA helicase specifically recognizes damaged DNA structures and thereby initiates the formation of the primosome which, in its final state, comprises of at least six other proteins: DnaB helicase, DnaC, DnaT, DnaG, PriC, and PriB<sup>11-17</sup>. Multiple and specific protein - protein, and protein - DNA interactions constitute integral part of these large molecular machines and dictate how those molecular motors assemble<sup>5,11-17,25</sup>. However, the mechanisms of these complex interactions are unknown (Figure 1.2)<sup>5-26</sup>.

The research goal of the research project described here was to obtain the first, comprehensive, quantitative model of the initial steps of helicase-directed formation of the primosome by examining an essential role the PriA helicase in the assembly process. By utilizing recombinant, highly purified components of the primosome and a combination of biophysical and biochemical methods, we accomplished that goal. As a result, we present first quantitative description of the initial step of the assembly process of the primosome, paradigm of a large molecular machine of DNA replication.

In order to understand, at the molecular level, how a multi-component system, like the primosome, assembles and functions, one has to identify how its components, interact between one another. In other words, it is crucial to identify under what circumstances the binary complexes of each protein with ssDNA, dsDNA, gapped DNA, and nucleotide cofactors, if any, form. Only when such information is available, tertiary complexes can be studied. In turn, different proteins and different nucleic acid conformations could be mixed, in ordered fashion, and relevant information on formed

complexes could be extracted. Needless to say, finding suitable buffering solution which will make all the components of the system stable, in both high and low concentrations is of crucial importance. This has proven to be a challenge, but it can be dealt with when comprehensive buffering screening is applied.

To this end, in Chapter 2, the recognition of damaged DNA structures by the PriA helicase was addressed<sup>27</sup>. The studies included energetics of the recognition of the gapped ssDNA substrates, and the allosteric role of ATP and ADP in the recognition process<sup>27</sup>. Using quantitative fluorescence titration techniques and hydrodynamic methods it was demonstrated that the PriA-gapped DNA complex has a surprisingly low total site-size corresponding to  $\sim 7$  nucleotides, as compared to the site-size of  $\sim 20$  nucleotides of the enzyme-ssDNA complex<sup>1,27,56,126</sup>. The strong DNA-binding subsite of the PriA helicase was indicated to be involved in these interactions<sup>27</sup>. It was revealed that the helicase has a strong preference for short ssDNA gaps with 4 - 5 nucleotides with the affinity,  $\sim 3$  and  $\sim 2$  orders of magnitude larger than the affinities for the ss and dsDNAs, respectively<sup>27</sup>. Furthermore, it was discovered that binding of ATP to the strong and weak nucleotide-binding sites of the helicase eliminates the selectivity of the enzyme for the size of the gap, while saturation of both sites with ADP leads to amplified affinity for the ssDNA gap containing 5 nucleotides and engagement of additional protein area in interactions with the nucleic acid<sup>27</sup>. One of the most interesting results, presented in Chapter 2, is that PriA helicase possesses the ability to bind to dsDNA<sup>27</sup>. This intriguing characteristic of the PriA helicase may be important in the formation of the primosome and was validated quantitatively in Chapter 3 and Chapter 6<sup>27,81,99</sup>.

Using the fluorescence titration, analytical ultracentrifugation, and photo-cross-linking techniques it was shown in Chapter 3 that the *E. coli* PriA helicase, indeed, binds to dsDNA with high affinity<sup>92</sup>. The PriA protein binds the dsDNA using the strong DNA-

binding subsite located on the helicase domain of the PriA protein, and the total site-size of the PriA-dsDNA complex is only  $5 \pm 1$  bps<sup>92</sup>. PriA's dsDNA intrinsic affinity is considerably higher than the affinity for ssDNA affinity and the binding process is accompanied by a significant positive cooperativity<sup>92</sup>. Association of cofactors with strong and weak nucleotide-binding sites of PriA profoundly affects the intrinsic affinity and cooperativity, without affecting the stoichiometry of PriA-dsDNA complex<sup>92</sup>. The coordinated action of both nucleotide-binding sites on the PriA - dsDNA interactions depends on the structure of the phosphate group which is interesting in the context of the PriA helicase function in recognizing primosome assembly site (PAS) (Chapter 6)<sup>92,99</sup>.

Trypsin digestion experiments show that the PriA helicase is build out of two functional domains (Figure 3.10)<sup>92,97</sup>. The strong DNA-binding subsite located on the helicase domain of the PriA helicase has been implemented in the recognition of the ssDNA gap structures, dsDNA, and ssDNA interactions<sup>27,56,81</sup>. Chapter 4, in turn, is devoted to the functional energetics of interactions of the PriA helicase 181aa N-terminal domain with the DNA and nucleotide cofactors. Using the quantitative fluorescence titration, photo-cross-linking, and analytical ultracentrifugation methods, we have shown that isolated 181aa N-terminal domain of PriA forms a stable dimer in solution. Only one monomer of the domain dimer binds the DNA and the DNA-binding subsite engages in direct interactions with  $5 \pm 1$  nucleotides. The results presented in Chapter 4 provide additional experimental evidence that the strong and weak DNA subsites of the intact PriA helicase molecule are spatially separated<sup>56,61</sup>. The subsite located on 181aa N-terminal domain has a slight preference for the 3'-end OH group of the DNA and lacks any significant base specificity, though it has a significant dsDNA affinity. One of the most exciting findings, described in Chapter 4, has to do with the discovery of the nucleotide-binding site on the 181aa N-terminal domain of PriA. The specific ADP effect

on the domain DNA-binding subsite indicates that in the intact helicase, ADP not only opens the subsite but also increases its intrinsic affinity of PriA for the DNA. It stands to reason that the allosteric effect of the weak nucleotide-binding site has to do with the translocation or unwinding of the duplex DNA by the helicase. These findings are the first experimental results pointing to the mechanism of the PriA helicase translocation and/or hydrolysis and will be further evaluated by the Bujalowski's group.

The interactions of PriB with PriA-PAS complex are proposed to be a crucial step in the assembly process of the primosome. However, in order to be able to dissect, at the molecular level, the assembly of the primosome and the nature of multiple protein - protein and protein - nucleic acid interactions, it is essential to understand energetic of PriB - ssDNA, PriB - dsDNA complex formation. Therefore, in Chapter 5, quantitative analysis of the interactions of the *Escherichia coli* primosomal PriB protein with a single-stranded DNA was carried out using quantitative fluorescence titration, photo-cross-linking, and analytical ultracentrifugation techniques<sup>81</sup>. The total site-size of the PriB dimer-ssDNA complex is  $12 \pm 1$  nucleotides<sup>81</sup>. The protein dimer has a single, functionally homogeneous, DNA binding site as shown by the photo-cross-linking experiments<sup>81</sup>. The intrinsic binding process is an entropy-driven reaction, suggesting strongly that the DNA association induces a large conformational change in the protein<sup>81</sup>. The PriB protein shows a dramatically strong preference for the homo-pyrimidine oligomers with an intrinsic affinity higher by about three orders of magnitude, as compared to the homo-purine oligomers<sup>81</sup>. This dramatic preference for the homo-pyrimidine oligomers is very intriguing in the context of the physiological functions of PriA helicase. Since PriA is proposed to be involved in the recognition of the specific DNA structures, like the damaged DNA, and PAS, it is tempting to speculate that the recognition process may be facilitated by the base composition around the damaged DNA



site or PAS structure. This interesting possibility is being currently examined in the Bujalowski's lab.

Finally, knowing intricate nature of PriA - ssDNA / - dsDNA and PriB - ssDNA / - dsDNA interactions, in Chapter 6, thermodynamics of the binary PriA-PriB and tertiary PriA-PriB-ssDNA, PriA-PriB-dsDNA, PriA-PriB-PAS complexes was examined. As a result, direct quantitative analysis of the initial steps in the primosome assembly, involving the PriA and PriB proteins and the minimal primosome assembly site (PAS) of phage phiX174, has been performed using fluorescence intensity and anisotropy titration, and fluorescence resonance energy transfer techniques<sup>99</sup>. It was shown that the primosome assembly site has two discrete PriA binding sites<sup>99</sup>. Binding of the PriB dimer to the PriA-PAS complex, a next step in the formation of the primosome, dramatically increases the affinity of PriA for the strong binding site<sup>99</sup>. Moreover, it was shown that the PriA-PriB complex can form independently of the DNA and is able to directly recognize the PAS with the affinity much higher than PriA alone; therefore, the high affinity state of PriA is generated through PriA - PriB interactions<sup>99</sup>. These surprising results change a current thinking about the initial steps involved in the primosome formation, and establish the first quantitative framework to study, at the molecular level, the assembly mechanism of a large molecular machine involved in DNA replication.

## **7.2 FUTURE DIRECTIONS**


By building on the framework established in this research project subsequent steps in the primosome assembly will be examined. In turn, comprehensive molecular model of the helicase-directed formation of the primosome will be established.

In order to be able to build a scaffold for the primosome assembly the association of the DnaT protein with the PriA-PAS-PriB complex will be addressed. The studies will include examination of energetics, topology and dynamics of the DnaT - ssDNA, DnaT - dsDNA, and the recognition of the PriA-PAS-PriB complex by DnaT, as well as the allosteric role of ATP and ADP in the recognition process. Although absolutely necessary, the specific role of DnaT in the primosome is still unknown<sup>15,25,130,131</sup>. Our hypothesis is that DnaT binds to the PriA-PAS-PriB complex and provide stopping signal for the PriA unwinding activity, and/or serves as a specific element in a subsequent step of the recognition by the DnaB-DnaC complex. However, the association process may be much more involved than that and several possible complexes can form. The stability of the DnaT trimer in solution has never been addressed and it could affect the interactions and the stoichiometry of the PriA-PAS-PriB complex<sup>15,25,130,131</sup>. Moreover, nothing is known about DnaT - ssDNA and DnaT - dsDNA interactions which may influence the assembly process of the primosome at the molecular level. Thus, it is crucial to address the DnaT interactions with different conformations of the DNA *prior* to any attempt to characterize interactions of DnaT with a PriA-PAS-PriB complex.

The next step in the assembly of the primosome is the recognition of formed multi-protein scaffold PriA - PAS - PriB - DnaT by the DnaB - DnaC complex<sup>15,24,25,47,129,130</sup>. A fascinating aspect of the primosome assembly is the role of the DnaC protein. Because the DnaC protein is absolutely necessary for the DnaB helicase to enter the primosome complex it has been proposed that all the interactions between DnaB and primosome components are transmitted through the DnaC protein<sup>129,130</sup>. Nevertheless, how the DnaB-DnaC complex binds to the PriA-PAS-PriB-DnaT scaffold is unknown, even at the level of the stoichiometry of the components of the reaction<sup>15,25,47,130</sup>. Current thinking about this complex process is that a single DnaB -


DnaC complex, with six DnaC molecules bound to the hexameric DnaB helicase enter the pre-primosome, but subsequently all DnaC molecules are proposed to leave the complex, although firm experimental evidence for the complete release of all DnaC molecules from the pre-primosome are not available<sup>129</sup>. Galletto *et. al.*, has shown that DnaB-DnaC complex may exist, in solution, with a different numbers of DnaC molecules, indicating that less than six DnaC molecules may be present in the mature primosome<sup>77</sup>.

## Appendix

 **Copyright Clearance Center**

**RightsLink®**

[Home](#) [Account Info](#) [Help](#)



**Title:** The Escherichia coli PriA Helicase Specifically Recognizes Gapped DNA Substrates: EFFECT OF THE TWO NUCLEOTIDE-BINDING SITES OF THE ENZYME ON THE RECOGNITION PROCESS

**Author:** Michal R. Szymanski, Maria J. Jezewska, Włodzimierz Bujalowski

**Publication:** Journal of Biological Chemistry

**Publisher:** The American Society for Biochemistry and Molecular Biology

**Date:** Mar 26, 2010

Copyright © 2010, by the American Society for Biochemistry and Molecular Biology

Logged in as:  
Michal Szymanski  
Account #:  
3000427606

[LOGOUT](#)

### Welcome to Rightslink for Commercial Use

The American Society for Biochemistry and Molecular Biology has partnered with Copyright Clearance Center's Rightslink service to offer a variety of options for reusing ASBMB content **for Commercial Use, including authors reusing content by a commercial publisher**. Select the "I would like to ..." drop-down menu to view the many reuse options available to you.

I would like to...

**For Non-profit/Non-commercial uses: You are FREE to copy, distribute, transmit and to adapt the work under the following conditions:**

**Attribution.** You must attribute the work in the manner specified by the author or licensor (but not in any way that suggests that they endorse you or your use of the work).

**Non-commercial.** You may not use the work for commercial purposes; including original authors reusing content by a commercial publisher.

Supplier	Elsevier Limited The Boulevard, Langford Lane Kidlington, Oxford, OX5 1GB, UK
Registered Company Number	1982084
Customer name	Michal R Szymanski
Customer address	The University of Texas Medical Branch Galveston, TX 77555
License number	2705410653859
License date	Jul 10, 2011
Licensed content publisher	Elsevier
Licensed content publication	Journal of Molecular Biology
Licensed content title	The <i>Escherichia coli</i> PriA Helicase–Double-Stranded DNA Complex: Location of the Strong DNA-Binding Subsite on the Helicase Domain of the Protein and the Affinity Control by the Two Nucleotide-Binding Sites of the Enzyme
Licensed content author	Michal R. Szymanski, Maria J. Jezewska, Włodzimierz Bujalowski
Licensed content date	17 September 2010
Licensed content volume number	402
Licensed content issue number	2
Number of pages	19
Start Page	344
End Page	362
Type of Use	reuse in a thesis/dissertation
Portion	full article
Format	both print and electronic
Are you the author of this Elsevier article?	Yes
Will you be translating?	No
Order reference number	
Title of your thesis/dissertation	Helicase Initiated Assembly of Macromolecular Machines Involved in DNA Replication
Expected completion date	Aug 2011



RightsLink®

[Home](#)

[Account Info](#)

[Help](#)



ACS Publications  
High quality. High impact.

**Title:** The N-Terminal Domain of the E. coli PriA Helicase Contains Both the DNA- and the Nucleotide-Binding Sites. Energetics of Domain-DNA Interactions and Allosteric Effect of the Nucleotide Cofactors

**Author:** Michal R. Szymanski et al.

**Publication:** Biochemistry

**Publisher:** American Chemical Society

**Date:** Sep 1, 2011

Copyright © 2011, American Chemical Society

Logged in as:

Michal Szymanski

Account #:

3000427606

[LOGOUT](#)

#### PERMISSION/LICENSE IS GRANTED FOR YOUR ORDER AT NO CHARGE

This type of permission/license, instead of the standard Terms & Conditions, is sent to you because no fee is being charged for your order. Please note the following:

- Permission is granted for your request in both print and electronic formats.
- If figures and/or tables were requested, they may be adapted or used in part.
- Please print this page for your records and send a copy of it to your publisher/graduate school.
- Appropriate credit for the requested material should be given as follows: "Reprinted (adapted) with permission from (COMPLETE REFERENCE CITATION). Copyright (YEAR) American Chemical Society." Insert appropriate information in place of the capitalized words.
- One-time permission is granted only for the use specified in your request. No additional uses are granted (such as derivative works or other editions). For any other uses, please submit a new request.

Supplier	Elsevier Limited The Boulevard, Langford Lane Kidlington, Oxford, OX5 1GB, UK
Registered Company Number	1982084
Customer name	Michal R Szymanski
Customer address	The University of Texas Medical Branch Galveston, TX 77555
License number	2705410945900
License date	Jul 10, 2011
Licensed content publisher	Elsevier
Licensed content publication	Journal of Molecular Biology
Licensed content title	Interactions of the <i>Escherichia coli</i> Primosomal PriB Protein with the Single-stranded DNA. Stoichiometries, Intrinsic Affinities, Cooperativities, and Base Specificities
Licensed content author	Michal R. Szymanski, Maria J. Jezewska, Wlodzimierz Bujalowski
Licensed content date	23 April 2010
Licensed content volume number	398
Licensed content issue number	1
Number of pages	18
Start Page	8
End Page	25
Type of Use	reuse in a thesis/dissertation
Portion	full article
Format	both print and electronic
Are you the author of this Elsevier article?	Yes
Will you be translating?	No
Order reference number	
Title of your thesis/dissertation	Helicase Initiated Assembly of Macromolecular Machines Involved in DNA Replication
Expected completion date	Aug 2011

Supplier	Elsevier Limited The Boulevard, Langford Lane Kidlington, Oxford, OX5 1GB, UK
Registered Company Number	1982084
Customer name	Michal R Szymanski
Customer address	The University of Texas Medical Branch Galveston, TX 77555
License number	2720350483960
License date	Aug 01, 2011
Licensed content publisher	Elsevier
Licensed content publication	Journal of Molecular Biology
Licensed content title	Binding of Two PriA–PriB Complexes to the Primosome Assembly Site Initiates Primosome Formation
Licensed content author	Michal R. Szymanski, Maria J. Jezewska, Włodzimierz Bujalowski
Licensed content date	27 May 2011
Licensed content volume number	n/a
Licensed content issue number	n/a
Number of pages	1
Start Page	
End Page	
Type of Use	reuse in a thesis/dissertation
Intended publisher of new work	other
Portion	full article
Format	both print and electronic
Are you the author of this Elsevier article?	Yes
Will you be translating?	No
Order reference number	
Title of your thesis/dissertation	Helicase Initiated Assembly of Macromolecular Machines Involved in DNA Replication
Expected completion date	Aug 2011



## References

1. Bujalowski, W. (2006). Thermodynamic and kinetic methods of analyses of protein-nucleic acid interactions. From simpler to more complex systems. *Chem Rev* **106**, 556-606.
2. Delagoutte, E. & von Hippel, P. H. (2002). Helicase mechanisms and the coupling of helicases within macromolecular machines. Part I: Structures and properties of isolated helicases. *Q Rev Biophys* **35**, 431-478.
3. Yao, N. Y. & O'Donnell, M. (2009). Replisome structure and conformational dynamics underlie fork progression past obstacles. *Curr Opin Cell Biol* **21**, 336-343.
4. Johnson, A. & O'Donnell, M. (2005). Cellular DNA replicases: components and dynamics at the replication fork. *Annu Rev Biochem* **74**, 283-315.
5. Kornberg, A. & Baker, T. A. (1992). DNA Replication, pp. 275–293, Freeman, San Francisco, CA.
6. Kong, X. P., Onrust, R., O'Donnell, M. & Kuriyan, J. (1992). Three-dimensional structure of the beta subunit of E. coli DNA polymerase III holoenzyme: a sliding DNA clamp. *Cell* **69**, 425-437.
7. Bujalowski, W. & Jezewska, M. J. (1995). Interactions of Escherichia coli primary replicative helicase DnaB protein with single-stranded DNA. The nucleic acid does not wrap around the protein hexamer. *Biochemistry* **34**, 8513-8519.
8. Jezewska, M. J., Rajendran, S., Bujalowska, D. & Bujalowski, W. (1998). Does single-stranded DNA pass through the inner channel of the protein hexamer in the complex with the Escherichia coli DnaB Helicase? Fluorescence energy transfer studies. *J Biol Chem* **273**, 10515-10529.

9. Galletto, R., Jezewska, M. J. & Bujalowski, W. (2004). Unzipping mechanism of the double-stranded DNA unwinding by a hexameric helicase: the effect of the 3' arm and the stability of the dsDNA on the unwinding activity of the Escherichia coli DnaB helicase. *J Mol Biol* **343**, 101-114.
10. Frick, D. N. & Richardson, C. C. (2001). DNA primases. *Annu Rev Biochem* **70**, 39-80.
11. Heller, R. C. & Marians, K. J. (2006). Replication fork reactivation downstream of a blocked nascent leading strand. *Nature* **439**, 557-562.
12. Heller, R. C. & Marians, K. J. (2007). Non-replicative helicases at the replication fork. *DNA Repair (Amst)* **6**, 945-952.
13. Xu, L. & Marians, K. J. (2003). PriA mediates DNA replication pathway choice at recombination intermediates. *Mol Cell* **11**, 817-826.
14. Jones, J. M. & Nakai, H. (1999). Duplex opening by primosome protein PriA for replisome assembly on a recombination intermediate. *J Mol Biol* **289**, 503-516.
15. Ng, J. Y. & Marians, K. J. (1996). The ordered assembly of the phiX174-type primosome. II. Preservation of primosome composition from assembly through replication. *J Biol Chem* **271**, 15649-15655.
16. Lopper, M., Boonsombat, R., Sandler, S. J. & Keck, J. L. (2007). A hand-off mechanism for primosome assembly in replication restart. *Mol Cell* **26**, 781-793.
17. Jones, J. M. & Nakai, H. (2001). Escherichia coli PriA helicase: fork binding orients the helicase to unwind the lagging strand side of arrested replication forks. *J Mol Biol* **312**, 935-947.
18. Ng, J. Y. & Marians, K. J. (1996). The ordered assembly of the phiX174-type primosome. I. Isolation and identification of intermediate protein-DNA complexes. *J Biol Chem* **271**, 15642-15648.

19. Hanawalt, P. C. (1994). Transcription-coupled repair and human disease. *Science* **266**, 1957-1958.
20. Ellis, N. A. (1997). DNA helicases in inherited human disorders. *Curr Opin Genet Dev* **7**, 354-363.
21. Tanaka, K. & Wood, R. D. (1994). Xeroderma pigmentosum and nucleotide excision repair of DNA. *Trends Biochem Sci* **19**, 83-86.
22. Delagoutte, E. & von Hippel, P. H. (2003). Helicase mechanisms and the coupling of helicases within macromolecular machines. Part II: Integration of helicases into cellular processes. *Q Rev Biophys* **36**, 1-69.
23. Enemark, E. J. & Joshua-Tor, L. (2006). Mechanism of DNA translocation in a replicative hexameric helicase. *Nature* **442**, 270-275.
24. Marians, K. J. (1999). PriA: at the crossroads of DNA replication and recombination. *Prog Nucleic Acid Res Mol Biol* **63**, 39-67.
25. Allen, G. C., Jr. & Kornberg, A. (1993). Assembly of the primosome of DNA replication in Escherichia coli. *J Biol Chem* **268**, 19204-19209.
26. Arai, K., Arai, N., Shlomai, J. & Kornberg, A. (1980). Replication of duplex DNA of phage phi X174 reconstituted with purified enzymes. *Proc Natl Acad Sci U S A* **77**, 3322-3326.
27. Szymanski, M. R., Jezewska, M. J. & Bujalowski, W. (2010). The Escherichia coli PriA helicase specifically recognizes gapped DNA substrates: effect of the two nucleotide-binding sites of the enzyme on the recognition process. *J Biol Chem* **285**, 9683-9696.
28. Leipec, D. D., Wolf, Y. I., Koonin, E. V. & Aravind, L. (2002). Classification and evolution of P-loop GTPases and related ATPases. *J Mol Biol* **317**, 41-72.

29. Fairman-Williams, M.E., Guenther, U-P. & Jankowsky E. (2010). SF1 and SF2 helicases: family matters. *Curr Opin Stru Biol* **20**, 313-324.
30. Pyle, A.M. (2008). Translocation and unwinding mechanisms of RNA and DNA helicases. *Annu Rev Biophys* **37**, 317–336.
31. Abdelhaleem, M. (2004). Do human RNA helicases have a role in cancer? *Biochim Biophys Acta* **1704**, 37-46.
32. Masai, H., Tanaka, T. & Kohda, D. (2010). Stalled replication forks: making ends meet for recognition and stabilization. *Bioessays* **32**, 687-697.
33. Cox, M. M., Goodman, M. F., Kreuzer, K. N., Sherratt, D. J., Sandler, S. J. & Marians, K. J. (2000). The importance of repairing stalled replication forks. *Nature* **404**, 37-41.
34. Marians, K. J. (2000). PriA-directed replication fork restart in Escherichia coli. *Trends Biochem Sci* **25**, 185-189.
35. Sandler, S. J. & Marians, K. J. (2000). Role of PriA in replication fork reactivation in Escherichia coli. *J Bacteriol* **182**, 9-13.
36. Marians, K. J. (2004). Mechanisms of replication fork restart in Escherichia coli. *Philos Trans R Soc Lond B Biol Sci* **359**, 71-77.
37. Courcelle, J., Crowley, D. J. & Hanawalt, P. C. (1999). Recovery of DNA replication in UV-irradiated Escherichia coli requires both excision repair and recF protein function. *J Bacteriol* **181**, 916-922.
38. Lee, E. H. & Kornberg, A. (1991). Replication deficiencies in priA mutants of Escherichia coli lacking the primosomal replication n' protein. *Proc Natl Acad Sci U S A* **88**, 3029-3032.

39. Nurse, P., Zavitz, K. H. & Marians, K. J. (1991). Inactivation of the Escherichia coli priA DNA replication protein induces the SOS response. *J Bacteriol* **173**, 6686-6693.
40. Zavitz, K. H. & Marians, K. J. (1992). ATPase-deficient mutants of the Escherichia coli DNA replication protein PriA are capable of catalyzing the assembly of active primosomes. *J Biol Chem* **267**, 6933-6940.
41. Masai, H., Asai, T., Kubota, Y., Arai, K. & Kogoma, T. (1994). Escherichia coli PriA protein is essential for inducible and constitutive stable DNA replication. *Embo J* **13**, 5338-5345.
42. Kogoma, T., Cadwell, G. W., Barnard, K. G. & Asai, T. (1996). The DNA replication priming protein, PriA, is required for homologous recombination and double-strand break repair. *J Bacteriol* **178**, 1258-1264.
43. Sandler, S. J. (2000). Multiple genetic pathways for restarting DNA replication forks in Escherichia coli K-12. *Genetics* **155**, 487-497.
44. Gregg, A. V., McGlynn, P., Jaktaji, R. P. & Lloyd, R. G. (2002). Direct rescue of stalled DNA replication forks via the combined action of PriA and RecG helicase activities. *Mol Cell* **9**, 241-251.
45. Sandler, S. J., Marians, K. J., Zavitz, K. H., Coutu, J., Parent, M. A. & Clark, A. J. (1999). dnaC mutations suppress defects in DNA replication- and recombination-associated functions in priB and priC double mutants in Escherichia coli K-12. *Mol Microbiol* **34**, 91-101.
46. Heller, R. C. & Marians, K. J. (2005). Unwinding of the nascent lagging strand by Rep and PriA enables the direct restart of stalled replication forks. *J Biol Chem* **280**, 34143-34151.

47. Schekman, R., Weiner, J. H., Weiner, A. & Kornberg, A. (1975). Ten proteins required for conversion of phiX174 single-stranded DNA to duplex form in vitro. Resolution and reconstitution. *J Biol Chem* **250**, 5859-5865.
48. Wickner, S. & Hurwitz, J. (1975). Association of phiX174 DNA-dependent ATPase activity with an Escherichia coli protein, replication factor Y, required for in vitro synthesis of phiX174 DNA. *Proc Natl Acad Sci U S A* **72**, 3342-3346.
49. Lee, E. H., Masai, H., Allen, G. C., Jr. & Kornberg, A. (1990). The priA gene encoding the primosomal replicative n' protein of Escherichia coli. *Proc Natl Acad Sci U S A* **87**, 4620-4624.
50. Nurse, P., DiGate, R. J., Zavitz, K. H. & Marians, K. J. (1990). Molecular cloning and DNA sequence analysis of Escherichia coli priA, the gene encoding the primosomal protein replication factor Y. *Proc Natl Acad Sci U S A* **87**, 4615-4619.
51. Gorbalenya, A. E., Koonin, E. V., Donchenko, A. P. & Blinov, V. M. (1989). Two related superfamilies of putative helicases involved in replication, recombination, repair and expression of DNA and RNA genomes. *Nucleic Acids Res* **17**, 4713-4730.
52. Gorbalenya, A. E. & Koonin, E. V. (1993). Helicases: amino acid sequence comparisons and structure-function relationship. *Curr Opin Struct Biol* **3**, 419-429.
53. Singleton, M. R., Dillingham, M. S. & Wigley, D. B. (2007). Structure and mechanism of helicases and nucleic acid translocases. *Annu Rev Biochem* **76**, 23-50.

54. Shlomai, J. & Kornberg, A. (1980). A prepriming DNA replication enzyme of *Escherichia coli*. I. Purification of protein  $\eta$ : a sequence-specific, DNA-dependent ATPase. *J Biol Chem* **255**, 6789-6793.
55. Lee, M. S. & Marians, K. J. (1987). *Escherichia coli* replication factor Y, a component of the primosome, can act as a DNA helicase. *Proc Natl Acad Sci U S A* **84**, 8345-8349.
56. Jezewska, M. J., Rajendran, S. & Bujalowski, W. (2000). *Escherichia coli* replicative helicase PriA protein-single-stranded DNA complex. Stoichiometries, free energy of binding, and cooperativities. *J Biol Chem* **275**, 27865-27873.
57. Jezewska, M. J. & Bujalowski, W. (2000). Interactions of *Escherichia coli* replicative helicase PriA protein with single-stranded DNA. *Biochemistry* **39**, 10454-10467.
58. Galletto, R., Jezewska, M. J. & Bujalowski, W. (2004). Multistep sequential mechanism of *Escherichia coli* helicase PriA protein-ssDNA interactions. Kinetics and energetics of the active ssDNA-searching site of the enzyme. *Biochemistry* **43**, 11002-11016.
59. Lucius, A. L., Jezewska, M. J. & Bujalowski, W. (2006). The *Escherichia coli* PriA helicase has two nucleotide-binding sites differing dramatically in their affinities for nucleotide cofactors. 1. Intrinsic affinities, cooperativities, and base specificity of nucleotide cofactor binding. *Biochemistry* **45**, 7202-7216.
60. Lucius, A. L., Jezewska, M. J., Roychowdhury, A. & Bujalowski, W. (2006). Kinetic mechanisms of the nucleotide cofactor binding to the strong and weak nucleotide-binding site of the *Escherichia coli* PriA helicase. 2. *Biochemistry* **45**, 7217-7236.

61. Lucius, A. L., Jezewska, M. J. & Bujalowski, W. (2006). Allosteric interactions between the nucleotide-binding sites and the ssDNA-binding site in the PriA helicase-ssDNA complex. 3. *Biochemistry* **45**, 7237-7255.
62. Jezewska, M. J., Rajendran, S. & Bujalowski, W. (1998). Functional and structural heterogeneity of the DNA binding site of the Escherichia coli primary replicative helicase DnaB protein. *J Biol Chem* **273**, 9058-9069.
63. Jezewska, M. J., Galletto, R. & Bujalowski, W. (2003). Tertiary conformation of the template-primer and gapped DNA substrates in complexes with rat polymerase beta. Fluorescence energy transfer studies using the multiple donor-acceptor approach. *Biochemistry* **42**, 11864-11878.
64. Edelhoch, H. (1967). Spectroscopic determination of tryptophan and tyrosine in proteins. *Biochemistry* **6**, 1948-1954.
65. Gill, S. C. & von Hippel, P. H. (1989). Calculation of protein extinction coefficients from amino acid sequence data. *Anal Biochem* **182**, 319-326.
66. Cantor, R. C. & Schimmel, P. R. (1980). Biophysical Chemistry, vol. II, pp. 591–641 W. H. Freeman, New York.
67. Bujalowski, W., Klonowska, M. M. & Jezewska, M. J. (1994). Oligomeric structure of Escherichia coli primary replicative helicase DnaB protein. *J Biol Chem* **269**, 31350-31358.
68. Schuck, P. (2000). Size-distribution analysis of macromolecules by sedimentation velocity ultracentrifugation and lamm equation modeling. *Biophys J* **78**, 1606-1619.
69. Tanford, C. (1961). Physical Chemistry of Macromolecules, pp. 364–390, John Wiley & Sons, Inc., New York, NY.



70. Lee, J. C. & Timasheff, S. N. (1979). The calculation of partial specific volumes of proteins in 6 M guanidine hydrochloride. *Methods Enzymol* **61**, 49-57.
71. Kuntz, I. D. (1971). Hydration of macromolecules. IV. Polypeptide conformation in frozen solutions. *J Am Chem Soc* **93**, 516-518.
72. Galletto, R., Maillard, R., Jezewska, M. J. & Bujalowski, W. (2004). Global conformation of the Escherichia coli replication factor DnaC protein in absence and presence of nucleotide cofactors. *Biochemistry* **43**, 10988-11001.
73. Bull, H. B. & Breese, K. (1968). Protein hydration. I. Binding sites. *Arch Biochem Biophys* **128**, 488-496.
74. Correia, J. J., Chacko, B. M., Lam, S. S. & Lin, K. (2001). Sedimentation studies reveal a direct role of phosphorylation in Smad3:Smad4 homo- and heterotrimerization. *Biochemistry* **40**, 1473-1482.
75. Stafford, W. F., 3rd. (1992). Boundary analysis in sedimentation transport experiments: a procedure for obtaining sedimentation coefficient distributions using the time derivative of the concentration profile. *Anal Biochem* **203**, 295-301.
76. Marcinowicz, A., Jezewska, M. J. & Bujalowski, W. (2008). Multiple global conformational states of the hexameric RepA helicase of plasmid RSF1010 with different ssDNA-binding capabilities are induced by different numbers of bound nucleotides. Analytical ultracentrifugation and dynamic light scattering studies. *J Mol Biol* **375**, 386-408.
77. Galletto, R., Jezewska, M. J. & Bujalowski, W. (2003). Interactions of the Escherichia coli DnaB helicase hexamer with the replication factor the DnaC protein. Effect of nucleotide cofactors and the ssDNA on protein-protein interactions and the topology of the complex. *J Mol Biol* **329**, 441-465.

78. Roychowdhury, A., Szymanski, M. R., Jezewska, M. J. & Bujalowski, W. (2009). Interactions of the Escherichia coli DnaB-DnaC protein complex with nucleotide cofactors. 1. Allosteric conformational transitions of the complex. *Biochemistry* **48**, 6712-6729.
79. Andreeva, I. E., Roychowdhury, A., Szymanski, M. R., Jezewska, M. J. & Bujalowski, W. (2009). Mechanisms of interactions of the nucleotide cofactor with the RepA protein of plasmid RSF1010. Binding dynamics studied using the fluorescence stopped-flow method. *Biochemistry* **48**, 10620-10636.
80. Andreeva, I. E., Szymanski, M. R., Jezewska, M. J., Galletto, R. & Bujalowski, W. (2009). Dynamics of the ssDNA recognition by the RepA hexameric helicase of plasmid RSF1010: analyses using fluorescence stopped-flow intensity and anisotropy methods. *J Mol Biol* **388**, 751-775.
81. Szymanski, M. R., Jezewska, M. J. & Bujalowski, W. (2010). Interactions of the Escherichia coli primosomal PriB protein with the single-stranded DNA. Stoichiometries, intrinsic affinities, cooperativities, and base specificities. *J Mol Biol* **398**, 8-25.
82. Jezewska, M. J., Rajendran, S. & Bujalowski, W. (2001). Energetics and specificity of Rat DNA polymerase beta interactions with template-primer and gapped DNA substrates. *J Biol Chem* **276**, 16123-16136.
83. Record, M. T., Jr., Lohman, M. L. & De Haseth, P. (1976). Ion effects on ligand-nucleic acid interactions. *J Mol Biol* **107**, 145-158.
84. Record, M. T., Jr., Anderson, C. F. & Lohman, T. M. (1978). Thermodynamic analysis of ion effects on the binding and conformational equilibria of proteins and nucleic acids: the roles of ion association or release, screening, and ion effects on water activity. *Q Rev Biophys* **11**, 103-178.

85. Lohman, T. M. & Bujalowski, W. (1991). Thermodynamic methods for model-independent determination of equilibrium binding isotherms for protein-DNA interactions: spectroscopic approaches to monitor binding. *Methods Enzymol* **208**, 258-290.
86. McGhee, J. D. & von Hippel, P. H. (1974). Theoretical aspects of DNA-protein interactions: co-operative and non-co-operative binding of large ligands to a one-dimensional homogeneous lattice. *J Mol Biol* **86**, 469-489.
87. Jezewska, M. J. & Bujalowski, W. (1996). A general method of analysis of ligand binding to competing macromolecules using the spectroscopic signal originating from a reference macromolecule. Application to Escherichia coli replicative helicase DnaB protein nucleic acid interactions. *Biochemistry* **35**, 2117-2128.
88. Epstein, I. R. (1978). Cooperative and non-cooperative binding of large ligands to a finite one-dimensional lattice. A model for ligand-oligonucleotide interactions. *Biophys Chem* **8**, 327-339.
89. Bujalowski, W., Lohman, T. M. & Anderson, C. F. (1989). On the cooperative binding of large ligands to a one-dimensional homogeneous lattice: the generalized three-state lattice model. *Biopolymers* **28**, 1637-1643.
90. Tolman, G. L., Barrio, J. R. & Leonard, N. J. (1974). Chloroacetaldehyde-modified dinucleoside phosphates. Dynamic fluorescence quenching and quenching due to intramolecular complexation. *Biochemistry* **13**, 4869-4878.
91. Ledneva, R. K., Razjivin, A. P., Kost, A. A. & Bogdanov, A. A. (1978). Interaction of tobacco mosaic virus protein with synthetic polynucleotides containing a fluorescent label: optical properties of poly(A,epsilonA) and poly(C,epsilonC) copolymers and energy migration from the tryptophan to 1,N6-

- ethenoadenine or 3,N4-ethenocytosine residues in RNP. *Nucleic Acids Res* **5**, 4225-4243.
92. Szymanski, M. R., Jezewska, M. J. & Bujalowski, W. (2010). The Escherichia coli PriA helicase-double-stranded DNA complex: location of the strong DNA-binding subsite on the helicase domain of the protein and the affinity control by the two nucleotide-binding sites of the enzyme. *J Mol Biol* **402**, 344-362.
  93. Sambrook, J., Fritsch, E. F. & Maniatis, T. (1989). Molecular Cloning. Laboratory Manual, vol. 1, pp. 6 - 39, Cold Spring Harbor Laboratory Press, Cold Spring Harbor, NY.
  94. Bujalowski, W. & Jezewska, M. J. (2000). In Spectrophotometry and Spectrofluorimetry. A Practical Approach (Gore,M.G., ed.), pp. 141–165, Oxford University Press, New York.
  95. Jezewska, M. J. & Bujalowski, W. (1997). Quantitative analysis of ligand-macromolecule interactions using differential dynamic quenching of the ligand fluorescence to monitor the binding. *Biophys Chem* **64**, 253-269.
  96. Connors, K. A. (1990). Chemical Kinetics. The Study of Reaction Rates in Solution, pp. 187–200, VCH Publishers, New York, NY.
  97. Tanaka, T., Mizukoshi, T., Taniyama, C., Kohda, D., Arai, K. & Masai, H. (2002). DNA binding of PriA protein requires cooperation of the N-terminal D-loop/arrested-fork binding and C-terminal helicase domains. *J Biol Chem* **277**, 38062-38071.
  98. Chen, H. W., North, S. H. & Nakai, H. (2004). Properties of the PriA helicase domain and its role in binding PriA to specific DNA structures. *J Biol Chem* **279**, 38503-38512.

99. Szymanski, M. R., Jezewska, M. J. & Bujalowski, W. (2011). Binding of Two PriA-PriB Complexes to the Primosome Assembly Site Initiates Primosome Formation. *J Mol Biol* **411**(1), 123-142.
100. Szymanski, M.R., Bujalowski, P.J., Jezewska, M.J., Gmyrek, A.M., Bujalowski, W. (2011). The N-Terminal Domain of the *Escherichia coli* PriA Helicase Contains Both the DNA- and Nucleotide-Binding Sites. Energetics of Domain-DNA Interactions and Allosteric Effect of the Nucleotide Cofactors. *Biochemistry* **50**(43), 9167-9183.
101. Bujalowski, W. & Klonowska, M. M. (1993). Negative cooperativity in the binding of nucleotides to *Escherichia coli* replicative helicase DnaB protein. Interactions with fluorescent nucleotide analogs. *Biochemistry* **32**, 5888-900.
102. Williams, K. R. & Konigsberg, W. H. (1991). Identification of amino acid residues at interface of protein-nucleic acid complexes by photochemical cross-linking. *Methods Enzymol* **208**, 516-539.
103. Shlomai, J. & Kornberg, A. (1980). An *Escherichia coli* replication protein that recognizes a unique sequence within a hairpin region in phi X174 DNA. *Proc Natl Acad Sci U S A* **77**, 799-803.
104. Sasaki, K., Ose, T., Okamoto, N., Maenaka, K., Tanaka, T., Masai, H., Saito, M., Shirai, T. & Kohda, D. (2007). Structural basis of the 3'-end recognition of a leading strand in stalled replication forks by PriA. *Embo J* **26**, 2584-2593.
105. Wickner, S. & Hurwitz, J. (1974). Conversion of phiX174 viral DNA to double-stranded form by purified *Escherichia coli* proteins. *Proc Natl Acad Sci U S A* **71**, 4120-4124.

106. Low, R. L., Shlomai, J. & Kornberg, A. (1982). Protein n, a primosomal DNA replication protein of Escherichia coli. Purification and characterization. *J Biol Chem* **257**, 6242-6250.
107. Zavitz, K. H., DiGate, R. J. & Marians, K. J. (1991). The priB and priC replication proteins of Escherichia coli. Genes, DNA sequence, overexpression, and purification. *J Biol Chem* **266**, 13988-13995.
108. Allen, G. C., Jr. & Kornberg, A. (1991). The priB gene encoding the primosomal replication n protein of Escherichia coli. *J Biol Chem* **266**, 11610-11613.
109. Liu, J., Nurse, P. & Marians, K. J. (1996). The ordered assembly of the phiX174-type primosome. III. PriB facilitates complex formation between PriA and DnaT. *J Biol Chem* **271**, 15656-15561.
110. Liu, J. H., Chang, T. W., Huang, C. Y., Chen, S. U., Wu, H. N., Chang, M. C. & Hsiao, C. D. (2004). Crystal structure of PriB, a primosomal DNA replication protein of Escherichia coli. *J Biol Chem* **279**, 50465-50471.
111. Shioi, S., Ose, T., Maenaka, K., Shiroishi, M., Abe, Y., Kohda, D., Katayama, T. & Ueda, T. (2005). Crystal structure of a biologically functional form of PriB from Escherichia coli reveals a potential single-stranded DNA-binding site. *Biochem Biophys Res Commun* **326**, 766-776.
112. Lopper, M., Holton, J. M. & Keck, J. L. (2004). Crystal structure of PriB, a component of the Escherichia coli replication restart primosome. *Structure* **12**, 1967-1975.
113. Huang, C. Y., Hsu, C. H., Sun, Y. J., Wu, H. N. & Hsiao, C. D. (2006). Complexed crystal structure of replication restart primosome protein PriB reveals a novel single-stranded DNA-binding mode. *Nucleic Acids Res* **34**, 3878-3886.

114. Low, R. L., Arai, K. & Kornberg, A. (1981). Conservation of the primosome in successive stages of phi X174 DNA replication. *Proc Natl Acad Sci U S A* **78**, 1436-1440.
115. Kowalczykowski, S. C., Lonberg, N., Newport, J. W. & von Hippel, P. H. (1981). Interactions of bacteriophage T4-coded gene 32 protein with nucleic acids. I. Characterization of the binding interactions. *J Mol Biol* **145**, 75-104.
116. Jezewska, M. J., Kim, U. S. & Bujalowski, W. (1996). Binding of Escherichia coli primary replicative helicase DnaB protein to single-stranded DNA. Long-range allosteric conformational changes within the protein hexamer. *Biochemistry* **35**, 2129-2145.
117. Jezewska, M. J., Marcinowicz, A., Lucius, A. L. & Bujalowski, W. (2006). DNA polymerase X from African swine fever virus: quantitative analysis of the enzyme-ssDNA interactions and the functional structure of the complex. *J Mol Biol* **356**, 121-141.
118. Hill, T. L. & Levitzki, A. (1980). Subunit neighbor interactions in enzyme kinetics: half-of-the-sites reactivity in a dimer. *Proc Natl Acad Sci U S A* **77**, 5741-5745.
119. von Hippel, P. H. & Schleich, T. (1969). In *Structure of Biological Macromolecules* (Timasheff, S. & Fasman, G. D., eds), pp. 417-575, Marcel Dekker, NY.
120. Raghunathan, S., Kozlov, A. G., Lohman, T. M. & Waksman, G. (2000). Structure of the DNA binding domain of E. coli SSB bound to ssDNA. *Nat Struct Biol* **7**, 648-652.

121. Sandler, S. J. (2005). Requirements for replication restart proteins during constitutive stable DNA replication in *Escherichia coli* K-12. *Genetics* **169**, 1799-1806.
122. Greenbaum, J. H. & Marians, K. J. (1985). Mutational analysis of primosome assembly sites. Evidence for alternative DNA structures. *J Biol Chem* **260**, 12266-12272.
123. Marcinowicz, A., Jezewska, M. J., Bujalowski, P. J. & Bujalowski, W. (2007). Structure of the tertiary complex of the RepA hexameric helicase of plasmid RSF1010 with the ssDNA and nucleotide cofactors in solution. *Biochemistry* **46**, 13279-13296.
124. Yang, M. & Millar, D. P. (1997). Fluorescence resonance energy transfer as a probe of DNA structure and function. *Methods Enzymol* **278**, 417-444.
125. Vamosi, G. & Clegg, R. M. (1998). The helix-coil transition of DNA duplexes and hairpins observed by multiple fluorescence parameters. *Biochemistry* **37**, 14300-14316.
126. Bujalowski, W. & Jezewska, M. J. (2011). Macromolecular competition titration method accessing thermodynamics of the unmodified macromolecule-ligand interactions through spectroscopic titrations of fluorescent analogs. *Methods Enzymol* **488**, 17-57.
127. Bujalowski, W. & Jezewska, M. J. (2009). Thermodynamic Analysis of the Structure-Function Relationship in the Total DNA-Binding Site of Enzyme-DNA Complexes. *Methods Enzymol* **466**, 293-324.
128. Lasken, R. S. & Kornberg, A. (1988). The primosomal protein n' of *Escherichia coli* is a DNA helicase. *J Biol Chem* **263**, 5512-5518.



129. Wahle, E., Lasken, R. S. & Kornberg, A. (1989). The dnaB-dnaC replication protein complex of Escherichia coli. I. Formation and properties. *J Biol Chem* **264**, 2463-2468.
130. Marians, K. J. (1992). Prokaryotic DNA replication. *Annu Rev Biochem* **61**, 673-719.
131. Masai, H., Bond, M. W. & Arai, K. (1986). Cloning of the Escherichia coli gene for primosomal protein i: the relationship to dnaT, essential for chromosomal DNA replication. *Proc Natl Acad Sci U S A* **83**, 1256-1260.
132. Blandamer, M. J., Engberts, J. B., Gleeson, P. T. & Reis, J. C. (2005). Activity of water in aqueous systems; a frequently neglected property. *Chem Soc Rev* **34**, 440-458.
133. Marcolli, C. & Peter, T. (2005). Water activity in polyol/water systems: new UNIFAC parameterization. *Atmos Chem Phys Discuss* **5**, 1501-1527.

## Vita

Michal Roman Szymanski was born on August 13, 1982 in Leszno, Poland, to Dr. Lidia and Roman Szymanski. Michal graduated from high school in Leszno, Poland, and moved to Houston, Texas in 2002 to pursue his undergraduate studies at the University of Houston. During that time he enrolled in the Cooperative Education Program at the University of Houston to work in the Polyorganix Inc., Houston, Texas, as a Research Assistant. In 2005 he joined laboratory of Dr. H.J. Yeo, Biology and Biochemistry Department, at the University of Houston. During his tenure there, Michal focused on the purification and crystallization of HMW1B, a membrane protein from *Haemophilus influenza*, a common respiratory pathogen and important cause of morbidity in humans. He obtained membrane protein crystals which diffracted to 2.8Å and directed his research to label proteins purification and further exploration of the HMW1B structure. In 2007 Michal graduated cum laude from the University of Houston with a B.S. in Biochemical and Biophysical Sciences and a minor in Chemistry. Following graduation, Michal was enrolled in the Molecular Biophysics Educational Track (MBET), the Ph.D. program in the Department of Biochemistry and Molecular Biology at the University of Texas Medical Branch at Galveston, Texas, (UTMB) and has resided there since 2007. After completion of the first year of rotations, Michal joined the laboratory of Dr. Wlodek Bujalowski to conduct his research focusing on the helicase initiated assembly of macromolecular machines involved in DNA replication. During his time at UTMB he received numerous awards including Robert A. Welch Award for Excellence in Graduate Research in Chemistry and Barbara Bowman Memorial Award for Research Excellence in 2009. In 2010 he was awarded with Marianne Blum, Ph.D. Endowed Scholarship, Irma Mendoza Scholarship, and Biological Chemistry Student Organization (BCSO) Award. In 2011 he was nominated for Harold M. Weintraub Graduate Student Award and Who's Who Among Students in American Universities and Colleges. Michal has presented his research orally at Annual Structural Biology Symposium, Galveston, Texas in 2009, 2010 and 2011. Annual Gibbs Conference on Biothermodynamics, Carbondale, Illinois, 2009, 2010, 2011. 54<sup>th</sup> and 55<sup>th</sup> Annual Biophysical Society Meeting. 2010 and 2011 in San Francisco, California, and Baltimore, Maryland. Protein Society Meeting. 2010. San Diego, California. For the presentation on his research he received the Best Student Poster Award at 16<sup>th</sup> Annual Structural Biology Symposium. Galveston, Texas. 2011. Michal has also been a lecturer for Graduate School of Biomedical Sciences (GSBS), Biochemistry Course (BBSC 6401) in the Fall of 2010. In the summer of 2011 Michal received Kempner Postdoctoral Fellowship and following the completion of his dissertation he will continue his scientific training, starting October 2011, under the supervision of Dr. Wlodek Bujalowski at UTMB.

#### Permanent address

ul. Marszałka Focha 14, 64-125 Poniec, Poland

#### Education

B.S., May 2007, The University of Houston, Houston, Texas

#### Publications

Szymanski, M.R., Bujalowski, P.J., Jezewska, M.J., Gmyrek, A.M., Bujalowski, W. (2011). The N-Terminal Domain of the *Escherichia coli* PriA Helicase Contains Both the DNA- and Nucleotide-Binding Sites. Energetics of Domain-DNA Interactions and Allosteric Effect of the Nucleotide Cofactors. *Biochemistry* **50**(43), 9167-9183.

Szymanski, M. R., Jezewska, M. J., Bujalowski, P. J., Bussetta, C., Ye, M., Choi, K. H. & Bujalowski, W. (2011). Full-length dengue virus RNA-dependent RNA polymerase - RNA/DNA complexes. Stoichiometries, intrinsic affinities, cooperativities, base, and conformational specificities. *J Biol Chem.* **286**(38), 33095-108.

Szymanski, M. R., Jezewska, M. J. & Bujalowski, W. (2011). Binding of Two PriA-PriB Complexes to the Primosome Assembly Site Initiates Primosome Formation. *J. Mol. Biol.* **411**(1), 123-42.

Jezewska, M. J., Szymanski, M. R. & Bujalowski, W. (2011). Interactions of the DNA polymerase X from African Swine Fever Virus with the ssDNA. Properties of the total DNA-binding site and the strong DNA-binding subsite. *Biophys Chem* **158**, 26-37.

Jezewska, M. J., Szymanski, M. R. & Bujalowski, W. (2011). Kinetic mechanism of the ssDNA recognition by the polymerase X from African Swine Fever Virus. Dynamics and energetics of intermediate formations. *Biophys Chem* **158**, 9-20.

Jezewska, M. J., Szymanski, M. R. & Bujalowski, W. (2011). The primary DNA-binding subsite of the rat pol beta. Energetics of interactions of the 8-kDa domain of the enzyme with the ssDNA. *Biophys Chem* **156**, 115-27.

Szymanski, M. R., Jezewska, M. J. & Bujalowski, W. (2010). The *Escherichia coli* PriA helicase-double-stranded DNA complex: location of the strong DNA-binding subsite on the helicase domain of the protein and the affinity control by the two nucleotide-binding sites of the enzyme. *J Mol Biol* **402**, 344-62.

Szymanski, M. R., Jezewska, M. J. & Bujalowski, W. (2010). Interactions of the *Escherichia coli* primosomal PriB protein with the single-stranded DNA. Stoichiometries, intrinsic affinities, cooperativities, and base specificities. *J Mol Biol* **398**, 8-25.

Szymanski, M. R., Jezewska, M. J. & Bujalowski, W. (2010). The Escherichia coli PriA helicase specifically recognizes gapped DNA substrates: effect of the two nucleotide-binding sites of the enzyme on the recognition process. *J Biol Chem* **285**, 9683-96.

Andreeva, I. E., Roychowdhury, A., Szymanski, M. R., Jezewska, M. J. & Bujalowski, W. (2009). Mechanisms of interactions of the nucleotide cofactor with the RepA protein of plasmid RSF1010. Binding dynamics studied using the fluorescence stopped-flow method. *Biochemistry* **48**, 10620-36.

Szymanski, M. R., Fiebach, A. R., Tratschin, J. D., Gut, M., Ramanujam, V. M., Gottipati, K., Patel, P., Ye, M., Ruggli, N. & Choi, K. H. (2009). Zinc binding in pestivirus N(pro) is required for interferon regulatory factor 3 interaction and degradation. *J Mol Biol* **391**, 438-49.

Roychowdhury, A., Szymanski, M. R., Jezewska, M. J. & Bujalowski, W. (2009). Interactions of the Escherichia coli DnaB-DnaC protein complex with nucleotide cofactors. 1. Allosteric conformational transitions of the complex. *Biochemistry* **48**, 6712-29.

Roychowdhury, A., Szymanski, M. R., Jezewska, M. J. & Bujalowski, W. (2009). Mechanism of NTP hydrolysis by the Escherichia coli primary replicative helicase DnaB protein. 2. Nucleotide and nucleic acid specificities. *Biochemistry* **48**, 6730-46.

Roychowdhury, A., Szymanski, M. R., Jezewska, M. J. & Bujalowski, W. (2009). Escherichia coli DnaB helicase-DnaC protein complex: allosteric effects of the nucleotides on the nucleic acid binding and the kinetic mechanism of NTP hydrolysis. 3. *Biochemistry* **48**, 6747-63.

Andreeva, I. E., Szymanski, M. R., Jezewska, M. J., Galletto, R. & Bujalowski, W. (2009). Dynamics of the ssDNA recognition by the RepA hexameric helicase of plasmid RSF1010: analyses using fluorescence stopped-flow intensity and anisotropy methods. *J Mol Biol* **388**, 751-75.

Duret, G., Szymanski, M., Choi, K. J., Yeo, H. J. & Delcour, A. H. (2008). The TpsB translocator HMW1B of haemophilus influenzae forms a large conductance channel. *J Biol Chem* **283**, 15771-8.

#### Abstracts and Poster Presentations

Michal R. Szymanski, Maria M. Jezewska and Wlodzimierz Bujalowski. The *Escherichia coli* PriA Helicase Specifically Recognizes Gapped DNA Substrates. 16<sup>th</sup> Annual Structural Biology Symposium. 2011. Galveston, Texas.

Michal R. Szymanski, Maria M. Jezewska and Wlodzimierz Bujalowski. The *Escherichia coli* PriA Helicase Specifically Recognizes Gapped DNA Substrates. Biophysical Society 55th Annual Meeting. March 5-9, 2011. Baltimore, Maryland.

Michal R. Szymanski, Maria M. Jezewska and Wlodzimierz Bujalowski. Interactions of the E. coli Primosomal PriB Protein with the Single-stranded DNA. Solution vs. Crystallographic Studies. Protein Society Meeting. August 1-5, 2010. San Diego, California.

Michal R. Szymanski, Maria M. Jezewska and Wlodzimierz Bujalowski. Interactions of the E. coli Primosomal PriB Protein with the Single-stranded DNA. Solution vs. Crystallographic Studies. 15<sup>th</sup> Annual Structural Biology Symposium. 2010. Galveston, Texas.

Emilio Reyes-Aldrete, Mengyi Ye, Jebamony J. Robert, Michal R. Szymański, Cécile Bussetta, Wlodzimierz Bujalowski, Kyung Choi and Marc Morais. Preliminary structural, biochemical, and biophysical characterization of the ATPase from a dsDNA bacteriophage genome packaging motor. 15<sup>th</sup> Annual Structural Biology Symposium. 2010. Galveston, Texas.

Wlodek Bujalowski, Maria J. Jezewska, Iraida E. Andreeva, Michal R. Szymanski, Roberto Galletto. Dynamics of the recognition by the RepA Hexameric helicase of plasmid RSF1010. Analyses using fluorescence stopped-flow intensity and anisotropy methods. Biophysical Society 54th Annual Meeting. February 20-24, 2010. San Francisco, California.

Michal R. Szymanski, Maria J. Jezewska, Wlodzimierz Bujalowski. Energetics of the E. Coli PriA Helicase Interactions with the Double Stranded DNA. Biophysical Journal, 98(3) 1 January 2010. Biophysical Society 54th Annual Meeting. February 20-24, 2010. San Francisco, California.

Maria J. Jezewska, Iraida E. Andreeva, Michal R. Szymanski, Wlodek Bujalowski. Mechanism of Nucleotide Cofactor Interactions with the RepA Protein of Plasmid RSF1010. Biophysical Society 54th Annual Meeting. February 20-24, 2010. San Francisco, California.

Michal R. Szymanski, Maria M. Jezewska and Wlodzimierz Bujalowski. Energetics of the E. coli PriA Helicase Interactions with the Double Stranded DNA. The Twenty-third Annual Gibbs Conference on Biothermodynamics. October 3-6, 2009. Carbondale, Illinois.

Michal R. Szymanski, Joseph W. St. Geme & Hye-Jeong. Towards the crystal structure of the Haemophilus influenzae Omp-85 protein. Sigma Xi Research Day. 2006. Houston, Texas.

Michal R. Szymanski, Joseph W. St. Geme & Hye-Jeong. Towards the crystal structure of the *Haemophilus influenzae* Omp-85 protein. 11<sup>th</sup> Annual Structural Biology Symposium. 2006. Galveston, Texas.

Hye-Jeong Yeo, Katarzyna Walkiewicz, Michal Szymanski, Takeshi Yokoyama, Joseph St. Geme. Towards the Structural Basis for Bacterial Two-Partner Secretion. The 2006 Meeting of the American Crystallographic Association. 2006. Honolulu, Hawaii.

This dissertation was typed by Michal R. Szymanski.